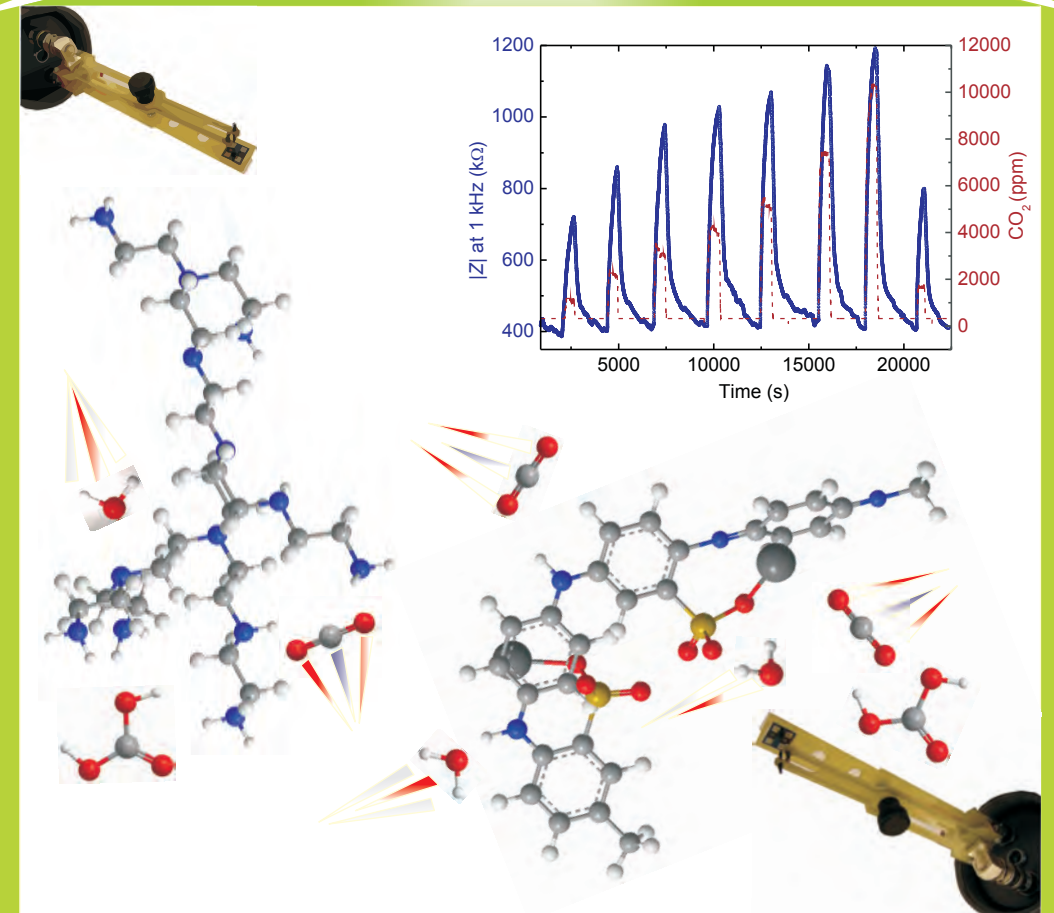


Conductive Polymers for Carbon Dioxide Sensing



Tin C. D. Doan

Conductive Polymers for Carbon Dioxide

Tin C. D. Doan

Propositions

1. Sulfonation of polyaniline enables detection of CO₂ due to shifting of the pH-induced conductivity to the carbonic acid pH regime. (*This thesis*)
2. ‘Direct’ CO₂ sensing via a reaction between CO₂ and amine groups of polyethyleneimine and its blends yields better sensitivity than ‘indirect’ CO₂ sensing via carbonic acid formation. (*This thesis*)
3. Dip-pen nanolithography using electrostatic interactions as a driving force, proposed by Mirkin and co-worker, is the best way to obtain patterned nanowires of water-soluble conductive polymers. (*J.H. Lim, C.A. Mirkin, Advanced Materials, 14 (2002) 1474-1477*)
4. Just heating poly(anthranilic acid) is not sufficient for complete removal of its ionized carboxyl groups (–COO[–]), as claimed by Ogura et al.
(*K. Ogura et al., Journal of Electroanalytical Chemistry, 522 (2002) 173-178,*
K. Ogura, H. Shiigi, Electrochemical and Solid-State Letters, 2 (1999) 478-480,
K. Ogura et al., Journal Polymer Science, Part A: Polymer Chemistry, 37 (1999) 4458-4465.)
5. Polymer thin films for highly selective, sensitive and reversible CO₂ sensors still have a long journey to practical applications.
6. Interdisciplinary research is a good thing, transdisciplinary research is better.
7. Doing measurements with high CO₂ concentrations on weekends has a higher risk of creating doziess than motorbike riding in Ho Chi Minh City during rush hours.
8. The large number of motorbikes in Ho Chi Minh promotes plant growth within the city.

Propositions belonging to the thesis, entitled

“Conductive Polymers for Carbon Dioxide Sensing”

Tin Chanh Duc Doan

Wageningen, 29 October 2012

Conductive Polymers for Carbon Dioxide Sensing

Tin C. D. Doan

Thesis committee

Thesis supervisor

Prof. dr. C.J.M. van Rijn

Professor of Microsystem and Nanotechnology for Agro, Food and Health

Wageningen University

Other members

Prof. dr. E.J.R. Sudhölter	Delft University of Technology
----------------------------	--------------------------------

Prof. dr. ir. F.A.M. Leermakers	Wageningen University
---------------------------------	-----------------------

Prof. dr. ing. E.J. Woltering	Wageningen University
-------------------------------	-----------------------

Prof. dr. S.G. Lemay	University of Twente, Enschede
----------------------	--------------------------------

This research was conducted under the auspices of the Graduate school VLAG (Advanced studies in Food Technology, Agrobiotechnology, Nutrition and Health Sciences).

Conductive Polymers for Carbon Dioxide Sensing

Tin C. D. Doan

Thesis

submitted in fulfillment of the requirements for the degree of doctor

at Wageningen University

by the authority of the Rector Magnificus

Prof. dr. M.J. Kropff,

in the presence of the

Thesis Committee appointed by the Academic Board

to be defended in public

on Monday 29 October 2012

at 4 p.m. in the Aula.

Tin C. D. Doan

Conductive Polymers for Carbon Dioxide Sensing

Thesis, Wageningen University, Wageningen, The Netherlands (2012)

With references, with summaries in English, Dutch and Vietnamese

ISBN: 978-94-6173-410-5

“I can accept failure but I can’t accept not trying” – Michael Jordan

Dedicated to my older sister, my family and Little Turtle

Table of Contents

Chapter 1	General Introduction	1
Chapter 2	Carbon Dioxide Sensing with Sulfonated Polyaniline	27
Chapter 3	Decoupling Intrinsic and Ionic Conduction in Sulfonated Polyaniline in the Presence of Water Vapor as Analyte	47
Chapter 4	Carbon Dioxide Detection at Room Temperature with Polyethyleneimine-based Chemiresistor	77
Chapter 5	Improved Carbon Dioxide Sensing of Polyethyleneimine Blended with Other Polyelectrolytes	99
Chapter 6	General Discussion	123
Appendix 1	Supplementary Information for Chapter 2	143
Appendix 2	Supplementary Information for Chapter 3	149
Appendix 3	Supplementary Information for Chapter 4	165
Appendix 4	Supplementary Information for Chapter 5	167
Summary		173
Samenvatting		177
Tóm Tắt		181
Curriculum Vitae		185
List of Publications		187
Overview of Completed Training Activities		189
Acknowledgement		191

Chapter 1. General Introduction

The aim of this research is to develop a low power carbon dioxide (CO₂) gas sensor based on conductive polymer/polyelectrolyte composites operating at ambient temperature. Detection of CO₂ is performed by measuring a specific change in the electrical conductivity of a thin film sensing layer at a specific frequency. The intended application is for integration into low power wireless CO₂ sensor nodes to monitor and control CO₂ levels in offices and greenhouses.

1.1. Role of CO₂ in Greenhouses - Monitoring of CO₂ Levels

Carbon dioxide (CO₂) has a significant influence on stimulating plant growth through photosynthesis. Elevated CO₂ concentrations are widely expected to increase crop photosynthesis and yield [1]. The review of CO₂ effects on harvestable yield was presented by Kimball [2] who examined effects of CO₂ enrichment on the economic yields and growth of 24 crops and 14 other species. It has been shown that yields increased by 33% with a doubling of atmospheric CO₂ concentration. Another study on effect of CO₂ concentration on wheat yield [3] also showed that doubling CO₂ concentration from 350 ppm to 700 ppm increased wheat yield about 31%.

As a result, monitoring CO₂ gas levels plays a significant role in plant growth control in greenhouses. For optimal plant growth, greenhouses need continuous stable monitoring and regulation of CO₂ levels. Wireless sensor networks are suggested to be used for continuous monitoring CO₂ levels over large area of greenhouses [4] and these networks require sensors operating at low power. The commercial non-dispersive infrared CO₂ sensors are available but they are expensive, large scale, and consume a great deal of power [5]. Hence these IR sensors are not suitable for the sensor network because of high running cost. Conventional CO₂ sensors based on solid state electrolytes (metal oxides) are only sensitive at high temperature. Continuous operation of such sensors in greenhouses leads to increased thermal degradation and large power consumption [6]. Thus solid electrolyte-based CO₂ sensors are also not suitable for wireless application. Therefore a highly selective, sensitive, low power CO₂ sensor is desired and polymer-based sensors are considered as promising candidates.

1.2. Polymer-Based CO₂ Sensors

Polymers have been used as active layers in CO₂ sensor because CO₂ detection can take place at room temperature [7, 8]. Absorption and desorption of CO₂ molecules interacting with functional groups of polymer molecules will induce an appropriate change in an electrical bulk property, such as conductivity and dielectric permittivity of the polymer film [9]. Several types of amino-group-containing polymers have been employed so far for CO₂ detection such as polyethyleneimine (PEI) [10-12], acrylamide and isooctylacrylate [13], polyacrylamide and polysiloxane [14], poly (γ -aminopropylethoxy/propylethoxysiloxane), poly(γ -aminopropylethoxy/octadecylethoxysiloxane), poly(propyleneimine), aminoalkyl poly(dimethylsiloxane), polystyrene-bound ethylenediamine [11, 15], alkylamine

functionalized polysilsesquioxanes [16], heteropolysiloxane containing 3-aminopropyltrimethoxysilane (AMO) and propyltrimethoxysilane (PTMS) [17-21]. AMO-PTMS was first used in chemi-capacitive sensor with integrated micro-heater (60-75 °C) for sensing 100-3,000 ppm CO₂ [17]. Recently, work function change of AMO-PTMS [18-21] in presence of 400-4,000 ppm CO₂ has been intensively investigated with suspended gate FET and Kelvin probe for measurement of contact potential difference. However, strong drift under humidity of 40% RH was observed.

Most of the polymers used as CO₂ sensing materials have hetero polysiloxane containing primary amino groups blended with a hydrophobic polymer to reduce effect of water vapor. Interaction of CO₂ and amino groups is based on acid-base reaction [11, 15, 22]. CO₂ is considered a hard acid and can interact with primary and secondary amines which are hard bases [22, 23]. The interaction is ionic and reversible, yielding to carbamates [22]. Branched polyethyleneimine (PEI) with three types of amine (primary, secondary and tertiary) (**Figure 1**) can react directly with CO₂ at room temperature (**Figure 2**) [24]. Therefore, PEI has been explored widely for CO₂ capture [24-29] and CO₂ sensing [10-12, 30].

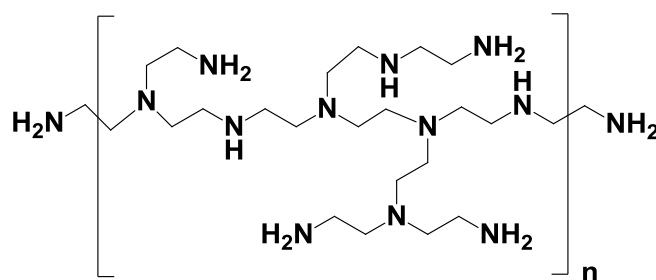
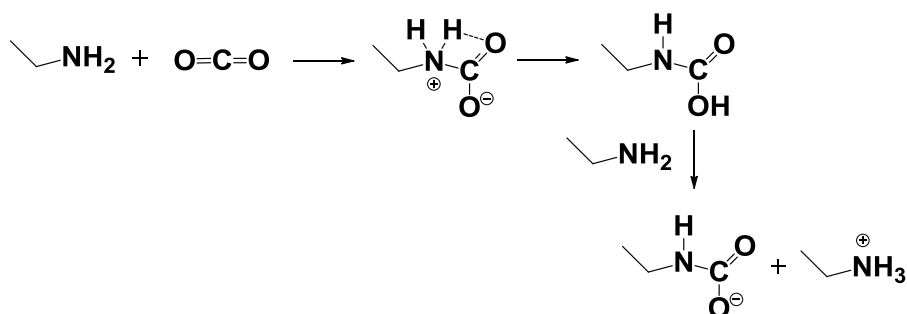
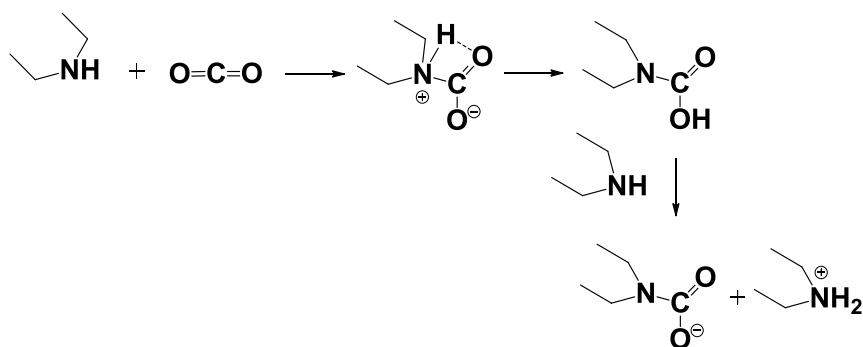


Figure 1. Chemical structure of polyethyleneimine (PEI).

a. Primary amines



b. Secondary amines



c. Tertiary amines

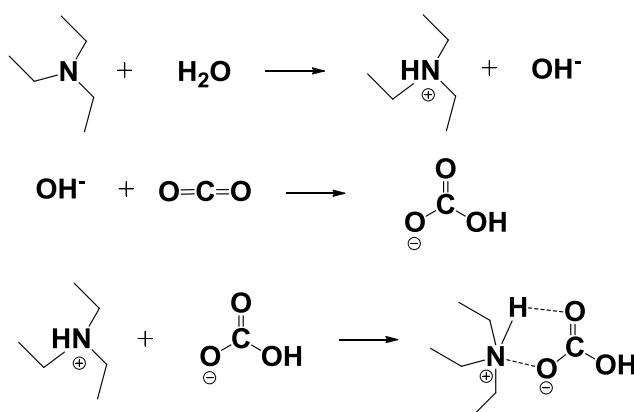


Figure 2. Mechanism of reaction between CO_2 and (a) primary amines (under dry condition), (b) secondary amine (under dry condition) and (c) tertiary amines (under humid condition) [24].

PEI-based CO_2 sensors have been developed with various transducing mechanisms. PEI-coated surface acoustic wave transduction (SAW) [10] was found to be not suitable for practical sensors due to baseline drift and undetermined recovery time. Quartz microbalance transduction (QCM) with PEI coating was used for CO_2 detection at 60 °C but the response was affected strongly by humidity due to polymer swelling and viscosity changes [11]. PEI/starch blend coated on QCM [12] showed higher sensitivity than PEI coating but both sensors suffer from poor signal and long recovery time (more than 20 minutes) at 25 °C. PEI/starch was also coated on AlGaIn/GaN High Electron Mobility Transistors (HEMT) [30] exhibiting (high) sensitivity in CO_2 range of 0.9-50% at high temperature of 108 °C. A PEI/starch-coated carbon nanotube (CNT) with field effect transistor (FET) [31] showed fast response (below 1 minute) and good reproducibility from 500 ppm to 10% and is a promising candidate. However, a PEI/starch-coated CNT with SAW as a transduction principle seems only suitable for monitoring high CO_2 concentrations of 2.5-40% [32].

Other polymers have also been employed for CO₂ sensing, for example fluoropolymer Teflon AF 2400 [33]. A ~10 µm thick film was deposited onto an interdigitated metal grid on a quartz substrate and a change in capacitance was measured. CO₂ adsorption causes an increase in dielectric constant of the Teflon film. The CO₂ response of the sensor was measured with respect to an air reference for both 100% CO₂ and ambient CO₂ levels (~420 ppm). However, the sensor exhibited poor selectivity to CO₂ and the measurement was done only in dry condition because water vapor created large interference.

1.3. Conductive Polymers for CO₂ Sensing

1.3.1. Conductive Polymers

A polymer that possesses the electrical, magnetic and/or optical properties of a metal is termed a “synthetic metal” [34, 35]. Conductive polymers often have alternating single and double bonds along the polymer chain, which enable the delocalization or mobility of charge carriers along the polymer backbone; therefore, conductive polymers are also called “conjugated polymers” [36, 37]. Among many developed conductive polymers, the conjugated systems based on aromatic rings such as polyacetylene (PA), polyaniline (PANI), polypyrrole (PPy), polythiophene (PT), polyphenylene (PPP), poly(phenylene vinylene) (PPV) (**Figure 3**) and their derivatives have attracted much attention [35].

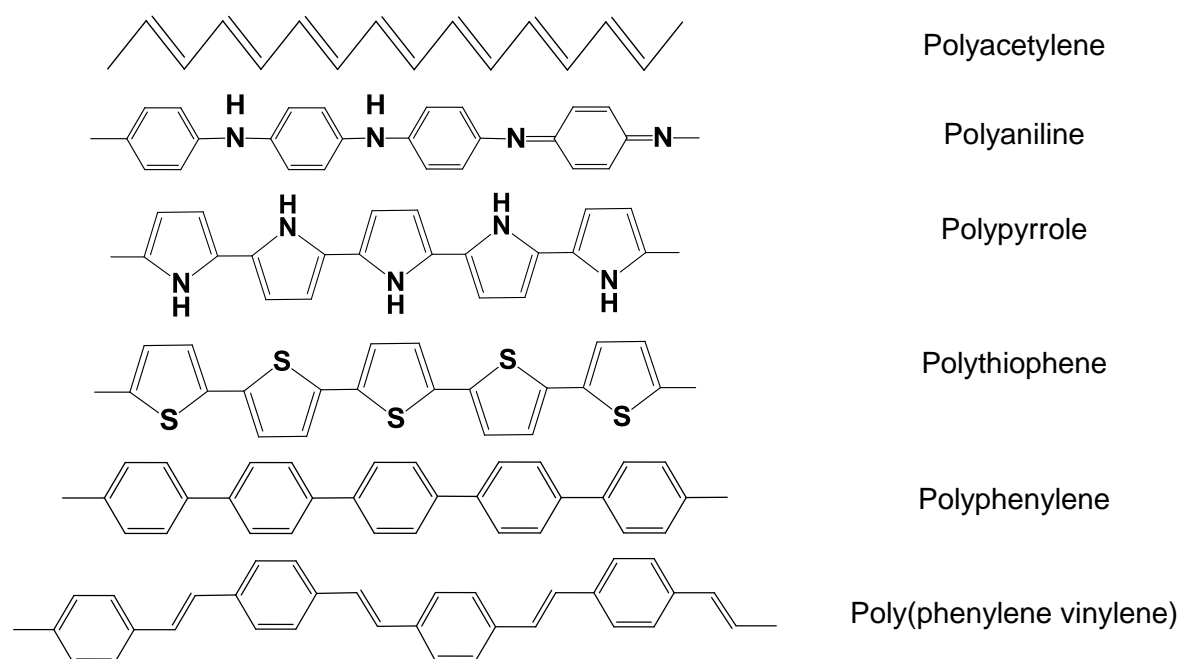


Figure 3. Chemical structures of some popular conjugated polymers [35].

Normal (undoped) conjugated polymers are semiconductors with band gaps ranging from 1 to several eV, therefore their room temperature conductivities are very low, typically in the range of 10^{-5} to 10^{-10} S.cm⁻¹ or lower [34, 35]. To make conjugated polymers electronically more conductive, additional (mobile) charge carriers are required to couple chemically with the conjugated system, which is called “doping” [35, 37]. The term “doping” is used by analogy with conventional semiconductors like silicon or germanium in which dopants like phosphorous or boron are introduced [38] in the semiconductor lattice. However, doping in conjugated polymers is quite different from that in conventional semiconductors [35, 37]. In conventional semiconductors, dopant in small quantity occupies positions in the atomic lattice, resulting in large change in conductivity due to a relative increase in charge carriers such as electrons and electron holes in the solid state material. Some of the semiconductor atoms are then replaced by electron-rich (e.g. phosphorus) or electron-poor (e.g. boron) atoms to create n-type (electron) and p-type (electron hole) semiconductors, respectively [37]. In contrast, the primary method of doping a conductive polymer is through an oxidation-reduction (redox) process. Upon doping, conductivity of conjugated polymers can increase by many orders of magnitude and can become “metallic” with conductivities in the order of 1 to 10^4 S.cm⁻¹ [34, 35] as shown in **Figure 4**. The highest conductivity value reported to date has been obtained in iodine-doped polyacetylene (10^5 S.cm⁻¹) [35, 39].

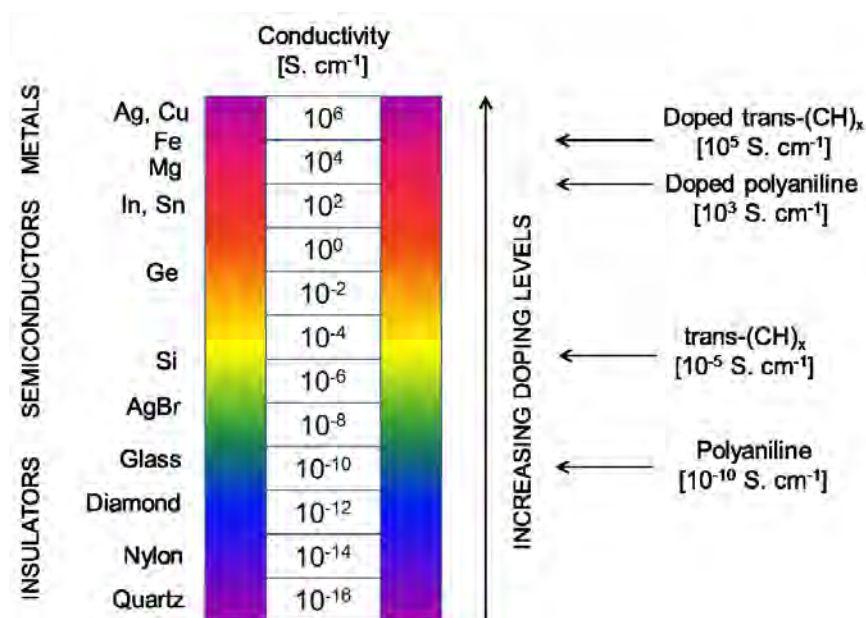


Figure 4. Conductivity of undoped and doped conjugated polymers [34, 39].

The doping of conductive polymers can be accomplished by redox doping or protonic acid doping [34, 35]. Redox doping involves insertion of electron acceptor molecules (oxidation)

or electron donor molecules (reduction) and the obtained polymer is then a p-type or an n-type one, respectively [38]. Protonic doping differs from redox doping in that the number of electrons associated with the polymer backbone does not change during the doping process [38, 40, 41]. Polyaniline (PANI) is a special conductive polymer because its conductivity can be increased either through oxidation of polyleucoemeraldine base or protonation of polyemeraldine base [38, 41]. The protonation mechanism of emeraldine base polyaniline (EB-PANI) via acidic doping has been well studied [40-48]. Upon exposure to an acid, insulating EB-PANI with a non-conjugated structure is converted to a conjugated conductive emeraldine salt after protonation doping (**Figure 5**). The imine nitrogen atoms can be protonated in whole or in part, resulting in the formation of a delocalized poly-semiquinone radical cation which is called “polaron” in solid state physics [35] with an increase in conductivity of about 10^{10} [39]. Besides, the doping process is inter-conversional, when conducting salt PANI is treated with a strong base (NH_3 , for example) or aqueous alkali, the imines are deprotonated resulting in conversion to the emeraldine base form (**Figure 5**).

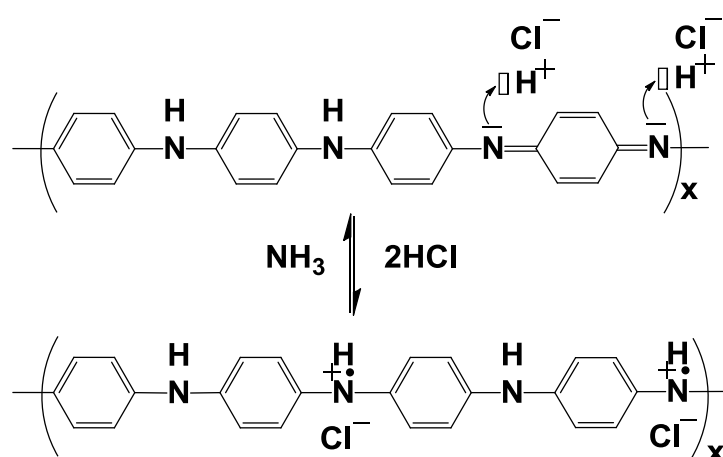


Figure 5. (Inter)conversion of the insulating EB-PANI (undoped) to conducting emeraldine salt PANI (doped) upon exposure to an acid or base [38].

In general, mobile charges in doped conductive polymers are positive charges (polarons or bipolarons - a bound pair of two polarons) along the polymer chains [35]. To maintain charge neutrality it requires incorporation of anions such as Cl^- , HSO_4^- , ClO_4^- , NO_3^- , p-toluene sulfonate, camphor-10-sulfonate, or polyelectrolytes such as poly(styrene sulfonate), as well as amino acids and biopolymers [35, 38]. These incorporated anions result in tuning the properties of the conductive polymers, leading to a wide range of properties and applications. However, in some doping processes such as photo-doping and charge injection there is no counter dopant ion involved [35].

1.3.2. Literature Review on Conductive Polymers for CO₂ Sensing

In recent years, many sensors using conductive polymers to detect different kinds of gases have been developed. Most of which have been reviewed by Basudam Adhikari [8], Ulrich Lange [49], and Hua Bai [9]. In the latter review, three popular conductive polymers including PANI, PPy and poly (3,4-ethylenedioxythiophene) used as active layers in various types of gas sensors have been reviewed. Two popular conductive polymers including PPy and PANI have been reported to be used for CO₂ detection. Measured sensing parameters, configurations of the sensors, sensing mechanism and the factors that affect the performances of these sensors will be briefly addressed.

a. CO₂ Sensor Based on Polyethylene (PE) Composite

C. Jouve et al. [50] used thin films (2 μm) of low density PE containing crystalline tetrathiofulvalinium-tetracyanoquinodimethane (TTF - TCNQ) organic salts casted on ITO glass substrates. Dc measurements were performed to investigate the gas detection properties of the composite film in the presence of CO₂, NO₂, H₂O and O₂ species in an argon atmosphere. A decrease to 15% of the initial conductivity was observed when the sample was exposed to 100 ppm CO₂ in argon at ambient temperature. After reaching a minimum (at 15% of the initial conductivity), the conductivity drifted and increased up to 95% of the initial conductivity. The response time was 5 minutes and the reversible response (recovery) in CO₂ was also noticed. The decrease in conductivity was explained by the modification of the conduction between dendritic conducting paths in the presence of CO₂ molecules. In this research, the conductivity of the composite film with gases was measured at very high relative humidity of 100%; however, the humidity value was not mentioned when dry argon gas was flowed to stimulate the desorption rate. A cross-interference of humidity on the measured signals might hamper a consequent interpretation of the sensitivity to CO₂.

b. CO₂ Sensor Based on PPy Composite

i. Komilla Suri et al. [51] used composites of iron oxide and PPy in pellet form to study humidity and gas (CO₂, N₂, CH₄) sensing properties. The resistance variations were studied as a function of gas pressures. The sensitivity increased linearly with the concentration of PPy for all pressures. At the highest pressure (40 psi), the sensors exhibited the highest sensitivity to CO₂ gas with a sensitivity approaching more than 100. The high sensitivity to CO₂ gas was ascribed to the molecular size and its effect on permeability of the gases. The kinetic diameter of CO₂ is smallest among the three tested gases including CO₂, N₂ and CH₄. Therefore

permeability of CO₂ is maximum, which results in good response and sensitivity. The gas sensitivity could be affected by the interference of water vapour which was not clearly investigated.

ii. In another study the composite of PPy was also used as a sensing material for CO₂ detection. S.A. Waghuley et al. [52] used the films of PPy-FeCl₃ to build a CO₂ sensor. Thick films (22-32 μ m) were deposited by screen-printing technique on a glass substrate. Sensitivity of sensors at different concentrations of CO₂ gas was measured by a voltage drop method at room temperature (303 K). The resistance of the sensors was found to increase with an increase in CO₂ concentration (100 ppm, 400 ppm and 700 ppm). The response values varied linearly with the CO₂ concentration for an exposure time of 15 minutes at room temperature. At certain higher concentration of CO₂ gas, a saturation effect was observed. The response time was 4 minutes and recovery time of the sensors was about 30 minutes. In addition, the effect of temperature on CO₂ response was also investigated. The CO₂ response of both sensors decreased when the temperature increased from 303 K to 343 K. The response to CO₂ gas was also ascribed to the kinetic diameter of CO₂ molecule and the gas permeability. The CO₂ sensing mechanism of the composite PPy-FeCl₃ was also proposed. CO₂ molecules might form weak bonds with π -electrons of PPy. The number of delocalized π -electrons of the PPy structure will then diminish. This causes then an increase in resistance of the material in the presence of CO₂ gas. However, the effect of humidity and the cross-sensitivity of other gases were not investigated. Investigating temperature effects on the resistance of the film at different CO₂ concentrations, it was observed that at 70 °C the resistance of the composite film remained unchanged in variation of CO₂ concentrations. Therefore, the effect might also possibly be due to water vapour that made the resistance change at room temperature.

c. CO₂ Sensor Based on PANI and Its Composite with Poly(Vinyl Alcohol) (PVA)

i. S. Takeda [53] used plasma polymerized PANI thin film (200-300 nm) deposited between parallel Au electrodes on a Pyrex glass substrate to detect CO₂. Dc measurement was performed in a stream of CO₂ gas (2 L/minute) and dry air. A fast increase (within 0.5 s) of the dc current was noticed when the polymer was exposed to CO₂ and a decrease in current was observed when dried air was used to purge. A reaction mechanism between adsorbed CO₂ molecules and the amino groups of the polymer chains was proposed. However, the relative humidity was not shown in the experiments. The change in current might at least partly be ascribed to the variation of humidity when CO₂ and dried air were introduced in the

measurement chamber. Moreover, the measurement was done with only 100% CO₂ (high flow rate 2 L/minute of CO₂). Therefore, the results can only be taken as a proof of concept.

ii. K. Ogura and H. Shiigi [5] reported on the electrical conductivity of a composite film comprising heat-treated poly(anthranilic acid) (PANA) and PVA. PANA underwent a heat-treatment at temperatures of 250 °C and 280 °C to eliminate carboxyl groups. After heat-treatment, PANA was claimed to be converted to base-type PANI. Heated PANA:PVA composite film (100 nm) was casted on comb-shaped Pt electrodes on glass substrates. The conductivity was measured by a two-probe dc technique. A linear relation between conductivity and CO₂ concentration was noticed at 30% RH. However, at 50% and 70% RH, the linear relationship was only in a limited range, and no response to CO₂ was observed in the concentration range higher than 10³ ppm. The response to humidity of PANA with and without heat-treatment at 280 °C for 8 hours was compared and it was concluded that the carboxyl group might be eliminated from PANA, preventing possible interference by water vapour during CO₂ sensing. The heat treatment of PANA at 280 °C at 8 hours was found to give the best linearity in conductivity on varying CO₂ concentration. The high conductivity of PANA treated at 250 °C for 2 hours was attributed to un-eliminated –COOH groups in the composite. The residual –COOH group made the polymer self-doped and gave rise in conductivity. Interestingly, the change in conductivity of the heat-treated PANA:PVA composite was observed towards 2,870 ppm CO₂ at 28% RH. The composite showed quick response (29 seconds) and good reversibility. The increase in conductivity of the composite film in proportion to the CO₂ concentration was attributed to the transformation of the insulating base-type PANI to the conducting salt-type which was caused by the incorporation of carbonate ions formed by the hydrolysis of H₂CO₃ into the base-type PANI. This is the first paper of this group in which the CO₂ detection principle by acidic doping was proposed. The mechanism is based on doping the base-type PANI by carbonic acid formed in the presence of CO₂ and water molecules. However, the acidic doping effect of base-type PANI resulting in the observed response to CO₂ was disputed in other papers [40, 42, 46, 54].

iii. Following this paper, T. Oho and K. Ogura [55] reported on a composite film consisting of base-type PANA and PVA exposed to CO₂ under high humidity. In the previous research [5], the authors reported that the change in dc resistance of the composite film depended on the CO₂ concentration at a constant humidity. However, the change in resistance upon the variation of CO₂ concentration became quite small at higher than 60% RH. The measurement of ac impedance instead of dc resistance was found to determine the CO₂ concentration with

accuracy under a high humidity. In this paper, the authors also used the same chip configuration. The same linearity of dc resistance and CO₂ concentration at 30% and 50% RH was obtained. However, at 20% and 70% RH, the linear relationship was valid only in a limited region of CO₂ concentration. At 20% RH, the dc resistance was independent of CO₂ concentration. It was attributed to small changes in concentration of hydrogen carbonate ion (HCO₃⁻) under such dry condition. At 70% RH, it was suggested that the base-type PANA was completely converted to the salt-type with a higher concentration of CO₂; hence the dc resistance was independent of CO₂ concentration. However, the ac method showed very good linearity in a highly humid atmosphere with CO₂. Moreover, smaller ratio of PANA to PVA resulted in complete conversion of the base-type PANA to the salt-type with a smaller amount of carbonate ions, i.e. with a lower concentration of CO₂. The ac impedance was found to be affected by the CO₂ concentration when the frequency was larger than 100 Hz at 80% RH. A good linear relationship of impedance versus CO₂ concentration was shown at 100 kHz in the concentration range between 3×10^2 and 1.5×10^5 ppm at 80% RH. The response of the composite film to CO₂ concentration was not affected in the presence of NH₃ (below 1,000 ppm) and HCl (10 ppm). In addition, no effect of coexisting gases such as O₂ and N₂O on dc resistance versus CO₂ concentration was observed.

iv. In addition to using base-type PAN as a result of heat-treated PANA at 280 °C for 2 hours, K.Ogura et al. also used directly emeraldine base polyaniline (EB-PANI) and PVA [56, 57]. The composites consisting of the EB-PANI and PVA served as a promising CO₂ sensor operating at room temperature with a high sensitivity. One noticeable point in the polymer synthesis is that p-toluene sulfonic acid (TSA) was used in synthesis of PANI. After dedoping TSA-doped PANI with 3% NH₄OH, PANI powder was heated at 380 °C for 1 hour in a helium gas atmosphere. The purpose was to complete the detachment of TSA. The thermal treatment of PANA and PANI could get the EB-PANI form and thermal conversion of the salt-type was much more advanced for PANI than PANA. The linear relation between electrical conductivity of the EB-PANI:PVA composite with CO₂ concentration was observed. For the composite with 13 wt % EB-PANI and 87 wt % PVA, the linear relationship held in the concentration range from 50 ppm to 5% at 30% RH. With the composite consisting of 25 wt % EB-PANI and 75 wt % PVA, the linearity was valid over a wide range from 100 ppm to 100% although the sensitivity for the detection of CO₂ was inferior to that in the case of the composite with lower content of EB-PANI. The weight percentage of PANI was varied from 11% to 25 wt % at 50% RH. As the content of the EB-

PANI was increased, the minimum concentration of CO₂ giving a limitation of conductivity became larger, and eventually the composite with higher than 13 wt % EB-PANI gave no limitation of conductivity in the range of CO₂ concentration from 50 ppm to 1%. The composite with higher content of EB-PANI gave higher concentration of carbonate ion and was rather conductive even at low concentration of CO₂. Conversely, the composite with lower content of EB-PANI gave low conductivity at lower concentration of CO₂ and a constant conductivity at higher concentration.

v. Mihai Irimia-Vladu [54] developed CO₂ sensor with the same procedure of Ogura [56, 57]. However, their sensor showed very small response magnitude $\Delta R/R$ (2% and 15%) in comparison to Ogura's sensor (2 orders of magnitude). The drift of the sensor exceeded half the dynamic range after three or four cycles between Ar and Ar + 5% CO₂, whereas Ogura's sensor was stable with minimal drift for 35 days. The 90% time response in this work was much slower (few hours to 24 hours) than reported by Ogura (second to few minutes). The poor performance of the sensor was explained based on the relationship between doping percentage of EB-PANI by protonic acids and the pH of the protonating bath. With PANI compressed pellet there was no change in conductivity due to very little protonation if pH was greater than 4 [40, 46]. However, the tested upper limit in Ogura's research was 50,000 ppm CO₂ corresponding to pH 4.6. Therefore, it was claimed that CO₂ would not protonate EB-PANI films because pH range in Ogura's experiment was greater than 4. The authors concluded that the proposed mechanism of CO₂ detection did not explain the observed response. In addition, these authors [58] also used impedance spectroscopy to investigate the conductivity of an EB-PANI thin film on an interdigitated electrode in hydrochloric acid solutions of various pH between 2.25 and 6. In this work, the polymer coated electrodes were immersed in carbonic solution and pH solutions. Impedance spectroscopy was used to measure pH changes resulting from bubbling argon-CO₂ mixtures through water. It was observed that impedance spectroscopy detected changes in the conductivity at pH levels between 6 and 4, which were not observable in total conductivity change measured with a dc technique. However, this measurement method is not suitable for practical application of CO₂ gas sensor.

vi. Recently, Michael Freund et al. [59] developed a CO₂ sensor based on self-doped PANI by boronic acid (PABA) attached to the main chain. The film was coated by drop-casting 2 μ L of the PABA solution with micro pipette on comb-shaped gold electrodes patterned on printed circuit boards. Nafion (2 μ L) or PVA (4 μ L) were used to attract water were dropped on top

of PABA film, so the total thickness of the film was quite large. The resistance of the sensor decreased when RH increased from 20% to 50% but increased when RH increased from 50% to 70%. It was attributed to polymer swelling due to water absorption and there might be breakdown or increase in contact between the dispersed conductive nano-particles affecting the resistance with the change in humidity. The film's response to change in analyte concentrations at various humidity levels was stable until 70% RH and became noisy above 70% RH. The sensors displayed a saturation effect above 2,455 ppm of CO₂ and severe drift in dc resistance signal was observed. The influence of temperature on the performance of the sensors was also evaluated. The decrease in the resistance value upon increase in temperature was explained due to the loss of protonation and expulsion of water molecules from the polymer composite. Exposure to 1% (vapour pressure) of methanol (1,618 ppm), acetone (3,157 ppm) and 1-propanol (276 ppm) in air for 3 minutes, followed by various levels of CO₂ did not change the resistivity of the sensor.

1.3.3. CO₂ Sensing Based on the Protonic Doping Concept in PANI

The chemical inertness of CO₂ makes the CO₂ detection difficult by conventional methods except infrared spectroscopy and gas chromatography. However, CO₂ can be detected “indirectly” when CO₂ is dissolved in water or in a humid environment (e.g., in a greenhouse with humidity of 80-90%) to form carbonic acid. In principle, carbonic acid with pH4-pH6 can be detected by a pH sensor with a conductive polymer as a sensing material.

The mechanism of CO₂ sensing based on protonation of EB-PANI with carbonic acid was firstly proposed by Ogura and his co-workers [5, 56, 57, 60] when they showed a working CO₂ sensors based on a composite film of EB-PANI and PVA. The acidic doping of EB-PANI by carbonic acid occurs in a similar way with HCl acid (**Figure 6**). At high humidity, there is hydrolysis of CO₂ and carbonate ions, resulting in formation of carbonic acid. Hence EB-PANI is assumed to be protonated and an increase in conductivity is observed [5, 56, 57, 60].

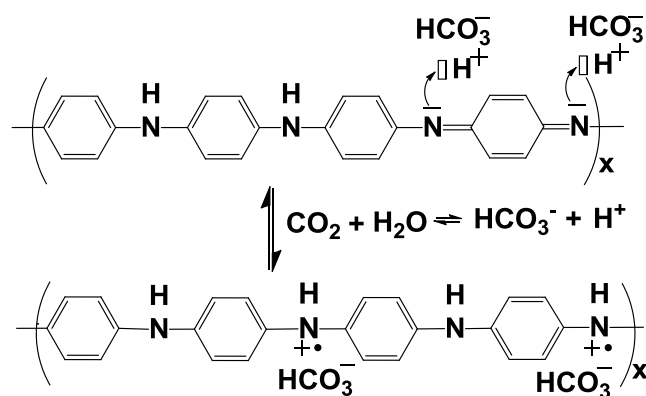


Figure 6. Acidic doping of the insulating EB-PANI results in conducting PANI (doped) by carbonic acid [5, 56].

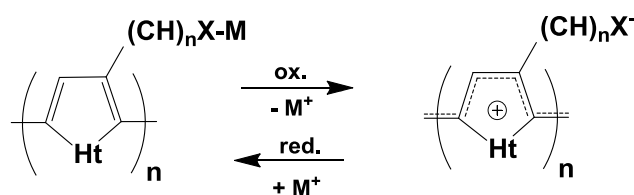
Ogura claimed that the conductivity change of the composite film was due to the doping of EB-PANI by carbonic acid which was formed by CO_2 and moisture trapped in the PVA matrix. However, this mechanism is debatable because it is not consistent with other reports on pH-dependent conductivity of EB-PANI [42, 43, 46]. The results of MacDiarmid and co-workers showed that with PANI compressed pellet very little protonation occurs if pH is greater than 4. According to calculation of Irimia-Vladu [54] the CO_2 detection range in Ogura's work was from pH 6 (50 ppm CO_2) to pH 4.6 (5% CO_2) and this pH range was greater than 4, so CO_2 would not protonate EB-PANI film. Therefore, the doping mechanism of EB-PANI with carbonic acid which was proposed by Ogura et al. still needs clarification.

1.4. Self-Doped Sulfonated PANI with Extended pH Response for CO_2 Sensing

1.4.1. Self-Doping in Conductive Polymers

As mentioned above, for oxidation doping or protonation doping (p-doping) of conductive polymers, it requires intrusion of charged dopants and counterions into the polymer in order to preserve charge neutrality during the charge injection process [35, 38]. Upon reduction or dedoping, the corresponding counterions (anions) should be expelled too. A self-doped conductive polymer however has an ionizable functional group attached to the polymer via a covalent bond acting as an immobile anion (e.g. SO_3^-) holding dopant molecules (e.g. H^+) that promote protonation at the imine sites [61, 62]. The principle of self-doping in a conjugated polymer is shown in **Figure 7**. During oxidation process, in the presence of immobilized larger anion, the smaller mobile proton or other monovalent cation is expelled from the polymer into the electrolyte to maintain charge neutrality. Upon reduction that cation moves into the polymer to compensate the immobilized anion. Due to higher mobility of the smaller

cations, the rate of the charging (redox) process is significantly increased [35].



Ht = NH, S; $n = 1, 2, \dots$; $X = \text{CO}_2, \text{SO}_3$; $M = \text{H, Na, Li, } \dots$

Figure 7. Redox reactions of a conjugated polymer showing self-doping during the oxidation reactions [62].

Moreover, attachment of ionizable functional groups which form negatively charged sites to polymer chain in self-doped conductive polymers is one of the most successful way to increase the solubility [35, 38, 63]. The increased solubility can be attributed to the hydrophilic interactions between the covalently attached ionized group and polar water molecules. In water, the steric and ionic repulsive interactions overcome the interchain interactions and allow for the rapid solvation of polymer backbone [35].

Solubility limitation of undoped and acid-doped PANI in common solvents stimulated development of various approaches to improve solubility [38] such as attachment of substituents (alkyl, alkoxy, aryl hydroxyl, amino or halogen groups) to PANI backbone. However, this modification results in lower conductivity and lower molecular weight due to steric effects [35]. In 1990, Epstein and co-workers [64-66] reported successful synthesis of sulfonated polyaniline (SPANI), the first water-soluble self-doped conductive PANI derivative.

1.4.2. Self-Doped Sulfonated Polyaniline with Extended pH-Dependent Conductivity

a. Self-Doped Sulfonated Polyaniline

Self-doped SPANI was synthesized by introduction of an acid group on the EB-PANI polymer chain via sulfonation reaction with fuming sulphuric acid [64, 65]. In sulfonation process a hydrogen atom of the phenyl ring is substituted by a sulfonic acid group ($-\text{SO}_3\text{H}$). Benzenesulfonic acid is a strong acid and can protonate the imine nitrogen atoms in a similar manner to the protonation of EB-PANI by HCl (**Figure 8**). In addition, approximately half of the aromatic rings contain negatively charged sulfonate groups (sulfonation degree of 50% [67]) which act as inner dopant anions that sufficiently compensate all positive charges at protonated nitrogen atoms on the polymer backbone thus replacing auxiliary solution dopant

molecules [65].

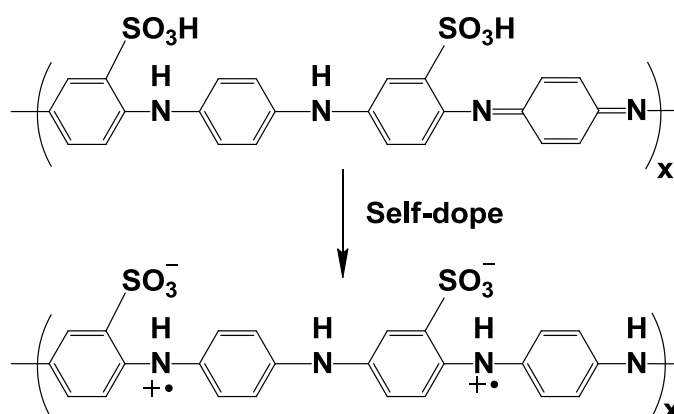


Figure 8. Self-doping of SPANI [65].

The positive charge carriers are much more localized at the nitrogen atoms of SPANI than in the case of hydrochloride-doped EB-PANI [65]. This is attributed to the strong electrostatic interaction between SO_3^- groups (with strong electron-withdrawing property) and cationic radical nitrogen atoms or hydrogen bonding to form five- or six-member rings, which are in an energetically favorable configuration [65, 67] as shown in **Figure 9**. The interaction between SO_3^- groups and cation radical nitrogen atoms or amine hydrogens may take place in intrachain (**Figure 9 - top row**) or between two adjacent chains, which is called interchain (**Figure 9 - bottom row**) [65].

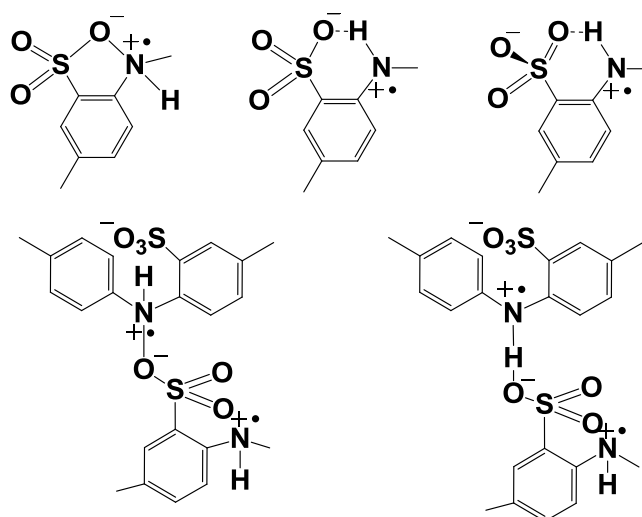


Figure 9. Intrachain (top row) and interchain (bottom row) interactions in SPANI [65].

b. Solubility of SPANI

In contrast to the parent PANI, self-doped SPANI is soluble in diluted aqueous base such as NaOH resulting in dedoped (insulating) salt form - sodium salt SPAN-Na. The water soluble

sodium salt of the SPANI can be reversibly converted back to the self-doped conducting form by treatment with aqueous acid [65, 68]. Nevertheless, SPANI is only very slightly soluble in water and stable SPANI aqueous solution can be obtained by further treatment of sodium salt SPAN-Na [69]. SPAN-Na in NaOH solution undergoes dialysis with a semipermeable membrane to remove excess NaOH. Then Na^+ is converted to H^+ with H^+ -type ion-exchange resin to give SPANI aqueous solution which is claimed to be stable for more than one year and can be cast into free-standing films with a room temperature conductivity of $10^{-2} \text{ S.cm}^{-1}$. In addition, this approach ensures that the SPANI has no external acid doping [69].

c. Conductivity and Sulfonation Degree

The SPANI with sulfonation degree of 50% (SPANI 50%) exhibited a lower conductivity ($\sim 0.1 \text{ S.cm}^{-1}$) in comparison to externally doped PANI (typically $1\text{--}10 \text{ S.cm}^{-1}$). It can be explained by steric effects of sulfonic acid substituents associated with the presence of a bulky substituent on the phenyl ring [70]. Substituent groups induce additional ring twisting along the polymer backbone due to the increased steric interactions and lower the crystallographic order of the polymer chains [65, 70]. The induced ring twisting increases the energy barrier for charge transport and reduces the extent of polaron delocalization along the polymer chain [69]. Moreover, conductivity of SPANI has much stronger temperature dependence than that of emeraldine hydrochloride, indicating greater electron localization in SPANI [65].

The conductivity of SPANI also depends on the degree of sulfonation, the position and nature of the substituent [70]. Fully sulfonated SPANI (with 100% sulfonation) has room temperature conductivity of 0.02 S.cm^{-1} [71], which is lower than SPANI 50% ($\sim 0.1 \text{ S.cm}^{-1}$) [65] and leucoemeraldine base SPANI (LEB-SPANI) with a degree of sulfonation 75% ($\sim 1 \text{ S.cm}^{-1}$) [72]. It is attributed to the larger twist of the phenyl rings relative to one another and increased interchain separation both due to the introduction of methoxy side groups and the higher density of SO_3^- groups [71].

d. pH-Dependent Conductivity of SPANI

Unlike the parent PANI the conductivity of SPANI is independent of external protonation over a broad pH range [64-66, 72, 73] as shown in **Figure 10**. SPANI 50% shows conductivity independent of external protonation in the pH range 1-7. It can be attributed to the electrostatic interactions which prevent the diffusion of protons away from the negatively charged polymer chain. The high local concentration of protons in the vicinity of the polymer

backbone is responsible for the retention of doping at neutral pH [64, 65]. LEB-SPANI with a degree of sulfonation 75% [72] shows the same conductivity over the entire pH range of 1-12. This is likely due to the enhancement of the doping strength of protons from sulfonic acid groups on the imine nitrogen atoms by the formation of “-C₂NHOS-” six-member-ring complexes. As a result, the doped imines are more difficult to dedope. Even after exchange of protons with cations, the six-member-ring conformation still exists and thus these imines may be doped by weaker metal cation Lewis acids. Therefore, even samples treated with alkaline aqueous solutions are still highly conducting [72].

Reported works on the conductivity of PANI and its derivatives with respect to pH have shown that pH-dependent conductivity of PANI can be tuned by sulfonation at different degrees/percentages. Undoped imine nitrogen atoms and the associated quinoid groups are expected to behave as barriers for electron conduction along a chain as well as between chains [65]. Hence if the imine nitrogen atoms of SPANI are not fully doped, the conductivity will depend on pH in the range of 0-7.5 [65]. For CO₂ sensing, the target polymer should demonstrate a conductivity change in the range of pH4–pH7. Therefore, the self-doped PANI such as SPANI and its derivatives could have potential use in CO₂ sensing because it has an extended pH range of electrical conductivity and a wide range of solubility.

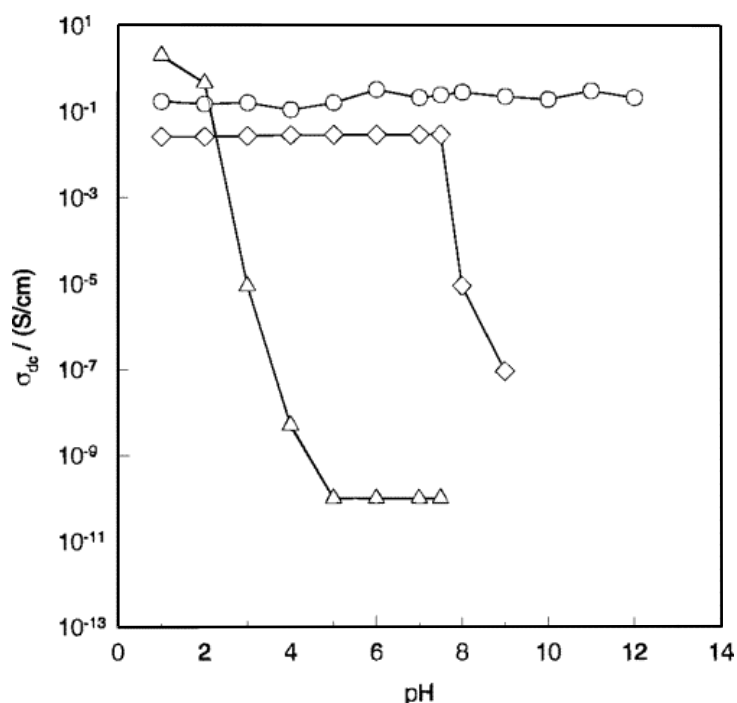


Figure 10. pH-dependent conductivity of conductive polymers, PANI doped by HCl (Δ), SPANI 50% (◇), LEB-SPANI 75% (○) [72].

1.5. Outline of This Thesis

The development of a CO₂ sensor based on conductive polymers working at room temperature with good selectivity and sensitivity is still a big challenge. To get a good selectivity and sensitivity, it requires strong chemical interaction between the polymer and CO₂. However, it also requires weak chemical interaction for fast reversibility. Moreover, in greenhouses the humidity is maintained at a high level between 70-90% RH. Exposure to high humidity and different analytes in greenhouse environment for a long time normally leads to rapid deterioration of the polymers. Therefore, the motivation of this research is to develop a CO₂ gas sensor modules based on conductive polymers/composites with high selectivity and sensitivity. The CO₂ sensor modules are aimed to be integrated in a low power wireless sensor network in greenhouses. CO₂ detection principle is measured by specific change in conductivity of polymer/composite films (chemiresistor).

First, PANI, SPAN-Na and its blends with PVA were explored for sensing CO₂ at room temperature in *Chapter 2*. Aqueous pH buffers were used to study pH-dependent conductivity of SPAN-Na to identify a good candidate polymer for CO₂ sensing. In addition, frequency-dependent ac measurements were carried out to detect changes in impedance of the polymer, drop casted on interdigitated electrodes, when exposed to CO₂ gas.

Second, CO₂ sensors in greenhouse work under high humidity 75-90% RH. Water vapor is needed for CO₂ indirect sensing to create carbonic acid to protonate the conductive polymers. Hence, humidity is also a main analyte which can interfere with the CO₂ response. Water vapor may induce similar response as CO₂ or improve the CO₂ response, conductivity strongly depends on RH. Therefore, the effect of humidity on intrinsic conductivity of PANI, SPANI and ionic conductivity of SPAN-Na and their composites was investigated by impedance spectroscopy in *Chapter 3*. These results could be used to compensate for the contribution of humidity in CO₂ measurement, by building a calibration curve for CO₂ sensor. Besides, doping mechanism of humidity sensing was also explored.

Third, in an effort to detect CO₂ at low concentrations, branched polyethyleneimine (PEI)-based chemiresistors were investigated in *Chapter 4*. The formation of carbamates and bicarbonates at amine sites of PEI chain in the presence of CO₂ and carbonic acid (from CO₂ and water vapour) can induce variation in conductivity of PEI films. This is the first report on PEI-based chemiresistor used for low-power CO₂ sensing.

In addition, mixing PEI with polyelectrolytes has been found to enhance CO₂

adsorption/desorption hence can improve CO₂ sensing characteristics. Therefore, blends of PEI and other polyelectrolytes containing sodium sulfonate groups including SPAN-Na, poly(sodium 4-styrenesulfonate) and Nafion sodium sulfonate were explored for CO₂ sensing at low concentrations (below 3,000 ppm) in *Chapter 5*.

Finally, the major achievements of this research are summarized and discussed in *Chapter 6*. In addition, discussions on different aspects of CO₂ sensing based on conductive polymers and organic polymers are presented. Furthermore, some perspectives and further researches are suggested to develop CO₂ sensors for use in greenhouses.

References

- [1] J.D. Cure, B. Acock, Crop responses to carbon dioxide doubling: a literature survey, *Agr. Forest. Meteorol.*, 38 (1986) 127-145.
- [2] B.A. Kimball, S.B. Idso, Increasing atmospheric CO₂: effects on crop yield, water use and climate, *Agricultural Water Management*, 7 (1983) 55-72.
- [3] J.S. Amthor, Effects of atmospheric CO₂ concentration on wheat yield: review of results from experiments using various approaches to control CO₂ concentration, *Field Crop. Res.*, 73 (2001) 1-34.
- [4] T. Ahonen, R. Virrankoski, M. Elmusrati, *Ieee*, Greenhouse Monitoring with Wireless Sensor Network, in: *Proceedings of 2008 IEEE/ASME International Conference on Mechatronic and Embedded Systems and Applications*, IEEE, New York, 2008, pp. 403-408.
- [5] K. Ogura, H. Shiigi, A CO₂ sensing composite film consisting of base-type polyaniline and poly(vinyl alcohol), *Electrochem. Solid St.*, 2 (1999) 478-480.
- [6] D. James, S.M. Scott, Z. Ali, W.T. O'Hare, Chemical sensors for electronic nose systems, *Microchimica Acta*, 149 (2005) 1-17.
- [7] H. E.C.M, CO, CO₂, CH₄ and H₂O sensing by polymer covered interdigitated electrode structures, *Sensors and Actuators*, 5 (1984) 181-186.
- [8] B. Adhikari, S. Majumdar, Polymers in sensor applications, *Prog. Polym. Sci.*, 29 (2004) 699-766.
- [9] H. Bai, G.Q. Shi, Gas sensors based on conducting polymers, *Sensors*, 7 (2007) 267-307.
- [10] M.S. Nieuwenhuizen, A.J. Nederlof, A SAW gas sensor for carbon dioxide and water. Preliminary experiments, *Sensors and Actuators B: Chemical*, 2 (1990) 97-101.

- [11] R. Zhou, D. Schmeisser, W. Göpel, Mass sensitive detection of carbon dioxide by amino group-functionalized polymers, *Sensors and Actuators, B: Chemical*, 33 (1996) 188-193.
- [12] B. Sun, G. Xie, Y. Jiang, X. Li, Comparative CO₂-Sensing Characteristic Studies of PEI and PEI/Starch Thin Film Sensors, *Energy Procedia*, 12 (2011) 726-732.
- [13] Q.Y. Cai, A. Cammers-Goodwin, C.A. Grimes, A wireless, remote query magnetoelastic CO sensor, *J. Environ. Monit.*, 2 (2000) 556-560.
- [14] P. Arquint, A. van den Berg, B.H. van der Schoot, N.F. de Rooij, H. Bühler, W.E. Morf, L.F.J. Dürselen, Integrated blood-gas sensor for pO₂, pCO₂ and pH, *Sensors and Actuators B: Chemical*, 13 (1993) 340-344.
- [15] R. Zhou, S. Vaihinger, K.E. Geckeler, W. Göpel, Reliable CO₂ sensors with silicon-based polymers on quartz microbalance transducers, *Sensors and Actuators B: Chemical*, 19 (1994) 415-420.
- [16] S. Patel, S. Hobson, S. Cemalovic, T. Mlsna, Materials for capacitive carbon dioxide microsensors capable of operating at ambient temperatures, *J. Sol-Gel Sci. Technol.*, 53 (2010) 673-679.
- [17] H.-E. Endres, R. Hartinger, M. Schwaiger, G. Gmelch, M. Roth, A capacitive CO₂ sensor system with suppression of the humidity interference, *Sensors and Actuators B: Chemical*, 57 (1999) 83-87.
- [18] S. Stegmeier, M. Fleischer, A. Tawil, P. Hauptmann, K. Egly, K. Rose, Mechanism of the interaction of CO₂ and humidity with primary amino group systems for room temperature CO₂ sensors, *Procedia Chemistry*, 1 (2009) 236-239.
- [19] S. Stegmeier, M. Fleischer, A. Tawil, P. Hauptmann, H.E. Endres, Detection of CO₂ with (Hetero-) Polysiloxanes sensing layers by the change of work function at room temperature, *Procedia Chemistry*, 1 (2009) 646-649.
- [20] S. Stegmeier, M. Fleischer, A. Tawil, P. Hauptmann, Stepwise improvement of (hetero-) polysiloxane sensing layers for CO₂ detection operated at room temperature by modification of the polymeric network, *Sensors and Actuators B: Chemical*, 148 (2010) 450-458.
- [21] S. Stegmeier, M. Fleischer, A. Tawil, P. Hauptmann, H.E. Endres, Sensing of CO₂ at room temperature using work function readout of (hetero-)polysiloxanes sensing layers, *Sensors and Actuators B: Chemical*, 154 (2011) 206-212.
- [22] B. Serban, A.K.S. Kumar, M. Brezeanu, C. Cobianu, O. Buiu, C. Bostan, N. Varachiu, S. Costea, Amino groups-based polymers for CO₂ detection; A comparison between two sensing mechanism models, in, 2011, pp. 127-130.

- [23] R.G. Pearson, Hard and Soft Acids and Bases, *J. Am. Chem. Soc.*, 85 (1963) 3533-3539.
- [24] Y.G. Ko, S.S. Shin, U.S. Choi, Primary, secondary, and tertiary amines for CO₂ capture: Designing for mesoporous CO₂ adsorbents, *J. Colloid Interface Sci.*, 361 (2011) 594-602.
- [25] J.C. Hicks, J.H. Drese, D.J. Fauth, M.L. Gray, G. Qi, C.W. Jones, Designing Adsorbents for CO₂ Capture from Flue Gas-Hyperbranched Aminosilicas Capable of Capturing CO₂ Reversibly, *J. Am. Chem. Soc.*, 130 (2008) 2902-2903.
- [26] B. Li, B. Jiang, D.J. Fauth, M.L. Gray, H.W. Pennline, G.A. Richards, Innovative nano-layered solid sorbents for CO₂ capture, *Chem. Commun.*, 47 (2011) 1719-1721.
- [27] E.P. Dillon, C.A. Crouse, A.R. Barron, Synthesis, Characterization, and Carbon Dioxide Adsorption of Covalently Attached Polyethyleneimine-Functionalized Single-Wall Carbon Nanotubes, *ACS Nano*, 2 (2008) 156-164.
- [28] A. Sayari, Y. Belmabkhout, Stabilization of Amine-Containing CO₂ Adsorbents: Dramatic Effect of Water Vapor, *J. Am. Chem. Soc.*, 132 (2010) 6312-6314.
- [29] H. Matsuyama, A. Terada, T. Nakagawara, Y. Kitamura, M. Teramoto, Facilitated transport of CO₂ through polyethylenimine/poly(vinyl alcohol) blend membrane, *Journal of Membrane Science*, 163 (1999) 221-227.
- [30] T. Anderson, F. Ren, S. Pearton, B.S. Kang, H.-T. Wang, C.-Y. Chang, J. Lin, Advances in Hydrogen, Carbon Dioxide, and Hydrocarbon Gas Sensor Technology Using GaN and ZnO-Based Devices, *Sensors*, 9 (2009) 4669-4694.
- [31] A. Star, T.R. Han, V. Joshi, J.C.P. Gabriel, G. Grüner, Nanoelectronic Carbon Dioxide Sensors, *Adv. Mater.*, 16 (2004) 2049-2052.
- [32] S. Sivaramakrishnan, R. Rajamani, C.S. Smith, K.A. McGee, K.R. Mann, N. Yamashita, Carbon nanotube-coated surface acoustic wave sensor for carbon dioxide sensing, *Sensors and Actuators B: Chemical*, 132 (2008) 296-304.
- [33] P.L. Kebabian, A. Freedman, Fluoropolymer-based capacitive carbon dioxide sensor, *Meas. Sci. Technol.*, 17 (2006) 703.
- [34] A.G. MacDiarmid, Synthetic metals: a novel role for organic polymers, *Synth. Met.*, 125 (2001) 11-22.
- [35] M.S. Freund, B.A. Deore, Introduction, in: *Self-Doped Conducting Polymers*, John Wiley & Sons, Ltd, 2007, pp. 1-74.
- [36] J.H. Burroughes, D.D.C. Bradley, A.R. Brown, R.N. Marks, K. Mackay, R.H. Friend, P.L. Burns, A.B. Holmes, Light-emitting diodes based on conjugated polymers, *Nature*, 347 (1990) 539-541.

- [37] G. Inzelt, Redox Transformations and Transport Processes Conducting Polymers, in, Springer Berlin Heidelberg, 2012, pp. 191-244.
- [38] D. Nicolas-Debarnot, F. Poncin-Epaillard, Polyaniline as a new sensitive layer for gas sensors, *Anal. Chim. Acta*, 475 (2003) 1-15.
- [39] A.G. MacDiarmid, "Synthetic Metals": A Novel Role for Organic Polymers (Nobel Lecture), *Angew. Chem. Int. Ed.*, 40 (2001) 2581-2590.
- [40] A.G. Macdiarmid, J.C. Chiang, A.F. Richter, A.J. Epstein, Polyaniline: a new concept in conducting polymers, *Synth. Met.*, 18 (1987) 285-290.
- [41] J.Y. Shimano, A.G. MacDiarmid, Polyaniline, a dynamic block copolymer: key to attaining its intrinsic conductivity?, *Synth. Met.*, 123 (2001) 251-262.
- [42] J.-C. Chiang, A.G. MacDiarmid, 'Polyaniline': Protonic acid doping of the emeraldine form to the metallic regime, *Synth. Met.*, 13 (1986) 193-205.
- [43] W. Huang, B.D. Humphrey, A.G. MacDiarmid, Polyaniline, a novel conducting polymer. Morphology and chemistry of its oxidation and reduction in aqueous electrolytes, *J. Chem. Soc., Faraday Trans. 1*, 82 (1986) 2385-2400.
- [44] A.J. Epstein, J.M. Ginder, F. Zuo, R.W. Bigelow, H.S. Woo, D.B. Tanner, A.F. Richter, W.S. Huang, A.G. MacDiarmid, Insulator-to-metal transition in polyaniline, *Synth. Met.*, 18 (1987) 303-309.
- [45] A.G.M.a.A.J. Epstein, Polyanilines: A Novel Class of Conducting Polymers, *Faraday Discuss. Chem. Soc.*, (1989) 317 - 332.
- [46] M.E. Józefowicz, A.J. Epstein, X. Tang, Protonic acid doping of two classes of the emeraldine form of polyaniline, *Synth. Met.*, 46 (1992) 337-340.
- [47] A.G. Macdiarmid, A.J. Epstein, The concept of secondary doping as applied to polyaniline, *Synth. Met.*, 65 (1994) 103-116.
- [48] A.G. MacDiarmid, A.J. Epstein, Secondary doping in polyaniline, *Synth. Met.*, 69 (1995) 85-92.
- [49] U. Lange, N.V. Roznyatovskaya, V.M. Mirsky, Conducting polymers in chemical sensors and arrays, *Anal. Chim. Acta*, 614 (2008) 1-26.
- [50] C. Jouve, D. Jullien, B. Remaki, Conductive Polyethylene as Sensitive Layer for Gas-Detection, *Sens. Actuator B-Chem.*, 28 (1995) 75-80.
- [51] K. Suri, S. Annapoorni, A.K. Sarkar, R.P. Tandon, Gas and humidity sensors based on iron oxide-polypyrrole nanocomposites, *Sensors and Actuators, B: Chemical*, 81 (2002) 277-282.

- [52] S.A. Waghuley, S.M. Yenorkar, S.S. Yawale, S.P. Yawale, Application of chemically synthesized conducting polymer-polypyrrole as a carbon dioxide gas sensor, *Sensors and Actuators B: Chemical*, 128 (2008) 366-373.
- [53] S. Takeda, A new type of CO₂ sensor built up with plasma polymerized polyaniline thin film, *Thin Solid Films*, 343-344 (1999) 313-316.
- [54] M. Irimia-Vladu, J.W. Fergus, Suitability of emeraldine base polyaniline-PVA composite film for carbon dioxide sensing, *Synth. Met.*, 156 (2006) 1401-1407.
- [55] T. Oho, T. Tonosaki, K. Isomura, K. Ogura, A CO₂ sensor operating under high humidity, *J. Electroanal. Chem.*, 522 (2002) 173-178.
- [56] K. Ogura, A CO₂ sensor with polymer composites operating at ordinary temperature, *J. Electrochem. Soc.*, 147 (2000) 4351-4355.
- [57] T. Tonosaki, T. Oho, H. Shiigi, K. Isomura, K. Ogura, Highly Sensitive CO₂ Sensor with Polymer Composites operating at room temperature, *Anal. Sci.*, Vol. 17 Supplement (2001) i249.
- [58] M. Irimia-Vladu, J.W. Fergus, Impedance spectroscopy of thin films of emeraldine base polyaniline and its implications for chemical sensing, *Synth. Met.*, 156 (2006) 1396-1400.
- [59] S. Neethirajan, M.S. Freund, D.S. Jayas, C. Shafai, D.J. Thomson, N.D.G. White, Development of carbon dioxide (CO₂) sensor for grain quality monitoring, *Biosyst. Eng.*, 106 (2010) 395-404.
- [60] H. Shiigi, T. Oho, T. Tonosaki, K. Ogura, CO₂-sensitive characteristics of base-type polyaniline poly(vinyl alcohol) composites at room temperature and effects of coexisting gases, *Electrochemistry*, 69 (2001) 997-1001.
- [61] A.O. Patil, Y. Ikenoue, F. Wudl, A.J. Heeger, Water soluble conducting polymers, *J. Am. Chem. Soc.*, 109 (1987) 1858-1859.
- [62] A.O. Patil, Y. Ikenoue, N. Basescu, N. Colaneri, J. Chen, F. Wudl, A.J. Heeger, Self-doped conducting polymers, *Synth. Met.*, 20 (1987) 151-159.
- [63] D.F.A. Maria C. Miras, Natalia Monge, Evelina Frontera, Claudia R. Rivarola and Cesar A. Barbero, Organic Chemistry of Polyanilines: Tailoring Properties to Technological Applications, *The Open Macromolecules Journal*, (2008) 58-73.
- [64] J. Yue, A.J. Epstein, Synthesis of self-doped conducting polyaniline, *J. Am. Chem. Soc.*, 112 (1990) 2800-2801.
- [65] J. Yue, Z.H. Wang, K.R. Cromack, A.J. Epstein, A.G. MacDiarmid, Effect of sulfonic acid group on polyaniline backbone, *J. Am. Chem. Soc.*, 113 (1991) 2665-2671.

- [66] J. Yue, G. Gordon, A.J. Epstein, Comparison of different synthetic routes for sulphonation of polyaniline, *Polymer*, 33 (1992) 4410-4418.
- [67] J. Yue, A.J. Epstein, XPS study of self-doped conducting polyaniline and parent systems, *Macromolecules*, 24 (1991) 4441-4445.
- [68] J. Yue, A.J. Epstein, A.G. Macdiarmid, Sulfonic Acid Ring-Substituted Polyaniline, A Self-Doped Conducting Polymer, *Molecular Crystals and Liquid Crystals Incorporating Nonlinear Optics*, 189 (1990) 255-261.
- [69] S.-A. Chen, G.-W. Hwang, Structure Characterization of Self-Acid-Doped Sulfonic Acid Ring-Substituted Polyaniline in Its Aqueous Solutions and as Solid Film, *Macromolecules*, 29 (1996) 3950-3955.
- [70] M.S. Freund, B.A. Deore, Self-Doped Derivatives of Polyaniline, in: *Self-Doped Conducting Polymers*, John Wiley & Sons, Ltd, 2007, pp. 75-155.
- [71] W. Lee, G. Du, S.M. Long, A.J. Epstein, S. Shimizu, T. Saitoh, M. Uzawa, Charge transport properties of fully-sulfonated polyaniline, *Synth. Met.*, 84 (1997) 807-808.
- [72] X.-L. Wei, Y.Z. Wang, S.M. Long, C. Bobeczko, A.J. Epstein, Synthesis and Physical Properties of Highly Sulfonated Polyaniline, *J. Am. Chem. Soc.*, 118 (1996) 2545-2555.
- [73] X.H. Wang, J. Li, L.X. Wang, X.B. Jing, F.S. Wang, Structure and properties of self-doped polyaniline, *Synth. Met.*, 69 (1995) 147-148.

Chapter 2. Carbon Dioxide Sensing with Sulfonated Polyaniline

Abstract

The use of polyaniline and especially sulfonated polyaniline (SPANI) is explored for sensing carbon dioxide (CO_2) at room temperature. Frequency-dependent ac measurements were carried out to detect changes in impedance of the polymer, drop casted on interdigitated electrodes, when exposed to CO_2 gas. Aqueous pH buffers were first used to study pH-dependent conductivity to identify a good candidate polymer for CO_2 sensing. Emeraldine base polyaniline exhibits only a significant conductivity change below pH 4 whereas SPANI shows also a conductivity change between pH 4 and pH 7. This makes SPANI more suitable for CO_2 sensing than emeraldine base polyaniline. The impedance of SPANI films is found to decrease when exposed to CO_2 concentrations above 20,000 ppm. Blending SPANI with poly(vinyl alcohol) further increases the sensitivity for CO_2 .

This chapter is published as:

“Carbon Dioxide Sensing with Sulfonated Polyaniline”, Tin C. D. Doan, Rajesh Ramaneti, Jacob Baggerman, J. Franc van der Bent, Antonius T. M. Marcelis, Hien D. Tong, and Cees J. M. van Rijn, *Sensors and Actuators B: Chemical* 168 (2012) 123–130.

1. Introduction

Detection and monitoring of carbon dioxide (CO₂) is important in various applications [1]. For example, the CO₂ level in greenhouses significantly influences plant growth and consequently productivity [2–5]. For optimal plant growth continuous reliable monitoring and regulation of the CO₂ level is required. The application of wireless sensor networks enables to monitor and control homogeneous CO₂ concentrations over large surface areas. This ensures uniform growth conditions in large greenhouses for precision agriculture [5–9]. Wireless sensor networks today require low power, typically 20–50 μ W [8]. Commonly used non-dispersive-infra-red (NDIR) CO₂ sensors and solid state electrochemistry-based CO₂ have high power consumption (>50 mW) [10, 11] and are unsuitable for use in low power nodes.

For the development of low-power gas sensors several approaches have been explored, for example, nanowire-based sensors [12–14], field-effect transistors [15, 16] and conductive polymer resistors [17, 18]. Conductive polymers are associated with low cost and room temperature operation [19, 20]. Change in conductivity of the undoped polymer may occur through interaction with specific target gas species, inducing doping with a corresponding change of the electronic band structure [21]. This process of doping occurs at sites along the polymer chain where positively charged species (holes/protons) are added or removed from the material [22]. The interaction of gases with conducting polymers is based on either chemical reactivity or physical adsorption of the target gas [17]. For example, reduction of polypyrrole, an n-type conducting polymer, with hydrogen shows an increase in resistance [23]. Otherwise, acid–base reactions can change the doping of p-type conductive polymers, e.g., HCl vapor decreases the resistivity of the polyaniline (PANI) [24]. “Indirect” detection of CO₂ is made possible by formation of carbonic acid in water as with potentiometers using Severinghaus electrodes [25, 26] and in pH-sensitive hydrogel-based sensing [27]. Ogura and co-workers described a CO₂ gas sensor based on the doping level of emeraldine base polyaniline (EB-PANI) [28–31]. By applying a mixture of EB-PANI and poly(vinyl alcohol) (PVA) onto interdigitated electrodes, an increase in conductivity over two orders of magnitude with increasing CO₂ concentrations was reported. It was proposed that in a humid environment, CO₂ forms carbonic acid followed by dissociation into H⁺ and HCO₃[−] and that protonation occurs on the imine sites along the polymer chain of EB-PANI due to interaction of H⁺ ions. Consequently, the material changes from an insulating base to a conducting salt.

Irimia-Vladu and Fergus [32, 33] could not reproduce the work of Ogura and co-workers. At 5% CO₂ and a various relative humidities (RH) only a small change in impedance was reported. It was concluded that the proposed protonation by carbonic acid is inconsistent with studies on the pH dependence of the doping level of EB-PANI [34–37]. They inferred that EB-PANI shows only significant doping below pH 4, while the intended CO₂ detection range of 50–50,000 ppm corresponds to a pH range between 6.0 and 4.5 in water [32]. This indicates that EB-PANI is an unsuitable material for detection of CO₂ due to insufficient protonation above pH 4.

The pH doping range of PANI can be tuned to a higher pH by means of adding self-doping functional groups to the polymer backbone, in particular negatively charged sulfonic acid groups acting as inner dopant anions [38, 39]. Sulfonation of PANI with fuming sulfuric acid gives a polymer with about 50% phenyl groups in the backbone being substituted with sulfonic acid groups (–SO₃H). Sulfonated polyaniline (SPANI) or its sodium salt (SPAN-Na) (see **Figure 1**) is reported to have a protonation range extending up to pH 7 [40–42]. Alternatively, the attachment of other functional groups such as boronic acid [43, 44] and carboxylic acid [45, 46] on the PANI chain can also extend the pH sensing regime in a similar way and make them suitable for “indirect” sensing of CO₂.

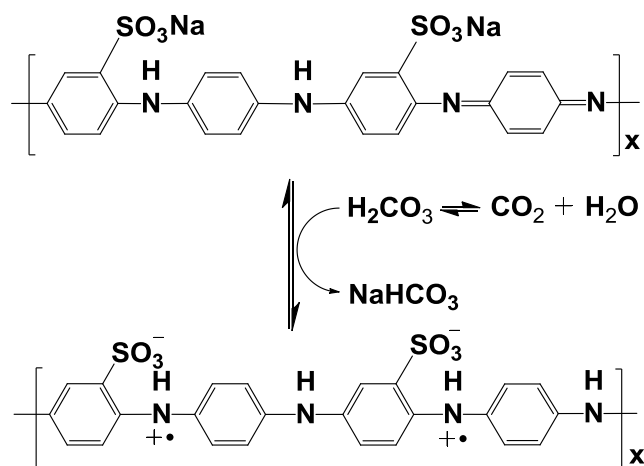


Figure 1. Reversible change from an insulating sulfonated polyaniline SPAN-Na (undoped) to conducting SPANI (self-doped) due to interaction with carbonic acid and subsequent protonation.

In this Chapter an investigation towards the suitability of PANI and the SPAN-Na for sensing CO₂ is described. Electronic transport measurements were carried out using impedance spectroscopy and dc measurements to determine the conductivity (impedance) of PANI and SPAN-Na films drop casted onto interdigitated electrodes [47]. The pH dependence of the conductivity of PANI and SPAN-Na as thin films in polyacrylamide (PAA) gels is described.

The response to CO₂ of PANI and SPAN-Na and the influence of adding PVA to the polymer film on the sensing characteristics are studied. The results show that whereas CO₂ sensing with PANI is not possible, SPAN-Na is a much better candidate material for CO₂ sensing.

2. Materials and methods

2.1. Materials

EB-PANI (Mw 20,000), PVA (Mw 89,000–98,000), fuming sulfuric acid (30% SO₃), ion-exchange resin (Amberlite IR 120 hydrogen form), N,N'-methylene bis-acrylamide, acrylamide, ammonium persulfate, N, N, N', N'-tetramethyl ethylene diamine and pH buffer solutions were purchased from Sigma–Aldrich. Dimethyl sulfoxide (DMSO; 99.9%) was obtained from Acros. CO₂ (99.99%) and N₂ (99.999%) were purchased from Linde Gas Benelux.

2.2. Spectroscopy

XPS analysis was performed using a JPS-9200 Photoelectron Spectrometer (JEOL, Japan). High-resolution spectra were obtained at a take-off angle of 80° under UHV conditions using monochromatic Al K_α X-ray radiation at 12 kV and 25 mA, using analyzer pass energy of 20 eV. A Bruker Tensor 27 was used for Fourier transformed infrared spectroscopy (FTIR) of powdered samples of EB-PANI and SPAN-Na in the transmittance mode. A Cary 100 Scan was used to obtain UV–vis absorption spectra of polymer solutions.

2.3. Polymer Solutions and Sensor Preparation

Emeraldine base polyaniline: EB-PANI was washed with 0.1 M NH₄OH for four times, each time for a duration of 30 minutes, followed by filtration and washing with several portions of deionized water and a final drying step at 50 °C for 24 hours in vacuum. Stock solutions were prepared by dissolving 25 mg EB-PANI in 5 ml DMSO to obtain a solution with a concentration of 0.5% (w/w) PANI in DMSO.

Composite EB-PANI:PVA: For the composite with PVA, 25 mg of PVA was dissolved in 5 ml of DMSO (0.5%, w/w) at 90 °C. This stock solution was mixed with EB-PANI in DMSO stock solution in different volumetric ratios of (EB-PANI:PVA) to produce polymer composite mixtures in ratios of 1:1, 1:2.

Sulfonated polyaniline (SPANI) and its sodium salt (SPAN-Na): For the preparation of SPANI the procedure described by Yue and Epstein et al. was followed [40, 41]. The SPANI cake

was then converted to SPAN-Na via a method described by Chen [48]. The sodium salt was prepared by dissolving 0.5 g of SPANI in 20 mL of 0.1 M NaOH. The SPAN-Na aqueous solution was purified to remove excess NaOH by dialysis with a semipermeable membrane (Membra-cel Dialysis Tubing, molecular weight cutoff 3500, Serva) in deionized water, which was refreshed 3 times per day during 4 days. The water was removed in vacuum and the product was further dried in a vacuum oven at 60 °C for 24 hours. 1%, w/w SPAN-Na stock solutions in DMSO were prepared by dissolving 50 mg SPAN-Na in 5 ml DMSO.

The SPAN-Na in the aqueous solution was converted back to SPANI by exchanging Na^+ for H^+ using an H^+ -type ion-exchange resin to give a stable green-colored SPANI solution in water. This approach ensured that the SPANI had no external acid doping [48].

Composite SPAN-Na:PVA: The composite SPAN-Na:PVA was prepared in a similar way to the EB-PANI:PVA composite. Stock solutions of SPAN-Na were prepared by dissolving 50 mg of SPAN-Na in 5 ml of DMSO (1%, w/w) at room temperature, while stock solutions of PVA were prepared by dissolving 150 mg of PVA in 5 ml of DMSO (3%, w/w) at 90 °C. Samples were extracted from the two stock solutions and mixed to obtain composite mixtures with different ratios of SPAN-Na:PVA.

SPAN-Na/polyacrylamide (PAA) cross-linked hydrogel: Since SPAN-Na dissolves easily in aqueous solutions, testing the pH range of SPAN-Na using salt pH buffer solutions can be quite challenging. An approach is to use a hydrogel which is not pH sensitive while the SPAN-Na does not undergo dissolution when exposed to pH buffers. A mixture of SPAN-Na trapped in PAA was prepared following the procedure described by Tao et al. [49]. Briefly, 0.1 g (0.63 mmol) *N,N'*-methylene bis-acrylamide (BAA), 4.5 g (63 mmol) acrylamide (AA) (molar ratio of BAA to AA 1:100), 0.1 g SPAN-Na, 24 mg (0.1 mmol) ammonium persulfate and 12 mg (0.1 mmol) *N, N, N', N'*-tetramethyl ethylene diamine was dissolved in 50 ml of water and stirred for 3 hours. This composition was chosen because the equilibrium swelling degree (defined by the ratio of the mass of the gel sample swollen in aqueous solution to mass of the dry gel) is minimal in the pH 1–8 range [49]. Pure PAA hydrogel (without adding SPAN-Na) was prepared in the similar way followed by spin coating on top of the EB-PAN film for testing the pH response of EB-PAN. In this study, EB-PAN (PAA) was chosen as a reference for comparison with SPAN-Na:PAA. To rule out the contribution of ionic conductivity from PAA gels, I–V measurements were carried out to verify that there is negligible conductivity in pure PAA.

1 μL of the polymer solution was drop casted onto a silicon chip having Pt interdigitated electrodes (thickness ~ 170 nm) of dimensions $300\text{ }\mu\text{m}$ (length) \times $9\text{ }\mu\text{m}$ (width) and $6\text{ }\mu\text{m}$ spacing. The drop-casted polymer was dried at $60\text{ }^{\circ}\text{C}$ for 24 hours in a vacuum oven. The thickness of the films was determined using a surface profiler Dektak 6 M (Veeco). The EB-PANI films had an average thickness of ~ 500 nm, while the SPAN-Na films had a thickness of 200 nm.

2.4. pH-Dependent Conductivity Measurements

The conductivity of the polymers as a function of pH was studied using impedance spectroscopy and dc measurements. The polymer coated chip was exposed to phosphate-based pH buffers. Reference impedance and dc measurements were made prior to the exposure. The pH buffer solutions (from pH 2 to 9) was dropped on the polymer composite film and kept in a closed box for 30 minutes. It was observed previously that the presence of salt on the surface of the chip without a polymer can also induce an impedance change. Therefore a filter paper was used to absorb the buffer solutions to reduce the influence of residual salt after drying. Impedance and dc measurements were carried out after every exposure to a pH buffer.

2.5. Gas Sensing Setup

A dedicated gas sensor characterization setup was used to carry out electrical measurements in controlled environments with the sample mounted on a probe holder placed inside a flow chamber (**Figure 2**).

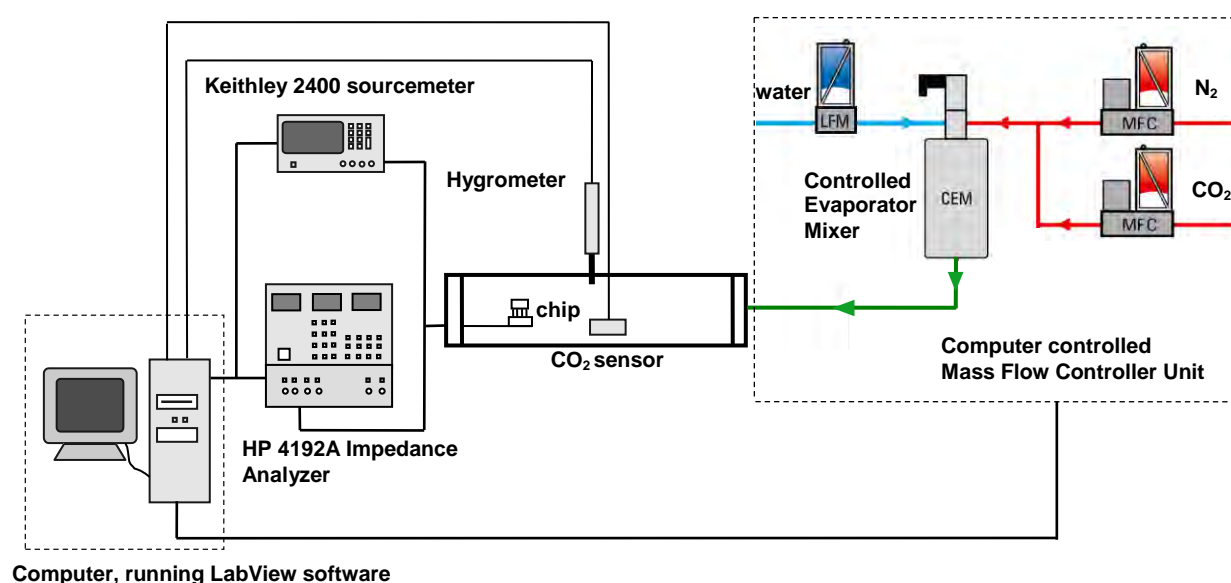


Figure 2. Schematic overview of the automated gas sensing measurement setup.

The air flow, humidity and CO₂ concentration inside the chamber were regulated with two mass flow controllers (MFC's), a liquid flow meter (LFM) and a controlled evaporator mixer (CEM) from Bronkhorst, The Netherlands. The pure CO₂ gas was mixed with water in the CEM to create a humidified CO₂ environment during the sensing experiments. The flow chamber was equipped with a PCMini52 hygrometer (Michell Instruments, The Netherlands) to measure the relative humidity, accuracy $\pm 2\%$ RH and temperature, accuracy ± 0.2 °C. A reference CO₂ sensor (K33, SenseAir, Sweden) based on the NDIR principle was used with an upper detection limit of 100,000 ppm.

Ac impedance spectroscopy was carried out using an HP 4192A LF impedance analyzer. Bias voltages in the range of 0.3–1.0 V were applied during the measurements. The impedance change was expressed in terms of Nyquist plots, imaginary impedance (Z'') is plotted vs. the real impedance (Z') derived from the measured absolute impedance ($|Z|$) and phase angle (θ) values, when the frequency is scanned from 5 Hz to 1 MHz. Fitting of the data was done with EIS spectrum analyzer software [51].

Two-point dc resistivity (conductivity) was measured with a Keithley 2400 source meter. The dc conductivity ($\sigma = 1/\rho$) was determined from two-point dc measurements using the relation resistivity (ρ) = $(V/I)/k$ meant for interdigitated/comb electrodes where k is the Zaretsky cell constant ($k = 0.215 \text{ cm}^{-1}$; see **Appendix 1** for details), which is related to the ratio of sample geometry (electrode spacing, width and the number of interdigitated fingers), V is voltage applied between the probes and I is the current measured [50]. The V/I values were determined from the linear slope of the I–V curves. All measurements were carried out in a dark enclosed chamber under low humidity (5% RH) to prevent cross-effects of light and humidity on the conductivity of the films.

The dc measurement experiments were applied for studying the pH dependence of conductivity. Different samples were used for each pH buffer to avoid cross contamination. The baseline resistivity of all the samples was checked for reproducibility prior to each pH measurement. Ac measurements were carried out for sensing experiments on a separate set of samples. Measurement of the time dependent changes in impedance of the polymers was done at two fixed frequencies: 140 kHz and 0.7 kHz. The 140 kHz (i.e. 100 kHz range) was chosen based on previously reported work and were used for comparison with literature [32] while we observed that a good signal to noise ratio can be obtained in the 1 kHz range (0.7 kHz). Hence two frequency ranges were studied.

3. Results and Discussion

3.1. pH Sensing Range of EB-PANI and Its Suitability for Sensing CO₂

Previous reports on the CO₂ sensing capability of EB-PANI are not consistent [32] and therefore the response of an EB-PANI film to different concentrations of CO₂ was first studied for verification. Films with and without PVA were studied, PVA was added to the polymer to increase the water retention capability. The films were exposed to CO₂ under constant relative humidity and an absolute impedance $|Z|$ was measured to observe possible change in $|Z|$. The impedance was measured at 140 kHz because on the Bode plot of $|Z|$ vs. frequency a maximum in $(\Delta Z/Z_0)$ was observed in the kHz range [47, 52]. In this frequency range, the nature of charge carrier transport is unaffected by polarization effects of oscillating currents (at high frequency) [53]. **Figure 3** shows the $|Z|$ response of a EB-PANI:PVA (1:1 ratio) film as a function of time under an applied positive voltage bias of 300 mV at 140 kHz at constant RH of 75%. CO₂ gas was introduced into the flow chamber in discrete steps ranging from 1% to 5% (indicated by the curves measured from the reference CO₂ sensor). No significant change (defined by $\Delta Z/Z_0$) was observed when CO₂ was introduced. The fluctuations in the impedance are around 50 Ω and comparable to the noise level of the baseline. This indicates that the EB-PANI films are not sensitive to CO₂ concentrations in the range of 1.5–5%. The results are consistent with the data reported by Irimia-Vladu and Fergus [32], who suggested that pH changes induced by CO₂ are insufficient for protonation of the EB-PANI films and therefore unable to change the bulk conductivity of the films.

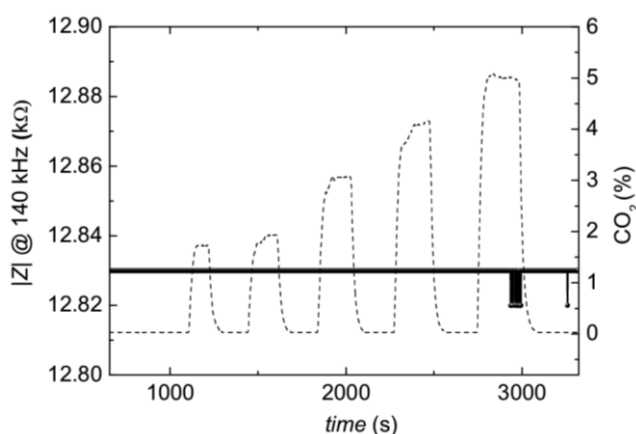


Figure 3. Absolute impedance response to CO₂ as a function of time of EB-PANI:PVA (1:1) at 140 kHz at 75% RH. The dashed line is the response from the reference CO₂ sensor.

The pH sensing range was determined for EB-PANI films by doping with pH buffers to validate the pH response of the films. The films were covered with a PAA hydrogel coating to

have a better comparison between EB-PANI and SPAN-Na (see below in **Figure 5**). pH buffer solutions were dropped on top of the gels and after 30 minutes removed by a filter paper. **Figure 4** shows the Nyquist plots of EB-PANI films after exposure to pH buffer solutions, ranging from pH 2 to 9. Above pH 6 the film impedance was high and no dependence of Z'' on Z' was observed. Below pH 6 semicircles were observed, which indicates a decrease in impedance.

Dc conductivity measurements on pure EB-PANI as a function of pH (**Figure 4**) showed a conductivity change of EB-PANI in the pH range from 1 to 4 and above pH 4 the conductivity remains nearly constant ($\sim 5 \times 10^{-9} \text{ S.cm}^{-1}$), consistent with earlier reports [54]. The decrease in impedance, i.e., increase in conductivity due to exposure to pH buffers is attributed to doping of the polymer by protonation of the imine sites [34]. Above pH 5 there is minimal protonation due to the low concentration of H^+ ions. At pH 5, partial doping could be assumed, while from pH 4 onwards the conductivity starts to increase. At pH 2, it could be assumed that the sample is completely doped and metal-like conductivity behavior is approached. The change in conductivity can be attributed to the formation of a bipolaron band (evidence from UV-vis spectra) due to the increased number of charge carriers [55]. Both the ac and dc measurements confirm that the response of the film on the sensor chip can be represented by an equivalent parallel electrical circuit consisting of a capacitive and resistive component of the polymer film. The conductivity of the polymer at high pH is mainly due to the capacitance part of the film, whereas at low pH the resistance of the polymer film dominates. The resultant pH dependent conductivity of EB-PANI films is in agreement with earlier findings [34–37] and confirms that doping of EB-PANI occurs outside the pH range (pH 5–7) that is necessary for CO_2 sensing.

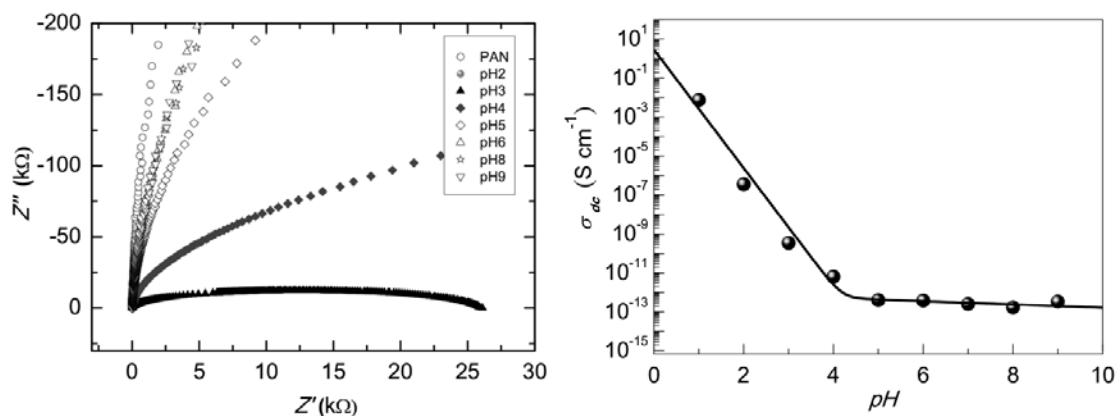


Figure 4. (Left) Nyquist plots of EB-PANI film upon exposure to pH buffers from pH 2 to pH 9. (Right) Dc conductivity of EB-PANI films as a function of pH.

3.2. pH Dependent Conductivity of Sulfonated Polyaniline Sodium Salt

It is known that self-doped derivatives of polyaniline are conductive in an extended pH-range [41]. For example, sulfonation with fuming sulfuric acid of EB-PANI results in attachment of sulfonic groups to the phenyl rings of the PANI chain (SPANI). The sulfonic acid groups cause self-doping of the polymer and a measurable conductivity change up to pH 7. This extended conductivity range might render it suitable for CO₂ sensing. Therefore, we explored SPANI in the deprotonated form (SPAN-Na).

SPANI was prepared by sulfonation of EB-PANI in fuming sulfuric acid. The chemical and structural characterization was carried out using Fourier transform infra-red (FTIR), UV-vis absorption, and X-ray photoelectron spectroscopy (XPS) (see **Appendix 1**). The FTIR spectrum is in good agreement with published literature values [40, 48]. The absorption maxima at 1066, 1015, 701, and 606 cm⁻¹ are consistent with the presence of sulfonate groups attached to the aromatic rings. The UV-vis spectrum of SPAN-Na in water shows an absorption band at 320 nm and two other absorption bands at 435 nm and 800 nm. The absorption at 320 nm is assigned to the π - π^* transition of the benzenoid rings. The other two absorption bands at 435 nm and 800 nm have been assigned to the optical absorption of the polaron band [40, 48].

The ratio between sulfur (S) and nitrogen (N) was about 50% (as obtained by XPS), which indicates that approximately one SO₃⁻ group is attached to every two phenyl rings [40, 41, 48]. The sulfonation occurs relatively rapidly and 50% sulfonation was obtained within 30 minutes. Extending the reaction time to 2 hours gave no higher substitution degree. This is consistent with earlier reports from Yue et al. [56]. The deprotonated form was obtained by dissolving the SPANI in sodium hydroxide 0.1 M and subsequently removing the excess salt by dialysis.

Experiments to determine the pH dependence of the conductivity of SPAN-Na coated chips were performed in a similar way as the EB-PANI coated chips. To prevent dissolution of SPAN-Na in water, SPAN-Na was trapped in PAA-cross-linked hydrogels for the experiments with pH buffers. It was shown that a pure PAA gel does not physically swell up in a wide range of pH solutions, while PAA gel with SPANI showed a swelling response above pH 8 [49]. Control experiments using pure PAA hydrogel without SPAN-Na did not show any change of conductivity when exposed to buffers with high and low pH (see **Figure**

A5 in Appendix 1). This rules out the possibility that the observed conductivity change is due to increased ionic conductivity of the hydrogel itself.

The SPAN-Na:PAA hydrogel coated chips were exposed to various pH buffer solutions (pH 1–9) to validate the pH response of the SPAN-Na films. pH buffer solutions were dropped on top of the gels and after 30 minutes removed by a filter paper. The dc resistance of SPAN-Na:PAA gels was determined from I–V sweep curves of the gel-coated chips with voltage range from –5 V to +10 V at a RH below 5%. The conductivity (σ) of SPAN-Na:PAA was calculated from two-point probe dc measurement in the same way as for EB-PANI:PAA films. The pH-dependent conductivity obtained for SPAN-Na:PAA gels is depicted in **Figure 5**. The higher conductivity of SPAN-Na compared to EB-PANI at pH 4–7 could be attributed to the self-doping mechanism characteristics of the sulfonated groups and is in agreement with findings from literature [41]. The observed conductivity change in the pH range between pH 4 and 7 might make the material a good candidate for sensing CO₂ in the range between 500 and 50,000 ppm.

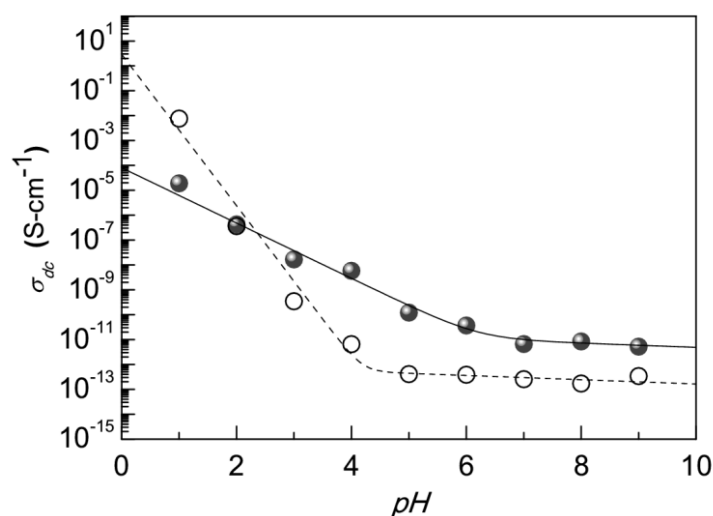


Figure 5. Relationship between conductivity of the SPAN-Na:PAA hydrogel and pH (closed circles). For comparison, EB-PANI:PAA is shown (open circles).

3.3. Influence of Humidity on CO₂ Sensing with Sulfonated Polyaniline Sodium Salt

Humidity is an important factor to be considered during the development of a CO₂ sensor. An influence of humidity on the sensitivity and selectivity for the gas to be sensed cannot be ruled out. Hence, we first investigated the effect of humidity on the impedance of SPAN-Na films and composite films of SPAN-Na with addition of PVA (1:1 ratio) to reduce the humidity dependence (**Figure 6**).

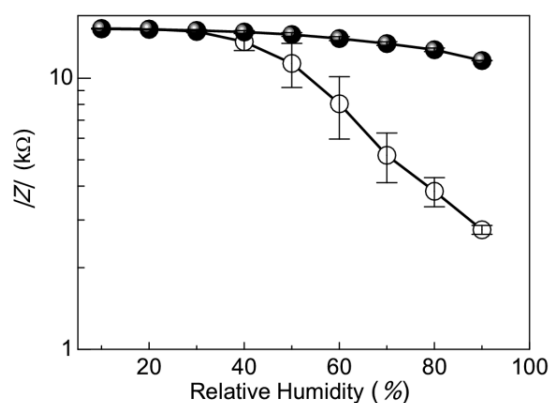


Figure 6. Absolute impedance of SPAN-Na (open circles) and SPAN-Na:PVA (1:1, closed circles) films measured at 140 kHz as a function of relative humidity.

The impedance of the SPAN-Na films gradually drops from 15 kΩ to 3 kΩ with ~0.2 kΩ per 1% RH when the RH increases from 40% to 90%. The SPAN-Na:PVA films show much smaller drop in impedance in this RH range. In addition, at higher humidity, the impedance of the composite films remains higher. These observations suggest that SPAN-Na:PVA composite films are less sensitive to humidity than pure SPAN-Na films. However, the impedance change due to humidity is significantly larger in comparison to composite PANI:PVA films doped with p-toluenesulfonic acid [57]. The presence of sulfonic groups on the polymer chain attracts water vapor via hydrogen bonding. The influence of humidity on impedance of SPAN-Na films will be discussed in more detail in Chapter 3.

3.4. CO₂ Sensing with Sulfonated Polyaniline Sodium Salt

The response of undoped SPAN-Na films towards CO₂ was investigated by impedance spectroscopy at constant humidity. The impedance spectrum was measured with a frequency scan from 1 MHz to 5 Hz. **Figure 7** shows the Nyquist plots of undoped SPAN-Na exposed to N₂ and 50,000 ppm CO₂ at 72% RH. The SPAN-Na shows a semi-circular response curve with a peak at 200 kHz (breakpoint frequency corresponding to a phase angle of 45°) followed by a second semicircle down to low frequencies. The high-frequency semicircle is related to the bulk conductance of the polymer film while the low-frequency semicircle contains information about the process related to reactions at the electrode surface [58]. Around 200 kHz a small shift was observed when the sample was measured with and without CO₂ (inset **Figure 7**). A reasonable fit of the impedance data is obtained using equivalent circuit consisting of resistive components related to bulk resistivity of the film and non-linear semi-empirical defined constant phase elements (CPEs) which are related to capacitive nature

of the film and diffusive components of the analyte species [59]. The details of the circuit model and fitting parameters are included in the **Appendix 1**.

Previous studies suggested that the sensitivity towards CO_2 can be improved by making a PANI:PVA composite [32, 52]. The addition of PVA to SPAN-Na in the ratio 1:1 changed the impedance behavior of the polymer. A semicircle in the high to middle frequency range with a maximum at 140 kHz (breakpoint frequency) was observed for SPAN-Na:PVA exposed to 50,000 ppm CO_2 (**Figure 7**). Furthermore, a shift in maximum of the semicircle was observed under pure N_2 flow and an additional linear component was observed instead of a second semicircle. The low-frequency diffusion tail in the spectra of SPAN-Na:PVA corresponding to a 45° slope shows that the rate of diffusion of species (i.e. water molecules, protons, ions) through the pores of the composite films becomes slower than the charge transfer process on the film [58]. In this case, the equivalent electrical circuit consists of a resistive component and CPE in parallel with a second CPE. The first CPE describes the capacitive nature of the film, whereas the second CPE relates to the diffusion of the analyte species at the electrode polymer interface, i.e. the Warburg element for semi-infinite thickness. Details on the fitting parameters are shown in the **Appendix 1**.

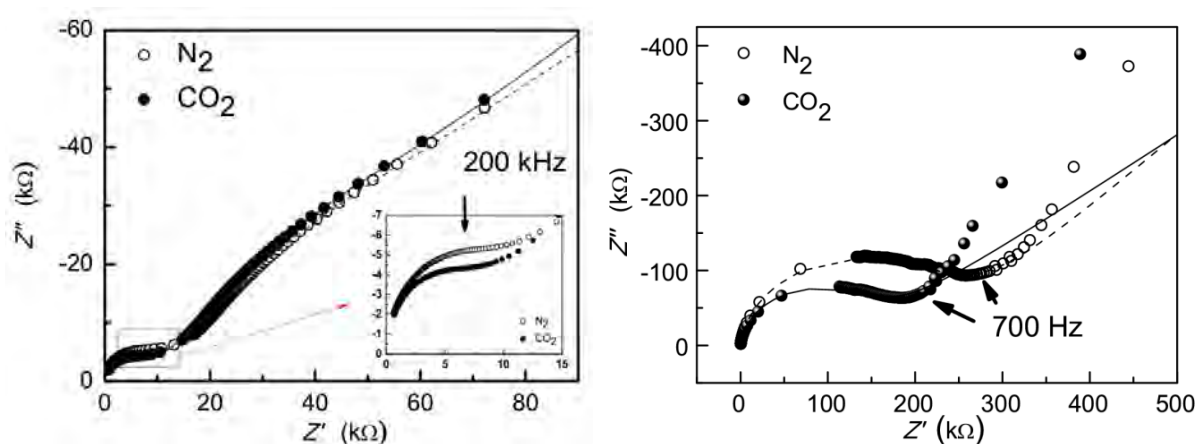


Figure 7. Nyquist plots of SPAN-Na (left), SPAN-Na:PVA (1:1) (right) exposed to N_2 and 50,000 ppm CO_2 at 72% RH.

The presence of CO_2 at 50,000 ppm results in a remarkable decrease in the overall impedance, with the linear component shifting from 300 $\text{k}\Omega$ to 200 $\text{k}\Omega$ at 700 Hz (minimum phase angle frequency) [58, 60]. This behavior is consistent with earlier studies on composite films of base-type poly(anthranilic acid) and PVA [52]. It could be that the presence of PVA in the vicinity of SPAN-Na slows down the diffusion rate of species in comparison with pure

SPAN-Na. This might explain the difference in the frequency at which the maximum impedance change induced by CO₂ was observed for the two films.

Next, the response of SPAN-Na and SPAN-Na:PVA films was studied for different concentrations of CO₂ at constant humidity at 0.7 kHz, where the maximum difference was observed. The absolute impedance of the SPAN-Na coated chips was measured as a function of time at 75% RH with CO₂ concentration increasing up to 50,000 ppm (5%) (**Figure 8**). The SPAN-Na films exhibited sensitivity toward CO₂ starting at 20,000 ppm CO₂. A relative decrease ($\Delta Z/Z_0$) in impedance of SPAN-Na is observed when CO₂ is introduced into the chamber and the ratio $\Delta Z/Z_0$ increases with the CO₂ concentrations (**Figure 9**).

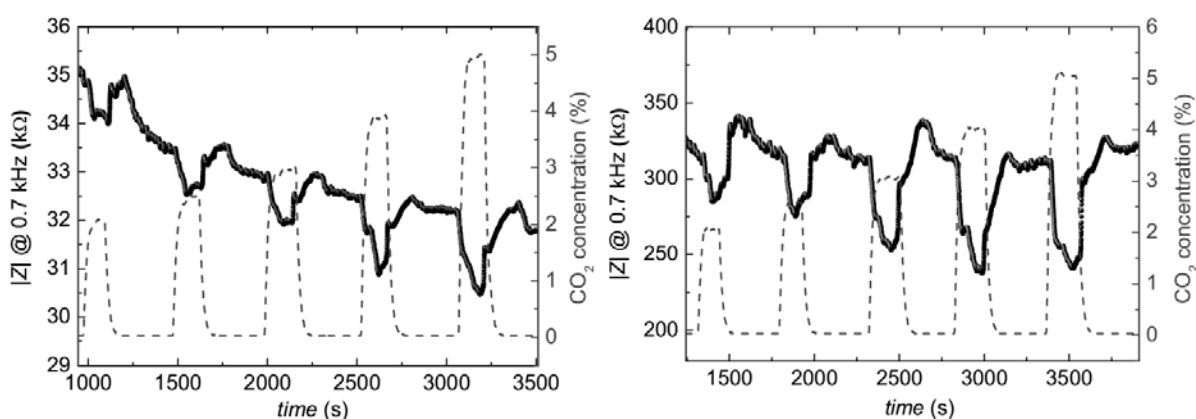


Figure 8. $|Z|$ as a function of time for SPAN-Na (left) and SPAN-Na:PVA (1:2) (right), when exposed to different CO₂ concentrations at 0.7 kHz. The dashed lines are the responses from the reference CO₂ sensor.

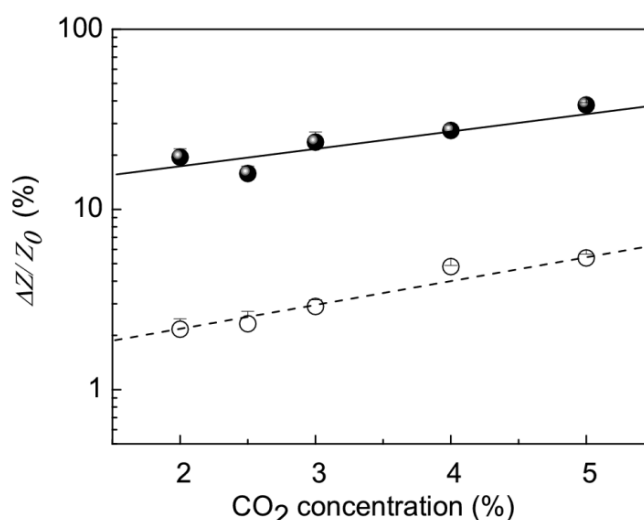


Figure 9. Relative change of impedance ($\Delta Z/Z_0$) at 0.7 kHz of SPAN-Na (open circles) and SPAN-Na:PVA (1:1, closed circles).

The addition of PVA to SPAN-Na makes the response more pronounced (**Figure 8**). The baseline resistance of the polymer is a factor 10 higher with PVA, consistent with earlier observations [46]. PVA is a non-conducting material and thereby contributes to a higher resistance. In the presence of PVA the $\Delta Z/Z_0$ is $\sim 20\%$ at 50,000 ppm CO_2 in comparison to 4% for pure SPAN-Na. For SPAN-Na a drift of 9% in the baseline was observed during the measurement, which is in the same order magnitude as the impedance changes due to presence of CO_2 . The high baseline drift of SPAN-Na arises due to the high sensitivity of the conducting polymer to humidity variations (**Figure 6**). The addition of PVA gave a baseline with drift in the order of 10% between each CO_2 pulse, but the relative change in impedance due to CO_2 was much larger (**Figure 9**). The drift in the signal was also observed by Freund and coworkers in the earlier study on CO_2 sensing with films of self-doped boronated PANI with PVA [46]. Measurements of films with and without PVA carried out at frequencies above 100 kHz failed to discriminate signals arising from humidity associated fluctuations and CO_2 pulse measurements (data not shown). For similar reasons, also at low CO_2 concentrations, the signal variations cannot be detected.

Based on these observations, the presence of sulfonated groups on the PANI enables the measurement of the presence of CO_2 . But the presence of CO_2 remains undetected below 1%. It is well known that the solubility of CO_2 in water changes the pH of the solution. We hypothesize that since the concentration between 2% and 5% has been measured, the pH sensing range lies in the range 4.5–5.5. Measuring below 10,000 ppm down to 400 ppm indicates that pH range should be around 5.5 to 7 as proposed by Irimia-Vladu and Fergus [32].

4. Conclusions

A sodium salt of sulfonated derivative of polyaniline with PVA composite demonstrates capability to sense CO_2 at room temperature. The sensing is possible due to the presence of the sulfonic groups on the polymer, acting as inner dopant anions, which make it possible to measure changes in conductivity in the pH range of 4–5.5. We showed that sensing of CO_2 with a reasonable signal to noise ratio is feasible at levels above 20,000 ppm. This work enables the development of low-cost sensors operating at room temperature. Future work will focus on approaches to enable sensing of lower CO_2 concentrations with conducting polymers. A method to improve the sensing range is to increase the conductivity of the SPAN-Na under a field effect bias. Applying an electric field in a FET configuration could

lead to an increase in conductivity in the higher pH range, thereby allowing for greater sensitivity at lower CO₂ concentrations.

References

- [1] J. Zosel, W. Oelssner, M. Decker, G. Gerlach, U. Guth, The measurement of dissolved and gaseous carbon dioxide concentration, *Meas. Sci. Technol.* 22 (2011) 072001.
- [2] J.D. Cure, B. Acock, Crop responses to carbon dioxide doubling: a literature survey, *Agric. Forest Meteorol.* 38 (1986) 127–145.
- [3] J.S. Amthor, Effects of atmospheric CO₂ concentration on wheat yield: review of results from experiments using various approaches to control CO₂ concentration, *Field Crop Res.* 73 (2001) 1–34.
- [4] B.A. Kimball, K. Kobayashi, M. Bindi, Responses of agricultural crops to free-air CO₂ enrichment, *Adv. Agron.* 77 (2002) 293–368.
- [5] G. Luciano, C. Carlos Eduardo, A proposal of greenhouse control using wireless sensor networks, in: *Computers in Agriculture and Natural Resources, 4th World Congress Conference, Proceedings*, 2006.
- [6] V.L. Narasimhan, A.A. Arvind, K. Bever, Greenhouse asset management using wireless sensor-actor networks, in: *International Conference on Mobile Ubiquitous Computing, Systems, Services and Technologies (UBICOMM'07)*, 2007, pp. 9–14.
- [7] T. Ahonen, R. Virrankoski, M. Elmusrati, Greenhouse monitoring with wireless sensor network, in: *Proceedings of 2008 IEEE/ASME International Conference on Mechatronic and Embedded Systems and Applications*, IEEE, New York, 2008, pp. 403–408.
- [8] L. Ruiz-Garcia, L. Lunadei, P. Barreiro, J.I. Robla, A review of wireless sensor technologies and applications in agriculture and food industry: state of the art and current trends, *Sensors* 9 (2009) 4728–4750.
- [9] A. Zerger, R.A.V. Rossel, D.L. Swain, T. Wark, R.N. Handcock, V.A.J. Doerr, G.J. Bishop-Hurley, E.D. Doerr, P.G. Gibbons, C. Lobsey, Environmental sensor networks for vegetation, animal and soil sciences, *Int. J. Appl. Earth Obs. Geoinf.* 12 (2010) 303–316.
- [10] S. Neethirajan, D.S. Jayas, S. Sadistap, Carbon dioxide (CO₂) sensors for the agrifood industry—a review, *Food Bioprocess Technol.* 2 (2009) 115–121.
- [11] D. James, S.M. Scott, Z. Ali, W.T. O'Hare, Chemical sensors for electronic nose systems, *Microchim. Acta* 149 (2005) 1–17.

- [12] P. Offermans, H.D. Tong, C.J.M. van Rijn, P. Merken, S.H. Brongersma, M. Crego-Calama, Ultralow-power hydrogen sensing with single palladium nanowires, *Appl. Phys. Lett.* 94 (2009).
- [13] J. Xu, P. Offermans, G. Meynants, H. Duy Tong, C.J.M. van Rijn, P. Merken, A low-power readout circuit for nanowire based hydrogen sensor, *Microelectron. J.* 41 (2010) 733–739.
- [14] I.M. Feigel, H. Vedala, A. Star, Biosensors based on one-dimensional nanostructures, *J. Mater. Chem.* 21 (2011) 8940–8954.
- [15] A. Star, T.R. Han, V. Joshi, J.C.P. Gabriel, G. Gruner, Nanoelectronic carbon dioxide sensors, *Adv. Mater.* 16 (2004) 2049–2052.
- [16] C.Y. Chang, B.S. Kang, H.T. Wang, F. Ren, Y.L. Wang, S.J. Pearton, D.M. Dennis, J.W. Johnson, P. Rajagopal, J.C. Roberts, E.L. Piner, K.J. Linthicum, CO₂ detection using polyethylenimine/starch functionalized AlGa_N/Ga_N high electron mobility transistors, *Appl. Phys. Lett.* 92 (2008) 232102.
- [17] U. Lange, N.V. Roznyatovskaya, V.M. Mirsky, Conducting polymers in chemical sensors and arrays, *Anal. Chim. Acta* 614 (2008) 1–26.
- [18] D.W. Hatchett, M. Josowicz, Composites of intrinsically conducting polymers as sensing nanomaterials, *Chem. Rev.* 108 (2008) 746–769.
- [19] H. Bai, G.Q. Shi, Gas sensors based on conducting polymers, *Sensors* 7 (2007) 267–307.
- [20] D. Nicolas-Debarnot, F. Poncin-Epaillard, Polyaniline as a new sensitive layer for gas sensors, *Anal. Chim. Acta* 475 (2003) 1–15.
- [21] E. Kang, K. Neoh, K. Tan, X-ray photoelectron spectroscopic studies of electroactive polymers, in: *Polymer Characteristics*, Springer, Berlin, Heidelberg, 1993, pp. 135–190.
- [22] M.S. Freund, B.A. Deore, Introduction, in *Self-Doped Conducting Polymers*, John Wiley & Sons, Ltd., Chichester, UK, 2007, <http://dx.doi.org/10.1002/9780470061725.ch1>.
- [23] L. Torsi, M. Pezzuto, P. Siciliano, R. Rella, L. Sabbatini, L. Valli, P.G. Zambonin, Conducting polymers doped with metallic inclusions: new materials for gas sensors, *Sens. Actuator B: Chem.* 48 (1998) 362–367.
- [23] L. Torsi, M. Pezzuto, P. Siciliano, R. Rella, L. Sabbatini, L. Valli, P.G. Zambonin, Conducting polymers doped with metallic inclusions: new materials for gas sensors, *Sens. Actuator B: Chem.* 48 (1998) 362–367.
- [24] S. Virji, J. Huang, R.B. Kaner, B.H. Weiller, Polyaniline nanofiber gas sensors: examination of response mechanisms, *Nano Lett.* 4 (2004) 491–496.

- [25] B.J.V. Tongol, C.A. Binag, F.B. Sevilla, Surface and electrochemical studies of a carbon dioxide probe based on conducting polypyrrole, *Sens. Actuators B: Chem.* 93 (2003) 187–196.
- [26] J.W. Severinghaus, A.F. Bradley, Electrodes for blood PO₂ and PCO₂ determination, *J. Appl. Physiol.* 13 (1958) 515–520.
- [27] S. Herber, W. Olthuis, P. Bergveld, A swelling hydrogel-based PCO₂ sensor, *Sens. Actuators B: Chem.* 91 (2003) 378–382.
- [28] K. Ogura, A CO₂ sensor with polymer composites operating at ordinary temperature, *J. Electrochem. Soc.* 147 (2000) 4351–4355.
- [29] K. Ogura, H. Shiigi, A CO₂ sensing composite film consisting of base-type polyaniline and poly(vinyl alcohol), *Electrochem. Solid State Lett.* 2 (1999) 478–480.
- [30] H. Shiigi, T. Oho, T. Tonosaki, K. Ogura, CO₂-sensitive characteristics of base-type polyaniline poly(vinyl alcohol) composites at room temperature and effects of coexisting gases, *Electrochemistry* 69 (2001) 997–1001.
- [31] T. Tonosaki, T. Oho, H. Shiigi, K. Isomura, K. Ogura, Highly sensitive CO₂ sensor with polymer composites operating at room temperature, *Anal. Sci.* 17 (Suppl.) (2001) i249.
- [32] M. Irimia-Vladu, J.W. Fergus, Suitability of emeraldine base polyaniline-PVA composite film for carbon dioxide sensing, *Synth. Met.* 156 (2006) 1401–1407.
- [33] M. Irimia-Vladu, J.W. Fergus, Impedance spectroscopy of thin films of emeraldine base polyaniline and its implications for chemical sensing, *Synth. Met.* 156 (2006) 1396–1400.
- [34] J.-C. Chiang, A.G. MacDiarmid, ‘Polyaniline’: protonic acid doping of the emeraldine form to the metallic regime, *Synth. Met.* 13 (1986) 193–205.
- [35] W. Huang, B.D. Humphrey, A.G. MacDiarmid, Polyaniline, a novel conducting polymer. Morphology and chemistry of its oxidation and reduction in aqueous electrolytes, *J. Chem. Soc. Faraday Trans. 1* (82) (1986) 2385–2400.
- [36] A.G. Macdiarmid, J.C. Chiang, A.F. Richter, A.J. Epstein, Polyaniline: a new concept in conducting polymers, *Synth. Met.* 18 (1987) 285–290.
- [37] M.E. Jozefowicz, A.J. Epstein, X. Tang, Protonic acid doping of two classes of the emeraldine form of polyaniline, *Synth. Met.* 46 (1992) 337–340.
- [38] M.S. Freund, B.A. Deore, Self-doped derivatives of polyaniline, in: *Self-Doped Conducting Polymers*, John Wiley & Sons, Ltd., Chichester, UK, 2007, <http://dx.doi.org/10.1002/9780470061725.ch2>.
- [39] A. Malinauskas, Self-doped polyanilines, *J. Power Sources* 126 (2004) 214–220.

- [40] J. Yue, A.J. Epstein, Synthesis of self-doped conducting polyaniline, *J. Am. Chem. Soc.* 112 (1990) 2800–2801.
- [41] J. Yue, Z.H. Wang, K.R. Cromack, A.J. Epstein, A.G. MacDiarmid, Effect of sulfonic acid group on polyaniline backbone, *J. Am. Chem. Soc.* 113 (1991) 2665–2671.
- [42] X.-L. Wei, Y.Z. Wang, S.M. Long, C. Bobeczko, A.J. Epstein, Synthesis and physical properties of highly sulfonated polyaniline, *J. Am. Chem. Soc.* 118 (1996) 2545–2555.
- [43] B.A. Deore, S. Hachey, M.S. Freund, Electroactivity of electrochemically synthesized poly(aniline boronic acid) as a function of pH: role of self-doping, *Chem. Mater.* 16 (2004) 1427–1432.
- [44] B.A. Deore, I. Yu, M.S. Freund, A switchable self-doped polyaniline: interconversion between self-doped and non-self-doped forms, *J. Am. Chem. Soc.* 126 (2004) 52–53.
- [45] A.A. Karyakin, A.K. Strakhova, A.K. Yatsimirsky, Self-doped polyanilines electrochemically active in neutral and basic aqueous solutions: electropolymerization of substituted anilines, *J. Electroanal. Chem.* 371 (1994) 259–265.
- [46] S. Neethirajan, 618 M.S. Freund, D.S. Jayas, C. Shafai, D.J. Thomson, N.D.G. White, Development of carbon dioxide (CO₂) sensor for grain quality monitoring, *Biosyst. Eng.* 106 (2010) 395–404.
- [47] P.D. Harris, W.M. Arnold, M.K. Andrews, A.C. Partridge, Resistance characteristics of conducting polymer films used in gas sensors, *Sens. Actuators B: Chem.* 42 (1997) 177–184.
- [48] S.-A. Chen, G.-W. Hwang, Structure characterization of self-acid-doped sulfonic acid ring-substituted polyaniline in its aqueous solutions and as solid film, *Macromolecules* 29 (1996) 3950–3955.
- [49] Y. Tao, J.X. Zhao, C.X. Wu, Polyacrylamide hydrogels with trapped sulfonated polyaniline, *Eur. Polym. J.* 41 (2005) 1342–1349.
- [50] L. Yang, A. Guiseppi-Wilson, A. Guiseppi-Elie, Design considerations in the use of interdigitated microsensor electrode arrays (IMEs) for impedimetric characterization of biomimetic hydrogels, *Biomed. Microdev.* 13 (2011) 279–289.
- [51] A.S. Bondarenko, G.A. Ragoisha, EIS Spectrum Analyzer v0.1b, 2008, <http://www.abc.chemistry.bsu.by/vi/analyser/>.
- [52] T. Oho, T. Tonosaki, K. Isomura, K. Ogura, A CO₂ sensor operating under high humidity, *J. Electroanal. Chem.* 522 (2002) 173–178.

- [53] S.H. Kim, T. Zyung, H.Y. Chu, L.-M. Do, D.-H. Hwang, Charge transport in a π -conjugated polymer: generalized Langevin equation analysis, *Phys. Rev. B* 61 (2000) 15854–15857.
- [54] N.E. Agbor, M.C. Petty, A.P. Monkman, Polyaniline thin films for gas sensing, *Sens. Actuators B: Chem.* 28 (1995) 173–179.
- [55] M. Nowak, S.D.D.V. Rughooputh, S. Hotta, A.J. Heeger, Polarons and bipolarons on a conducting polymer in solution, *Macromolecules* 20 (1987) 965–968.
- [56] J. Yue, G. Gordon, A.J. Epstein, Comparison of different synthetic routes for sulphonation of polyaniline, *Polymer* 33 (1992) 4410–4418.
- [57] K. Ogura, T. Saino, M. Nakayama, H. Shiigi, The humidity dependence of the electrical conductivity of a soluble polyaniline-poly(vinyl alcohol) composite film, *J. Mater. Chem.* 7 (1997) 2363–2366.
- [58] W.M. Bos, Electrochemical techniques for coating characterisation – early detection using electrochemical methods, Ph.D. thesis, Delft University of Technology, Delft, The Netherlands, 2008.
- [59] I.D. Raistrick, D.R. Franceschetti, J.R. Macdonald, in: E. Barsoukov, J.R. Macdonald (Eds.), *Theory, in Impedance Spectroscopy: Theory, Experiment, and Applications*, second ed., John Wiley & Sons, Inc., Hoboken, NJ, USA, 2005, pp. 80–117, <http://dx.doi.org/10.1002/0471716243.ch2>.
- [60] A. Amirudin, D. Thierry, Application of electrochemical impedance spectroscopy to study the degradation of polymer-coated metals, *Prog. Org. Coat.* 26 (1995) 1–28.

Chapter 3. Decoupling Intrinsic and Ionic Conduction in Sulfonated Polyaniline in the Presence of Water Vapor as Analyte

Abstract

The influence of humidity on the conductivity of Sulfonated Polyaniline (SPANI) is investigated with electrochemical impedance spectroscopy (EIS). Both SPANI and Polyaniline (PANI) were investigated to separate the intrinsic (q) and ionic charge (i) transport at varying humidity concentrations from 5 to 90% RH. A combination of ac and dc impedance measurements was necessary to distinguish between the intrinsic and ionic conductivity in the polymer. Nyquist plots for both PANI (acid doped) and SPANI show single semicircles at all humidity levels indicating pure intrinsic charge conduction. These semicircles are well described with a fairly constant capacitance ($C_I = 10^{-10}$ F) and with a large varying resistance (10 k Ω - 10 M Ω) of the polymer bulk with RC times in the order of 10^{-3} - 10^{-6} sec. In all samples the intrinsic charge conductivity increases for increasing humidity, with Emeraldine base PANI showing the highest change corresponding to a 2-order increase. A partial exchange of protons with sodium ions in SPANI (SPAN-Na) induces a second semicircle at humidity levels above 40% with large RC times (10^{-1} - 10^{-3} sec), which is attributed to a contribution of ionic mobility at the polymer/electrode interface. Blended samples of SPAN-Na with poly(vinyl alcohol) (PVA) and polyacrylamide (PAA) also show a second semicircle at slightly higher humidity levels from 50% RH onwards. In all cases this second semicircle is best described by a Constant Phase Element (CPE) with a value (order typical 10^{-9} - 10^{-7} F) increasing at higher humidity, and a varying coefficient ($0.5 < n < 0.8$), possibly due to a changing dispersion in the representative relaxation times for migration and accumulation of the ionic species. In addition for SPAN-Na samples blended with PVA a third semicircle is seen which can be described by an additional RC element representing an additional phase or grain boundary contribution.

This chapter will be submitted as:

“Intrinsic and Ionic Conduction in Humidity Sensitive Sulfonated Polyaniline”, Tin C. D. Doan, Rajesh Ramaneti, Jacob Baggerman, Antonius T. M. Marcelis, Hien D. Tong, and Cees J. M. van Rijn, submitted.

1. Introduction

Intrinsic charge carriers, such as electrons and holes, are usually transported in semiconductors and conductive polymers, while ions normally determine the conductive transport in polyelectrolyte solutions and solid state ionic conductors. A wide variety of systems such as sensors and electrochemical cells may exhibit both intrinsic and ionic transport. In battery electrodes, for example, more efficient charge transport can be enabled by a fine intercalation of electronic and ionic conducting microphases [1]. Organic semiconductors, especially conjugated polymers, have also long been considered as good active sensing material candidates. However constituted devices are frequently limited in operation by complicated organic polymer/metal interfaces, resulting in electronic drift, material degradation and complex humidity responses. Low power chemiresistive sensors for monitoring environmental gases, such as carbon dioxide, ammonia and NO_x are known to be co-sensitive for water vapor, especially in applications where humidity levels are controlled at 70-90% RH [2]. Low power chemiresistors (conjugated polymer and/or polyelectrolyte films) have therefore also been applied for humidity sensing themselves and have been studied for the last 20-30 years [3, 4] due to their ease of processability and low power consumption [5, 6]. The transduction principle of a chemiresistor is based on the relative change in conductivity of the polymer when exposed to the gas analyte. This change can originate from intrinsic charge transport (holes/electrons in conjugated polymers), proton hopping via water molecules (Grotthuss mechanism) and/or ionic transport in the polymer film, when it is subjected to an electrical dc/ac interrogation. Attachment of functional groups to the polymer backbone will promote specific interactions between the ionized groups and the polar water molecules [7, 8].

Polyaniline (PANI) and its derivatives have been well studied for humidity responses. Besides proton hopping and ionic transport, the intrinsic conductivity of the conjugated polymer backbone might also co-determine the humidity response. Most of the prior studies related to humidity effects on conductivity were done with emeraldine salt of PANI [9-11] and composites with poly(vinyl alcohol) (PVA) [12-15]. The addition of PVA is believed to minimize hysteresis, generally improving the humidity sensing response [15-17]. Formation of two different hydrogen bondings have been proposed for EB-PANI, one involving the imine nitrogen center facing a hydrogen atom of a nearby water molecule, and one involving the amine center facing the oxygen atom of the water molecule. EB-PANI is therefore

assumed to adsorb at least one water molecule at each nitrogen center (if temperature does not exceed 60 °C). Sulfonated polyaniline (SPANI) has an abundance of protons near the imine sites of the backbone and is called a “self-doped” conducting polymer with conductivity in the order of 0.01-100 mS.cm⁻¹ [18]. The water soluble sodium salt of the sulfonated polyaniline (SPAN-Na) however is an ion conducting polymer and therefore can be considered as an polyelectrolyte [18]. In this work we report inter alia on the humidity-dependent conductivity of undoped emeraldine base PANI (EB-PANI) and the sodium salt of sulfonated polyaniline (SPAN-Na). To our knowledge, until date, the humidity responses of SPAN-Na have not been reported. In addition, a systematic study on nature of intrinsic charge and ionic transport under humidity variations has not been carried out. This chapter aims to discriminate between the two conduction mechanisms as the water vapor concentration is varied. We first analyze the conductivity responses of EB-PANI (without the sulfonate groups) and SPAN-Na (with sulfonate groups) when the humidity levels are varied. Then, we investigate the role of intrinsic charge transport in the presence of humidity using acidic (pH 1) or self-doped polymers and compare them with the undoped films. Finally, the effect of blending with non-conducting hydrophilic polymers such as PVA in SPAN-Na and SPANI will be also reported.

Modeling Charge Transport

Understanding conductivity and related charge transfer processes in conductive polymers is a complicated task [19, 20]. The conductivity change of a polymer film exposed to humidity is attributed to a variation in both intrinsic and ionic conduction through the polymer film and also to the processes at the interface between the metal electrode(s) and the polymer film. Impedance spectroscopy has been extensively used to clarify charge transport, an approach involving the interpretation of experimental data in terms of an appropriate equivalent circuit model, wherein the individual circuit components are assumed to adequately describe the involved physical processes [21, 22]. However, there is not always consensus about the construction of the representative electrical circuit and the physical interpretation of the individual elements [21]. The chosen circuit should be informative on all related electrode, interfacial and film impedance contributions with fast relaxation times and also on slow charge transport processes, such as diffusion and migration of ions, dominating the low frequency response. Several equivalent circuits have been developed to represent the charge transport of conductive polymers in electrolyte solution such as Randle’s circuit [21, 23], extended Randle’s circuit [20, 24] and a transmission line model [19, 25]. The Randle’s circuit is originally used to describe polymer-coated metal electrodes dipped in electrolyte

solutions [21]. In humidity sensing different models were applied to describe the charge transport process of conducting polymer films [22, 26].

In this communication an extended Randle's circuit [23] was applied to give a general description aiming to de-convolute ionic and intrinsic charge transport in SPAN-Na and its blends when exposed to water vapor at low and high frequencies as shown in **Figure 1**. We expect both ion and electron conducting channels, and thus a parallel combination of the intrinsic (R_2 , C_1) and ion ($C(PE)_2$, $C(PE)_3$, R_3 , R_4) representative circuits seems appropriate. This model will also help to characterize the charge conduction inside the polymer film upon exposure to different levels of humidity. The overlap of the electrical circuit model with the film device structure in **Figure 1** aims to correlate the various analytical components with the device structure and the physical processes occurring within them. Here we assume that our polymer film can be partially porous [18, 27] but fully covers the interdigitated platinum electrode sensing area. A transmission line model has also been proposed to distinguish between the two conducting mechanisms [28]; however in our case, the polymer is not exposed to an electrolyte except at very high water vapor concentrations, hence this model cannot be applied and an extended Randle's circuit has been chosen as the first workable model.

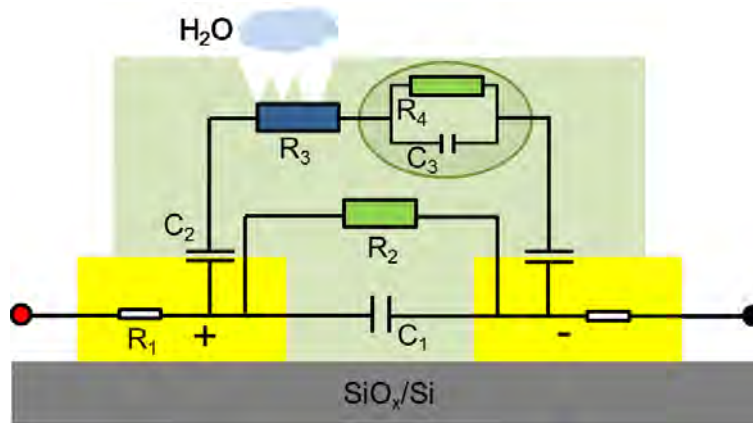


Figure 1. Generic extended Randle's circuit to characterize the charge conduction inside the polymer. Intrinsic charge conduction R_2 and ionic charge conduction R_3 are represented in parallel to the film capacitance C_1 .

The extended Randle's model seems also applicable to suit the polymorphous nature of polyaniline and its response in a wide humidity range. In order to build our model, four resistors R_1 , R_2 , R_3 and R_4 are incorporated into the model to match the measured resistances. The dc resistance varies from 10 k Ω to 100 G Ω and is described by the series resistance of R_2

and R_1 [29, 30]. For ac measurements we have to take into account mainly R_3 and sometimes also R_4 to describe more complex responses.

R_1 is the interdigitated electrode contact resistance. In our case, this applies specifically to electrode resistance arising from Cr/Pt interdigitated metal contacts having a fitted finite value of 28 Ω , whereas the calculated value is $35 \pm 5 \Omega$ (See **Appendix 2**). It is related to geometry of the electrode, including the spacing between the interdigitated comb structures.

C_1 is the sum capacitance of the polymer film and the capacitance of the blank interdigitated electrode (via the silicon substrate) and is normally quite small (~ 100 pF). This element dictates the response in the very high frequency domain. The measured value for the capacitance C_1 without any polymer film on the interdigitated electrode is typical 85 pF. It is also represented as a Constant Phase Element CPE_1 with a nearly ideal capacitance behavior ($n = 0.9-1$).

R_2 is related to intrinsic charge (q) electron/hole conduction within the polymer film and can vary from 10 k Ω to 100 G Ω for PANI and SPANI and can be strongly influenced by the charge doping by means of external doping: acidic or basic buffers (holes or electrons) or through self-doping: attachment of charged functional groups along the PANI backbone. Here R_2 is also represented as R_q .

Then, we have C_2 , which is associated with charge generation and accumulation at the polymer/electrode interface. Under humid conditions, this capacitance at the interface may lose its ideal properties so that this capacitance may transform into a constant phase element (CPE_2) with a varying phase value ($n = 0.6-0.9$). This element is assumed to describe the behavior in the medium to low frequency domain and is associated with relatively large values (order of 10-100 nF). In our samples, due to the frequency and compliance limitations of the measurement setup, measurements in high impedance samples have been limited to 5 Hz. In our case platinum is the metal electrode material in contact with the ion conducting polymer film. It is a blocking electrode for Na^+ and H^+ ions, therefore C_2 corresponds to the electrode/polymer interface capacitance.

Next, we have the resistance R_3 in series with C_2 and describes the ionic charge resistance from ionic charges out of the polymer film to condense on the electrode/polymer interface [29, 30]. The value of R_3 can be derived from the radius of the high frequency semicircle in the corresponding Nyquist plot, as will be explained later in this section. See **Appendix 2 - Figure A2** for ideal representation of the Nyquist plot.

Finally, we have a CPE_3/R_4 element which has been previously used to describe transport processes across grain boundaries or secondary phases present in hybrid conductors [31]. An equivalent physical analogy in describing an ion conducting polymer is not clear. This “sub” Randle’s circuit consisting of R_4 in parallel with a CPE_3 element will be used to describe the third semicircle which appears in the intermediate region between the high and low/medium frequency semicircles [30]. While in most cases, we see two semicircles, some samples measured under specific conditions (humidity in this case) show a third semicircle. To our knowledge, no analogous description with respect to ion conducting polymers is present [32].

2. Materials and Methods

2.1. Materials

The chemicals for synthesis of EB-PANI, SPAN-Na and blends with PVA, PAA were reported in our previous publication [27]. All chemicals were used without further purification.

2.2. Polymer Solutions and Sensor Preparation

The details of preparation of EB-PANI, SPAN-Na and blends with PVA can be found in our previous publication [27].

1 μL of the polymer solution was drop-casted onto a silicon chip with Pt interdigitated electrodes (thickness ~ 170 nm) of dimensions 300 μm (length) x 9 μm (width) and 6 μm spacing. For the polymer solutions using dimethylsulfoxide (DMSO) as solvent (with EB-PANI, SPAN-Na, SPAN-Na:PVA), the drop-casted polymer was dried at 60 $^{\circ}\text{C}$ for 24 hours in a vacuum oven. The thickness of the films was determined using a surface profiler Dektak 6M (Veeco). The EB-PANI films had an average thickness of ~ 500 nm, the SPAN-Na films had a thickness of 200 nm.

For the preparation of SPANI the procedure described by Yue and Epstein was followed [33, 34]. The acid doping of the films was carried out by dropping a 1 μL droplet of pH 1 buffer solution onto the chip and the excess pH buffer solution was removed with a filter paper. In the case of acid doping of SPAN-Na, a composite was obtained with PAA as an ionic hydrogel, which makes it sensitive to pH below 7 while dissolution in aqueous buffers is prevented. It was shown that a pure PAA gel does not show physically swelling in a wide range different pH solutions, while PAA gel with SPANI/SPAN-Na showed a swelling

response above pH 8. As a result a conductivity change at low pH is expected only from SPAN-Na. Further details of application of pH buffers can be found in [27].

2.3. pH-Dependent Conductivity Measurements

Acid-doped samples of SPAN-Na, SPANI, EB-PANI were obtained by exposing the polymer chips to the pH 1 buffer solution. Reference impedance and dc measurements were made prior to the exposure. The pH buffer solution was dropped onto the polymer composite film and kept in a closed box for 30 minutes. It was observed previously that the presence of salt on the surface of the chip without a polymer can also induce an impedance change. Therefore a filter paper was used to adsorb the buffer solution to reduce the influence of residual salt after drying. Impedance and dc measurements were carried out after exposure to the pH buffer.

2.4. Electrical Characterization of Humidity Sensing of Polymer Coated Chips using Ac Impedance and Dc Resistance Measurements

The polymer-coated chips were placed in the chamber with controlled relative humidity levels. More details of the gas sensor test characterization setup can be found in Chapter 2. To investigate the humidity sensing capability of SPAN-Na, SPANI and its blends, the polymer coated chip was exposed to different humidity levels from 10% to 90% RH, the ac impedance and dc resistance of polymer films were measured at room temperature (24 °C). Dc measurements identify the interfacial electronic properties of polymers (junction between metal/semiconductor contacts) in interaction with water vapor. The frequency-dependent studies are useful to obtain better understanding of the charge transport mechanism both within the bulk and interface [35, 36]. Two-point dc resistivity (conductivity) measurement and ac impedance spectroscopy were carried out using a Keithley 2400 source meter and a HP 4192A LF impedance analyzer respectively. Bias voltages in the range of 10 mV to 1.0 V were applied during the measurements to ensure minimum perturbation or to obtain steady state currents in the samples. This range was chosen in order to correspond with the dc measurements where samples were found ohmic between -1 V to +1 V (see **Appendix 2 - Figures A3-A6**). The impedance change was expressed in terms of Nyquist plots with the imaginary impedance (Z'') plotted against the real impedance (Z'), having been derived from the measured absolute impedance ($|Z|$) and phase angle (θ) values during a frequency scan ranging from 5 Hz to 1 MHz. To extract the parameters from electrical circuit described in **Figure 1**, the analysis was carried out using EIS Spectrum Analyser 2008 fitting software (A.S. Bondarenko and G.A.Ragoisha).

3. Results and Discussion

3.1. Dc Measurements on PANI, SPAN-Na, SPAN and Their Blends with PVA

Water adsorption in EB-PANI films has been studied extensively [37, 38]. Direct structural conformational changes are difficult to verify with X-Ray analysis or with Electron Spin Resonance [39]. Thermo gravimetric analysis, calorimetric experiments and Molecular Dynamics reveal a maximum adsorbed water content up to 15% w/w [40, 41]. Also dielectric constant changes have been reported [42], the real part of the dielectric constant was shown to approach more than 80 at higher humidity levels, suggesting the presence of oriented water molecules in a porous polymer matrix [43]. Matveeva et al. [42] proposed that a primary stage of protonation originating from hydrogen bond formation between the water molecules and the polymer chain was induced, which might result in an increase of the intrinsic electrical conductivity. Macdiarmid et al. [44] showed a two-fold increase in conductivity of EB-PANI film upon exposure to water vapor. Ogura et al. [45] stated that EB-PANI was still in the undoped form and water vapor would not protonate EB-PANI sufficiently to induce an increase in the intrinsic conductivity.

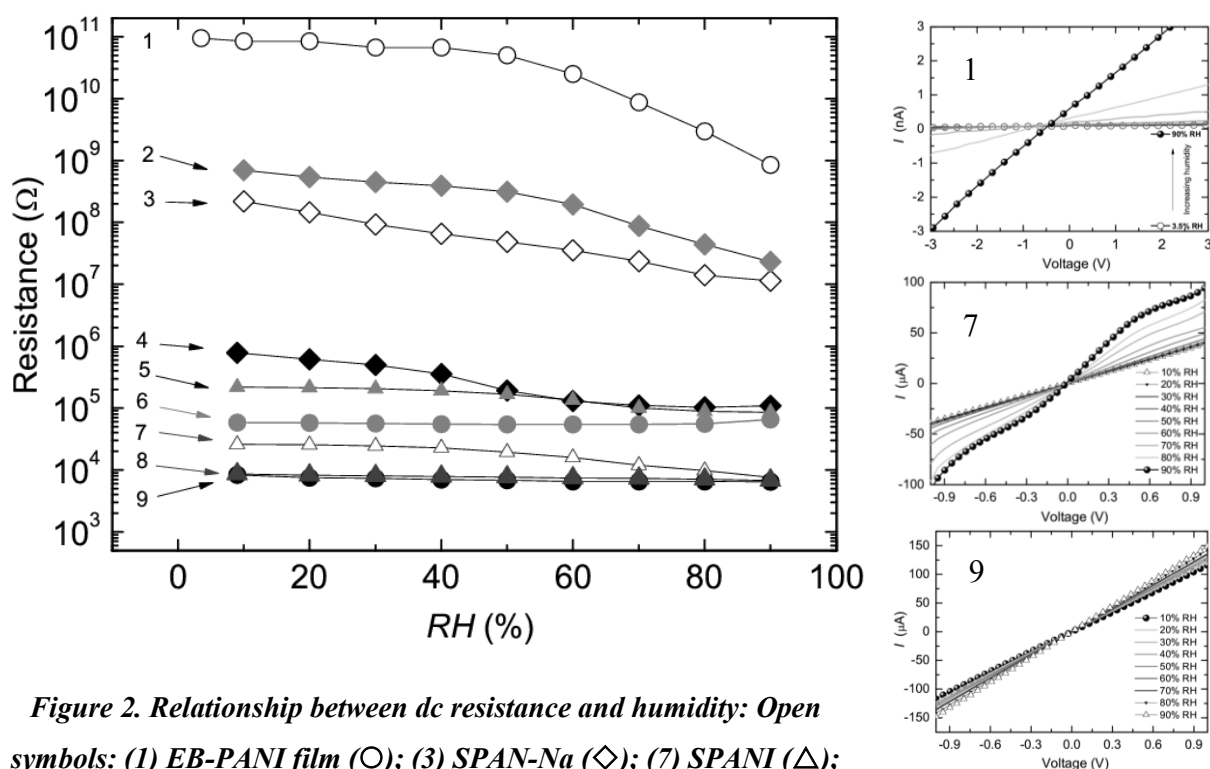


Figure 2. Relationship between dc resistance and humidity: Open symbols: (1) EB-PANI film (○); (3) SPAN-Na (◇); (7) SPANI (△);

Closed symbols (dark) (9) acid-doped PANI (●); (4) acid-doped SPAN-Na (◆); (8) acid-doped SPANI (▲); Grey shaded symbols Blends of PVA: (2) SPAN-Na:PVA (◇); (5) acid-doped SPANI:PVA (▲) and (6) acid-doped PANI:PVA (●) are also shown. For all our interdigitated

electrodes (IDE)-based devices, the Zaretsky cell constant is given by 0.215 cm^{-1} , hence the measured conductivity in all our samples is $\sigma = 0.215/R$ (Appendix 1). On right side are the I-V measurements of EB-PANI (top), SPANI (middle) and acid doped SPANI (bottom) (for details please see Appendix 2, Figures A3-A4).

To study the influence of humidity, measurements were carried out using a 2-point dc method to measure the resistance of the polymer films at varying water vapor concentration. **Figure 2** shows dc resistance (R) of undoped EB-PANI and SPAN-Na in the humidity range of 10 % to 90% RH. The I-V measurements from the samples were found to be linear (ohmic behavior) within the $\pm 0.3 \text{ V}$ range. A comparison is made with acid doping in PANI, SPANI and SPAN-Na films. The as-prepared EB-PANI films show very high resistance in the order of 10-100 G Ω while the resistance of the as-prepared SPAN-Na and SPANI films respectively is 3 to 7 orders of magnitude smaller. The observed difference can be explained in terms of the self-doping nature of SPAN-Na/SPANI films. The presence of sulfonic groups along the PANI backbone results in relatively higher protonation of the imine sites causing the resistance to decrease. The gap in resistance between SPAN-Na and SPANI is due to the presence of bound sodium ions preventing protonation [46].

External doping with protons from acidic buffer solutions can also lower the resistance. We observe this in the case of acid-doped SPANI and acid-doped PANI films which are almost in the same range, whereas the acidic doping of an EB-PANI film with pH 1 causes the resistance to drop by 7 orders of magnitude. However, in the case of acid doping in SPAN-Na, there is only a factor of 100 change. This relatively smaller change may be caused by the presence of still bound Na^+ ions to the sulfonate groups of the polymer backbone. Also steric hindering effects depending on the degree of sulfonation may influence the effect of self-doping [46].

The small difference between the dc conductivities of SPANI and acid-doped PANI can be explained due to the “self-steric effects” of the sulfonic groups [34]. The presence of the sulfonic groups causes a structural reorientation along the polymer chain which results in restricted sites available for protonation while in the case of EB-PANI, the amine and imine sites on the polymer chain are completely protonated by acid doping causing the resistance to decrease more significantly.

In the case of SPAN-Na, the acidic buffer will partially replace the sodium ions and protonation takes place at the “vacant” amine and imine sites as shown in **Figure 3**.

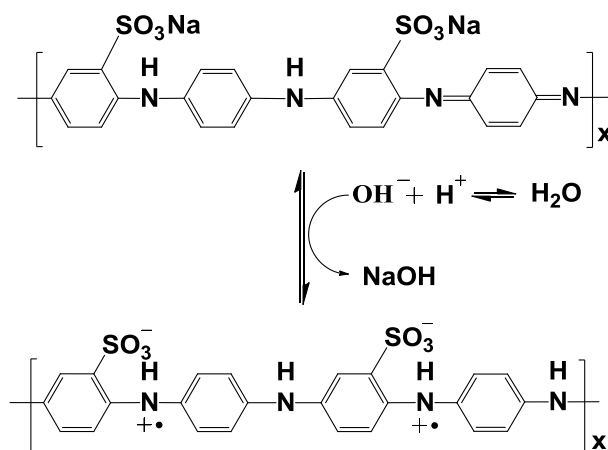


Figure 3. Conversion from insulating SPAN-Na to self-doped conducting SPANI through exchange of sodium ions to protons.

Also all ac resistances severely decrease when the films are gradually exposed up to 90% RH. In addition to the increase in the intrinsic (dc) conductivity we propose two possible ionic transport mechanisms for the observed increase in ac conductivity of the films upon exposure to water vapor. One, it is possible that the conductivity can change due to presence of water molecules with subsequent dissociation in H^+ and OH^- in the film facilitating hopping of protons over the water molecules aligned along the polymer backbone (Grotthuss mechanism) [47]. Two, the possibility could be due to the transport of (hydrated) sodium ions.

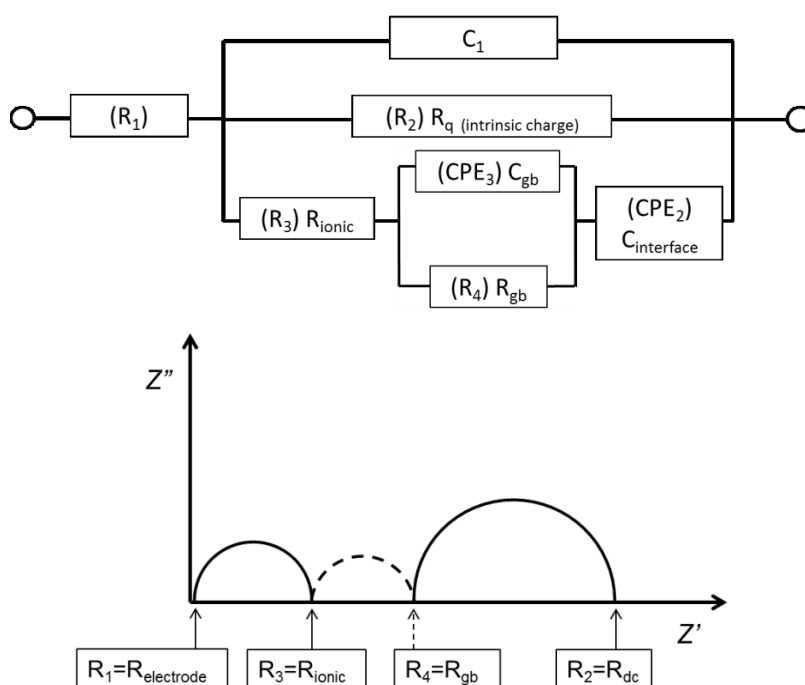


Figure 4. Analytical electrical circuit model aiming to discriminate between two distinct charge transport mechanisms within the conducting polymer films in the presence of humidity. R_1 represents the contact resistance of the blocking electrodes. A parallel branch of C_1 and R_2

represents the intrinsic charge transport through the film. The branch with R_3 represents ionic charge transport, and R_4/CPE_3 represent grain boundary effects in some samples. A typical corresponding Nyquist plot resulting from the circuit is depicted in the bottom graph, in the case that the ionic transport resistance is much smaller than intrinsic (dc) charge transport.

In **Figure 4** we put forward an equivalent model to unravel intrinsic charge transport (R_q) and ionic charge transport (R_{ionic}) based on the layout as presented in **Figure 1**. This model is hopefully generic to pure and blended materials and for all humidity conditions. R_q can be associated with doping of the polymer chain by external pH buffers, protonation of the polymer chain by water molecules and self-doping effects, whereas R_3 takes into account the resistance change due to the Grotthuss mechanism and the movement of free anions or cations in the presence of water molecules.

Please note that electron-hole transport via water molecules adsorbed on the polymer chain is also possible (similar to electron-hole transport in p-type semiconductors). Instead of proton (H^+) hopping (cf. Grotthuss mechanism), only the charge (as an electron-hole) is transferred to a neighboring water molecule, without a net movement of the nucleus (the proton). We consider this as an intrinsic conduction contribution. As mentioned earlier, R_q can range from 10^8 - $10^{11} \Omega$ for as-prepared undoped films and 10^3 - $10^6 \Omega$ for the doped films.

Since there are two time constants associated with film/chip capacitance (C_1) and the interfacial film/electrode capacitance (C_2), one should be able to use this model to represent Nyquist plots representing two semicircles. In some cases, a third semicircle appears in the intermediate frequency region which could be described by a third time constant (CPE_3 and R_4). While in the case of inorganic ionic conductors, it describes a grain boundary impedance and in some cases binary phase materials, it is difficult to ascertain the physical origin [30, 31]. Hence it is applied as a correction factor in this work and leave it open to interpretation.

Without the R_4/CPE_3 element in **Figure 4** we could have a simple Randle's circuit with a corresponding Nyquist plot comprising a high frequency semicircle and a low frequency second semicircle [28, 48].

Description of the fitting procedure: In order to fit our experimental data, we started out with a normal Randle's circuit model, consisting of one resistor R_3 and two capacitances CPE_1 , CPE_2 . Before the Randle's circuit a series resistance R_l was placed to include the interdigitated electrode contact resistance and in parallel with the Randle's circuit an extra resistance R_2 , to describe the (finite) dc resistance. After having obtained a reasonable fit for

R_2 and CPE_1 , we fix the latter parameters while CPE_2 and R_3 is then fitted, together with its coefficient n_2 (between 0.5 and 1.0). We see that it may occur a considerable deviation from $n \sim 0.5$ and this cannot be explained alone by a Warburg impedance effect. There are two issues to adopting this model. One, from literature, this model has been mainly applied to polymer-coated metal electrodes exposed to electrolytic solutions and non-blocking electrodes, where the diffusion component is correlated to the charge transfer resistance and double layer capacitance at the electrode. In our case, we have electrodes which block the ionic species in consideration. Secondly, it is not known to discriminate or distinguish between ionic and intrinsic charge transport. In literature it is known that the model does not fully describe the physical system and/or the physical processes associated with it, and should be considered as a pure phenomenological approach. We have chosen the extended Randle's model as described in **Figure 4** and we split up the cases with respect to the fitting procedures. Case I) Low humidity: This is described by a simple R-C element in parallel. Here R_2 was kept fixed while CPE_1 (C_1) (P_1 and n_1) were varied. Case II) Intermediate humidity: The R_2 was kept fixed, while C_1 was set free. Following this, R_2 and C_1 was fixed while R_3 and CPE_2 were kept free for fitting. Case III) High humidity: the same procedure as case 2 was followed. However an additional element comprising R_4 and CPE_3 was set free for fitting while the remaining parameters were kept constant. Thus, a stepwise analysis was carried out until all parts of the Nyquist plot gave a reasonable fit. As a final check, the analysis was extended to the entire curve with R_2 , C_1 , R_4 , CPE_3 was kept fixed while R_3 and CPE_2 was kept free. No deviation from the fit was observed in this case and a convergent iteration was verified. The Powell algorithm with amplitude functionality was applied and the total number of iterations was limited to 5. In most cases, the procedure was checked for the residuals errors less than 5%. We found that above 5 iterations, the quality of fit did not change significantly and we could obtain good agreement. In section 3.2 we figuratively describe the trends observed in the corresponding fits.

Samples with a purely intrinsic charge transport or purely ionic charge transport in combination with blocking electrodes can be described with a single semicircle, while a combination of intrinsic charge transport and ionic transport (involving e.g. Na^+ ions) may results in the appearance of a second semicircle [30]. Acidic doping of SPAN-Na:PAA and SPAN-Na:PVA blends would behave similarly due to hydrophilic nature associated with PAA and PVA. It can be argued that proton hopping (Grotthuss mechanism) may lead to protonation of imine and amine sites contributing to intrinsic conduction and as explained

above that proton hopping can in a way also be considered as electron-hole transport via water molecules, implying that a large part of the Grotthuss mechanism can be considered as pure intrinsic transport [49, 50]. In the following section we will investigate this.

3.2. Ac Measurements: Humidity Dependence in Acid-doped and Self-doped Films

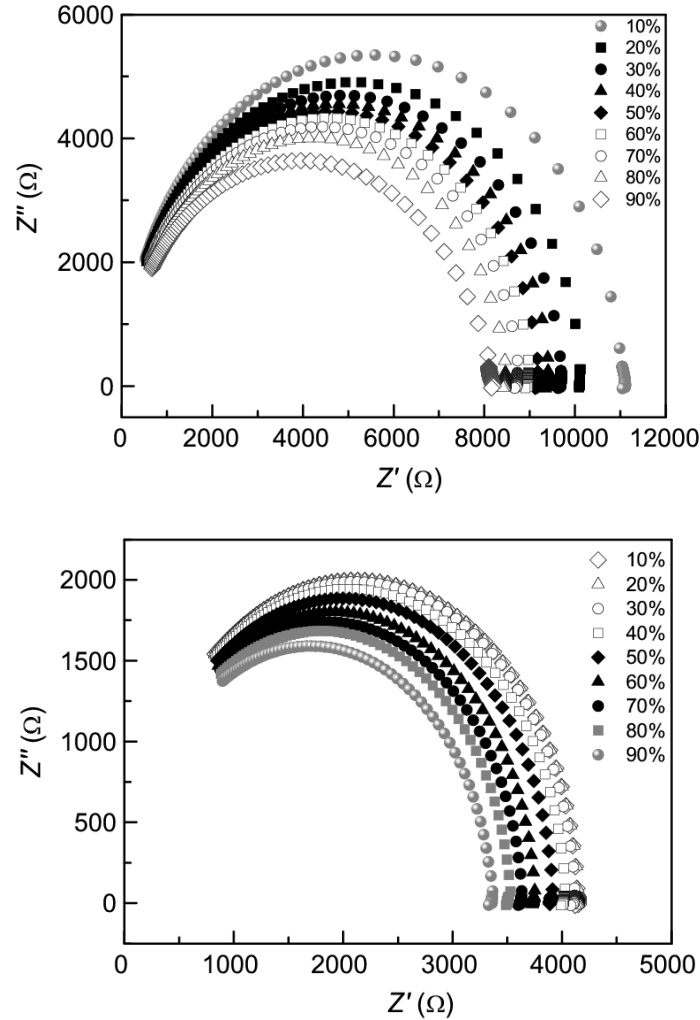


Figure 5. The Nyquist plots of acid-doped EB-PANI (1:1) (top) and acid-doped SPANI (bottom) measured in the humidity range from 10 to 90% RH.

In case of purely intrinsic charge transport, the model represented in **Figure 4** can be simplified to a single R-C circuit (R_2 , C_1). In the case of films where intrinsic charge transport R_q is truly dominant [51], the film resistance can drop from 1 k Ω to 10 k Ω . For our acid-doped PANI films and acid-doped SPANI films (**Figure 5**), we see that indeed a single semicircle is seen. Increasing the water vapor concentration up to 90% RH is also marked by only one semicircle and thus an absence of a second semicircle ruling out the possibility of a substantial additional ionic conduction mechanism leading to the built up of blocking ions at the polymer/electrode interface.

The blends of the as-prepared acid-doped SPAN-Na:PAA, SPANI:PVA and acid-doped PANI:PVA samples show a single semicircle only at very low humidity as seen in **Figure 6**.

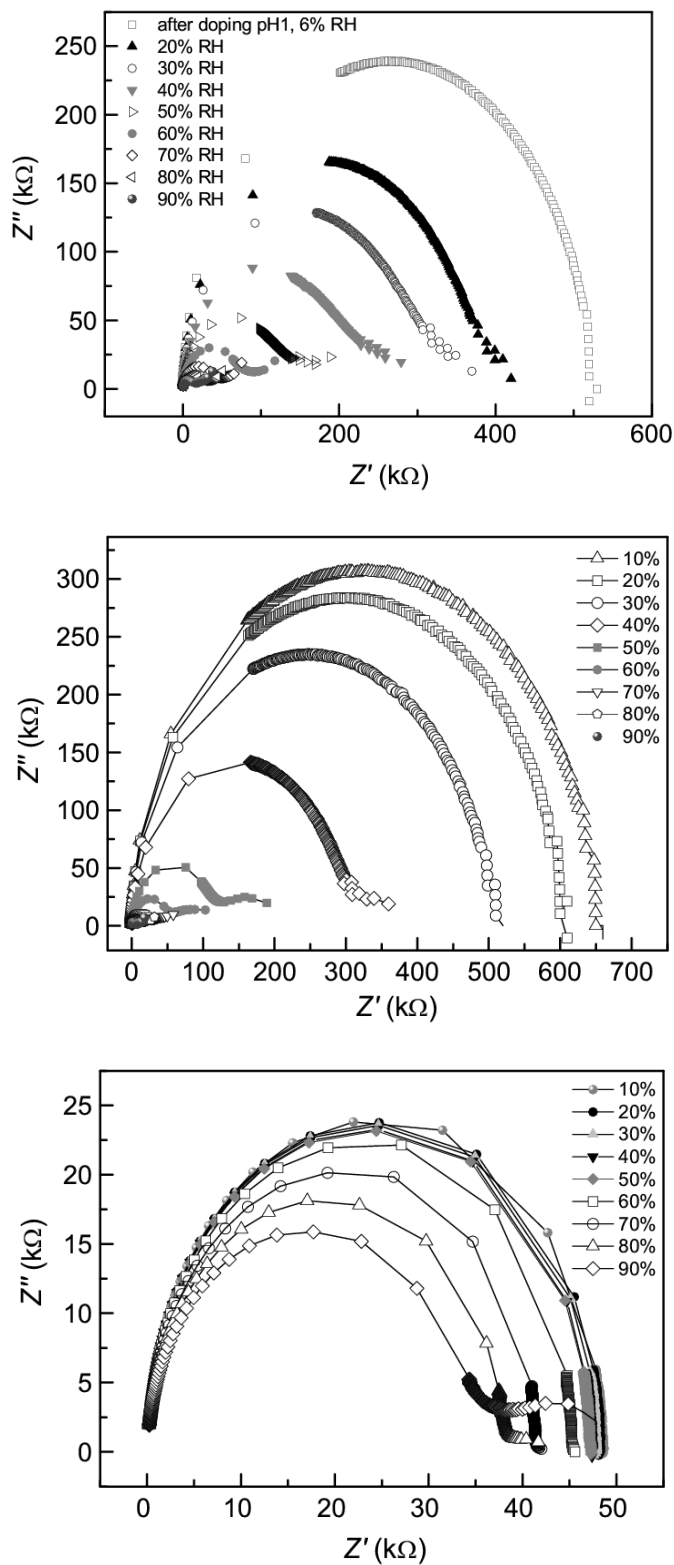
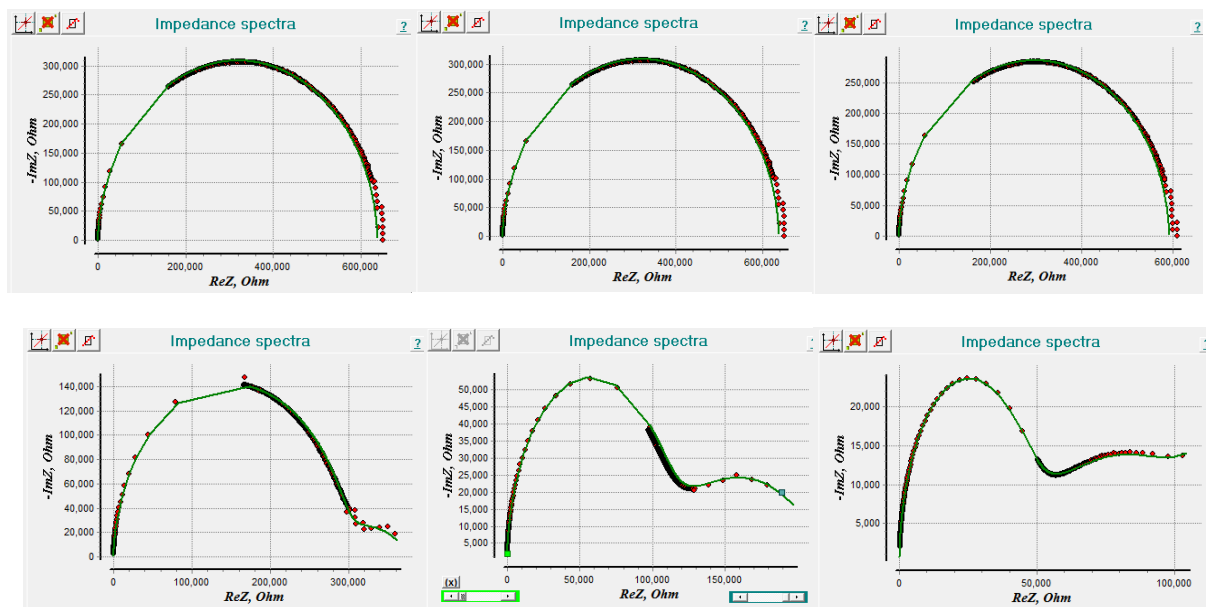


Figure 6. The Nyquist plot of acid-doped SPAN-Na:PAA (1:1) (top), SPANI:PVA (middle), acid-doped PANI:PVA (bottom) measured in the humidity range from 10% to 90% RH.

At high humidity above 40% RH the appearance of a second semicircle is observed for all three samples. Please note that, below 40% RH the (large) semicircle has a radius related to R_2 (intrinsic conductivity), whereas above 40% RH two semicircles appear, wherein the larger one (on the left of the plot) has a radius related to R_3 (ionic conductivity). R_3 in series with CPE_2 describes the ionic charge resistance from ionic charges out of the polymer film to condense on the electrode/polymer interface. $R_{Nyquistionic}$ is the radius of the high frequency semicircle in the Nyquist plot and can be derived from $1/R_{Nyquistionic} = 1/R_3 + 1/R_2$ [35]. We will see and explain that when R_3 decreases the value of CPE_2 increases (at higher humidity levels). A qualitative difference between the three samples is that while SPAN-Na has Na^+ ions, acid-doped PANI and SPAN-Na do not contain Na^+ ions. The ions accumulating at the polymer/electrode interface are presumably OH^- , H^+ and Na^+ . Please note that if the H^+ protons (including the nucleus) accumulate at the electrode interface this can be considered as a real ionic contribution (the same applies for the OH^- ions). It is known from literature that both H^+ and OH^- charges migrate much faster through the H_2O lattice bath than can be assumed from a pure mechanistically standpoint.

In **Figure 7** we represent the experimental trends of SPANI:PVA together with the fits in the humidity range from 10 to 90% RH.



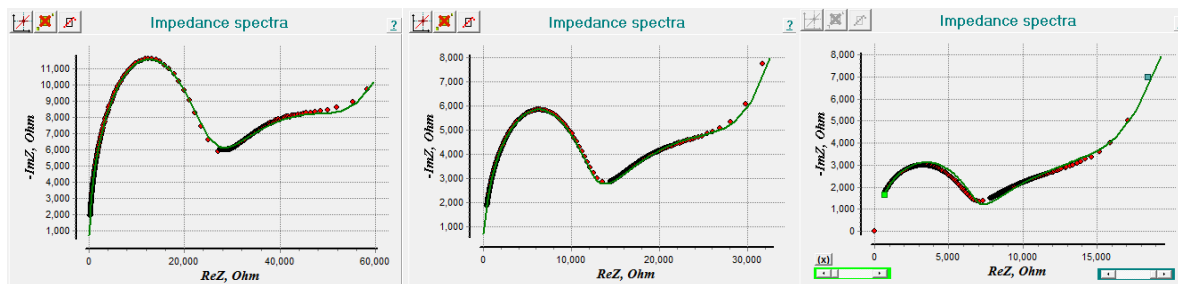


Figure 7. Nyquist plot with fits of SPANI:PVA measured in the humidity range from 10% to 90% RH (top row: 10% RH, 20% RH, 30% RH; middle row: 40% RH, 50% RH, 60% RH and bottom row: 70% RH, 80% RH and 90% RH). At higher humidity (above 70%) the first semicircle (on the left) is related to ionic transport at the polymer/electrode interface and has a Nyquist radius R_{Nionic} and can be derived $1/R_{Nionic} = 1/R_3 + 1/R_2$ with R_3 and R_2 - the fitted resistance values of the equivalent circuit. The second semi-circle could be related to ionic transport through the grain boundaries present in the bulk film, and the onset of the third semicircle is related to intrinsic transport of charge carriers through the bulk from one electrode to the other electrode.

It is very likely that when ionic conduction processes manifest themselves at the polymer/electrode interface due to protons, hydroxyl and sodium ion transport it is likely that they also play a measurable role in the bulk (from one electrode to the other electrode). In acid-doped SPAN-Na samples, sodium ions contribute to a combination of both ionic processes, while in acid-doped PANI:PVA and SPANI:PVA, the H^+ and OH^- ions contribute. Normally the Grotthuss mechanism is only associated with ionic transport of H^+ (mechanistically transport of the proton nucleus) and PVA has been known to enhance the Grotthuss mechanism as shown from previous studies [50]. A Nyquist measurement at 90% RH was carried out in pure PVA sample and more than one semicircle is observed, hinting at different transport processes (See **Appendix 2 - Figure A19**). A more quantitative analysis of the trends with respect to ionic (at the interface and in the bulk) and intrinsic charge transport is discussed in the next section. **Conclusion:** In acidic and self-doped films, it is purely intrinsic charge transport (charge doping by buffers and water molecules), while in the case of blended films, it is combination of intrinsic charge transport, ion transport processes at the polymer/electrode interface and a contribution of (unknown) grain boundaries effects in the bulk.

3.3. *Ac Measurements: Humidity Dependence in Undoped films (EB-PANI and SPAN-Na) and Their Blends*

For conducting polymers, which are not doped by acidic buffers, it is expected that protonic doping might originate from water molecules, from hydrogen bonding and/or dissociated protons. We consider here the case where the water vapor concentration is high at 80% RH. To enhance the water adsorbing mechanism, the samples are also blended with PVA. PVA is a nonionic, water-soluble polymer and the presence of -OH groups along the polymer backbone gives it a strong hydrophilic character [15]. In blending with EB-PANI, there is a proposed formation of hydrogen bonding between -OH groups of PVA and =N-H or -N-H groups of EB-PANI [52].

Figure 8 shows an overlay of Nyquist plots measured at 80% RH of blended and non-blended films, with and without sulfonation of PANI. Also a plot of a pure PVA film is depicted. We notice that the EB-PANI film has a very high dc resistance (10-100 G Ω) and full semicircle(s) can thus not be observed. The addition of PVA has little effect on the conductivity plot of the EB-PANI film. A pure PVA films has a similar shape and is even lower in absolute resistance than the undoped EB-PANI films for all measured frequencies (5 Hz - 1 MHz). Pure PVA can be made more conducting by addition of acids [53, 54] but without that proton hopping of dissociated water molecules (Grotthuss mechanism) is the main conduction mechanism [50, 55]. The measured conductivity in the blended films can therefore partially be explained by the hydrophilic nature of PVA where hydrogen bonding between -OH groups and dissociated water molecules allows for proton hopping transport to occur [56].

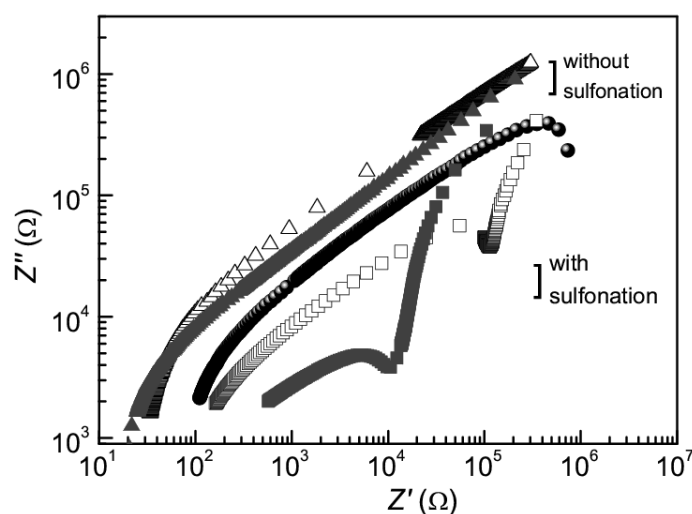


Figure 8. Nyquist log-log plots measured at 80% RH of EB-PANI (\blacktriangle), EB-PANI:PVA (1:1) (\triangle), PVA (\bullet), SPAN-Na (\blacksquare) and SPAN-Na:PVA (1:1) (\square).

The presence of charged sulfonate groups on the polymer backbone with sodium counterions is known to make the polymer film very hydrophilic and attract additional water molecules [34]. A qualitative look at the Nyquist plots of pure SPAN-Na film (**Figure 8**) shows that the film behaves like a polyelectrolyte at high humidity characterized by the appearance of a high frequency semicircle component and a low frequency semicircle probably associated with Warburg behavior. The SPAN-Na and SPAN-Na:PVA films show a lower absolute impedance and a clear start of a second semicircle. The ionic mobility along the SPANI chain could be hindered in the presence of PVA and could explain the observed lower conductivity in SPAN-Na:PVA [57, 58]. At a high water vapor concentration, there are polymer sites on the SPAN-Na backbone which are still not interlinked with PVA and reside in pores [59]. In such a possible scenario, the Na^+ ions under the influence of water molecules decouple from the sulfonate groups and become mobile in the porous regions of the blended polymer film [34]. Under high humidity, in SPAN-Na:PVA blends hydrogen bonding is not only created between -OH groups of PVA but also with the =N-H, -N-H groups [60]. Hence addition of PVA might change the interactions between SPAN-Na and water molecules. Differential scanning calorimetry DSC measurements have shown that up to two water molecules interact with each hydroxyl group of a PVA monomer [58].

We summarize the possible mechanisms for the observed conduction in the case of above discussed undoped films (with and without sulfonate groups) blended with PVA. One, the films are intrinsically doped by protonated species arising from water molecules [42]. Two, in the case of sulfonated films diffusion of ionic species such as Na^+ ions may contribute. Three, proton hopping via the Grotthuss mechanism contributes to (ionic and intrinsic) conductivity [41]. For pure EB-PANI films ionic transport mechanisms seem to be absent. In the case of undoped SPAN-Na films, intrinsic, sodium ion transport, and proton hopping influence the total impedance.

The systematical variation in humidity-dependent conductivity of SPAN-Na films by ac impedance spectroscopy is shown in **Figure 9**. The presence of hydrophilic sulfonate groups on the polymer backbone and the interaction of the dissociated water molecules can protonate the amine and imine nitrogen atoms in polymer backbone [41].

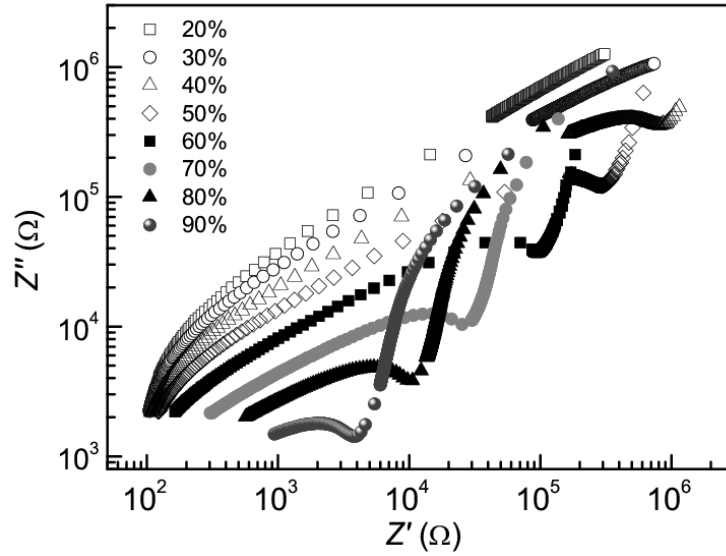


Figure 9. Nyquist plot of SPAN-Na as a function of humidity changes (10-90% RH).

In **Figure 9** a Nyquist plot of SPAN-Na film from 20% to 90% RH is represented. Below 50% RH, a single high frequency semicircle is anticipated and can possibly be explained with intrinsic charge transport (R_q) only. At higher humidity a full high frequency semicircle can be distinguished and fitted. Fitting of a constant phase element (CPE_I) gives a near ideal behaviour. The $CPE = P*(j\omega)^n$ where the exponential factor n accounts for non-ideality and can range in this case from 0.90 to 1 [61]. Please note that CPE_I is almost equivalent to the blank chip capacitance of 85 pF. The low frequency region displaces the onset of a second semicircle. When the ionic resistance R_3 becomes much lower than the dc resistance R_2 and at the same time the polymer/electrode interfacial capacitance C_2 becomes much larger than C_I it can be approximated that in the Nyquist plot the radius of the first semicircle on the Z' axis is almost the ionic resistance R_3 and the height (Z'') of the second semicircle is related to the ionic capacitance $1/i\omega C_2$. As mentioned earlier, ionic transport is present at low to intermediate frequencies with corresponding $R_3 C_2$ times. The interfacial capacitance (C_2) is due to the charge/ion accumulation at the blocking polymer/metal electrode interface.

Blended films of SPAN-Na:PVA give a good fit with two semicircles in the intermediate to lower frequency region (see fittings in **Appendix 2 - Figures A7-A9**), so in total these curves are fitted with three semicircles (cf. **Figure 7**). In all our samples we have used the model as described in **Figure 4** to extract the intrinsic charge conduction R_2 , ionic charge conduction – R_3 , capacitive double layer C_2 and the film/blank chip capacitance C_I . The trends for extracted parameters will be described in the next section. **Table 1** below qualitatively summarizes the conduction mechanisms in PANI and SPANI.

Table 1. Summarizing the possible interplay of conduction mechanisms in PANI, its derivatives and blends as humidity concentration is varied.

Polymer	Intrinsic charge conduction			Ionic conduction (Na ⁺ ions) Grotthuss mechanism (proton hopping)
	Intrinsic doping (ext) Acid pH buffers	Intrinsic doping (protonation from water molecules and electron-holes transport from Grotthuss)	Sulfonated	
EB-PANI	-	√	-	-
SPAN-Na	-	√	√	√
SPAN-Na:PVA	-	√	√	√
SPANI	-	√	√	-
SPANI:PVA	-	√	√	√
Acid-doped PANI:PVA	√	√	-	√
Acid-doped SPANI	√	√	√	-
Acid-doped PANI	√	√	-	-
Acid-doped SPAN-Na	√	√	√	√
PVA	-	-	-	√

3.4. Intrinsic versus Ionic Charge Transport in PANI, SPAN-Na and Its Derivatives

Most studies to date are focused on metal electrode coated films completely immersed in a solution. One can imagine this situation when the polymer is exposed to a very high humidity as shown in the work of Casalbore-Miceli et.al [43]. In addition, dc measurements are normally not explicitly coupled with ac measurements. In our study, we have specifically dealt with correlating dc with ac measurements so that the ionic and intrinsic charge transport conductivity can be extracted. From our experimental data we have seen that impedance of the films changes as a function of humidity. Using the discussed model in **Figure 4**, we analyzed the experimental data in terms of an electrical analytical circuit to distinguish between ionic and intrinsic charge transport. The trends for intrinsic charge transport resistance ($R_2 = R_q$ - indicated by closed symbols) and ionic resistance ($R_3 = R_{ionic}$ - indicated

by open symbols) for SPAN-Na, PANI, acid-doped samples, SPANI and their blends show linearity in the entire range as seen in **Figure 10**.

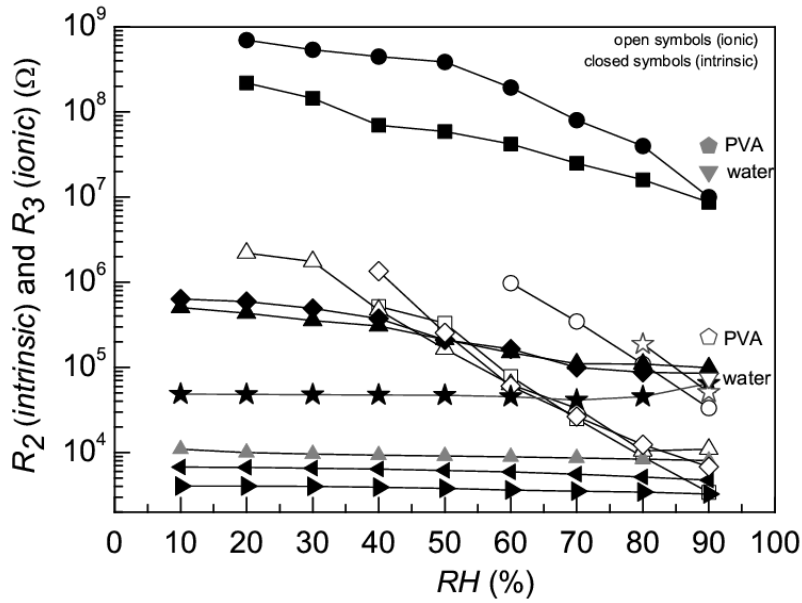


Figure 10. Dependence of intrinsic charge transport (R_2) on humidity is represented by closed symbols: pure SPAN-Na (■), SPAN-Na:PVA (●), acid-doped SPAN-Na (▲), SPANI (◄), acid-doped SPANI (►), SPANI:PVA (◆), acid-doped PANI (▲), acid-doped PANI:PVA (★).

Dependence of ionic charge transport (R_3) on humidity represented by open symbols as seen in SPAN-Na (□), SPAN-Na:PVA (○), acid-doped SPAN-Na (△), SPANI:PVA (◇) and acid-doped PANI:PVA (☆). In addition, the R_2 and R_3 values for pure PVA and DI water droplet are included for comparison. For all our IDE-based devices, the Zaretsky cell constant is given by 0.215 cm^{-1} , hence the conductivity in all our samples can be expressed as $\sigma = 0.215/R$ (Appendix 1).

In the undoped samples, a factor 100-10,000 difference is obtained between R_q and R_{ionic} . It is also seen that protonic conduction changes significantly as RH is increased. In the undoped samples, the decrease in resistance is caused likely by the source for protonation of sites along the polymer backbone. These can arise from two sources 1) from dissociated water molecules and/or 2) self-doping effects of sulfonate groups. If it is due to water molecules, the effect is partial but still significant. If it is due to sulfonate groups, then it should approach resistance values of pure SPANI (indicated by symbol (◄)), which is not observed in our case. Hence, change in $R_2 = R_q$ for SPAN-Na and SPAN-Na:PVA is most likely caused by protonation from water molecules as water vapor concentration increases. The low $R_3 = R_{ionic}$ can be caused by the higher mobility of the Na^+ ions and other ionic species which increases as water vapor concentration is increased. This has an effect on the interfacial capacitance C_2 that strongly increases at higher humidity levels as seen in **Figure 11** and **Figure 12**. An

explanation for this is the increase of the relative dielectric constant at the polymer/electrode interface through the increase of the amount of water in the corresponding polymer film (see below). This effect in C_I is not observed because this value is overshadowed by the blank chip contribution (85 pF).

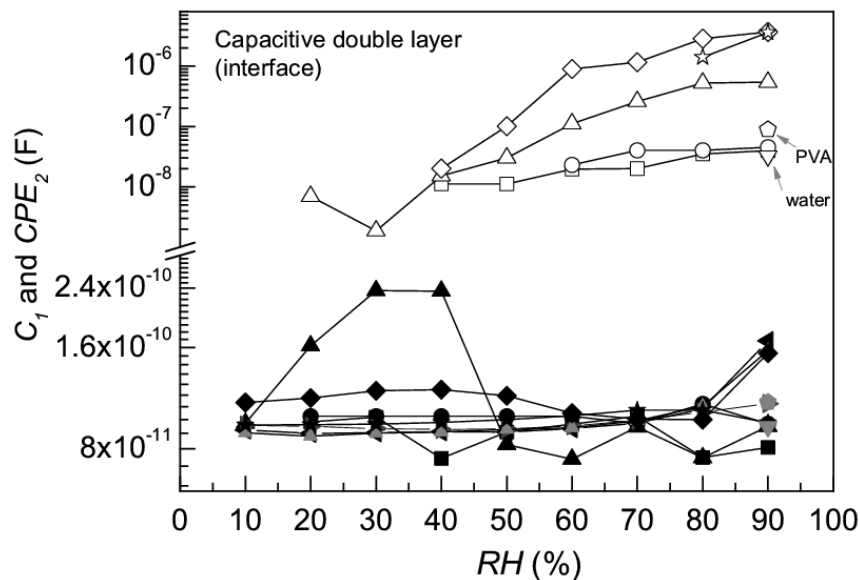


Figure 11. Dependence of capacitance C_1 (closed symbols) on the relative humidity in the case of SPAN-Na (■), SPAN-Na:PVA (●), acid-doped SPAN-Na (▲), SPANI (◄), SPANI:PVA (◆), acid-doped SPANI (►), acid-doped PANI (▲), acid-doped PANI:PVA (★). Dependence of interfacial electrode/polymer capacitance CPE_2 on the relative humidity is seen only in SPAN-Na (□), SPAN-Na:PVA (○), acid-doped SPAN-Na (△), SPANI:PVA (◇) and acid-doped PANI:PVA (☆).

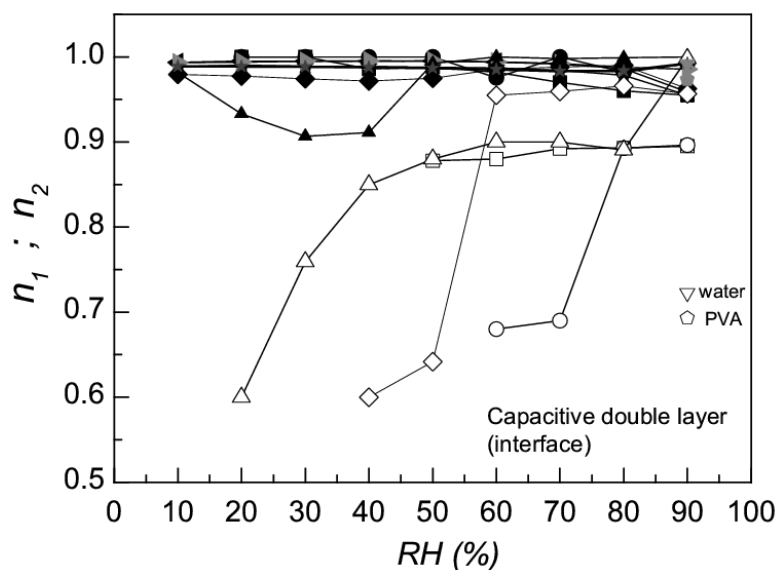


Figure 12. Dependence of n_1 (closed symbols) on RH of SPAN-Na (■), SPAN-Na:PVA (●), acid-doped SPAN-Na (▲), SPANI (◄), SPANI:PVA (◆), acid-doped SPANI (►), acid-doped PANI (▲)

and acid-doped PANI:PVA (★). Dependence of n_2 (open symbols) on the relative humidity is seen only in SPAN-Na (□), SPAN-Na:PVA (○), acid-doped SPAN-Na (△), SPANI:PVA (◇) and acid-doped PANI:PVA (☆). In addition, the C_1 , n_1 and C_2 and n_2 values for pure PVA and DI water droplet are included for comparison.

While the protonation due to water molecules is strongly visible in the case of undoped SPAN-Na and its blends, in the case of acid-doped (PANI, SPANI) and SPANI samples that intrinsic charge transport (due to external acid doping) is a dominant conduction mechanism and hence only R_q is visible. We see no second semicircle implying ionic conduction and the presence of a large interfacial capacitance layer is absent in the entire humidity range. While the film capacitance (as seen in **Figure 11**) is almost constant at ~ 100 pF [26, 62, 63], the decrease in R_q (at high RH) could be due to dissociated water species and subsequent protonation.

Finally, we consider the interesting situation of an intermediate case, where Nyquist plots are generated from acid-doped SPAN-Na:PAA (PAA is added to prevent dissolution of SPAN-Na during pH treatment), SPANI:PVA and acid-doped PANI:PVA samples. The plots are characterized by the appearance of an unambiguous third circle at intermediate frequencies (See **Appendix 2 – Figures A10-A18** for the plots). It has been argued this can be due to grain boundaries associated with binary phase systems or simply undefined as a correction factor to obtain a good fit [30]. This has also been observed earlier with respect to binary phase inorganic ionic conductors [31]. However it is difficult to verify the formation of a “secondary phase” in our homogeneously doped samples as seen in **Figure 7**, R_q in the acid-doped SPAN-Na competes with R_{ionic} and it is not only present in the same range but also overlaps with a similar trend from SPANI:PVA. A crossover form between R_q and R_{ionic} is observed in both cases probably suggesting that the intrinsic charge conduction and ionic conduction occur along closed spaced channels. While the film capacitance C_1 does not change much, the interfacial capacitance CPE_2 shows significant variation between the films. While the undoped films show a slight increase and saturate at $0.05 \mu\text{F}$, the self-doped and acid-doped films show a rather significant trend increasing up to $5 \mu\text{F}$. This is a factor 100 difference between the samples. The formation of a double layer is not only a result of the ionic species strongly adsorbing onto to the electrode surface but also on the concentration and the type of species involved. The electrode surface is always covered by some combination of anions and cations and the capacitance results from the change of their ratio on traversing the voltage range. A simple calculation can show that while the inner layer bulk

capacitance is independent of the voltage and bulk defect concentration given by $C_2 = \kappa \epsilon_0 / d_c$

where κ is relative dielectric constant of the medium, ϵ_0 is the effective dielectric constant ($8.854 \times 10^{-12} \text{ F.m}^{-1}$) and d_c is electrode gap (distance of closest approach of the charge centers of the current carrying ions). The ionic double layer charge appears as a slight excess of cations over anions in the interfacial ion layer depending on the polarity of the electrode. For the ionic double layer, we could assume $\kappa \sim 1$, $d_c \sim 1 \text{ \AA}$ for H^+ ions and Na^+ for 3 \AA we find that interfacial capacitance for an electrode area of $124 \times 300 \text{ \mu m} \times 9 \text{ \mu m}$, the interfacial capacitance per unit area for 0.05 to 5 \mu F varies between 15 - $1,500 \text{ F/cm}^2$. This is the range of capacitances consistent with earlier trends [64]. Second we also observe that magnitude of the interfacial capacitance is dependent not only the size of the adsorbed species but also on the concentration of the ionic species and the mobility of the ionic species [64]. To our understanding an explanation for the dependence on humidity is the increase of the relative dielectric constant at the polymer/electrode interface through the increase of the amount of water in the corresponding polymer film.

While in the case of acid-doped SPAN-Na, we could argue that despite the relatively low concentration of ionic species (Na^+), the ionic mobility of sodium ions under an applied electrical field leads to a substantial buildup of interfacial capacitance in comparison to SPANI:PVA or acid-doped PANI:PVA samples. In the latter the PVA merely adsorbs more water molecules in the film and a subsequent increase of the relative dielectric constant at the polymer/electrode interface yielding higher C_2 values.

4. Conclusions

Humidity-dependent conductivity of SPAN-Na and its blends with PVA have been studied. A comparison has been made of EB-PANI, SPANI and acid doped films blended with PVA. A generic equivalent circuit model to describe and discriminate between ionic and intrinsic conduction has been proposed and we were able to describe the ac/dc response in a wide range of humidity conditions for all samples.

Undoped films of PANI show partial protonation from dissociated water molecules and show a significant drop in resistance on increasing the humidity. Only intrinsic charge transport and no ionic conduction is observed. Addition of sulfonate groups increases the self-doping effect causing 4 orders of magnitude change in resistance. In SPANI and acid doped samples intrinsic charge conduction dominates at both low and high humidity levels. Both ionic

conduction and intrinsic charge transport mechanisms are normally present only at high humidity in samples with an intermediate dc resistance between 10^5 and $10^9 \Omega$ ($2 \mu\text{S}\cdot\text{cm}^{-1}$ to $0.2 \text{ nS}\cdot\text{cm}^{-1}$) depending on the type of samples. In Nyquist plots generated from acid doped SPAN-Na:PAA, SPANI:PVA and acid-doped PANI:PVA samples a third semicircle is seen which can be described by an additional RC element attributed to an additional phase or grain boundary structure.

References

- [1] M. Park, X. Zhang, M. Chung, G.B. Less, A.M. Sastry, A review of conduction phenomena in Li-ion batteries, *Journal of Power Sources*, 195 (2010) 7904-7929.
- [2] H. Gisleröd, A. Selmer-Olsen, L. Mortensen, The effect of air humidity on nutrient uptake of some greenhouse plants, *Plant and Soil*, 102 (1987) 193-196.
- [3] Z. Chen, C. Lu, Humidity sensors: A review of materials and mechanisms, *Sensor Letters*, 3 (2005) 274-295.
- [4] Y. Sakai, Y. Sadaoka, M. Matsuguchi, Humidity sensors based on polymer thin films, *Sensors and Actuators B: Chemical*, 35 (1996) 85-90.
- [5] J. Janata, M. Josowicz, Conducting polymers in electronic chemical sensors, *Nat. Mater.*, 2 (2003) 19-24.
- [6] M. Gerard, A. Chaubey, B.D. Malhotra, Application of conducting polymers to biosensors, *Biosensors and Bioelectronics*, 17 (2002) 345-359.
- [7] M.S. Freund, B.A. Deore, Self-Doped Derivatives of Polyaniline, in: *Self-Doped Conducting Polymers*, John Wiley & Sons, Ltd, 2007, pp. 75-155.
- [8] V.N. Prigodin, F.C. Hsu, J.H. Park, O. Waldmann, A.J. Epstein, Electron-ion interaction in doped conducting polymers, *Physical Review B*, 78 (2008) 035203.
- [9] M.V. Kulkarni, A.K. Viswanath, R.C. Aiyer, P.K. Khanna, Synthesis, characterization, and morphology of p-toluene sulfonic acid-doped polyaniline: A material for humidity sensing application, *Journal of Polymer Science Part B: Polymer Physics*, 43 (2005) 2161-2169.
- [10] Y.S. Sonawane, M.V. Kulkarni, B.B. Kale, R.C. Aiyer, Electrical and humidity sensing properties of synthesized hydrophosphoric acid doped polyaniline, *Polymers for Advanced Technologies*, 19 (2008) 60-65.

- [11] T. Taka, Humidity dependency of electrical conductivity of doped polyaniline, *Synthetic Metals*, 57 (1993) 5014-5019.
- [12] H.S.M.N.A.O. K. Ogura, Thermal properties of poly(anthranilic acid) (PANA) and humidity-sensitive composites derived from heat-treated PANA and poly(vinyl alcohol), *Journal of Polymer Science Part A: Polymer Chemistry*, 37 (1999) 4458-4465.
- [13] S. Jain, S. Chakane, A.B. Samui, V.N. Krishnamurthy, S.V. Bhoraskar, Humidity sensing with weak acid-doped polyaniline and its composites, *Sensors and Actuators B: Chemical*, 96 (2003) 124-129.
- [14] S.T. McGovern, G.M. Spinks, G.G. Wallace, Micro-humidity sensors based on a processable polyaniline blend, *Sensors and Actuators B: Chemical*, 107 (2005) 657-665.
- [15] K. Ogura, T. Saino, M. Nakayama, H. Shiigi, The humidity dependence of the electrical conductivity of a soluble polyaniline-poly(vinyl alcohol) composite film, *Journal of Materials Chemistry*, 7 (1997) 2363-2366.
- [16] Y. Li, B. Ying, L. Hong, M. Yang, Water-soluble polyaniline and its composite with poly(vinyl alcohol) for humidity sensing, *Synthetic Metals*, 160 (2010) 455-461.
- [17] H.S. K.Ogura, T.oho, T.Tonosaki, Selectively sensitive polymer composites to humidity and CO₂, (2000).
- [18] A.J. Epstein, Yue, Jiang, Sulfonated polyaniline salt compositions and uses thereof, United States Patent, Patent: 5,159,031 (1992).
- [19] A.J. Heeger, In Situ Studies of Electrochemical Charge Transfer Processes in Conducting Polymers, *Molecular Crystals and Liquid Crystals*, 125 (1985) 289-302.
- [20] V.V. Malev, V.V. Kondratiev, Charge transfer processes in conducting polymer films, *Russian Chemical Reviews*, 75 (2006) 147.
- [21] A. Amirudin, D. Thieny, Application of electrochemical impedance spectroscopy to study the degradation of polymer-coated metals, *Progress in Organic Coatings*, 26 (1995) 1-28.
- [22] E.B. James Ross Macdonald, *Impedance Spectroscopy: Theory, Experiment, and Applications*, 2nd ed., John Wiley & Sons, 2005.
- [23] A.A.H. (Ed), B. Wang and R. N. Vyas, Chapter 3, Ion Transfer in Layer-by-Layer Films, *Polymer Thin Films*, in, InTech, 2010.
- [24] E.S. Matveeva, R. Diaz Calleja, V. Parkhutik, Equivalent circuit analysis of the electrical properties of conducting polymers: electrical relaxation mechanisms in polyaniline under dry and wet conditions, *Journal of Non-Crystalline Solids*, 235-237 (1998) 772-780.

- [25] W.J. Albery, Z. Chen, B.R. Horrocks, A.R. Mount, P.J. Wilson, D. Bloor, A.T. Monkman, C.M. Elliott, Spectroscopic and electrochemical studies of charge transfer in modified electrodes, *Faraday Discussions of the Chemical Society*, 88 (1989) 247-259.
- [26] K. Nitsch, B.W. Licznarski, H. Teterycz, L.J. Golonka, K. Wiśniewski, AC equivalent circuits of thick film humidity sensors, *Vacuum*, 50 (1998) 131-137.
- [27] T.C.D. Doan, R. Ramaneti, J. Baggerman, J.F. van der Bent, A.T.M. Marcelis, H.D. Tong, C.J.M. van Rijn, Carbon dioxide sensing with sulfonated polyaniline, *Sensors and Actuators B: Chemical*, 168 (2012) 123-130.
- [28] J.F. Robinson, Y.P. Kayinamura, Charge transport in conducting polymers: insights from impedance spectroscopy, *Chemical Society Reviews*, 38 (2009) 3339-3347.
- [29] C.A.C. Sequeira, M.J.C. Plancha, L.P.S. Araújo, Conductivity studies on solid polymer electrolytes, *J. Phys. IV France*, 04 (1994) C1-17-C11-35.
- [30] A.E. Javier, S.N. Patel, D.T. Hallinan, V. Srinivasan, N.P. Balsara, Simultaneous Electronic and Ionic Conduction in a Block Copolymer: Application in Lithium Battery Electrodes, *Angewandte Chemie International Edition*, 50 (2011) 9848-9851.
- [31] E. Horopanitis, G. Perentzis, L. Papadimitriou, Impedance modelling of two-phase solid-state ionic conductors. Part I - Theoretical model and computer simulations, *Journal of Solid State Electrochemistry*, 11 (2007) 1171-1182.
- [32] R. Huggins, Simple method to determine electronic and ionic components of the conductivity in mixed conductors a review, *Ionics*, 8 (2002) 300-313.
- [33] J. Yue, A.J. Epstein, Synthesis of self-doped conducting polyaniline, *Journal of the American Chemical Society*, 112 (1990) 2800-2801.
- [34] J. Yue, Z.H. Wang, K.R. Cromack, A.J. Epstein, A.G. MacDiarmid, Effect of sulfonic acid group on polyaniline backbone, *Journal of the American Chemical Society*, 113 (1991) 2665-2671.
- [35] P. Dutta, S. Biswas, M. Ghosh, S.K. De, S. Chatterjee, The dc and ac conductivity of polyaniline–polyvinyl alcohol blends, *Synthetic Metals*, 122 (2001) 455-461.
- [36] P.G. A. Sarkar, A. K. Meikap, S. K. Chattopadhyay, S. K. Chatterjee, M. Ghosh, Alternate and direct current conductivity of conducting polyaniline dispersed with poly vinyl alcohol and blended with methyl cellulose, *Journal of Applied Physics*, 97 (2005) 113713.
- [37] H.H.S. Javadi, M. Angelopoulos, A.G. MacDiarmid, A.J. Epstein, Conduction mechanism of polyaniline: Effect of moisture, *Synthetic Metals*, 26 (1988) 1-8.
- [38] B.Z. Lubentsov, O.N. Timofeeva, M.L. Khidekel, Conducting polymer interaction with gaseous substances II. PANI-H₂O, PANI-NH₃, *Synthetic Metals*, 45 (1991) 235-240.

- [39] B. Lubentsov, O. Timofeeva, S. Saratovskikh, V. Krinichnyi, A. Pelekh, V. Dmitrenko, M. Khidekel, The study of conducting polymer interaction with gaseous substances IV. The water content influence on polyaniline crystal structure and conductivity, *Synthetic Metals*, 47 (1992) 187-192.
- [40] E.S. Matveeva, R. Diaz Calleja, V.P. Parkhutik, Thermogravimetric and calorimetric studies of water absorbed in polyaniline, *Synthetic Metals*, 72 (1995) 105-110.
- [41] M. Canales, D. Aradilla, C. Alemán, Water absorption in polyaniline emeraldine base, *Journal of Polymer Science Part B: Polymer Physics*, 49 (2011) 1322-1331.
- [42] E.S. Matveeva, Residual water as a factor influencing the electrical properties of polyaniline. The role of hydrogen bonding of the polymer with solvent molecules in the formation of a conductive polymeric network, *Synthetic Metals*, 79 (1996) 127-139.
- [43] G. Casalbore-Miceli, M.J. Yang, N. Camaioni, C.M. Mari, Y. Li, H. Sun, M. Ling, Investigations on the ion transport mechanism in conducting polymer films, *Solid State Ionics*, 131 (2000) 311-321.
- [44] M. Angelopoulos, A. Ray, A.G. Macdiarmid, A.J. Epstein, Polyaniline: Processability from aqueous solutions and effect of water vapor on conductivity, *Synthetic Metals*, 21 (1987) 21-30.
- [45] K. Ogura, A CO₂ sensor with polymer composites operating at ordinary temperature, *Journal of the Electrochemical Society*, 147 (2000) 4351-4355.
- [46] J. Yue, A.J. Epstein, A.G. Macdiarmid, Sulfonic Acid Ring-Substituted Polyaniline, A Self-Doped Conducting Polymer, *Molecular Crystals and Liquid Crystals Incorporating Nonlinear Optics*, 189 (1990) 255-261.
- [47] S. Cukierman, Et tu, Grotthuss! and other unfinished stories, *Biochimica et Biophysica Acta (BBA) - Bioenergetics*, 1757 (2006) 876-885.
- [48] C. Deslouis, M.M. Musiani, B. Tribollet, M.A. Vorotyntsev, Comparison of the AC Impedance of Conducting Polymer Films Studied as Electrode-Supported and Freestanding Membranes, *Journal of The Electrochemical Society*, 142 (1995) 1902-1908.
- [49] U. Thanganathan, Effects of imidazole on the thermal and conductivity properties of hybrid membrane based on poly(vinyl alcohol)/SiO₂, *Journal of Materials Chemistry*, 22 (2012) 9684-9689.
- [50] M. Hema, S. Selvasekerapandian, G. Hirankumar, Vibrational and impedance spectroscopic analysis of poly(vinyl alcohol)-based solid polymer electrolytes, *Ionics*, 13 (2007) 483-487.

- [51] A.J. Epstein, J.M. Ginder, F. Zuo, R.W. Bigelow, H.S. Woo, D.B. Tanner, A.F. Richter, W.S. Huang, A.G. MacDiarmid, Insulator-to-metal transition in polyaniline, *Synthetic Metals*, 18 (1987) 303-309.
- [52] R. Gangopadhyay, A. De, G. Ghosh, Polyaniline–poly(vinyl alcohol) conducting composite: material with easy processability and novel application potential, *Synthetic Metals*, 123 (2001) 21-31.
- [53] F. Tedjar, Multilayer thin-film batteries with poly(vinyl alcohol), *Journal of Power Sources*, 48 (1994) 285-291.
- [54] J. Przyłuski, W. Wieczorek, Proton polymeric electrolytes - a review, *Synthetic Metals*, 45 (1991) 323-333.
- [55] N. Verdel, I. Jerman, P. Bukovec, The “Autothixotropic” Phenomenon of Water and its Role in Proton Transfer, *International Journal of Molecular Sciences*, 12 (2011) 7481-7494.
- [56] R.M. Hodge, G.H. Edward, G.P. Simon, Water absorption and states of water in semicrystalline poly(vinyl alcohol) films, *Polymer*, 37 (1996) 1371-1376.
- [57] S.G. Greenbaum, Y.S. Pak, M.C. Wintersgill, J.J. Fontanella, NMR studies of Na⁺-anion association effects in polymer electrolytes, *Solid State Ionics*, 31 (1988) 241-245.
- [58] K.M. Krise, A.A. Hwang, D.M. Sovic, B.H. Milosavljevic, Macro- and Microscale Rheological Properties of Poly(vinyl alcohol) Aqueous Solutions, *The Journal of Physical Chemistry B*, 115 (2011) 2759-2764.
- [59] M.A. Hickner, Water-mediated transport in ion-containing polymers, *Journal of Polymer Science Part B: Polymer Physics*, 50 (2012) 9-20.
- [60] S.-A. Chen, G.-W. Hwang, Structures and properties of the water-soluble self-acid-doped conducting polymer blends: sulfonic acid ring-substituted polyaniline/poly(vinyl alcohol) and poly(aniline-co-N-propanesulfonic acid aniline)/poly(vinyl alcohol), *Polymer*, 38 (1997) 3333-3346.
- [61] F.M. C. H. Hsu, Concerning the Conversion of the Constant Phase Element Parameter Y_0 into a Capacitance, *Corrosion*, 57 (2001) 747.
- [62] B.W.L. Leszek J Golonka, Karol Nitsch and Helena Teterycz, Thick-film humidity sensors *Meas. Sci. Technol.*, 8 (1997) 92-98.
- [63] S. Feliu, J.C. Galván, M. Morcillo, The charge transfer reaction in Nyquist diagrams of painted steel, *Corrosion Science*, 30 (1990) 989-998.
- [64] M. Kleitz, Douglas O Raleigh, The electrochemical double layer in solid state electrolytes, *Electrode processes in solid state ionics*, (1976) 122-125.

Chapter 4. Carbon Dioxide Detection at Room Temperature with Polyethyleneimine-based Chemiresistor

Abstract

Branched polyethyleneimine (PEI) was studied as a chemiresistor for use in carbon dioxide (CO₂) detection. The dc and ac resistance of the drop-coated PEI films on interdigitated electrodes was studied at different CO₂ concentrations and humidity levels. PEI exhibited a noticeable decrease in conductivity upon exposure to CO₂ at room temperature. The increased impedance/resistance is attributed to the formation of carbamates and bicarbonates at amine sites of the PEI chain in the presence of CO₂ and water. The response with increasing CO₂ concentration followed a Langmuir isotherm, indicating that the response is caused by an adsorption process. Recovery times of the PEI sensor were in the order of 20 to 60 minutes. Ability of detecting a wide range of CO₂ concentrations makes PEI chemiresistors suitable for low power CO₂ sensing between 400 and 2,000 ppm in greenhouses and offices.

This chapter is part of a publication which is submitted as:

“Carbon Dioxide Detection at Room Temperature with Polyethyleneimine-based Chemiresistor”, Tin C. D. Doan, Rajesh Ramaneti, Jacob Baggerman, Antonius T. M. Marcelis, Hien D. Tong, and Cees J. M. van Rijn, submitted.

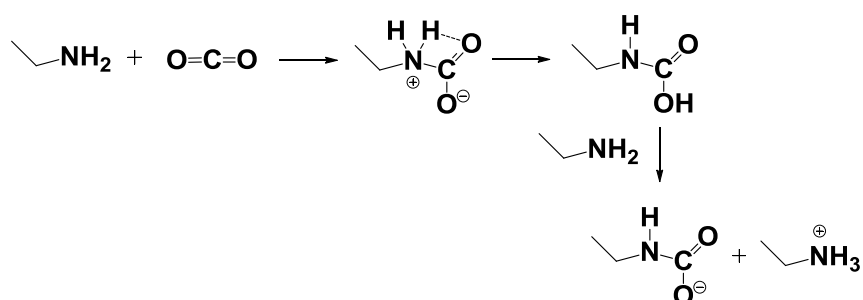
1. Introduction

Carbon dioxide (CO₂) is known to be important to increase crop yields in greenhouses [1], [2]. Therefore, continuous monitoring and controlling of CO₂ concentration in greenhouses is needed to control and optimize growth conditions. Wireless-sensor networks are developed to monitor climate conditions over the whole area of greenhouses [3]. Sensor nodes with simple sensing transducers and easy fabrication are needed for wireless networks. For this many new sensing materials are investigated to replace the existing expensive CO₂ sensors based on non-dispersive infrared (NDIR) detection [4]. For example, solid electrolytes based on metal oxides were used to develop simple miniaturized sensor devices. However, these materials require high operation temperatures leading to large power demand and short lifetime [5]. Hence there is still a strong demand for CO₂ sensors working at room temperature in an environment with high humidity, like greenhouses.

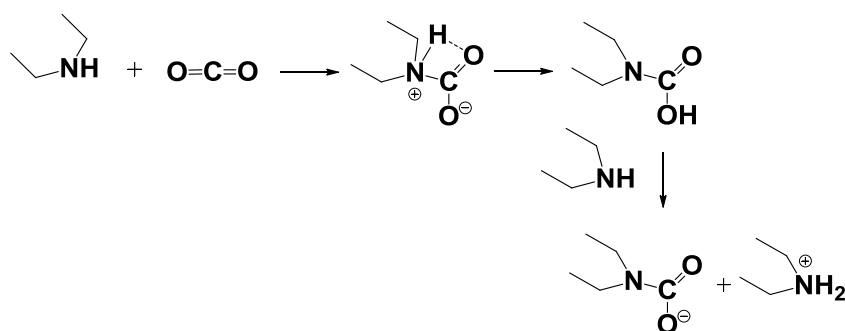
CO₂ sensors based on polymers as active layers are pursued because CO₂ detection with polymers can take place at room temperature [6, 7]. Several types of polymers containing amino groups have been employed for CO₂ detection such as polyethyleneimine (PEI) [8-10], poly(propyleneimine) and polystyrene-bound ethylene diamine [9, 11]. Sensing materials based on heteropolysiloxanes containing primary alkyl amino groups were developed. The hydrophobic polymer matrix reduces the influence of water vapor on the sensing characteristics, for example, aminoalkyl poly(dimethylsiloxane) [9, 11], alkylamine functionalized polysiloxanes [12] and heteropolysiloxane containing 3-aminopropyl-trimethoxysilane (AMO) and propyltrimethoxysilane (PTMS) [13-17] have been studied.

The binding of CO₂ to amino groups can be explained using the Hard Soft Acid Base (HSAB) rule [18, 19]. Hard acids and bases have a low polarizability whereas soft acids and bases are easily polarized. CO₂ is a hard acid according to this theory and can interact with hard bases such as amines. Primary and secondary amines react reversibly with CO₂, yielding carbamates (**Figure 1**) [19]. Tertiary amines can only act as base in the reaction of CO₂ with water that yields bicarbonate.

a. Primary amines



b. Secondary amines



c. Tertiary amines

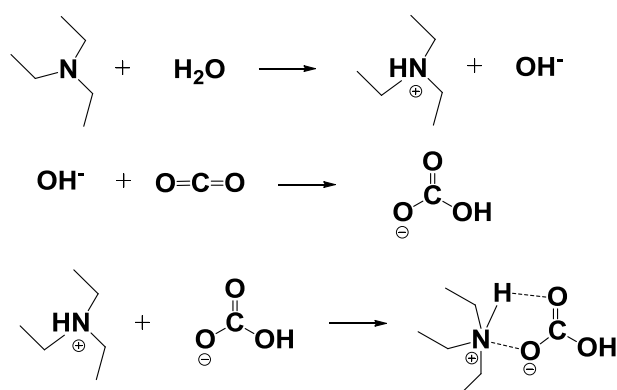


Figure 1. Mechanism of reaction between CO_2 and (a) primary amines (under dry condition), (b) secondary amine (under dry condition) and (c) tertiary amines (under humid condition) [20].

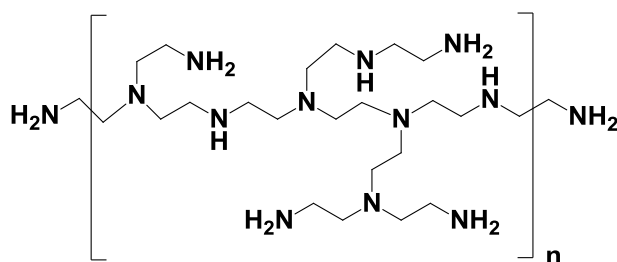


Figure 2. Chemical structure of polyethyleneimine (PEI).

Branched PEI contains three types of amine groups: primary, secondary and tertiary (**Figure 2**). These primary and secondary amino groups can react directly with CO₂ at room temperature (**Figure 1**) [20]. Therefore, PEI has been explored widely for CO₂ capture [21] and sensing [19]. Interaction (adsorption/desorption) between CO₂ and PEI can induce changes in electrical properties, such as conductivity and permittivity [22]. PEI-based CO₂ sensors were developed based on various transduction mechanisms. PEI-coated surface acoustic wave transducers (SAW) [8] were found to be unsuitable for practical sensors due to baseline drift and related imprecise recovery time. A quartz microbalance transducer (QCM) with PEI coating was used for CO₂ detection at 60 °C but the response was affected strongly by humidity due to polymer swelling and viscosity changes [9]. PEI/starch blends coated on QCM [10] showed higher sensitivity than PEI-coated QCM but both sensors had low signal to noise ratio and exhibited long recovery time (more than 20 minutes) at 25 °C. A PEI/starch blend was also coated on AlGaIn/GaN High Electron Mobility Transistors (HEMT) [23]. These sensors exhibited high sensitivity in the range of 0.9-50% CO₂ at high temperature (108 °C). Moreover, PEI/starch-coated carbon nanotube (CNT) field effect transistors (FET) [24] showed fast response and reproducibility from 500 ppm to 10% CO₂. However, PEI/starch coated-CNT sensors based on SAW are only suitable for sensing CO₂ concentrations in the range of 2.5-40% [25].

Although interaction between CO₂ and amino groups of PEI has been investigated thoroughly [20], the electronic properties of thin PEI layers and the influence of CO₂ on conductivity at high humidity (with formation of carbonic acid) have not been studied in detail. In this chapter the conductivity of PEI films is investigated upon exposure to CO₂ at high humidity. Ac impedance and dc resistance measurements of the PEI films were done. Furthermore, the feasibility of using PEI as a chemiresistor for CO₂ sensing is described.

2. Materials and Methods

2.1. Materials

PEI (branched, Mw ~25,000 by LS, Mn ~10,000 by GPC) was purchased from Sigma-Aldrich. All chemicals were used without further purification. CO₂ (99.99%) and N₂ (99.999%) were purchased from Linde Gas Benelux.

2.2. Polymer Solutions and Sensor Preparation

200 mg of PEI was dissolved in 20 ml of deionized water at room temperature by magnetic stirring for 24 hours to obtain a solution with a concentration of 1% w/w.

1 μL of the PEI solution was drop-casted onto a silicon chip with Pt interdigitated electrodes (thickness ~ 170 nm) of dimensions 300 μm (length) \times 9 μm (width) and 6 μm spacing. The drop-casted polymer was dried at room temperature for 24 hours in a vacuum desiccator. The thickness of the films was determined using a surface profiler Dektak 6M (Veeco). The PEI films had a thickness of ~ 1 μm .

2.3. Ac Impedance and Dc Resistance Measurement to Characterize CO₂ Sensing of the PEI Coated Chips

The polymer-coated chips were mounted in the chamber with controlled relative humidity (RH) levels and CO₂ concentrations. The details of the setup for gas sensor characterization can be found in Chapter 2. To investigate the CO₂ sensing capability of the PEI films, the polymer coated chip was exposed to different CO₂ concentrations (from 400 ppm to 10,000 ppm) at high humidity levels (from 60% to 90% RH) and the ac impedance and dc resistance of polymer films were measured at room temperature (24 °C). Two-point dc resistivity measurements were carried out using a Keithley 2400 source meter with voltage scanning from -5 V to +10 V. Ac impedance spectroscopy was measured using a HP 4192A LF impedance analyzer with applied voltage of 0.3 V. The impedance change was expressed in terms of Nyquist plots, imaginary impedance (Z'') is plotted against the real impedance (Z') derived from the measured absolute impedance ($|Z|$) and phase angle (θ) values when the frequency is scanned from 5 Hz to 1 MHz.

3. Results and Discussion

3.1. Dc Resistance of the PEI Films upon Exposure to CO₂ and Humidity

Dc measurements identify the interfacial electronic properties of polymers (junction between metal/semiconductor contacts) in interaction with an analyte gas (water vapor, CO₂). The change in dc resistance of the PEI films upon the variation of CO₂ concentrations was investigated by I-V curve measurements. The current through the PEI films was measured while the voltage was scanned from -5 V to +10 V for a sample exposed to 400 and 10,000 ppm CO₂ at constant humidity (75% RH) (**Figure 3**).

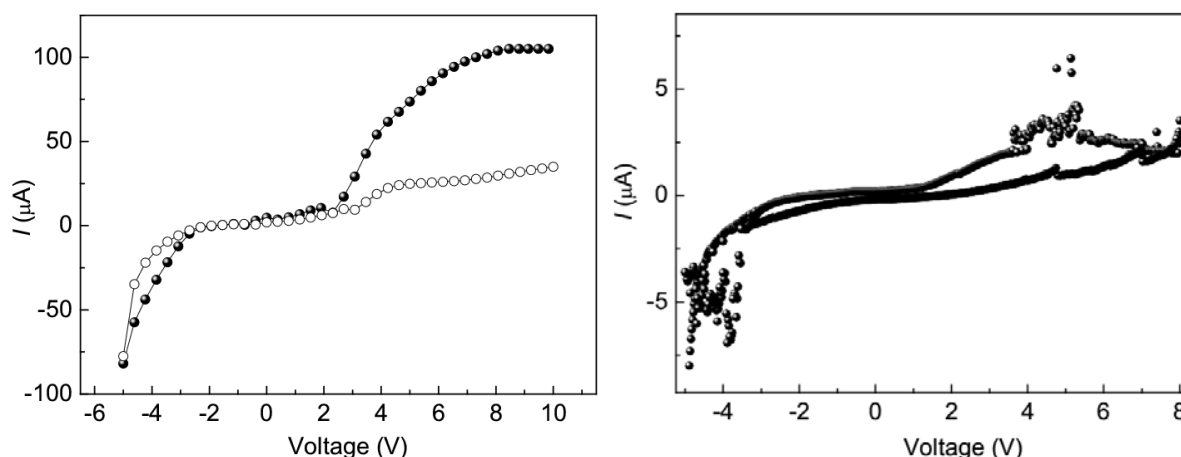


Figure 3. *I-V curves of PEI upon exposure to 400 ppm CO₂ (●) and 1% CO₂ (○) at 75% RH. Voltage scan from -5 V to +10 V with scan rate of 3 V.s⁻¹ (left), loop voltage scan from -5 V to +8 V with scan rate of 20 mV.s⁻¹ (right).*

The current through the PEI film is in the range of μA at relative humidity of 75% and low CO₂ concentration (400 ppm). It can be attributed to the presence of protons from water vapor in the PEI film. Branched PEI has amino groups (25% primary, 50% secondary and 25% tertiary), each type of amines has a different basicity (pK_a) and can be protonated at different pH values [26]. Under high humidity, the PEI film is hydrated because of hydrogen bonding between water vapor and amine groups. The amine groups are partly protonated due to their basicity. The conduction path in PEI film is mainly due to protons hopping from the protonated to the non-protonated amines [27].

The measured I-V curves are non-linear; at voltages $>2\text{ V}$ and $<-2\text{ V}$ the current increases more than expected for ohmic behavior. This non-linear behavior can be described using the space-charge-limited current model [28]. In this model three domains can be distinguished in the I-V curves. At low voltages the behavior is ohmic and $I \sim V$. At intermediate voltage, charge injection takes place and the contribution of injected charge carriers becomes larger, $I \sim V^2$. In case of a trapless material this increase continues to higher voltages. However, if there are traps in the film for the charge carriers, the increase will stop at the threshold voltage at which all the traps are filled. PEI has amine sites which are good electron donors and can easily accept an electron hole. At higher voltages when amine sites are oxidized the electron transport through the holes is facilitated, resulting in a higher current. This increase in current is limited by the amount of available amine groups. This explains the reduction of the current increase at high voltages in the presence of CO₂. Due to adsorption of CO₂ to amine groups,

there are fewer sites available for electron hole injection, resulting in a lower maximum number of injected charge carriers and a higher resistance.

When the CO₂ concentration increased from 400 ppm to 10,000 ppm, a decrease in current was observed indicating an increase in resistance of the PEI film. The dc resistance of the PEI films was calculated from the slopes in the linear parts of the I-V curves (between -2 V and 2 V). The dc resistance increases with a factor of 2.7 from 30 k Ω to 81.7 k Ω when the CO₂ concentration increases from 400 ppm to 10,000 ppm. This response is similar to the observations with PEI-coated CNT where the current decreased at higher concentrations of CO₂ [24]. The increase in resistance of the PEI films with increasing CO₂ concentration can be explained by the proton hopping mechanism. In the presence of water and CO₂, amine groups form carbamates and bicarbonates [20], which bind to the amine sites in the PEI (**Figure 1**) and reduce the number of free amine groups. This hinders proton hopping along the chain leading to a decrease in conductivity. Similar behavior was observed for PEI with different amounts of bound phosphoric acid groups [27]. Small amounts of phosphoric acid lead to some increase in the conductivity due to an increase in the amount of charge carriers (protons). However, with increasing amounts of phosphoric acid (up to 80% of the available amine sites) the conductivity drops two orders of magnitude due to a reduction in the number of amine sites available for proton hopping. As can be seen from **Figure 3**, the current increases rather steeply at a voltage above 3 V and saturates at a voltage of about 4.5 V, which is smaller than the saturating voltage at 400 ppm CO₂. It can be explained that in the presence of a high concentration of CO₂, the proton transport needs higher activation energy to overcome the barrier due to the negative charges. Nevertheless, the protonic conduction cannot be enhanced since most amine sites are occupied when the voltage increases above 4.5 V and a saturation in current is obtained.

Dc resistance as a function of CO₂ concentrations is plotted in **Figure 4**. The resistance increases when CO₂ concentration increases and saturates at some levels. The dependence of dc resistance of the PEI film on CO₂ concentrations was fitted with a Langmuir isotherm [29]. The Langmuir isotherm was also observed in adsorption kinetics of CO₂ onto PEI-based absorbents [20]. This indicates a direct proportional relation between the dc resistance and the adsorbed amount of CO₂ in the film.

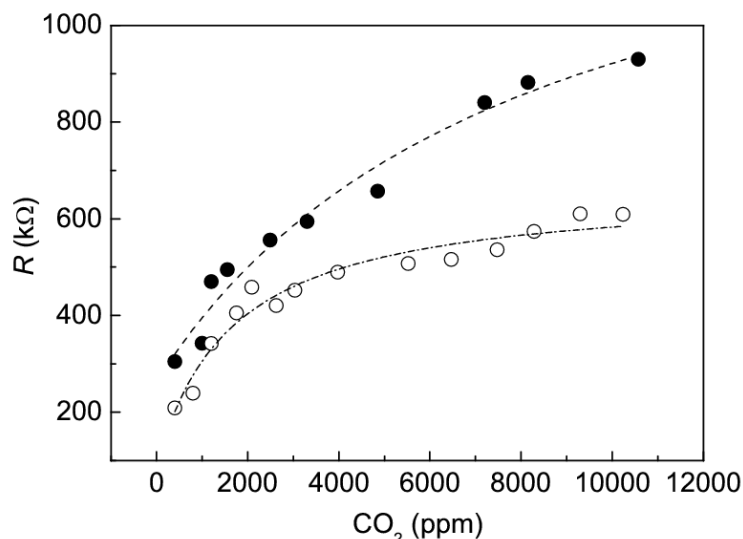


Figure 4. Relationship between dc resistance and CO₂ concentrations of PEI at 60% RH (●) and 75% RH (○).

The PEI-based chemiresistors are studied to work under high humid environment like greenhouses, hence humidity-dependent resistance measurements of the PEI films were also investigated. The PEI films were exposed to different CO₂ concentrations at 60% RH and 75% RH. The increase in dc resistance of the PEI films at 60% RH is about 2 times higher than at 75% RH with CO₂ concentrations higher than 1,000 ppm. This is attributed to the effect of water vapor on conductivity of the PEI films.

The effect of water vapor on the dc resistance of the PEI films was obtained from I-V curves measured at different humidity levels (from 10% to 90% RH). The dc resistance was calculated from the slope of I-V curves (linear parts in low voltage range of about 2 V). **Figure 5** shows the resistance of the PEI film as a function of humidity. It is known that humidity can affect the conductivity of the polyelectrolyte polymers [30]. PEI is considered as a weak cationic polyelectrolyte [26, 31, 32], so PEI is sensitive towards water vapor and it was used as a sensing layer for humidity sensors [33]. An increase in conductivity (or decrease in resistance) of PEI film is observed when humidity increases. This is similar to humidity response of PEI cross-linked with 1,4-butanediol diglycidyl ether [33].

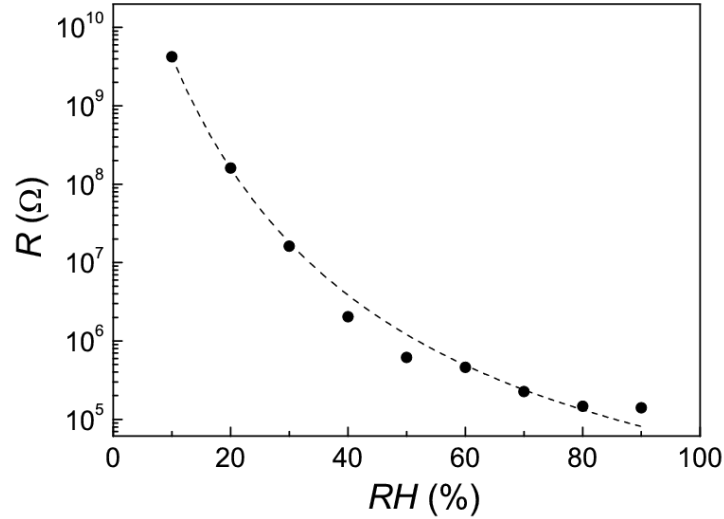


Figure 5. Relationship between dc resistance of PEI film and humidity from 10 to 90% RH.

The decrease in resistance with increasing humidity can have different reasons. It can be due to the creation of a new conduction path through the material by formation of water channels or due to facilitating proton conduction on the polymer chains. The first mechanism can be described by a percolation model [34-37] that is at low humidity there is no percolation path for conduction. Upon increasing the water concentration more percolation path open up and the resistance decreases. The percolation model predicts a power-law decreasing of the resistance starting from a certain critical water concentration [38]. This is often observed for polyelectrolytes.

$$\sigma \sim (p - p_c)^\mu$$

in which σ is conductivity, p is probability, p_c is critical probability of open percolation path.

The second mechanism follows an exponential curve and is often observed for hygroscopic materials [39].

$$\sigma \sim \exp\left(\frac{a}{M}\right)$$

in which σ is conductivity, M is amount of water in the film and a is exponential factor.

The data in **Figure 5** fit better with an exponential decrease if the resistance does not show a critical concentration for decrease of the resistance and the decrease seems to level. This can be better described with an exponential function than a power-law. Therefore, the decrease in resistance is most likely due to water facilitating the proton conduction in the film. The limiting resistance at high humidities is due to limitation of the proton mobility in water.

3.2. Impedance Spectroscopy of PEI Coated Chips upon Exposure to CO₂

The frequency-dependent ac impedance study is useful to obtain a better understanding of the charge transport mechanism and contributions to conduction. Ac impedance measurements of the PEI films were conducted to determine conductivity changes (including resistance and capacitance change) when the PEI films were exposed to CO₂. Variable-frequency capacitance (C) and ac absolute impedance ($|Z|$) were measured over the frequency range from 5 Hz to 1 MHz.

An increase in capacitance of the PEI film was observed when humidity increased from 10% to 75% RH (**Figure 6**). The water vapor adsorption leads to an increase in dielectric permittivity at low frequencies (<200 kHz), hence an increase in capacitance. This increase in dielectric permittivity at low frequencies is often observed in hydrated films [39]. This is associated with the formation of large dipole moment(s) along the conduction paths. Proton conduction occurs through the Grotthuss mechanism, the proton moves through the medium by means of forming and breaking of hydrogen bonds with water molecules [40, 41]. When there are defects in the hydrogen bonding network, i.e., if there is not a neighboring water molecule that can participate, the conduction will stop at that point. This results in an accumulation of charge at this point and a large dipole moment. At higher water concentrations the amount of defects is smaller and the dipole moments will become larger, thus dielectric permittivity increases.

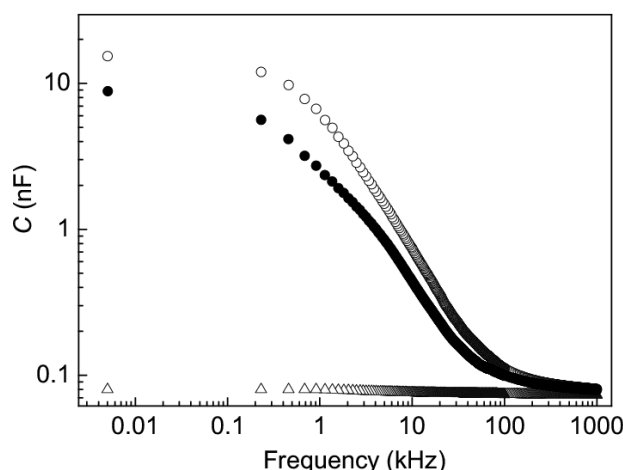


Figure 6. Capacitance of PEI film at 10% RH with 400 ppm CO₂ (Δ), at 75% RH with 400 ppm CO₂ (\circ) and at 75% RH with 10,000 ppm CO₂ (\bullet).

Upon increasing the CO₂ concentration from 400 ppm to 10,000 ppm the capacitance decreases at frequencies below 200 kHz. This trend was also observed with chemicapacitive

sensors using alkylamine-functionalized organic bridged polysilsesquioxanes [12]. Adsorption of CO_2 at high humidity leads to the reaction between amines and water with CO_2 . The formed carbamates and bicarbonates leads to more blocked conduction paths, which results in smaller dipole moments, as discussed before. The increase in resistance and decrease in capacitance when CO_2 is adsorbed on the PEI films result in an increase in total impedance Z as shown below. These results are in agreement with a proton conduction model for PEI.

The influence of CO_2 on the impedance was further investigated at 75% RH. The absolute impedance ($|Z|$) was measured when the films were exposed to 400 ppm (baseline) and 3,000 ppm CO_2 over the frequency range from 5 Hz to 1 MHz (**Figure 7**). From the Bode plots the frequency range of 1-5 kHz was determined at which the difference in impedance between 400 ppm and 3,000 ppm CO_2 is maximal. A frequency in this range (1 kHz) was chosen for time dependent impedance measurement of the PEI chemiresistors. An increase in impedance of the PEI films is observed when CO_2 concentration increases from 400 ppm to 3,000 ppm CO_2 . Differences in $|Z|$ amplitude are observed for the PEI films exposed to CO_2 concentrations between 400 ppm and 3,000 ppm in the frequency range of 100 Hz - 100 kHz. The low frequency range describes the diffusion process of ionic species through double layer at the interface between polymer films and metal electrodes and the high frequency range shows the response from the polymer film. The largest response to CO_2 is seen at higher frequencies, indicating that the response is mainly from the PEI itself. The increase in impedance of the PEI films upon exposure to CO_2 is consistent with the observed increase in dc resistance.

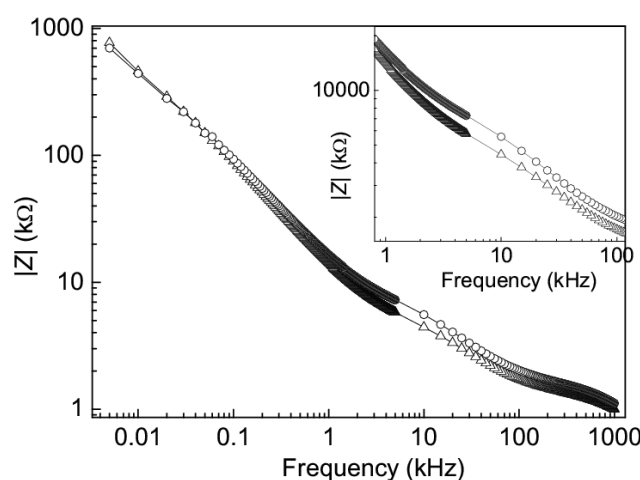


Figure 7. Absolute impedance $|Z|$ of the PEI films as a function of frequency at 75% RH upon exposure to 400 ppm (Δ) and 3,000 ppm (\circ) CO_2 . Inset: zoom in at frequency range of 1-100 kHz.

3.3. Effect of Humidity on Impedance of the PEI Films

The influence of humidity on the conductivity of the PEI films was investigated in more detail by impedance spectroscopy. **Figure 8** shows the Nyquist and Bode plots of PEI film at different humidity levels from 8% to 90% RH. When humidity increases above 50% RH the dependence in the lower frequency regime starts. This is related to the charge transfer at electrode surface and diffusion of ion species (protons and OH⁻) generated from water through the double layer.

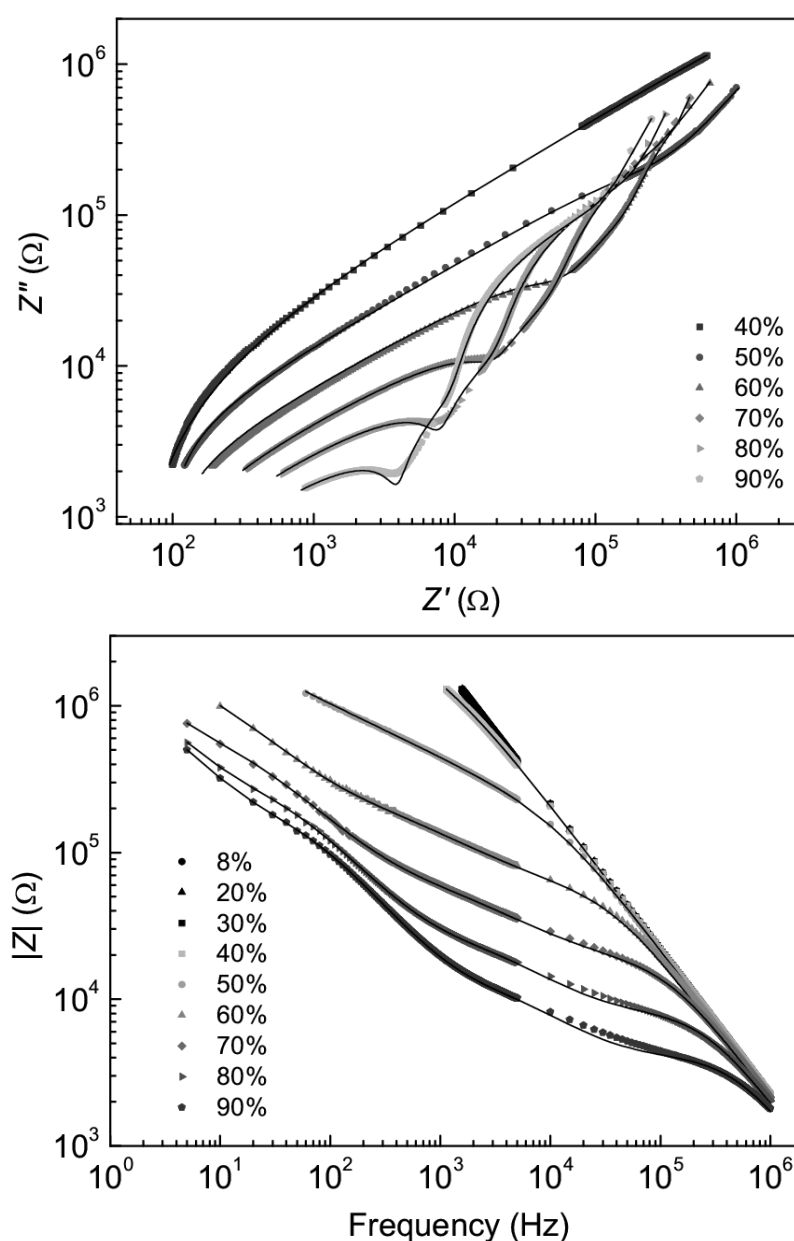


Figure 8. Nyquist plots (top) and Bode plots (bottom) of the PEI films at different humidity levels (8 - 90% RH).

The fitting of impedance data was performed to investigate the contribution of different conduction pathways in the PEI films due to water vapor. The details of data fitting (equivalent circuit and obtained fit parameters) can be found in **Appendix 3**. Here we used a slightly modified equivalent circuit from Chapter 3 (**Figure 9**). Similar to the model in Chapter 3 the resistance $R1$ describes the bulk polymer. However at high humidities there is not closed semicircle present in the Nyquist plot matching with the observed dc resistances. This indicates mainly a pure ionic (proton) conductor without a contribution of intrinsic electron or electron-hole transport. Therefore an additional constant phase element ($CPE1$) was added after resistance $R1$ to compensate for the (not steady or present) dc behavior. $R2$ and $CPE3$ describe the ionic or protonic conduction through water. $CPE2$ and $R3$ describe grain boundary effects due to presence of polymeric and water phase domains in the film. At lower humidities of 30-40% RH, $R2$ and $R3$ are too large to be observed in the frequency range of our measurements and the data can be fitted with a simple Randle's circuit with a large $R1$. The resistance at very low humidities is too high to be fitted accurately; the impedance response is almost a perfect capacitor.

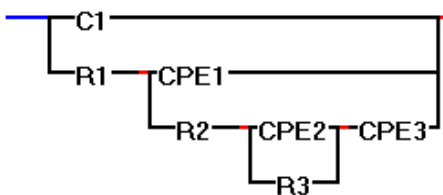


Figure 9. Equivalent circuit used for analysis of impedance data.

The resistance of the system decreases with increasing humidity, as observed with dc measurements. The impedance data shows the same behavior (**Figure 10**). Only a resistance in the order of $M\Omega$ can be obtained from the data due to limitation of the equipment used. Fitting shows that all resistances in the equivalent circuit are sensitive to humidity. This is not surprising since all conduction processes are protonic in nature. The protonic conduction along the PEI polymer is facilitated by more water in the polymer film. Besides that additional conduction is possible through the formation of water channels.

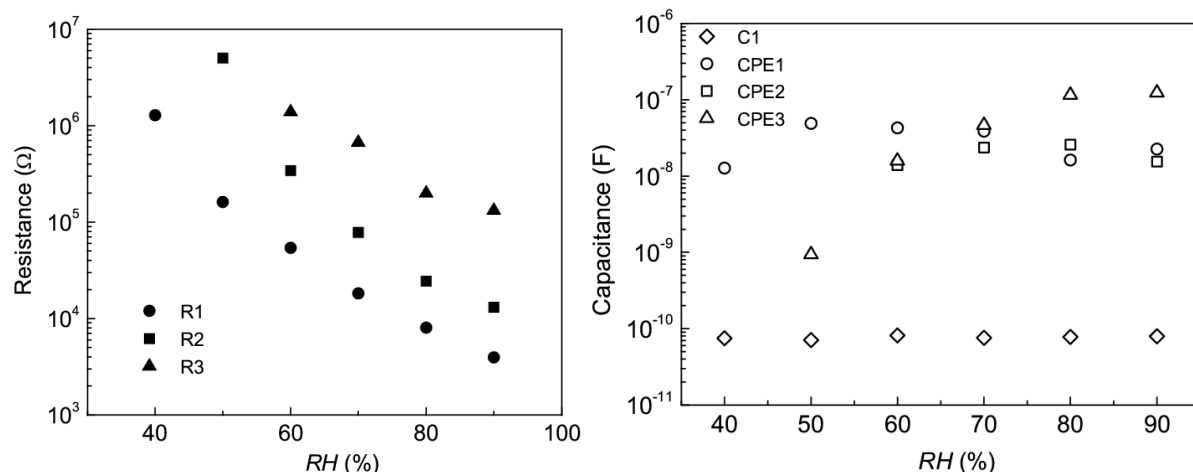


Figure 10. Obtained fit parameters as function of the relative humidity.

In **Figure 10** parameters of the equivalent circuit as a function of the relative humidity have been plotted. $C1$ is found constant and describes the blank chip (without polymer) capacitance of 85 pF. All the resistances (3x) and constant phase elements (4x) could be fitted relatively well. It can be seen in the corresponding log-log Nyquist plots in **Figure 8** that especially at high humidity (>60% RH) at least three R/CPE elements will be needed to fit the obtained plots. At 50% RH the obtained fit is less accurate because the polymer system appears to be in a transition mode. Looking at the $CPEs$ at higher humidity, it is clear that only $CPE3$ is strongly dependent on humidity. This indicates that $CPE3$ is related to the double layer capacitance of the polymer/electrode interface and is in agreement with an increased capacitance observed at low frequencies at high humidities, similar to our observation and discussion in Chapter 3.

3.4. Comparison of Relative Change in Impedance due to Humidity and CO_2

To investigate the effect of humidity on the CO_2 sensing, the PEI films were exposed to 60% RH without and with 1% CO_2 and then to 62% RH without any CO_2 . 60% RH was chosen because at this humidity level, the start of the second semicircle was observed. The impedance spectroscopy was measured at each exposure with frequency scanning from 5 Hz to 1 MHz (**Figure 11**). The PEI films exhibited the same behavior as at 75% RH mentioned above. CO_2 causes increase in impedance whereas humidity induces decrease in impedance. The decrease in impedance upon exposure to higher humidity levels is consistent with dc measurement results. The relative changes in impedance due to 1% change in RH and 1% CO_2 of the PEI films were calculated at three frequencies (100 kHz, 10 kHz and 1 kHz) where the significant difference in values of impedance was observed (**Figure 11**).

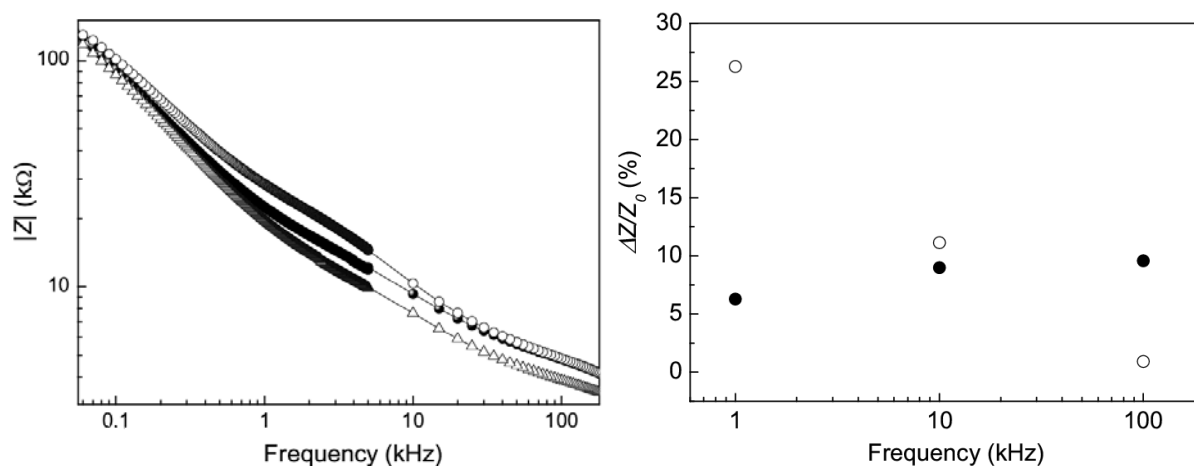


Figure 11. (Left) Absolute impedance ($|Z|$) of the PEI films as a function of frequency at 60% RH (●), at 60% RH with 1% CO_2 (○) and at 62% RH (△). (Right) Relative change in impedance $\Delta Z/Z_0$ at 1 kHz, 10 kHz and 100 kHz due to 1% change in RH (●) and 1% CO_2 (○).

As can be seen, the relative change in impedance at 1 kHz due to 1% CO_2 is 4.3 times larger than due to 1% change in RH whereas at 10 kHz these values are more or less the same. At 100 kHz, the relative change in impedance due to 1% CO_2 is smaller 10 times. Therefore, 1 kHz is suitable for impedance measurement to distinguish effects due to CO_2 or humidity with a good signal to noise ratio. The absolute impedance $|Z|$ of the PEI films was measured at a constant frequency under various conditions. Frequency of 1 kHz was chosen to measure time dependent impedance response of the PEI films upon exposure to different CO_2 concentrations.

3.5. Time Dependent Impedance Response of the PEI Films upon Exposure to CO_2

Time dependent measurement exhibits the dynamic response of the PEI films towards CO_2 including the response time, recovery time, drift, etc. which involves the adsorption/desorption of CO_2 on the polymers. As mentioned above, the time dependent measurements were measured at a fixed frequency as CO_2 concentration varies from 400 ppm (baseline) to 18,000 ppm.

The time dependent impedance response of the PEI films was measured at 1 kHz when CO_2 concentration varied from 400 ppm (baseline) to 3,000 ppm at 75% RH (**Figure 12**). The impedance of the PEI films was found to increase as CO_2 gas was introduced and the impedance increase was proportional to CO_2 concentrations. The impedance increase in ac measurement is consistent with the resistance increase in dc measurement discussed above. The response time was about 4-5 minutes; it can be explained by the fact that at high

humidity, all tertiary amines take part in reaction with CO_2 and H_2O , so the impedance increased quite fast. However, the impedance of the PEI films decreased very slowly after CO_2 was switched off, from 20 to 60 minutes depending on the concentrations of CO_2 . It might be attributed to the slow conversion of carbamates back to CO_2 and amine after CO_2 was removed out of the PEI films resulting in a long recovery time of the sensor. This behavior was also observed with PEI-coated SAW [8] and PEI/starch blends-coated QCM [10].

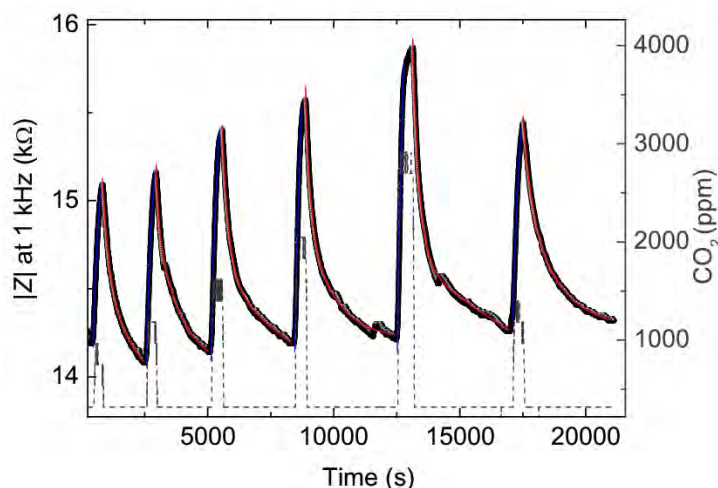


Figure 12. Time dependent impedance response of PEI measured at 1 kHz when the PEI film was exposed to different CO_2 concentrations (dash line) at 75% RH.

The impedance response and recovery when CO_2 was introduced and purged out correspond to adsorption and desorption of CO_2 on the PEI films. The fitting of these impedance curves was done with the data analysis and graphing software Origin version 8.1. The impedance increase curves when CO_2 was introduced follow single exponential (ExpDec1) equation as shown in **Equation 1** below.

$$y = A_1 * \exp(-x/t_1) + y_0 \quad (1)$$

Table 1. Fitting parameters of impedance decrease in CO_2 adsorption process.

CO_2 , ppm	t_1	Standard error
753	310	4.31
1,186	322	5.78
1,270	313	6.46
1,500	314	7.19
2,000	312	10.39
2,800	311	13.45

From **Table 1**, we can see that value of t_1 does not change much with different CO₂ concentrations. The rate of CO₂ adsorption on the PEI films is almost constant independently CO₂ concentrations.

The impedance decrease curves when CO₂ was purged out follow double exponential decay (ExpDecay2) equation (**Equation 2**). The results of parameters are shown in **Table 2**. The double exponential decay indicates that desorption takes place in two phases. CO₂ bound close to the surface can release fast (similar to adsorption speed). However, CO₂ bound in the film diffuses out later, which leads to a slower response.

$$y = y_0 + A_1 * \exp[-(x-x_0)/t_1] + A_2 * \exp[-(x-x_0)/t_2] \quad (2)$$

Table 2. Fitting parameters of impedance decrease in CO₂ desorption process.

<i>CO₂, ppm</i>	<i>Value</i>			
	<i>A₁</i>	<i>t₁</i>	<i>A₂</i>	<i>t₂</i>
753	738	324	1297	6129
1,186	353	115	824	1036
1,270	494	365	716	1363
1,500	844	263	799	4152
2,000	757	190	681	1125
2,800	1254	262	1240	9878

The recovery time and the relative change in impedance ($\Delta Z/Z_0$) of the PEI films at 75% RH was calculated from the time dependent impedance response in **Figure 12** and plotted against CO₂ concentrations in **Figure 13** and **Figure 14** correspondingly. The CO₂ sensitivity of the PEI films measured with ac impedance also follows Langmuir isotherm as dc measurement.

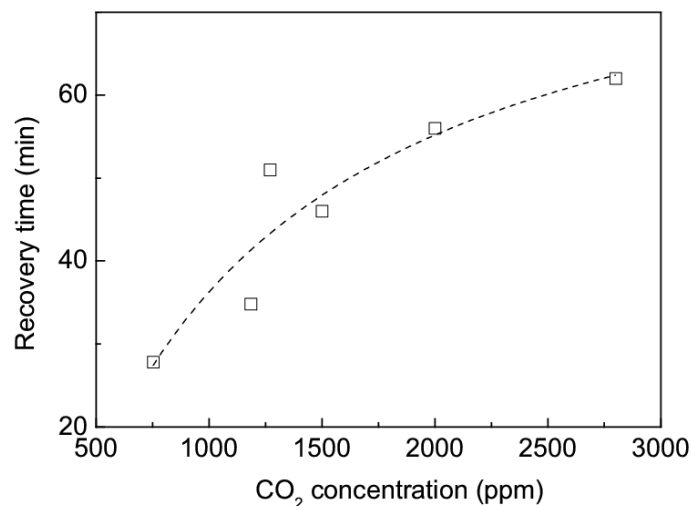


Figure 13. Recovery time as a function of CO₂ concentrations of the PEI films.

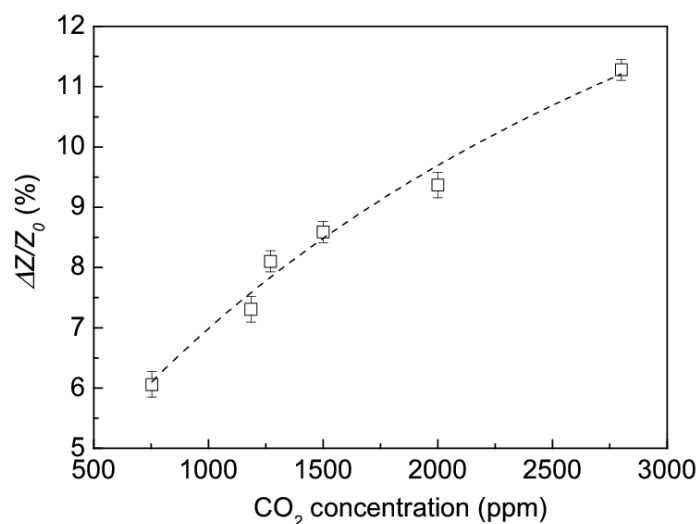


Figure 14. Relative change in impedance of the PEI films as a function of CO₂ concentrations at 75% RH.

4. Conclusions

In conclusion, PEI exhibited sensitivity to CO₂ at low concentrations. The increase in ac impedance and dc resistance was observed when the PEI films were exposed to CO₂ at high humidity. The impedance increase is attributed to formed carbamates and bicarbonates in the PEI chain when the PEI film is exposed to CO₂ at high humidity. Water vapor is the main cross-sensitive analyte because these CO₂ sensors are aimed for greenhouse application. However humidity induced an opposite response to conductivity in comparison to CO₂. PEI chemiresistors might thus be a potential candidate for low power CO₂ sensing operating at room temperature in greenhouses between 400 and 2,000 ppm.

References

- [1] J.D. Cure, B. Acock, Crop responses to carbon dioxide doubling: a literature survey, *Agricultural and Forest Meteorology*, 38 (1986) 127-145.
- [2] J.S. Amthor, Effects of atmospheric CO₂ concentration on wheat yield: review of results from experiments using various approaches to control CO₂ concentration, *Field Crops Research*, 73 (2001) 1-34.
- [3] T. Ahonen, R. Virrankoski, M. Elmusrati, Greenhouse Monitoring with Wireless Sensor Network, in: *Mechtronic and Embedded Systems and Applications*, 2008. MESA 2008. IEEE/ASME International Conference on, 2008, pp. 403-408.
- [4] K. Ogura, H. Shiigi, A CO₂ sensing composite film consisting of base-type polyaniline and poly(vinyl alcohol), *Electrochemical and Solid State Letters*, 2 (1999) 478-480.
- [5] D. James, S.M. Scott, Z. Ali, W.T. O'Hare, Chemical Sensors for Electronic Nose Systems, *Microchimica Acta*, 149 (2005) 1-17.
- [6] H. E.C.M, CO, CO₂, CH₄ and H₂O sensing by polymer covered interdigitated electrode structures, *Sensors and Actuators*, 5 (1984) 181-186.
- [7] B. Adhikari, S. Majumdar, Polymers in sensor applications, *Progress in Polymer Science*, 29 (2004) 699-766.
- [8] M.S. Nieuwenhuizen, A.J. Nederlof, A SAW gas sensor for carbon dioxide and water. Preliminary experiments, *Sensors and Actuators B: Chemical*, 2 (1990) 97-101.
- [9] R. Zhou, D. Schmeisser, W. Göpel, Mass sensitive detection of carbon dioxide by amino group-functionalized polymers, *Sensors and Actuators, B: Chemical*, 33 (1996) 188-193.
- [10] B. Sun, G. Xie, Y. Jiang, X. Li, Comparative CO₂-Sensing Characteristic Studies of PEI and PEI/Starch Thin Film Sensors, *Energy Procedia*, 12 (2011) 726-732.
- [11] R. Zhou, S. Vaihinger, K.E. Geckeler, W. Göpel, Reliable CO₂ sensors with silicon-based polymers on quartz microbalance transducers, *Sensors and Actuators B: Chemical*, 19 (1994) 415-420.
- [12] S. Patel, S. Hobson, S. Cemalovic, T. Mlsna, Materials for capacitive carbon dioxide microsensors capable of operating at ambient temperatures, *Journal of Sol-Gel Science and Technology*, 53 (2010) 673-679.
- [13] H.-E. Endres, R. Hartinger, M. Schwaiger, G. Gmelch, M. Roth, A capacitive CO₂ sensor system with suppression of the humidity interference, *Sensors and Actuators B: Chemical*, 57 (1999) 83-87.

- [14] S. Stegmeier, M. Fleischer, A. Tawil, P. Hauptmann, K. Egly, K. Rose, Mechanism of the interaction of CO₂ and humidity with primary amino group systems for room temperature CO₂ sensors, *Procedia Chemistry*, 1 (2009) 236-239.
- [15] S. Stegmeier, M. Fleischer, A. Tawil, P. Hauptmann, H.E. Endres, Detection of CO₂ with (Hetero-) Polysiloxanes sensing layers by the change of work function at room temperature, *Procedia Chemistry*, 1 (2009) 646-649.
- [16] S. Stegmeier, M. Fleischer, A. Tawil, P. Hauptmann, Stepwise improvement of (hetero-) polysiloxane sensing layers for CO₂ detection operated at room temperature by modification of the polymeric network, *Sensors and Actuators B: Chemical*, 148 (2010) 450-458.
- [17] S. Stegmeier, M. Fleischer, A. Tawil, P. Hauptmann, H.E. Endres, Sensing of CO₂ at room temperature using work function readout of (hetero-)polysiloxanes sensing layers, *Sensors and Actuators B: Chemical*, 154 (2011) 206-212.
- [18] R.G. Pearson, Hard and Soft Acids and Bases, *Journal of the American Chemical Society*, 85 (1963) 3533-3539.
- [19] B. Serban, A.K.S. Kumar, M. Brezeanu, C. Cobianu, O. Buiu, C. Bostan, N. Varachiu, S. Costea, Amino groups-based polymers for CO₂ detection: A comparison between two sensing mechanism models, in, 2011, pp. 127-130.
- [20] Y.G. Ko, S.S. Shin, U.S. Choi, Primary, secondary, and tertiary amines for CO₂ capture: Designing for mesoporous CO₂ adsorbents, *Journal of Colloid and Interface Science*, 361 (2011) 594-602.
- [21] J.C. Hicks, J.H. Drese, D.J. Fauth, M.L. Gray, G. Qi, C.W. Jones, Designing Adsorbents for CO₂ Capture from Flue Gas-Hyperbranched Aminosilicas Capable of Capturing CO₂ Reversibly, *Journal of the American Chemical Society*, 130 (2008) 2902-2903.
- [22] H. Bai, G.Q. Shi, Gas sensors based on conducting polymers, *Sensors*, 7 (2007) 267-307.
- [23] T. Anderson, F. Ren, S. Pearton, B.S. Kang, H.-T. Wang, C.-Y. Chang, J. Lin, Advances in Hydrogen, Carbon Dioxide, and Hydrocarbon Gas Sensor Technology Using GaN and ZnO-Based Devices, *Sensors*, 9 (2009) 4669-4694.
- [24] A. Star, T.R. Han, V. Joshi, J.C.P. Gabriel, G. Grüner, Nanoelectronic Carbon Dioxide Sensors, *Advanced Materials*, 16 (2004) 2049-2052.
- [25] S. Sivaramakrishnan, R. Rajamani, C.S. Smith, K.A. McGee, K.R. Mann, N. Yamashita, Carbon nanotube-coated surface acoustic wave sensor for carbon dioxide sensing, *Sensors and Actuators B: Chemical*, 132 (2008) 296-304.

- [26] A. Tanioka, Relationship Between Protonation and Ion Condensation for Branched Poly(Ethyleneimine), *Biophysical Chemistry*, 60 (1996) 45-51.
- [27] R. Tanaka, H. Yamamoto, A. Shono, K. Kubo, M. Sakurai, Proton conducting behavior in non-crosslinked and crosslinked polyethylenimine with excess phosphoric acid, *Electrochimica Acta*, 45 (2000) 1385-1389.
- [28] R.W.I. de Boer, A.F. Morpurgo, Influence of surface traps on space-charge limited current, *Physical Review B*, 72 (2005) 073207.
- [29] I. Langmuir, Chemical reactions at low pressures, *Journal of the American Chemical Society*, 37 (1915) 1139-1167.
- [30] G. Casalbore-Miceli, N. Camaioni, Y. Li, A. Martelli, M.-J. Yang, A. Zanelli, Water sorption in polymer electrolytes: kinetics of the conductance variation, *Sensors and Actuators B: Chemical*, 105 (2005) 351-359.
- [31] J. Koetz, K.-J. Linow, B. Philipp, L.P. Hu, O. Vogl, Effects of charge density and structure of side-chain branching on the composition of polyanion-polycation complexes, *Polymer*, 27 (1986) 1574-1580.
- [32] P.C. Griffiths, A. Paul, P. Stilbs, E. Petterson, Charge on Poly(ethylene imine): Comparing Electrophoretic NMR Measurements and pH Titrations, *Macromolecules*, 38 (2005) 3539-3542.
- [33] B. Chachulski, J. Gebicki, G. Jasinski, P. Jasinski, A. Nowakowski, Properties of a polyethyleneimine-based sensor for measuring medium and high relative humidity, *Measurement Science and Technology*, 17 (2006) 12.
- [34] J.W. Essam, Percolation theory, *Reports on Progress in Physics*, 43 (1980) 833.
- [35] B.J. Last, D.J. Thouless, Percolation Theory and Electrical Conductivity, *Physical Review Letters*, 27 (1971) 1719-1721.
- [36] P. Dutta, S. Biswas, M. Ghosh, S.K. De, S. Chatterjee, The dc and ac conductivity of polyaniline–polyvinyl alcohol blends, *Synthetic Metals*, 122 (2001) 455-461.
- [37] M. Parlar, Y.C. Yortsos, Percolation theory of vapor adsorption - desorption processes in porous materials, *Journal of Colloid and Interface Science*, 124 (1988) 162-176.
- [38] S. Kirkpatrick, Percolation and Conduction, *Reviews of Modern Physics*, 45 (1973) 574-588.
- [39] J.H. Christie, S.H. Krennek, I.M. Woodhead, The electrical properties of hygroscopic solids, *Biosystems Engineering*, 102 (2009) 143-152.
- [40] A. Noam, The Grotthuss mechanism, *Chemical Physics Letters*, 244 (1995) 456-462.

[41] S. Cukierman, Et tu, Grotthuss! and other unfinished stories, *Biochimica et Biophysica Acta (BBA) - Bioenergetics*, 1757 (2006) 876-885.

Chapter 5. Improved Carbon Dioxide Sensing of Polyethyleneimine Blended with Other Polyelectrolytes

Abstract

Branched polyethyleneimine (PEI) sensors showed sensitivity to carbon dioxide (CO₂) at low concentrations. However, the sensitivity is moderate (about 10% impedance change at 2,000 ppm CO₂) and a very long recovery time (about 40-60 minutes). In this chapter blends of PEI with several polyelectrolytes such as sodium salt of sulfonated polyaniline (SPAN-Na), poly(sodium 4-styrenesulfonate) (PSS-Na), Nafion sodium sulfonate (Nafion-Na) were studied for improved sensitivity and response times of PEI-based CO₂ sensors. The dc and ac resistance of the drop-coated PEI blends was studied as these blend films were exposed to different CO₂ concentrations and humidity regimes. Mixing of PEI with Nafion-Na has a significant increase in sensitivity (about ten times better) and shorter recovery time (10-20 minutes) than pure PEI (40-60 minutes). However, in blends of PEI and SPAN-Na much shorter recovery times were found after CO₂ exposure but also a decrease in sensitivity. Better signal to noise ratio of the PEI blends in comparison to the pure PEI films opens possibilities of using these blends as CO₂ sensors in greenhouses and offices.

This chapter is part of a publication which is submitted as:

“Carbon Dioxide Detection at Room Temperature with Polyethyleneimine-based Chemiresistor”, Tin C. D. Doan, Rajesh Ramaneti, Jacob Baggerman, Antonius T. M. Marcelis, Hien D. Tong, and Cees J. M. van Rijn, submitted.

1. Introduction

In Chapter 4 a branched polyethyleneimine (PEI)-based chemiresistor was described for CO₂ sensing at low concentrations. However, the sensitivity is still relatively small and recovery time is rather long (more than 20 minutes). In literature, bilayers of PEI and oppositely-charged polyelectrolytes such as polystyrene sulfonate (PSS) showed fast CO₂ adsorption and desorption in the CO₂ capture process [1]. This was attributed to the presence of the PSS layer which might facilitate the transport of CO₂ [1]. It was found that the permeability coefficient of a number of gases including CO₂ decreases with an increasing extent of sulfonation in PSS [2]. Furthermore, the gas transport in Nafion, a polymer with a polytetrafluoroethylene backbone and fluoride-containing side-chains with terminal $-\text{SO}_3^-\text{M}^+$ groups was also studied [3, 4]. Investigation on permeation of CO₂ in Nafion membrane [3, 5, 6] revealed that the presence of sulfonate groups and metal counterions improved CO₂ transport selectivity. Moreover, solubility of gases in the K⁺-form of Nafion membrane was greater than those in the acid-form [3].

Therefore, in this Chapter blends of PEI with several polyelectrolytes containing sodium sulfonate groups were studied for improving CO₂ sensitivity and response times. These polyelectrolytes include sodium salt of sulfonated polyaniline (SPAN-Na), poly(sodium 4-styrenesulfonate) (PSS-Na), Nafion sodium sulfonate (Nafion-Na). The chemical structures of SPAN-Na, PSS-Na and Nafion-Na are shown in **Figure 1**. These polymers are all ionic conductors [7], strong polyelectrolytes and contain negatively charged groups ($-\text{SO}_3^-$). Their presence in blends with PEI might lead to fast CO₂ adsorption and desorption resulting in improvement in the CO₂ sensing characteristics (response time, recovery time, sensitivity).

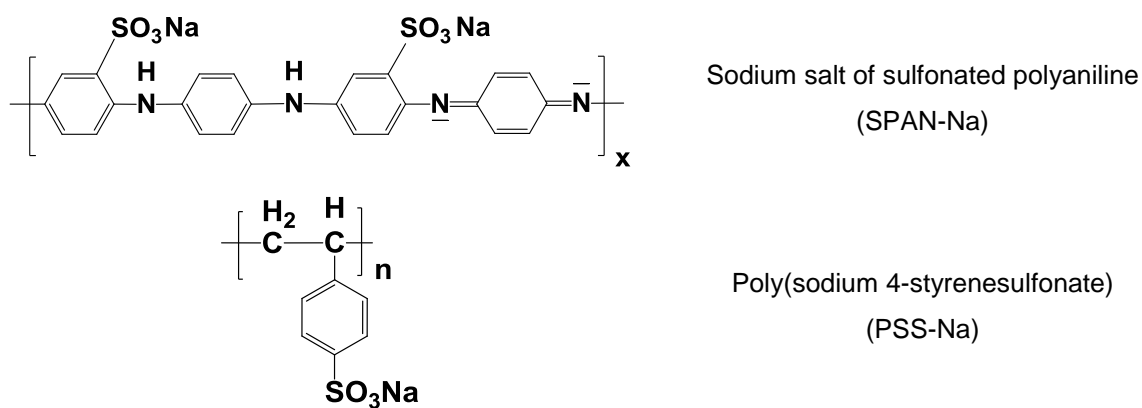




Figure 1. Chemical structures of polyelectrolytes used in blends with PEI.

In Chapter 2 undoped/unprotonated sulfonated polyaniline (SPAN-Na) exhibited CO₂ sensitivity but only at high concentrations (above 20,000 ppm) which are far from the desired concentrations for greenhouses (below 3,000 ppm). In this work PEI blends with SPAN-Na, PSS-Na, Nafion-Na were explored to detect lower CO₂ concentrations (below 3,000 ppm) with high sensitivity. 2-point ac impedance and dc resistance measurements of the PEI blend films showed a decrease in conductivity is proportional to CO₂ concentrations from 400 ppm to 3,000 ppm at different humidity regimes similar as the PEI sensors in Chapter 4. Nevertheless, the chemiresistive sensors with the PEI blends exhibited better CO₂ sensitivity in comparison to the pure PEI films.

2. Materials and Methods

2.1. Materials

Branched PEI (Mw ~25,000 by LS, Mn ~10,000 by GPC), Nafion 117 solution (~5% in a mixture of lower aliphatic alcohols and water) and PSS-Na (Mw ~70,000) were purchased from Sigma-Aldrich. All chemicals were used without further purification. Nafion-Na was prepared by mixing 3 ml Nafion 117 solution with 20 ml of 0.1 M NaOH for 2 hours at room temperature to replace protons of sulfonic acid in Nafion with sodium ions. Then the Nafion-Na aqueous solution was purified to remove excess NaOH by dialysis with a semipermeable membrane (Membra-cel Dialysis Tubing, molecular weight cutoff 3,500, Serva) in deionized water, which was refreshed 3 times per day during 4 days. Then the water was removed in vacuum and the product was further dried in a vacuum oven at 50 °C for 24 hours. The details of SPAN-Na synthesis can be found in Chapter 2. CO₂ (99.99%) and N₂ (99.999%) were purchased from Linde Gas Benelux.

2.2. Polymer Solutions and Sensor Preparation

PEI solution was prepared as described in Chapter 4. For the blend of PEI:SPAN-Na, 50 mg of SPAN-Na was dissolved in 5 ml of water (1% w/w). Similarly, for the blend of PEI:PSS-Na, 200 mg of PSS-Na was dissolved in 20 ml of water (1% w/w). 15 mg of Nafion-Na was

also dissolved in 1.5 ml of water (1% w/w) for the blend of PEI:Nafion-Na. All the polymer solutions were prepared at room temperature by magnetic stirring for 24 hours. These stock solutions were mixed with the PEI stock solution in different ratios of PEI:SPAN-Na, PEI:PSS-Na and PEI:Nafion-Na respectively to produce polymer blends in ratios of 1:1, 2:1, 3:1.

1 μL of the blend solutions was drop-casted onto a silicon chip with Pt interdigitated electrodes (thickness ~ 170 nm) of dimensions 300 μm (length) x 9 μm (width) and 6 μm spacing. The drop-casted polymer chips were dried at room temperature for 24 hours in a vacuum desiccator. The thickness of the blend films was determined using a surface profiler Dektak 6M (Veeco, USA). The PEI:SPAN-Na, PEI:PSS-Na and PEI:Nafion-Na blend films had a thickness of ~ 1 μm .

2.3. Ac Impedance and Dc Resistance Measurement to Characterize CO₂ Sensing of the Blend Coated Chips

The blend-coated chips were mounted in a chamber with controlled relative humidity (RH) levels and CO₂ concentrations. The details of the setup for gas sensor characterization can be found in Chapter 2. To investigate the CO₂ sensing capability of the PEI blends with SPAN-Na, PSS-Na and Nafion-Na, the blend-coated chips were exposed to different CO₂ concentrations (from 400 ppm to 10,000 ppm) at high humidity levels (from 60% to 90% RH) and the ac impedance and dc resistance of the blend films were measured at room temperature (24 °C). Two-point dc resistivity measurements were carried out using a Keithley 2400 source meter with voltage scanning from -5 V to +8 V. Ac impedance spectroscopy was measured using a HP 4192A LF impedance analyzer with applied voltage of 0.3 V and a frequency range of 5 Hz - 1 MHz. The impedance change was expressed in terms of Nyquist plots in which imaginary impedance (Z'') is plotted against the real impedance (Z') or Bode plots in which the measured absolute impedance ($|Z|$) and phase angle (θ) values are plotted against frequency.

3. Results and Discussion

3.1. Dc Resistance of the PEI:SPAN-Na Films upon Exposure to CO₂

The change in dc resistance of the PEI:SPAN-Na films upon the variation of CO₂ concentrations was investigated by I-V curve measurements (**Figure 2**). The two I-V curves of the PEI:SPAN-Na film at two CO₂ concentrations overlap when CO₂ increases from 400

ppm to 30,000 ppm. The resistance of the PEI:SPAN-Na film increases slightly (1%) upon exposure to CO₂ in comparison to the pure PEI films (Chapter 4). The increase in resistance indicates that the change is caused by binding of CO₂ to PEI. However, the addition of SPAN-Na to PEI reduces the increase in resistance of the PEI:SPAN-Na blend in the presence of CO₂. This might be due to the opposing effect of SPAN-Na. It was observed that the resistance of SPAN-Na films decreased upon exposure to CO₂ due to self-doping (Chapter 2). The lower response might also be due to the changes in binding characteristics of CO₂ to PEI.

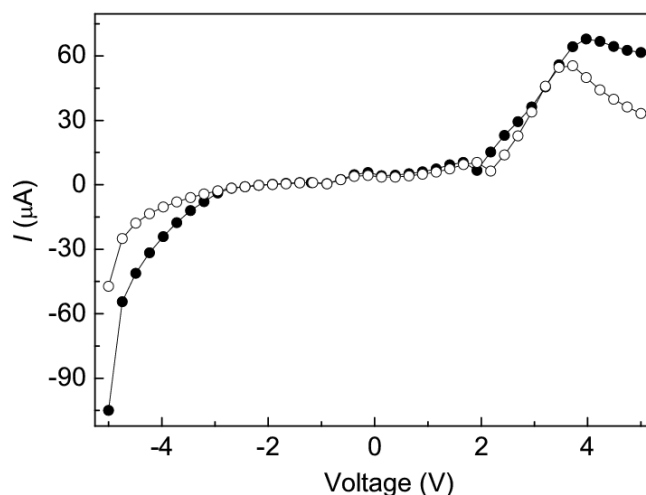


Figure 2. *I-V curves of the PEI:SPAN-Na 1:1 blend upon exposure to 400 ppm CO₂ (●) and 30,000 ppm CO₂ (○) at 75% RH.*

Similar to the pure PEI films, the current through the PEI:SPAN-Na blend also increases steeply at voltages larger than 2 V. Above 2 V, a decrease in current was observed indicating an increase in resistance of the blend film when CO₂ concentration increases starting from 400 ppm. Furthermore, oxidation peaks were observed in I-V curves at voltage of 3.5-4 V, indicating that some charge carrier injection in the film took place. To study this behavior in more detail, the voltage was scanned as a full loop and the current was measured. The blend of PEI:SPAN-Na was exposed to 80% RH without CO₂ and the voltage was scanned from -5 V to +5 V and then from +5V to -5 V. Right after that, the measurement was repeated with voltage scanned from -5V to +8 V and back from +8 V to -5 V. The scan rate was 20 mV.s⁻¹. The results are shown in **Figure 3** with oxidation peaks at ±3.5 V for both scanning processes. These peaks were also found in case of the pure PEI film. The redox reaction occurred when the blend films were exposed to water vapor at high humidity. This behavior was already observed with SPAN-Na upon exposure to high humidity (above 60% RH) (Chapter 3). The redox behavior was found in electronically/intrinsically conductive polymers and in case of

ion exchange polymers containing electrostatically bound redox centers including Nafion and PSS [8].

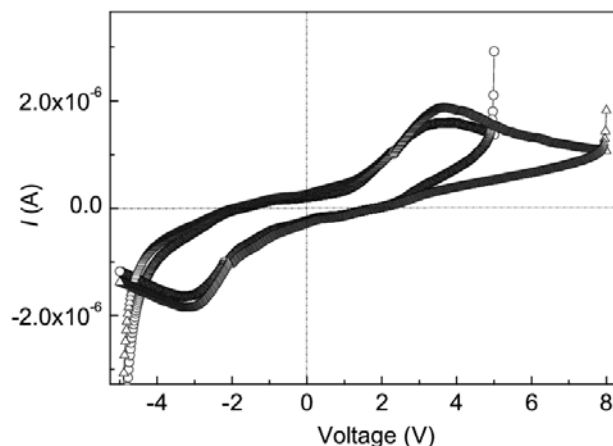


Figure 3. Loop scan *I-V* measurements of the PEI:SPAN-Na 1:1 blend film at humidity of 80% RH. Voltage scan from -5 V to +5 V (○), -5 V to +8 V (△) with scan rate of 20 mV.s^{-1} .

The non-linearity of *I-V* curves can be qualitatively understood from the space-charge-limited current model [9] as explained in Chapter 4.

3.2. Dc Resistance of the PEI:Nafion-Na Films upon Exposure to CO_2

The dc resistance of the PEI:Nafion-Na films in the presence of different CO_2 concentrations was also investigated by *I-V* measurements. The PEI blend film was exposed to 400-2,000 ppm CO_2 at 75% RH. Voltage was scanned from -5 V to +8 V and current was measured (Figure 4).

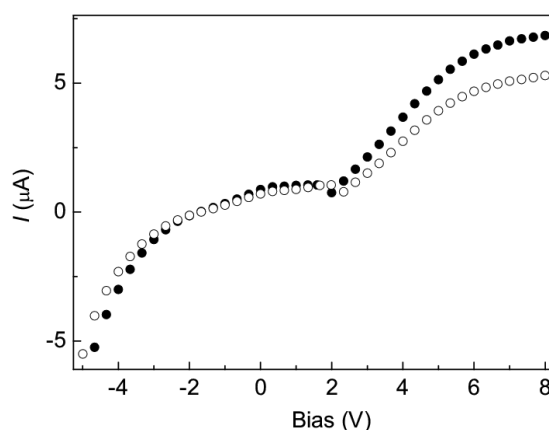


Figure 4. *I-V* curves of the PEI:Nafion-Na 1:1 blend upon exposure to 400 ppm CO_2 (●) and 2,000 ppm CO_2 (○) at 75% RH.

The shapes of the *I-V* curves of the PEI:Nafion-Na blend are similar to the ones of the pure PEI film but the current is about 6 times smaller (at 1 V) indicating a higher resistance of this

blend film. Dc resistance of the PEI:Nafion-Na films was calculated from the slopes in the linear parts of the I-V curves (between -2 V and 2 V). Dc resistance increases approximately 15% from 3.2 M Ω to 3.7 M Ω when the CO₂ concentration increases from 400 ppm to 2,000 ppm. This behavior is also similar to that of the pure PEI films (Chapter 4).

3.3. Impedance Spectroscopy of the PEI Blend Coated Chips upon Exposure to CO₂

Ac impedance measurement of the PEI blend films was conducted to determine conductivity change when the PEI blend films were exposed to CO₂. Variable-frequency ac absolute impedance ($|Z|$) was measured over the frequency range from 5 Hz to 1 MHz when the blend films were exposed to different CO₂ concentrations at 75% RH.

Increase in impedance of all the blend films are observed when CO₂ concentration increases from 400 ppm to 10,000 ppm CO₂ (**Figure 5**). Significant differences in absolute impedance amplitude $|Z|$ of the PEI blend films are observed between 400 ppm and 10,000 ppm CO₂ in a specific frequency range. For the PEI:SPAN-Na films the frequency range is 70 Hz - 500 kHz, for the PEI:PSS-Na blend the frequency range is 110 Hz - 1 MHz and for the PEI:Nafion-Na blend the frequency range is 1-10 kHz respectively. Blending of PSS-Na with PEI reduces difference in impedance at low frequency range (below 200 Hz). The impedance response of PEI:PSS-Na is reversed at frequency below 100 Hz, i.e. impedance decreases as CO₂ concentration increases. This frequency range describes the diffusion process of ionic species through double layer at the interface between polymer films and metal electrodes. The reversed response can be attributed to ionic conduction due to Na⁺ ions at low frequency.

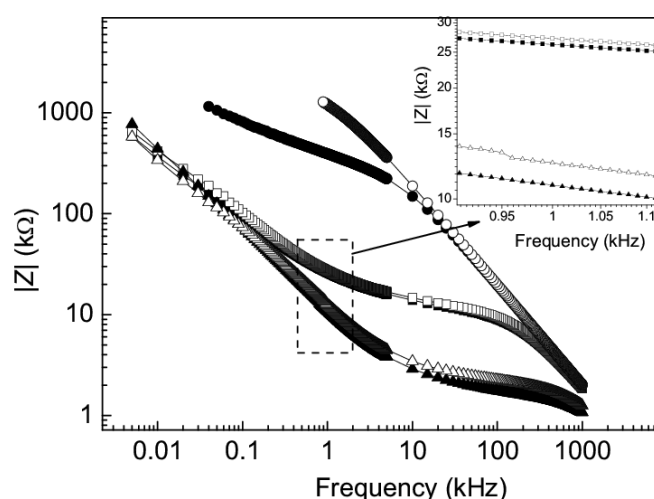


Figure 5. Absolute impedance ($|Z|$) of the blend films as a function of frequency at 75% RH upon exposure to 400 ppm CO₂ (closed symbol) and 10,000 ppm CO₂ (open symbol). PEI:SPAN-Na 1:1 (■, □), PEI:PSS-Na 1:1 (▲, △), PEI:Nafion-Na 1:1 (●, ○).

The relative change in impedance at 1 kHz of the PEI blends as a function of CO₂ concentrations is shown in **Figure 6**. The CO₂ sensitivity of the PEI:PSS-Na blend is equal in comparison to the pure PEI film (Chapter 4), whereas the PEI:SPAN-Na blend has a 5 time lower sensitivity. This is consistent with the dc measurement results of the PEI:SPAN-Na blend discussed above (**Figure 2**). However, the PEI:Nafion-Na blend showed a 15 times larger change in impedance than the pure PEI films. The changes in impedance as a function of CO₂ concentration follow a Langmuir isotherm for all the blends as well as the pure PEI films. These results are consistent with the impedance change from time dependent measurement (will be shown later).

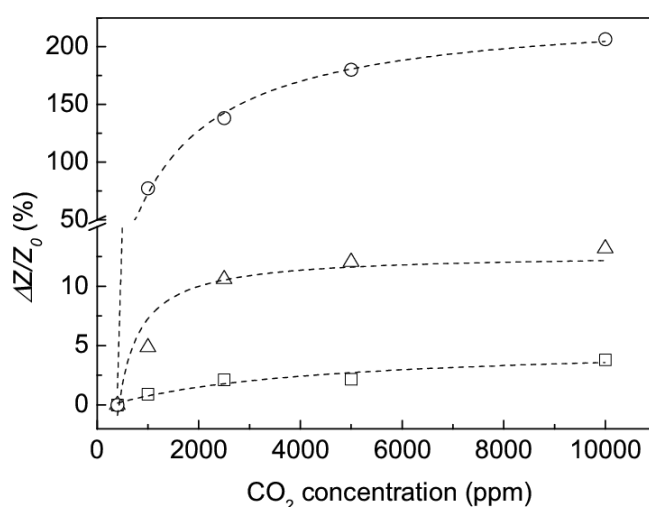


Figure 6. Relative change in impedance of the blends exposed to different CO₂ concentrations at 75% RH, frequency of 1 kHz. PEI:SPAN-Na 1:1 (□), PEI:PSS-Na 1:1 (Δ), PEI:Nafion-Na 1:1 (○).

Difference in the relative change in impedance of the blends can be explained by the structures of Nafion-Na, PSS-Na and SPAN-Na. Nafion has separate phases including hydrophobic (poly(tetrafluoroethylene) backbone) and hydrophilic regions (ionic sites (SO₃⁻)) with an intermediate phase containing the ether side-chains [10]. PSS-Na and SPAN-Na have a more rigid structure and do not allow the sulfonate groups to reorganize themselves into a separate phase. The interactions between the sulfonate groups of these polymers and the amine groups of PEI might lead to the different CO₂ sensing behavior as observed.

3.4. Dc Resistance of the PEI Blend Films upon Exposure to Humidity

The humidity-dependent resistance of the PEI:SPAN-Na and PEI:Nafion-Na blends was also investigated. I-V curves were measured when the blend films were exposed to different humidity levels (from 10% to 90% RH). Then the dc resistance was calculated from the slope

of I-V curves (linear parts at low voltage range of about 1 V). **Figure 7** shows the resistance of the blend films as a function of humidity. Similar to the response of the PEI films, the relationship between logarithmic dc resistance of the blend films and RH levels also follows the exponential equation presented in Chapter 4. The resistance of the PEI:Nafion-Na blend is larger than the resistance of the PEI:SPAN-Na blend at humidity above 20% RH. The reason might be attributed to the hydrophobic phase of Nafion hindering ionic and protonic conductions.

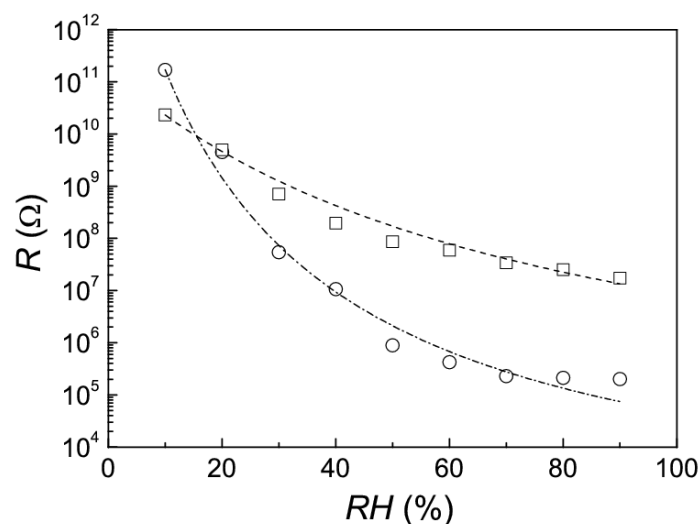


Figure 7. Relationship between resistance of PEI:SPAN-Na 1:1 (○) and PEI:Nafion-Na 1:1 (□) blend films and humidity from 10% RH to 90% RH.

3.5. Effect of Humidity on Impedance of the PEI Blend Films

Humidity-dependent conductivity of the PEI blend films was also investigated by impedance spectroscopy. **Figure 8** and **Figure 9** show the Nyquist plots and Bode plots of the PEI:SPAN-Na and PEI:Nafion-Na blend films at different humidity levels from 10% RH to 90% RH. The response to humidity of the PEI:SPAN-Na blend is similar to the PEI films. At low humidity 20% RH the real impedance (resistance - Z') does not show any change with frequency. At high humidities 40-90% RH the real impedance shows a strong dependence on imaginary impedance (reactance - Z'') indicated by semicircles. The radius of the semicircle decreases with increasing humidity, which indicates a decrease in resistance of the PEI blend films due to permeation of the water vapor into the films. The second semicircles and linear tails appearing at high humidities (from 40% RH onwards) relate to the charge transfer at electrode surface and diffusion of ionic species (protons and OH^-) generated from water through the double layer. Moreover, the angle of the diffusion tails also increases as humidity increases. This can be attributed to a delamination occurring in the PEI blend films when a

large amount of water diffuses and formed continuous channel water phase. In comparison to the PEI:SPAN-Na blends, the PEI:Nafion-Na blend has higher impedance even at high humidity regimes. This result is consistent with dc results mentioned above. The diffusion tail occurred at higher humidity levels (60% RH onwards). The high impedance of PEI:Nafion-Na is most likely due to hydrophobic regions (poly(tetrafluoroethylene) backbone) of Nafion leading to less water vapor bound to the blend film and hindered mobile charge (ions and protons) transport.

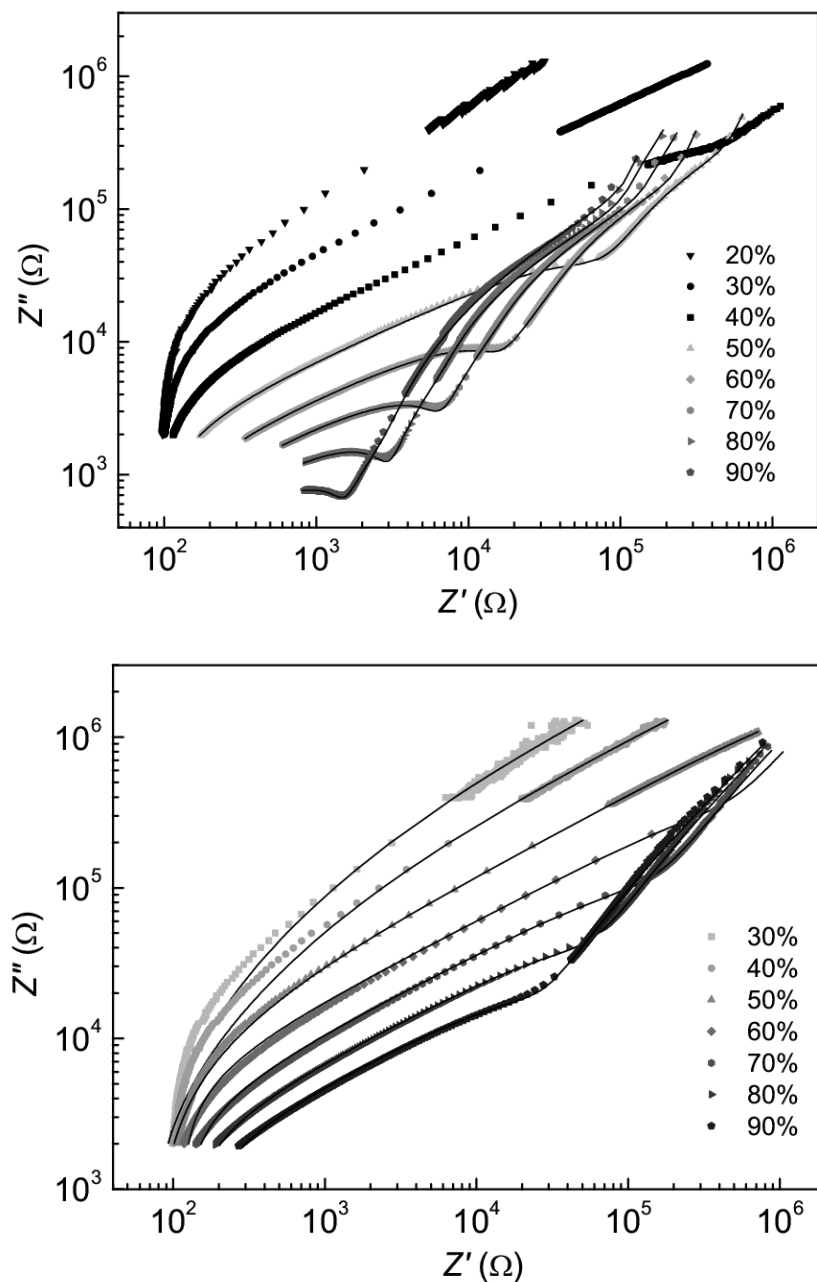


Figure 8. Nyquist plots of the blends PEI:SPAN-Na 1:1 (top) and PEI:Nafion-Na 1:1 (bottom) at different humidity levels (10-90% RH).

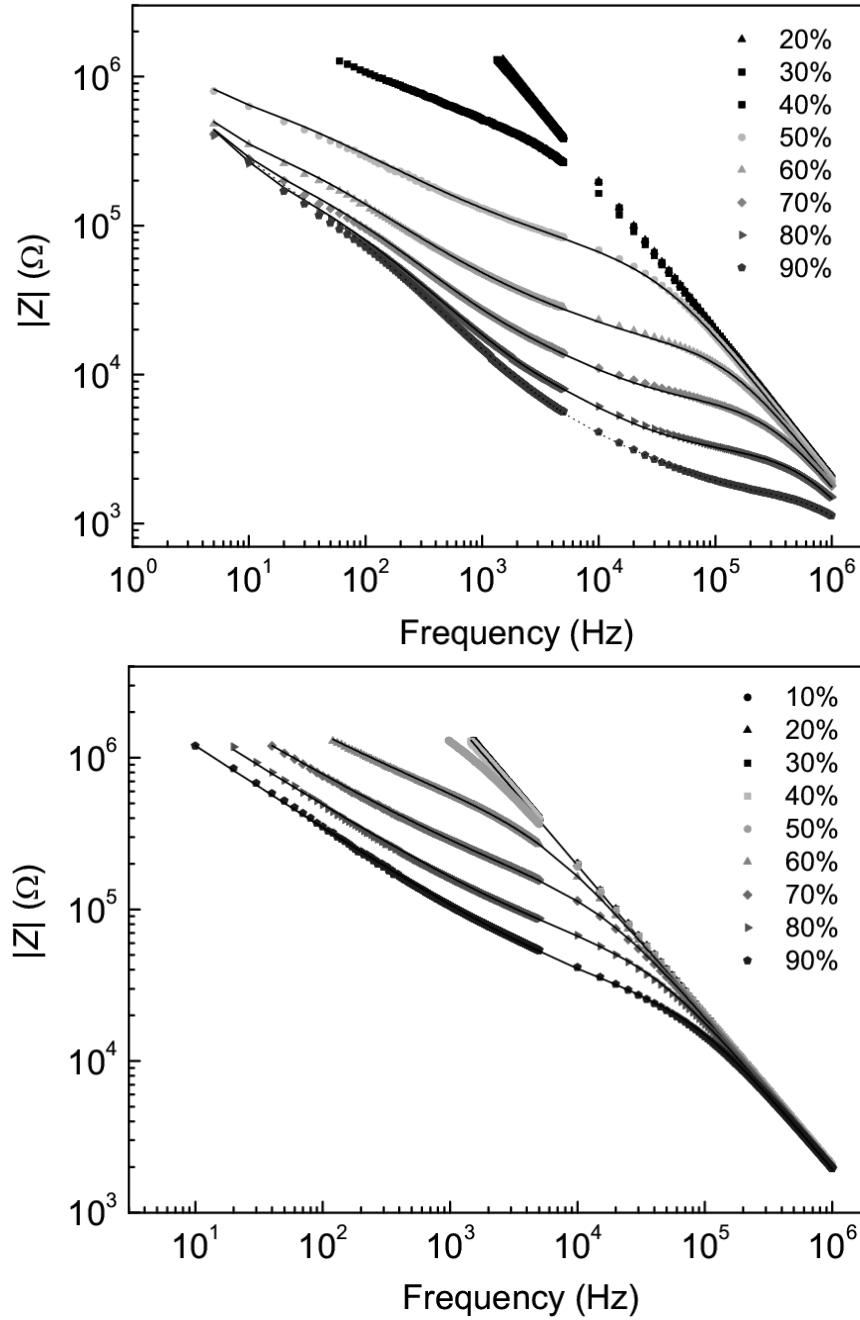


Figure 9. Bode plots of the blends $PEI:SPAN-Na$ 1:1 (top) and $PEI:Nafion-Na$ 1:1 (bottom) at different humidity levels (10-90% RH).

The impedance data were fitted to investigate conduction in the PEI blend films due to water vapor using the same model as presented in Chapter 4. The details of data fitting (equivalent circuit, values of elements) can be found in **Appendix 4**. The fitting shows a steady decrease of all resistances under influence of humidity for $PEI:SPAN-Na$ and $PEI:Nafion-Na$ (**Figure 10**). This is similar to our observation in the case of pure PEI (Chapter 4).

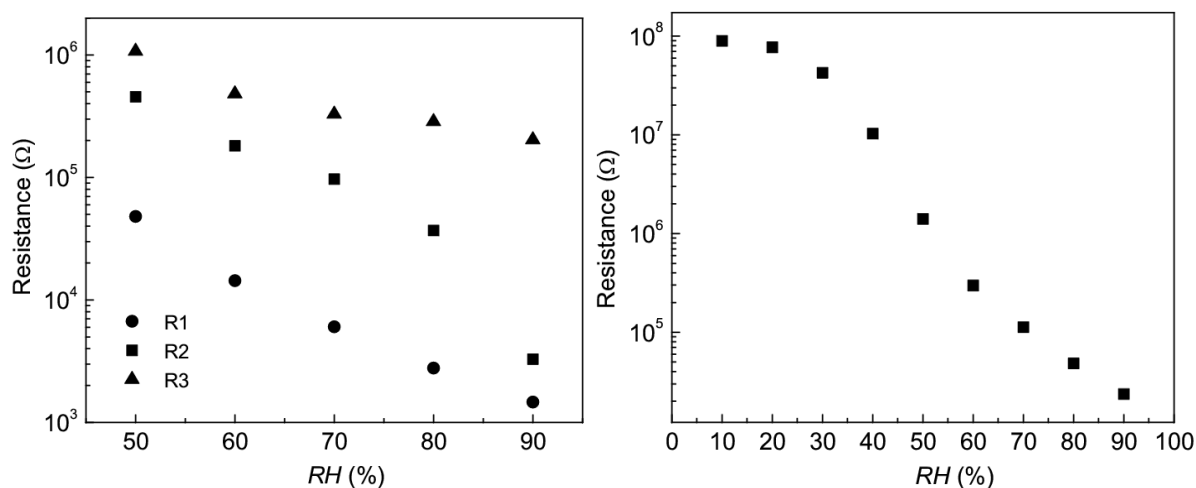


Figure 10. Fit parameters obtained at different humidities of the blends PEI:SPAN-Na 1:1 (left) and PEI:Nafion-Na 1:1 (right) at different humidity levels.

3.6. Comparison of Relative Change in Impedance due to Humidity and CO₂

All the polymers used to blend with PEI are hygroscopic due to their polar groups in the structures (as shown in **Figure 1**) hence the blends are all sensitive to humidity. To investigate the effect of humidity on CO₂ sensitivity of the PEI blends, all the blends with ratio of 1:1 were exposed to 60% RH without and with 1% CO₂ and then to 62% RH without any CO₂. The impedance was measured with frequency scanning from 5 Hz to 1 MHz (**Appendix 4 - Figure A7**). The measurements were repeated 2 times on the same interdigitated electrode chip to check reproducibility and the relative changes in impedance due to 1% change in RH and 1% CO₂ of the PEI blends were calculated and plotted in **Figure 11**. All the polymers at 60% RH exhibited the same behavior as at 75% RH mentioned above. CO₂ causes an increase in impedance whereas humidity induces a decrease in impedance. The decrease in impedance upon exposure higher humidity levels was observed as mentioned above.

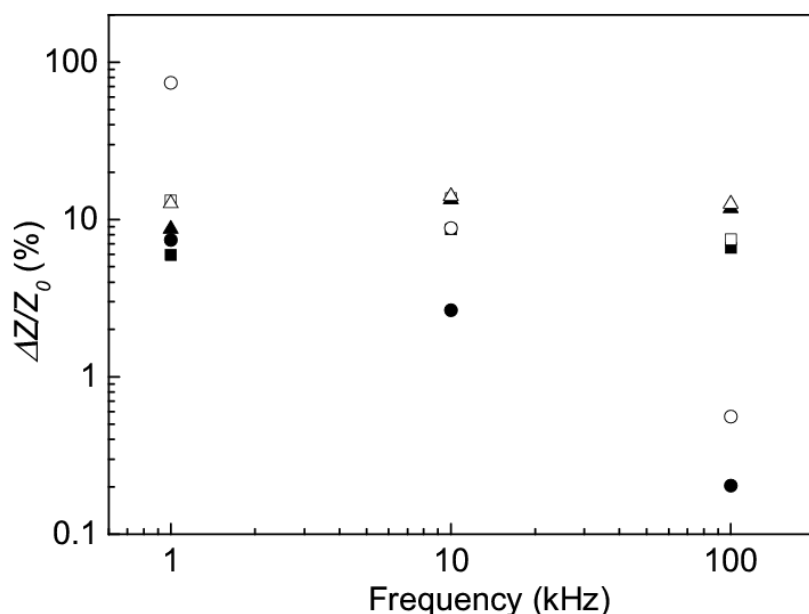


Figure 11. Relative change in impedance $\Delta Z/Z_0$ at 1 kHz, 10 kHz and 100 kHz due to 1% change in RH (closed symbol) and 1% CO₂ (open symbol). PEI:SPAN-Na 1:1 (□), PEI:PSS-Na 1:1 (Δ), PEI:Nafion-Na 1:1 (○).

For the PEI:SPAN-Na films, at 1 kHz and 10 kHz the relative change in impedance due to 1% CO₂ is 2.2 and 1.6 times larger respectively than due to a 1% change in RH. At 100 kHz, there is no significant change in relative change of the impedance between CO₂ and RH. Hence, measurements at 100 kHz cannot distinguish the effect of humidity and CO₂ on impedance of this blend (please notice some overlap of symbols in **Figure 11**). For the PEI:PSS-Na films, the relative change in impedance due to 1% CO₂ is about 1.4 times larger than due to a 1% change in RH at 1 kHz. At 10 kHz and 100 kHz, no significant difference in relative change is observed. For the PEI:Nafion-Na films, the relative change in impedance due to 1% CO₂ is 10, 3.4 and 3 times larger than due to 1% change in RH at 1 kHz, 10 kHz and 100 kHz respectively. From the results of all the blend films, it is apparent that 1 kHz gives the largest relative change in impedance, so 1 kHz is more suitable than other frequencies to distinguish the sensitivity towards CO₂.

Next the absolute impedance $|Z|$ of the blend films was measured at a constant frequency under various conditions. Frequency of 1 kHz was chosen to measure time dependent impedance response of PEI blend films upon exposure to different CO₂ concentrations. 10 kHz and 100 kHz were also used for time dependent measurement to verify the results of impedance spectroscopy.

3.7. Time Dependent Impedance Response of PEI Blend Films upon Exposure to CO₂

Time dependent measurement exhibits the dynamic response of the blends towards CO₂ including the response time, recovery time, drift, etc. which involves the absorption/desorption of CO₂ on the blends. As mentioned above, the time dependent measurements were measured at a fixed frequency as CO₂ concentration varies from 400 ppm (baseline) to 18,000 ppm.

3.7.1. PEI:SPAN-Na Films

SPAN-Na was found to be sensitive to CO₂ with a very fast response and recovery time (Chapter 2). Moreover, SPAN-Na is also a strong polyelectrolyte because it contains ionizable, negatively charged sulfonate groups bound to the backbone. Therefore, blending of PEI with SPAN-Na is expected to increase the conversion rate of carbamates and bicarbonates when CO₂ is removed, hence the recovery time might be reduced.

The time dependent impedance response of PEI:SPAN-Na films was measured at 1 kHz, CO₂ concentration ranged from 400 ppm to 18,000 ppm at 75% RH (**Figure 12**). The response time is about 1.5-4 minutes and the recovery time is much shorter, about 1.5-10 minutes compared to 20-60 minutes for the pure PEI film (Chapter 4). The PEI:SPAN-Na blend had very short response time and recovery time even at high CO₂ concentration of 18,000 ppm. However, a drift in impedance response of this blend was observed.

It is apparent that addition of SPAN-Na reduces the relative change in impedance but the presence of SPAN-Na shortens recovery time significantly. This is attributed to the fact that after removal of CO₂, SPAN-Na might shift the pH equilibrium because SPAN-Na is also a polymer having a pH-dependent conductivity (Chapter 2). Formed carbamates and bicarbonates might cause an increase in conductivity of SPAN-Na due to interactions of SPAN-Na with bicarbonates and carbamates resulting in an ionic conduction change. A drift in impedance response was observed with high ratio of SPAN-Na in the blend. This can be attributed to the effect of humidity on SPAN-Na. The blends of PEI:SPAN-Na were also measured at frequency of 10 kHz and 100 kHz but the impedance response showed smaller sensitivity and large drift (data not shown). Therefore, 10 kHz and 100 kHz frequency are not suitable for time dependent measurement.

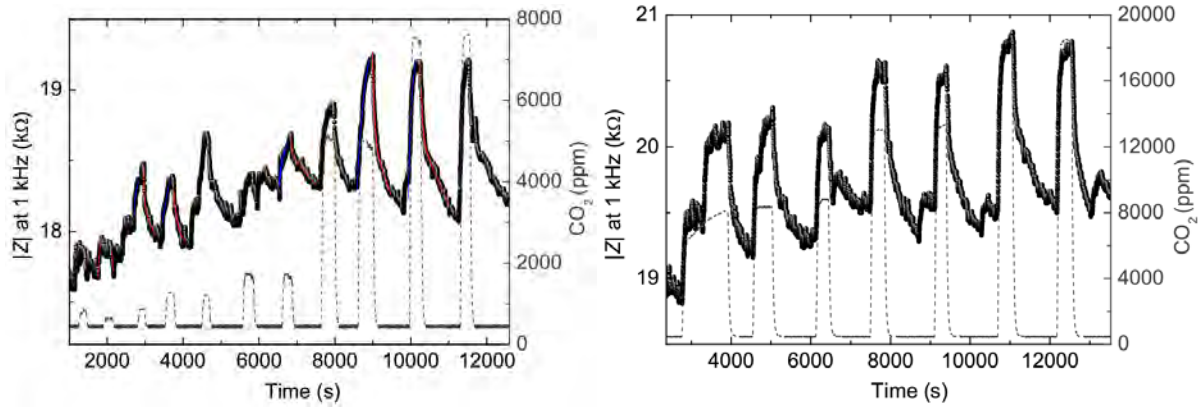


Figure 12. Time dependent impedance response of PEI:SPAN-Na 2:1 measured at 1 kHz when the blend was exposed to low (left) and high (right) CO₂ concentrations (dash line) at 75% RH.

Figure 13 shows the relative change in impedance ($\Delta Z/Z_0$) as a function of CO₂ concentrations of the PEI:SPAN-Na blends calculated from the time dependent impedance response measured at 1 kHz, 75% RH. The inset of **Figure 13** shows the sensitivity of the different ratios of PEI:SPAN-Na at high range of CO₂ concentrations (8,000-18,000 ppm) which were used to compare due to low sensitivity of the PEI:SPAN-Na blends. A Langmuir isotherm between relative change in impedance and CO₂ concentrations was observed for the PEI:SPAN-Na 2:1 blend. The relative change in impedance of the PEI:SPAN-Na 1:1 blend was found to be 2 times smaller at high CO₂ concentrations than the blends of ratio 2:1 and 3:1. Therefore, a decrease in the amount of SPAN-Na in the blend of PEI:SPAN-Na increases the relative change in impedance upon exposure to CO₂. This is in line with a response due to binding to PEI.

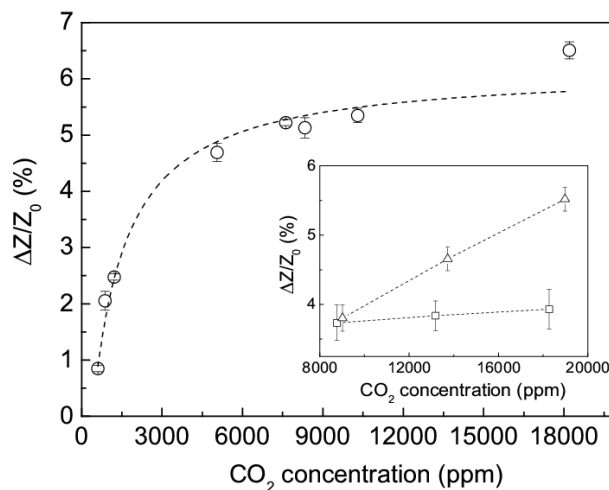


Figure 13. Relative change in impedance ($\Delta Z/Z_0$) as a function of CO₂ concentration at 75% RH of the PEI:SPAN-Na 2:1 blend (○). The inset: Smaller $\Delta Z/Z_0$ of PEI:SPAN-Na blends with ratio 1:1 (□) and ratio 3:1 (Δ) at 75% RH.

In comparison to the pure PEI films, the PEI:SPAN-Na 2:1 blend has a 3 time smaller sensitivity (e.g. at 1,200 ppm), leading to a much smaller change in impedance at low CO₂ concentrations. However, mixing PEI with SPAN-Na induced quite fast response and much shorter recovery time (about 15 times) as compared to pure PEI in CO₂ sensing.

3.7.2. PEI:PSS-Na Films

PSS-Na is an ionic conductor similar to SPAN-Na [7] and it exhibited fast CO₂ adsorption and desorption in the structure of polyelectrolyte multilayers with PEI [1]. Therefore, blending of PEI with PSS-Na was also investigated for CO₂ sensing in this research.

The time dependent impedance response of the PEI:PSS-Na films was measured at 1 kHz, CO₂ concentration was 400-10,000 ppm at 75% RH (**Figure 14**). The response time was a bit longer in comparison to the PEI:SPAN-Na blend (6-8 minutes). The recovery time was much longer than the PEI:SPAN-Na blend. The PEI:PSS-Na 3:1 blend has a recovery time of about 10-28 minutes, whereas the PEI:PSS-Na 1:1 blend has longer recovery time (about 35 minutes) at high CO₂ concentrations.

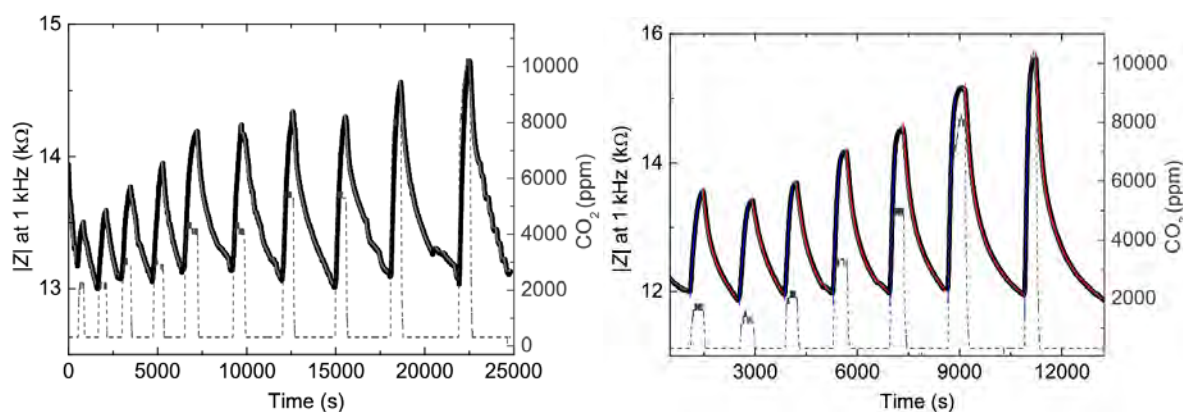


Figure 14. Time dependent impedance response of PEI:PSS-Na (1:1) (left) and PEI:PSS-Na (3:1) (right) measured at 1 kHz when the composite was exposed to different CO₂ concentrations (dash line) at 75% RH.

Figure 15 shows the relative change in impedance ($\Delta Z/Z_0$) as a function of CO₂ concentrations of the PEI:PSS-Na blends calculated from the time dependent impedance response measured at 1 kHz, 75% RH. A Langmuir isotherm between relative change in impedance and CO₂ concentrations was also observed for all the blends of PEI:PSS-Na. The relative change in impedance of the PEI:PSS-Na 1:1 blend was found to be 3 times smaller than the blend of ratio 3:1. This relative change in impedance of the PEI:PSS-Na 1:1 blend is consistent with the relative change in the Bode plots presented above (**Figure 5**).

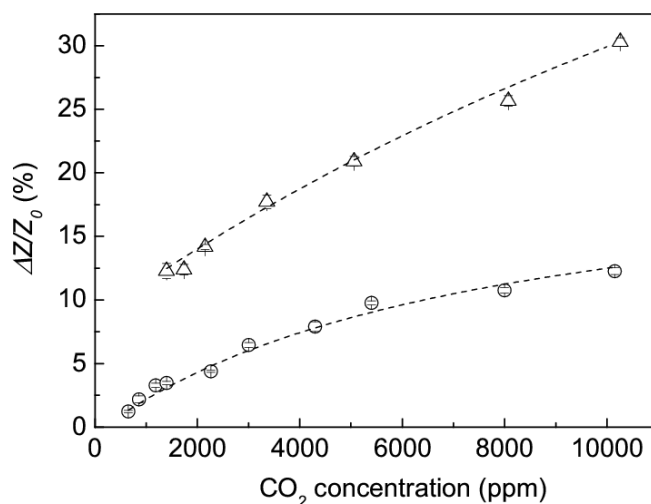


Figure 15. Relative change in impedance ($\Delta Z/Z_0$) in respect to CO_2 concentrations at 75% RH of the PEI:PSS-Na blends with ratio 1:1 (O) and ratio 3:1 (Δ).

In comparison to the pure PEI films, the sensitivity of the PEI:PSS-Na 3:1 blend is about 2 times higher. However, the recovery time is about 3 times shorter than the pure PEI films. Therefore, mixing of PEI with PSS-Na can improve the CO_2 sensing for the PEI films.

3.7.3. PEI:Nafion-Na Blend Films

To compare with SPAN-Na and PSS-Na which have sodium sulfonate groups, Nafion 117 was mixed with NaOH solution to replace protons of sulfonic acids with sodium ions. From the Bode plots (**Figure 5**), blending of PEI with Nafion-Na exhibited largest relative change in impedance when the PEI:Nafion-Na 1:1 blend was exposed to 400 ppm and 10,000 ppm CO_2 at 75% RH. Therefore, the blends of PEI:Nafion-Na were studied thoroughly. In addition, to compare with Na-form, Nafion 117 was also mixed with PEI and coated on chemiresistors for CO_2 sensing measurements.

The time dependent impedance response of PEI:Nafion-Na 1:1 blend films was measured at 1 kHz, CO_2 concentration was 400-10,000 ppm at 75% RH (**Figure 16-top left**). The PEI:Nafion-Na blend showed a high sensitivity towards CO_2 but some instability in the impedance response was observed. The same devices periodically measured after 2 weeks and 4 weeks showed however a decrease in baseline impedance and also a reduced sensitivity to CO_2 . **Figure 16-top right** and **Figure 16-bottom** show the responses of the PEI:Nafion-Na 1:1 blends after 2 weeks and 4 weeks. As can be seen, the absolute impedance $|Z|$ at 75% RH of the PEI:Nafion-Na 1:1 blend decreased from 400 k Ω to 200 k Ω and the increase in impedance in the presence of CO_2 was also reduced correspondingly. Nevertheless, the

impedance baseline of the PEI:Nafion-Na 1:1 blend was stable after 2 weeks but a further decrease in sensitivity was still observed (**Figure 16-top right**).

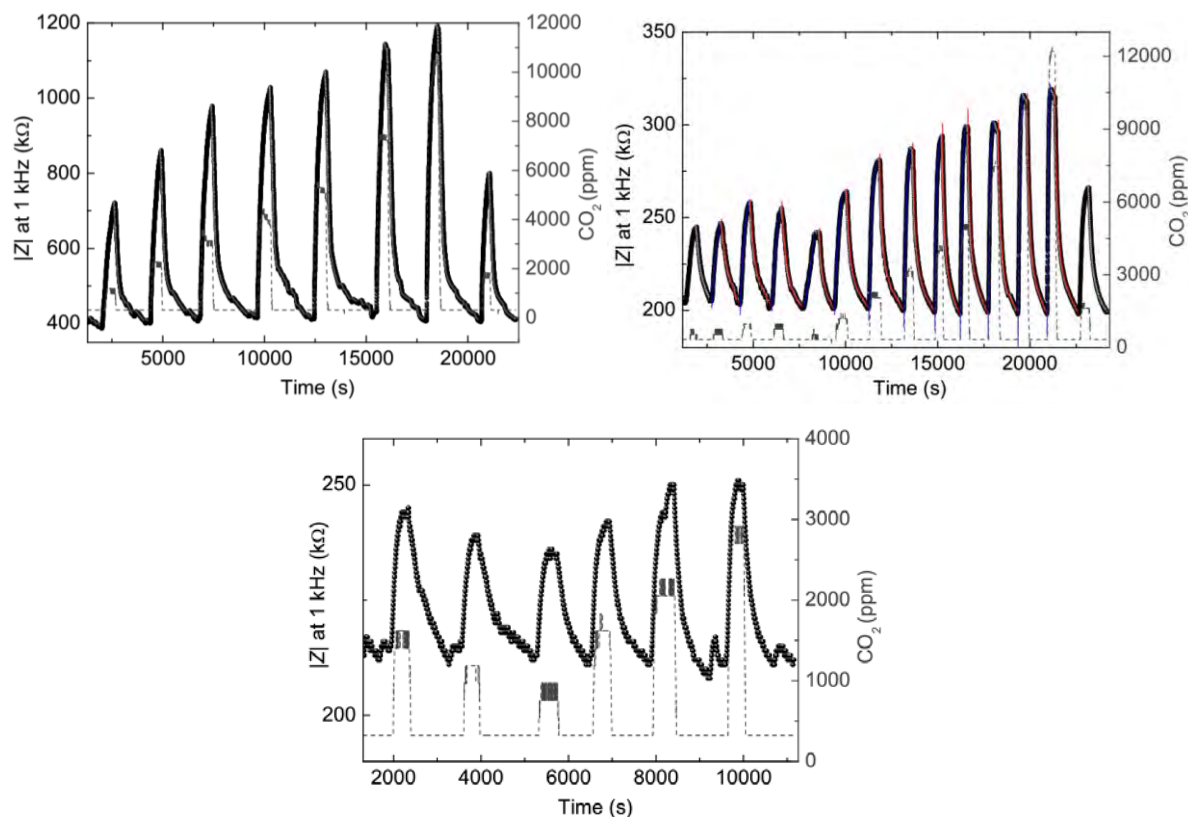


Figure 16. Time dependent impedance response of PEI:Nafion-Na 1:1 measured at 1 kHz when the blend was exposed to different CO_2 concentrations (dash line) at 75% RH. (Top left) as prepared - the first measurement, (top right) after 2 weeks, (bottom) after 4 weeks.

It should be noticed that the impedance values of the PEI:Nafion-Na 1:1 in the first measurement of time dependent impedance matched with the values obtained in impedance spectroscopy as shown in **Figure 5** above. To check the consistency the impedance spectroscopy of the PEI:Nafion-Na 1:1 blend was measured again after 2 weeks when the blend film was exposed to 400-3,000 ppm CO_2 at 75% RH (**Figure 17**). The impedance values at 1 kHz matched with the impedance values in time dependent measurement in **Figure 16-top left**, the impedance increased from 187 k Ω (at 400 ppm CO_2 - baseline) to 284 k Ω (at 3,000 ppm CO_2).

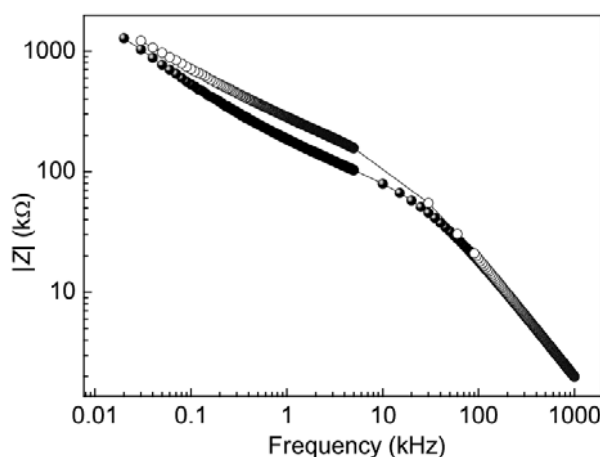


Figure 17. Absolute impedance ($|Z|$) of PEI:Nafion-Na 1:1 films after 2 weeks as a function of frequency at 75% RH with 400 ppm (●) and 3,000 ppm CO_2 (○).

The time dependent impedance responses of PEI:Nafion-Na 3:1 and PEI:Nafion 2:1 blend films were measured at 1 kHz, CO_2 concentration was 400-8,000 ppm at 75% RH (**Appendix 4 - Figure A8-A9**). The relative change in impedance ($\Delta Z/Z_0$) of the PEI:Nafion-Na blends was calculated from the time dependent impedance responses of the blends and plotted as function of CO_2 concentrations in **Figure 18**. The sensitivity of all the blends follows the Langmuir isotherms similar to the PEI films in Chapter 4. With increasing PEI content the signal ratio went down. This is in contrast with PSS and SPAN-Na blends which showed an increasing response with increasing PEI content. This shows that blending with Nafion-Na enhances the sensitivity of the PEI.

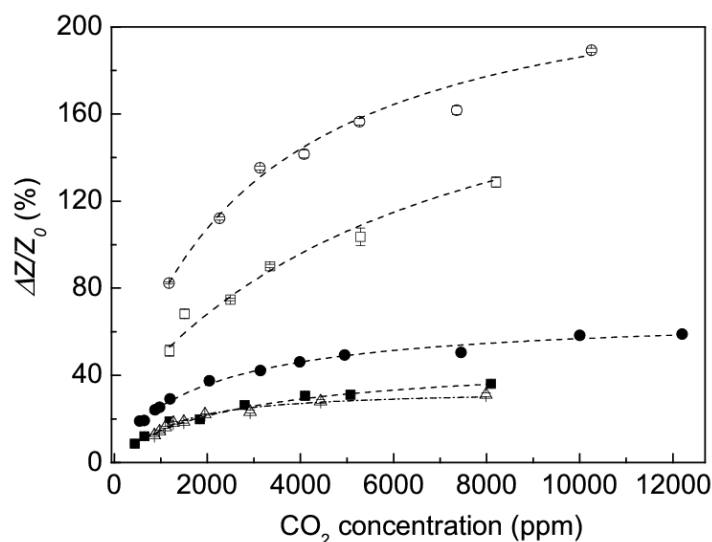


Figure 18. Relative change in impedance as a function of CO_2 concentrations of PEI:Nafion-Na 1:1 in the first measurement (○) and after 2 weeks (●), PEI:Nafion-Na 2:1 in the first

measurement after 2 weeks of storage (Δ), PEI:Nafion-Na 3:1 in the first measurement (\square), and after 2 weeks (\blacksquare) at 75% RH.

From the results of the PEI:Nafion-Na blends it can be concluded that after some time (2 weeks) of storage in a closed box (in case of PEI:Nafion-Na 2:1) or measurement with CO₂ at high humidity (PEI:Nafion-Na 1:1, 3:1), the PEI:Nafion-Na blends reached stability. The common trend is that both the impedance and the CO₂ sensitivity of these blends decrease.

The decrease in impedance of these blends before reaching stability after some time can be attributed to the instability of Nafion which was noticed and investigated in literature [4, 11, 12]. The chemical degradation of Nafion is due to generated peroxide radicals. H₂O₂, formed by reactions between oxygen and hydrogen, then decomposes, giving $\bullet\text{OH}$ or $\bullet\text{OOH}$ radicals that attack the H-containing terminal bonds ($-\text{CF}_2\text{COOH}$) and this initiates chemical decomposition [4, 11]. However, this form of chemical attack is most aggressive in the presence of peroxide radicals at low humidity and temperatures exceeding 90 °C [11]. In our case, the PEI:Nafion-Na blends were measured at high humidity and at room temperature (24 °C). Furthermore, all the samples were dried in a vacuum desiccator at room temperature after the measurement to remove any residues of water vapor and CO₂ gas. Therefore, the explanation of chemical degradation of Nafion seems not the only reason in our case. One possibility is that some Na⁺ ions could be replaced by protons in the preparation process (water was used as solvent) or protons coming from water electrolysis at high humidity under bias during quite long period of time dependent impedance measurements (more than 6 hours). These protons could not be replaced by Na⁺ ion resulting in some parts of Nafion-Na which contain acid form hence the blend film has a high ionic conductivity [10]. Therefore, reduced impedance was observed already after the first measurements of these blends.

3.8. Role of $-\text{SO}_3\text{Na}$ Group in the Interaction with CO₂

The sulfonate groups might be the main contribution to the better CO₂ sensitivity of the PEI blends. To check the effect of $-\text{SO}_3\text{Na}$ groups on CO₂ sensing of Nafion-Na blends, Nafion in acid form was also used as a component in PEI blend.

The impedance response of the PEI:Nafion 1:1 blend measured at 1 kHz was shown in **Figure 19** when the film was exposed to CO₂ at 75% RH. As can be seen, the impedance of this blend is much smaller (6.6 times) than the blend of PEI:Nafion-Na 1:1. It is due to the presence of sulfonic acid as discussed above. In addition, the relative change in impedance (sensitivity) of this blend was also much smaller (about 5 times) than the blend of Na-form.

The reduced sensitivity of the acid-form of Nafion is consistent with the decrease in CO₂ sensitivity of the PEI:Nafion-Na blends. Hence the hypothesis that some parts of Na⁺ ions were replaced by protons might be reasonable, resulting in higher conductivity and lower sensitivity as observed. Moreover, a drift in impedance response of the PEI:Nafion was observed. Therefore, the acid-form of Nafion seems not to be a good choice for PEI blends. However mixing with other hydrophobic polymers might have the same effect on the sensitivity.

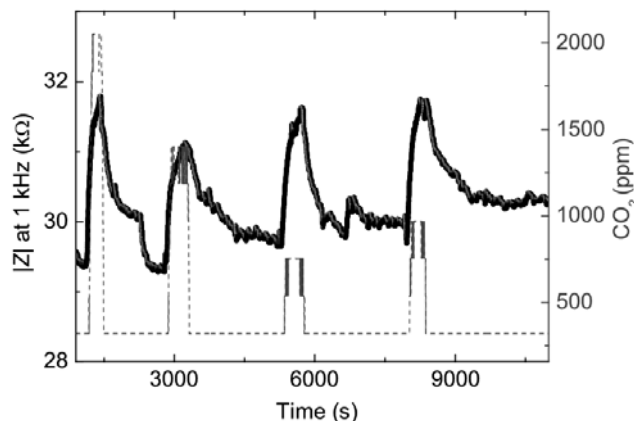


Figure 19. Time dependent impedance response measured at 1 kHz of PEI:Nafion 1:1 exposed to different CO₂ concentrations (dash line) at 75% RH.

The response time of the PEI:Nafion-Na blends was 7-8 minutes, the same as the PEI:PSS-Na blends. However, the recovery time of the PEI:Nafion-Na blend is the longest among the PEI blends, about 10-20 minutes (**Figure 20**). Nevertheless, the recovery time of this blend is about 2 times shorter in comparison to the pure PEI films.

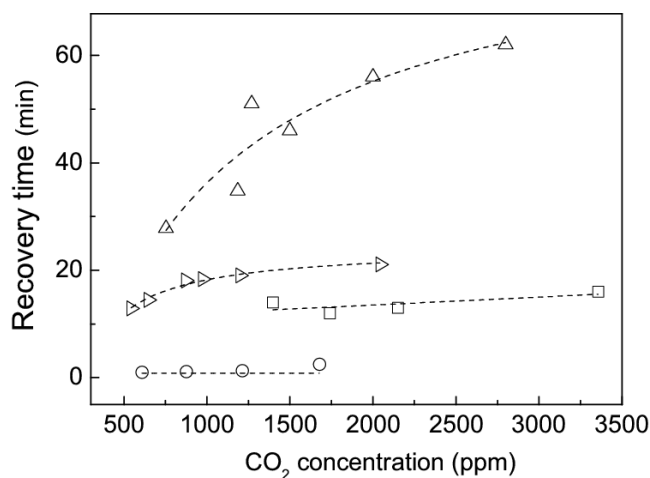


Figure 20. Recovery time as a function of CO₂ concentrations of PEI:SPAN-Na 2:1 (○), PEI:PSS-Na 3:1 (□), PEI:Nafion-Na 1:1 (▷) at 75% RH. Data of PEI (Δ) was taken from Chapter 4.

4. Conclusions

In conclusion, mixing PEI with other polyelectrolytes can result in better sensitivity or faster response times to CO₂ at low concentrations. Blending of PEI and SPAN-Na exhibited fast response and short recovery time (high reversibility) but reduced sensitivity in comparison to pure PEI. Furthermore, the blends of PEI with PSS-Na or Nafion-Na gave higher sensitivity and shorter recovery time. Water vapor is also the main cross-sensitive analyte and causes the same effect as observed in the PEI films. For all the PEI blends, measurements at 1 kHz can distinguish the relative change in impedance due to the effect of CO₂. Therefore, blending PEI with other polyelectrolytes improves CO₂ sensing characteristic of PEI and these PEI blends can be used for CO₂ sensor in greenhouses. A good candidate material seems to be PEI:Nafion-Na 1:1 with a relative humidity independent impedance change at 1 kHz of 40-110% for 2,000 ppm CO₂ with a fast response time in the order of minutes and a recovery time of less than 20 minutes.

References

- [1] B. Li, B. Jiang, D.J. Fauth, M.L. Gray, H.W. Pennline, G.A. Richards, Innovative nano-layered solid sorbents for CO₂ capture, *Chemical Communications*, 47 (2011) 1719-1721.
- [2] W.-J. Chen, C.R. Martin, Gas-transport properties of sulfonated polystyrenes, *Journal of Membrane Science*, 95 (1994) 51-61.
- [3] T. Sakai, H. Takenaka, E. Torikai, Gas Diffusion in the Dried and Hydrated Nafions, *Journal of The Electrochemical Society*, 133 (1986) 88-92.
- [4] R.B.M. Kenneth A. Mauritz, State of Understanding of Nafion, *Chemical Reviews*, 104 (2004) 4535–4585.
- [5] J.S. Chiou, D.R. Paul, Gas permeation in a dry Nafion membrane, *Industrial & Engineering Chemistry Research*, 27 (1988) 2161-2164.
- [6] T. Sakai, H. Takenaka, N. Wakabayashi, Y. Kawami, E. Torikai, Gas Permeation Properties of Solid Polymer Electrolyte (SPE) Membranes, *Journal of The Electrochemical Society*, 132 (1985) 1328-1332.
- [7] A.J. Epstein, Yue, Jiang, Sulfonated polyaniline salt compositions and uses thereof, Patent: 5159031, (1992).

- [8] G. Inzelt, Classification of Electrochemically Active Polymers Conducting Polymers, in, Springer Berlin Heidelberg, 2012, pp. 7-82.
- [9] R.W.I. de Boer, A.F. Morpurgo, Influence of surface traps on space-charge limited current, *Physical Review B*, 72 (2005) 073207.
- [10] S. Tan, D. Bélanger, Characterization and Transport Properties of Nafion/Polyaniline Composite Membranes, *The Journal of Physical Chemistry B*, 109 (2005) 23480-23490.
- [11] D.E. Curtin, R.D. Lousenberg, T.J. Henry, P.C. Tangeman, M.E. Tisack, Advanced materials for improved PEMFC performance and life, *Journal of Power Sources*, 131 (2004) 41-48.
- [12] F.M. Collette, C. Lorentz, G. Gebel, F. Thominette, Hygrothermal aging of Nafion®, *Journal of Membrane Science*, 330 (2009) 21-29.

Chapter 6. General Discussion

The major achievements of this research are summarized in this Chapter. Discussions on many different aspects of CO₂ sensing based on CO₂ sensitive polymers are presented. Furthermore, some perspectives and suggestions are proposed for further development of low power CO₂ sensors suitable for use in greenhouses.

In this research, several conductive polymers were investigated for carbon dioxide (CO_2) sensing as presented in the previous chapters. We examined amongst other ones the polymer sulfonated polyaniline, in which charge is transported by cations (H^+ , Na^+) and in which charge is transported along and between polymer molecules via generated charge carriers (e.g., holes, electrons, polarons). We studied blends of different polymers and derived Electrochemical Impedance Spectroscopy models capable of uncoupling ionic and intrinsic charge transport. CO_2 can induce in polymers a pH change provided that the polymer can retain water, and enables dissociation of H_2CO_3 into HCO_3^- and H^+ . The protons subsequently protonate the conducting polymers resulting in an increase in conductivity of sulfonated polyaniline. In *Chapter 2*, emeraldine base polyaniline (EB-PANI) was shown to be not suitable for CO_2 sensing because the active pH sensing range (below pH 4) is far from the pH range needed for CO_2 sensing (pH4 - pH7). Undoped sulfonated polyaniline sodium salt (SPAN-Na) exhibited a better matching pH-dependent conductivity and a measurable sensitivity towards CO_2 was found at high humidity (*Chapter 2*). However, a significant change in impedance of these polymer films was only observed at high CO_2 concentrations (above 2%) (*Chapter 2*).

An important achievement of this research is the demonstration of a CO_2 chemiresistive sensor based on polyethyleneimine (PEI) including its blends with SPAN-Na, sodium salt poly(styrene sulfonate) (PSS-Na) and Nafion sodium salt (Nafion-Na). These materials displayed a CO_2 sensing ability covering a wide CO_2 concentration range (from 400 ppm to 20,000 ppm) with a moderate to fast response (*Chapter 4* and *5*). At a high sensitivity we normally found a prolonged recovery time for some polymers (pure PEI, PEI:PSS-Na, PEI:Nafion), with a relatively low value for PEI:SPAN-Na (recovery in the order of a few minutes). In both greenhouse and office applications a fast response may be more relevant than a delayed recovery because the ascent towards a maximum CO_2 concentration is the primary critical steering parameter. Also these levels are relatively low (below 1,500 ppm) and they do not rapidly change as a certain level has been reached. Therefore, these polymers seem good candidates to be used as sensing layer for CO_2 sensors in greenhouses and offices.

However, to be used in greenhouses, factors affecting the accuracy and stability of the sensors should also be considered, such as variations in (high) humidity, fluctuations of temperature, solar radiation, air ventilation (as shown in **Figure 1**) and the presence of possible contaminant gases in the greenhouse environment.

Hence, in this chapter, the effects of these factors on the performance of the polymer sensors will be discussed. Furthermore, some perspectives and further researches are suggested to improve CO₂ sensitivity of the polymers and application in wireless sensor network for greenhouses will be outlined.

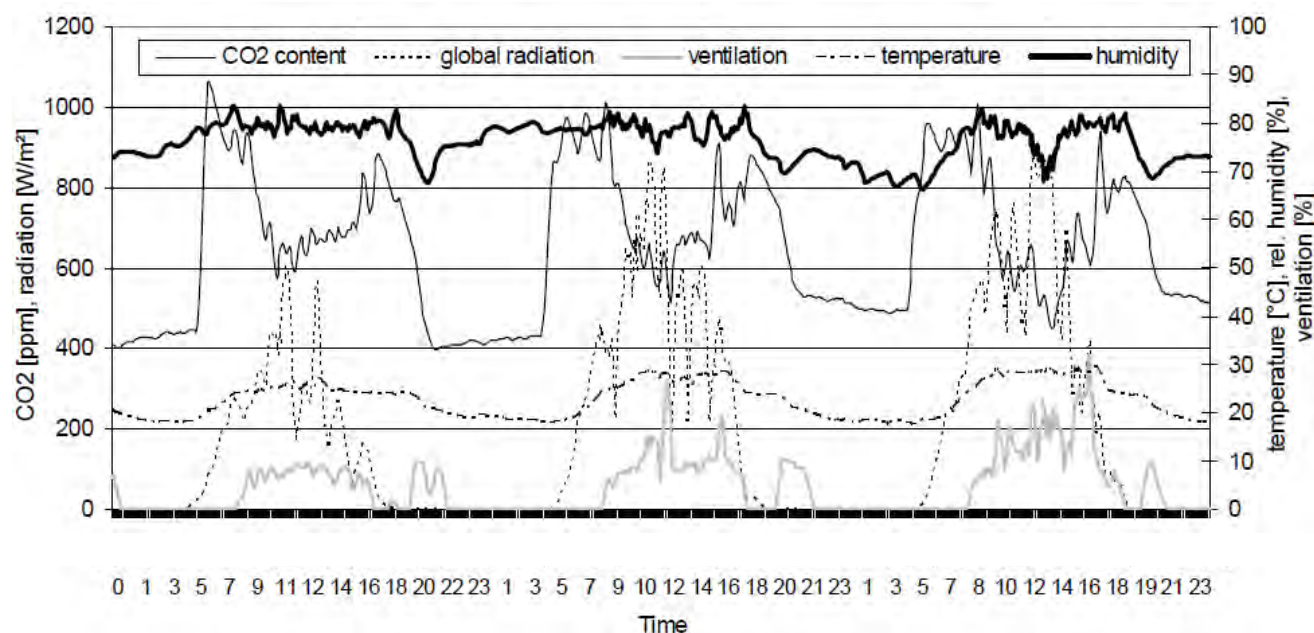


Figure 1. Typical climate data inside a greenhouse for tomatoes in three days [1]. CO₂ concentration in ppm, Global Solar Radiation in W/m², Temperature in °C, Relative Humidity and Ventilation in %.

1. Water Vapor - the Main Interference in CO₂ Sensing

In greenhouses, the relative humidity (RH) is in the range of 70-90% RH [1-3]. At high RH regime, fluctuations in humidity levels can cause a problem in the read-out stability of the polymer-based CO₂ sensor, because water vapor is an important analyte which can interfere the CO₂ sensing [4-11]. The concept of indirect CO₂ sensing via a pH shift involves the essential presence of water vapor. Moisture is needed for pH (CO₂) sensing but it is also a main interference analyte. All the investigated polymers in this research are hydrophilic due to polar groups, hence they can adsorb a large amount of water vapor. In *Chapter 2*, it was found that the effect of water on conductivity of the investigated conductive polymers is more dominant than CO₂. The relative change in impedance due to a 1% change in RH might be larger than an impedance change due to a 1% CO₂ concentration change in some cases. For SPAN-Na films, a 1% change in RH causes even a relative change in impedance of 2.5%, which is larger than 1% relative change in impedance due to 1% CO₂. However, with the

blend of SPAN-Na: poly(vinyl alcohol) (PVA), a 1% change in RH induces a relative change in impedance of 1.2%, which is much smaller than the 5% relative change in impedance due to a 1% CO₂ variation. Therefore, addition of PVA increases the CO₂ sensitivity of SPAN-Na as shown in *Chapter 2*. Also pure PVA is capable of sensing CO₂ via an indirect pH measurement at very high humidity levels (above 90% RH) and high CO₂ concentrations (5%). Hence, RH level in the experiments should be kept constant and should typically not exceed a 1% change during time dependent measurement. With CO₂ sensing based on pH sensitivity as in the case of SPAN-Na, only high CO₂ concentration (above 2%) can create a significant change in impedance.

With PEI and its blends, CO₂ sensing can be more “direct” because amine groups can react directly with CO₂. A little amount of CO₂ readily can take part in amines-CO₂ reaction; hence, direct sensing by reaction between CO₂ and polymer can be performed with low CO₂ concentrations in comparison to the pH sensing concept. Another remarkable difference is that with PEI, a higher RH leads to a higher conductance, but a higher CO₂ concentration leads to a lower conductance.

In all experiments some drift in ac and dc impedance signals due to water was observed. This drift is until now not explained clearly in previous works relating to gas sensing with CO₂ sensitive polymers [12, 13]. The drift might be attributed to water retention in polymer films which causes the drift in signal under bias applied. Also the interface between polymer and electrode material can initiate deteriorating reactions [14, 15]. Therefore, there is a serious need for control algorithms integrated in the sensor system to compensate for drift, to retrieve stable baselines after multiple operations, resulting in reproducible calibrations. Along, the durability and degradation of the conductive polymers should be monitored and compensated.

The relative humidity depends not only on temperature but also on the pressure of the system. Therefore, in testing chambers with varying pressures [16, 17], it is more difficult to control the accuracy of humidity because a variation in RH can cause a confusing response of the CO₂ sensor. In some cases it may even be better to take the absolute humidity as a controlling parameter instead of the relative humidity; however absolute humidity sensors are relatively difficult to integrate in the measurement system and do not warn in time if condensation effects may take place.

2. Effect of Temperature and Light in Greenhouses

Together with humidity, the temperature is one of the main factors affecting the accuracy of CO₂ measurements and the life-time of polymers. In our research, the effect of temperature on conductivity of the polymers was not investigated, the temperature inside our measurement chamber was always kept stable at 24 °C. However, the temperature in greenhouses in fact can vary in a wide range between day and night, for example in a greenhouse for tomatoes (**Figure 1**), temperature variation is in the range of 18-27 °C. The fluctuation of temperature can cause changes in relative humidity according to Mollier diagram as shown in **Figure 2**. According to this diagram, at a fixed mixing ratio of water vapor of 11 g/kg (11 g water to evaporate mixed with 1 kg dry air), when temperature increases from 18 °C to 30 °C, humidity will decrease from 80% RH to 40% RH. Hence, a 1 °C change induces roughly a 3.3% change in RH. A large decrease in humidity results in a large decrease in conductivity of the polymers as mentioned above.

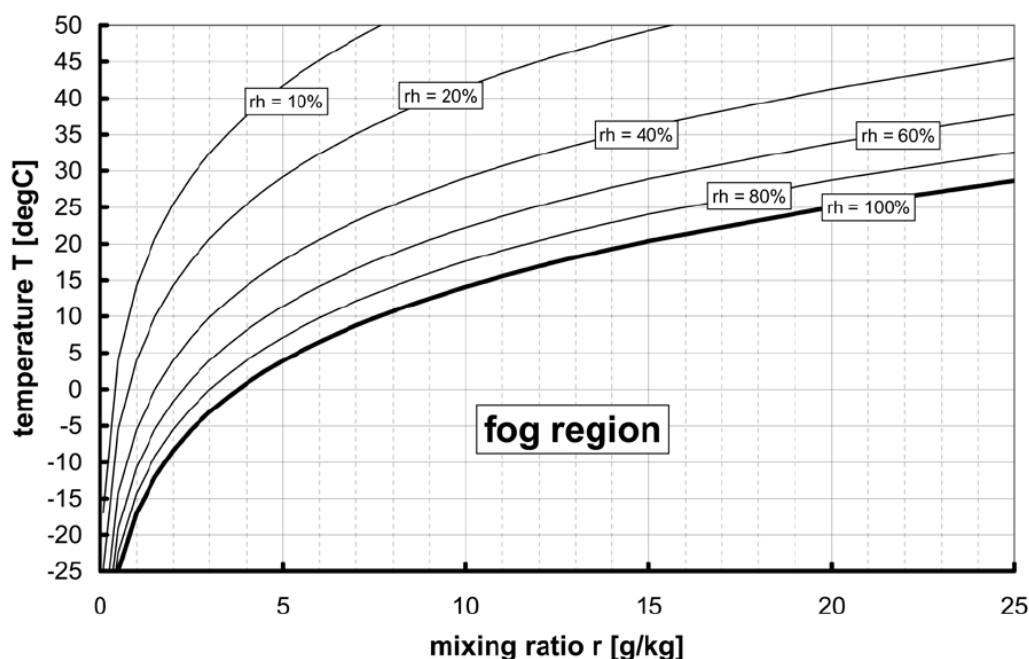


Figure 2. Mollier diagram: curves of constant relative humidity. The region below 100% (fog region) is not valid because condensation occurs [18].

In addition, like other semiconductors, the conductivity of conductive polymers increases with an increase in temperature [10]. This is anticipated for SPAN-Na because it was already observed in case of self-doped boronated polyaniline (PABA) [13]. When the temperature increased from 25 °C to 55 °C the resistance of the composite PABA:Nafion decreased from

6 k Ω to 1.044 k Ω on exposure to 2,455 ppm CO₂. The decrease in the resistance upon increase in temperature was attributed to the loss of protonation and expulsion of water molecules from the polymer composite [13].

Furthermore, the temperature can influence the sensing process involving the adsorption of analyte molecules in the sensing film and promoting reactions [10]. Adsorption prefers a low temperature and an increasing temperature will shift the equilibrium to more desorption. Sensitivity will normally decrease as the temperature increases in cases where an adsorption process is the predominant step [10]. For PEI, high temperatures were used to remove CO₂, for example 40 °C [19], or 110 °C [20] after capture. So, in case of PEI-based sensors, increasing temperature can decrease the recovery time due to fast desorption but also decrease sensitivity because of weak adsorption.

Light irradiation is another factor that can cause inaccuracy of CO₂ measurement due to the photo-doping effect [21]. Conductive polymers which are conjugated polymers can be affected by photo-excitation. Thus quickly changing conditions of the weather from sunny to cloudy can also affect the conductivity of the polymers, when exposed to light.

3. Effect of Other Contaminants (Gases, Organic Vapors)

Besides humidity, temperature and light as mentioned above, inaccuracy of the CO₂ measurement and the degradation of polymers might come from interference or even poisoning of other contaminants, especially in greenhouses with existence of many different chemicals, gases and vapors. In greenhouses, CO₂ is often supplied by combustion of fossil fuel [22, 23] such as natural gas, propane, kerosene, or directly from tanks of pure CO₂. Combustion with burners can produce nitric oxide (NO) which can be further oxidized to nitrogen dioxide (NO₂) [22-24]. Concentration of NO_x may reach levels of 0.5 to 5 volume parts per million (vpm) [22]. NO₂ acts as a strong oxidant and may convert the emeraldine form (half oxidized form) of PANI to its higher oxidized state [25]. Upon exposure to different concentration of NO₂ gas, the emeraldine salt form of PANI led to a large increase in resistance - greater than three orders of magnitude at 100 ppm NO₂ levels. NO₂ is also a strong acidic gas which can form nitric acid HNO₃ (much stronger than carbonic acid) at high RH and may protonate conductive polymers such as SPAN-Na and PEI. However, improvements in fuel burning (efficient burners, lower flaming temperature) can decrease concentration of NO_x down to a limit not affecting deterioration of the polymers.

In addition, if ammonia (NH_3) is present in greenhouses, it may reduce lifetime of the polymer sensors [11]. NH_3 can cause natural aging due to irreversible dedoping reaction inside the sensitive polymer film. Sometime regeneration is possible by heating up to 104-107 °C. A plus point is if the polymer sensor is exposed to NH_3 for a short time (e.g. less than 10 minutes) at a low concentration, then the response is totally reversible. Furthermore, in greenhouses vapor from liquid fertilizers containing NH_4NO_3 , KNO_3 , H_3PO_4 [26] will influence the conductivity. Ions can migrate into the polymer film and will increase the ionic conductivity of the polymers. A gas permeable membrane allowing only CO_2 molecules to pass through such as PTFE membrane [13] can be used to avoid cross sensitivity effect of other contaminants in greenhouses. Moreover, it should be noted that these contaminants can also contribute to corrosion of electronics and sensor electrodes.

4. Sulfonation Degree of SPANI and pH Range for CO_2 Sensing

Investigating reports on the conductivity of EB-PANI and its derivatives with respect to pH, it was found that sulfonation of EB-PANI at different degrees/percentages can modify the pH-dependent conductivity. It was claimed that if the imine nitrogen atoms of SPANI are not fully doped (protonated), the conductivity may vary in the pH range of 0-7.5 [27]. Therefore, SPANI with a sulfonation degree of 25% was expected to be more sensitive than PANI towards CO_2 because the conductivity of this SPANI is in the pH range of 0-7, instead of 1-4 for PANI. However, sulfonation of SPANI with fuming sulfuric to obtain 25% was a problem because sulfonation degree obtained by sulfonation reaction with fuming sulfuric acid is virtually independent of the sulfonation time over periods from 0.5 to 24 hours [28]. Sulfonation occurs relatively rapidly and finishes within 2 hours. The mean value of sulfonation degree is 0.5 with maximum conductivity at the sulfonation time of 1-2 hours. Prolonged sulfonation causes slow hydrolysis of EB-PANI in fuming sulfuric acid resulting in a decrease in conductivity [28]. In our research, SPANI with sulfonation for 0.5 hour was also prepared and the sulfonation degree was confirmed to be 50% by XPS. Hence, it is hard to control the sulfonation degree at 25% in sulfonation reaction with fuming sulfuric acid.

In *Chapter 2* it was claimed that SPAN-Na has a good conductivity dependence in the desired range for CO_2 sensing, from pH4 to pH7. However, similar to the principle of the potentiometric Severinghaus type CO_2 sensor [29-31] “indirect” sensing of the polymer films via “pH solution” requires a proper mixture of CO_2 and water vapor to obtain carbonic acid (H_2CO_3) to protonate the conductive polymers. The reversible reaction $\text{CO}_2 + \text{H}_2\text{O} \leftrightarrow \text{H}_2\text{CO}_3$

($\leftrightarrow \text{H}^+ + \text{HCO}_3^-$) is relatively slow and the dissolved $[\text{CO}_2]$ at equilibrium is found to be of the order of 1,000 times greater than the H_2CO_3 concentration [32]. Hence in fact only a small amount of CO_2 is converted to H_2CO_3 . Enzyme carbonic anhydrase was claimed to accelerate the reaction of CO_2 and H_2O so it has been added in several CO_2 sensors [31, 33]. This enzyme was also used in our experiments with SPAN-Na but this enzyme could not improve the sensing with low CO_2 concentrations. The reason could be attributed to the fact that carbonic anhydrase does not have an appreciable effect at pH5 [34] or this enzyme catalyzes the decomposition of bicarbonate to CO_2 [29]. As a result, low concentrations of CO_2 cannot create sufficiently strong acidic H_2CO_3 to protonate SPAN-Na to induce a significant change in impedance. Moreover, the pH of “solution” formed by CO_2 and water vapor cannot be measured in reality and the concentration of CO_2 is only reasonable with the knowledge of the pH of the analyzed medium [35]. Therefore it is rather difficult to determine at forehand which concentration of CO_2 is sufficient to create the change in pH needed for a good signal in varying humidity conditions.

5. Effect of (Surface) Morphology on Performance of Sensor

The sensitivity, response time and recovery time might depend on the (surface) morphology of the polymer films. Normally any change in morphology of the polymer layer may influence the performance of the sensor [10]. A film with high ratio of surface area to volume ($r_{A/V}$) helps gas molecules diffuse and interact with the polymer layer easily leading to a higher sensitivity and shorter response time [10]. Therefore, thin or porous films with higher $r_{A/V}$ have higher sensitivity [36, 37]. Increasing the volume ratio of micropores in the film was found to enhance the response [9] but the response of the film is insensitive to its thickness as the porosity of the film is sufficient [38].

Previous studies have shown that the morphology of doped PANI or self-doped SPANI films is different from that of their blends with another polymer such as poly(vinyl alcohol) (PVA), poly(methyl methacrylate) (PMMA), polystyrene (PSt) [9, 39]. The pure SPANI exhibited an aggregated granular morphology, while the SPANI:PVA blend films exhibited a much smoother surface morphology, in which no significant difference in morphology due to composition variation could be observed [39].

Similarly, a protonated PANI film exhibited small PANI aggregates [9], whereas in PANI:PSt blend film, PSt completely coated the PANI aggregates which were distributed homogeneously in the blend film. NH_3 and H_2O molecules were claimed unable to interact

directly with the doped PANI so this blend film was less sensitive to NH_3 than the plain PANI film. However, many pores were observed on the surface of PANI:PMMA blend film and the PANI aggregates were exposed inside the pores. The humidity effect was found larger for PANI:PMMA than PANI:PSt blend film and the humidity effect became less sensitive to the NH_3 response [9]. In another work [40], HCl-doped PANI in aqueous solution stabilized by PVA showed spherical and almost mono-dispersed (60-100 nm) PANI particles randomly distributed within the network of the support polymer PVA. On increasing PANI percentage in the composite, moisture absorption capacity increased but dropped above a certain fraction. It was claimed that beyond that particular composition the system became too highly cross-linked to incorporate water molecules in larger amount [40].

In addition, conductivity of PANI films has a significant dependence on morphology which depends on the method by which the polymer is processed and how the film was casted [41]. It was found that the nature of a cast film depends critically on the relative rate of solvent evaporation versus the rate at which changes in molecular interaction occur [41]. The evaporation process is often the determining factor of the gas sensor performance since the porosity of the film is responsible for the rate of uptake–release of the gas analyte by the polymer matrix [42]. Also the intrinsic and ionic conduction will adversely contribute to the dc and ac conductance in polymer blends (e.g. SPAN-Na:PVA) depending on the morphology of the blended polymer film (homogeneous, suspended in a matrix, etc.).

6. Conductive Polymer Nanowires for Gas Sensing

Polymer nanowires/nanofibers have a high surface to volume ratio so they seem interesting candidates for preparing sensors with a high sensitivity and a fast response [10]. All of our polymers used in this research (SPAN-Na, PEI) are difficult to process with standard lithography to pattern nanowires because they are well soluble in many solvents. Moreover, ultraviolet (UV) light exposure, electron beam or laser ablation cannot be applied because these processes can modify chemical structures leading to changing properties of the polymers.

A common solution is synthesis of polymer nanowires/nanofibers then deposition of these nanowires onto prefabricated interdigitated electrodes in thin film/sheet form [25, 38, 43-45]. PANI nanofibers with diameters of 30-50 nm and lengths from 500 nm up to several micrometers have been made, but tended to agglomerate into interconnected nanofiber networks, rather than bundles [38, 43, 44]. The PANI nanofiber thin film responded as

anticipated much faster than the conventional film to both acid and base, even when the total nanofiber film was more than twice as thick. The small diameter of the nanofibers and increased high surface area within the film enabled a fast access by the gas vapors. It was also found that the nanofiber films showed essentially no thickness (0.2-2.5 μm) dependence in their performance [38, 43]. However, the contact resistance between nanofibers and electrodes should be considered because nanofiber films exhibited lower sensitivity than conventional thin films due to imperfect contact between nanofibers and electrodes [46].

Electro or chemical polymerization inside an anodic aluminum oxide template has been used widely to make conductive polymer nanofibers such as PANI [47] and polypyrrole (PPy) nanowires [48]. PPy nanowire arrays with high density and small diameter (~ 50 nm) [49] showed a relatively high response (10%) towards 1.5 ppm NH_3 and a comparatively short response and recovery time.

Patterning by direct writing via dip-pen nanolithography can also be used to make polymer nanowires [50]. Poly(3,4-ethylenedioxythiophene) (PEDOT) nanowires with a diameter of 300 nm across a 55 μm gap between a pair of electrodes were fabricated by using dip-pen nanolithography [51]. The responses to nitric oxide (NO) were highly linear and reproducible with a minimal concentration of NO of 10 ppm.

Electrospinning is another method which has been used to make isolated and relatively long polymer nanofibers. This approach has also been used in fabricating conductive polymer nanowire such as sulfuric acid-doped PANI fibers [52] and isolated camphor sulfonic acid-doped PANI nanofibers [53]. Oriented PANI nanowires with diameters of 100 nm were deposited on gold electrodes by using a scanned-tip electrospinning [54]. The devices showed a rapid and reversible resistance change upon exposure to NH_3 gas at low concentration of 0.5 ppm. The response times of nanowire sensors with various diameters corresponded to radius-dependent differences in the diffusion time of ammonia gas into the wires. Electrospinning has also been extensively used to fabricate composite nanowires of PANI and poly(methyl methacrylate) (PMMA) [55]. The composite nanowires showed a linear, reversible and reproducible response towards triethylamine vapors ranging from 20 ppm to 500 ppm. The PANI doped with toluene sulfonic acid exhibited the highest sensing magnitude. A gas sensor based on polypyrrole (PPy):PMMA composite fibers [56] exhibited greatly improved performances towards NH_3 comparing with those of the device based on a PPy flat film.

The polymers used in this research including SPAN-Na, PEI were synthesized from available commercial polymers and then were post-modified as presented in the previous chapters. Therefore, the synthesis of nanowires by aqueous/organic interfacial synthesis [38, 43, 44] or UV synthesis [45] or polymerization incorporated with anodic aluminum oxide template has not been applied. Hence, electrospinning is probably the most suitable way to make conductive polymer nanowires in our case.

Electrospinning method was tried in our research to make SPAN-Na nanowires deposited on micro comb-shaped Pt electrodes. The setup for electrospinning is illustrated in **Figure 3**. SPAN-Na solution was filled in a 10 μL glass syringe bearing a metal capillary with internal diameter of 130 μm . This needle tip acted as an electrospinning source. The chip with interdigitated Pt electrodes was mounted as a fiber collector and the electrode contact pad was connected to the grounded counter electrode. The voltage of 5 kV was supplied from a high voltage power supply Teltron, England. The distance between the capillary tip and the chip was 500 μm - 3 mm. To obtain nanofibers, the electrical field strength should be maintained at 10^7 V.m^{-1} [57]. So in this process utilizing 5 kV, the distance was set 0.5 mm. However, with short distance of 0.5-2 mm, there was arc between needle and the chip (connected to the ground electrode), resulting in burnt polymer dots on the chip. The arc disappeared when the distance increased to 3 mm. The flow rate of SPAN-Na solution (0.2 mL/hour) was controlled by a syringe pump (NE-1000X2, USA). The polymer jet was electrostatically extracted from the tip and dried on the way to the substrate with comb-shaped electrodes.

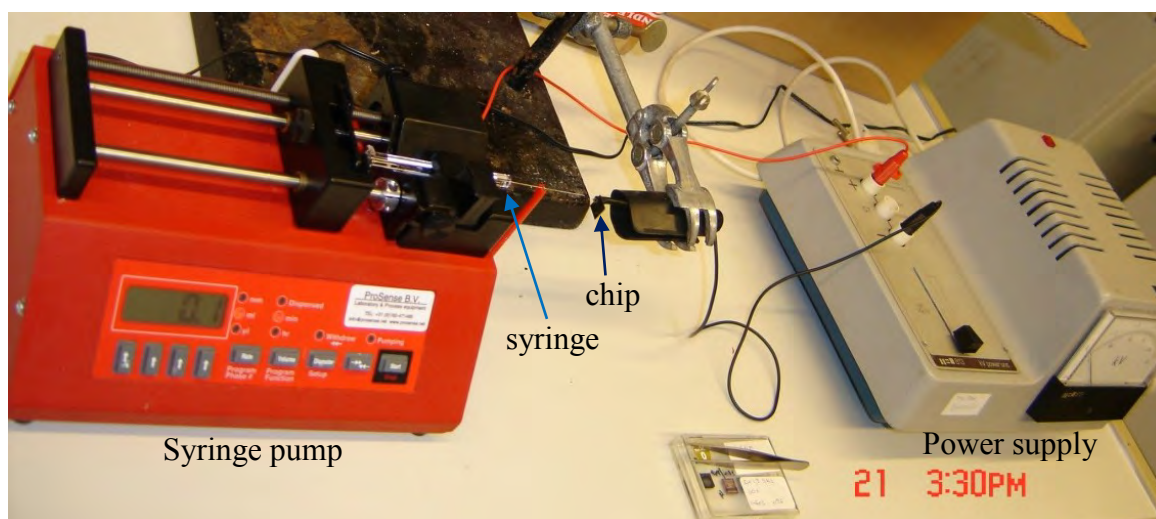


Figure 3. Setup for electrospinning process.

However, the electrospinning process did not yield adequate sensor material in our case. A spinning jet could be obtained but no suitable nanofibers were obtained. Co-spinning of SPAN-Na in DMSO with polyethylene oxide (PEO) to facilitate the formation of nanofibers [58, 59] was also employed, however not successful. Further research is needed to fabricate SPAN-Na, PEI and their blend nanofibers, probably a higher voltage of 10-15 kV should be used [52]. On the other hand the response time of our thin film sensor in the order of minutes seems sufficient for application in a greenhouse environment.

7. Chemiresistor and Field Effect Transistor (FET)

To improve sensitivity of the polymer sensors, besides morphology of the polymer films the configuration of the sensor should be considered. The sensor used in this research is a chemiresistor which principle has been widely used for gas sensing [8, 13, 16, 37, 60-68]. Platinum and gold are often used as building materials of the interdigitated electrodes. Platinum electrodes have a high affinity to many organic compounds and hence form good electrical contacts with PANI without the need of an additional adhesive layer, such as 4-aminothiophenol in the case of gold electrodes [69]. In our research, both platinum and gold were used and no discernible difference in sensing characteristic was found, even 4-aminothiophenol layer was not needed for our self-made gold electrode chips. The polymer thin films deposited on top of interdigitated electrodes are the sensing elements and the output signal can be dc resistance or ac impedance [17, 63, 68, 70], capacitance [71] or dc/ac current [61]. In addition, the use of alternating current (ac) allows an accurate measure of resistance to be made at a micro watt power level which does not heat the film [63]. Therefore, the CO₂ sensing characterization of the polymers in our research was performed with time dependent impedance measurement at a fixed frequency.

Using the field effect transistor (FET) measurement principle for SPAN-Na, it might be able to detect CO₂ at lower concentrations. However, the disadvantage of these FET devices is mainly the complex characterization which is much more difficult than a chemiresistor [10]. It should be noted that PEI and starch have been applied in an AlGaIn/GaN high electron mobility transistor (HEMT) [72] to detect CO₂ in a wide range of 0.9% - 50% balanced with nitrogen at temperature from 46-220 °C. In another study this mixture was also used in a carbon nanotube FET configuration to detect between 500 ppm and 10,000 ppm CO₂ [73]. A study of a FET with SPAN-Na and their blends as active materials for CO₂ sensing can be a good approach for further research.

8. Wireless CO₂ Sensor Network for Greenhouses and Other Applications

Polymer-based CO₂ sensors can be integrated together with other sensors such as humidity sensor, temperature sensor, light sensor, etc. to form multi sensor arrays in greenhouse. Arrays of chemiresistors with different chemically active layers have already been proposed to increase the selectivity for specific gases [74] so that other gases (such as NH₃, NO₂) can be monitored at the same time with CO₂. With proper algorithms for calibration and/or addition of a filter to prevent CO₂ and other gases, the signal for interfering gases, such as humidity can be compensated. For using in wireless sensor networks (WSN) these gas sensors may communicate spatially separated with readout/display components [74]. The advantages of a WSN do include high nodal density and low installation costs without the need for extensive wiring. In addition, a WSN provides simultaneous measurements of different parameters (gas concentrations, temperature) for a large area such as in greenhouses and office buildings. The challenges of WSNs for gas sensing are power consumption of individual sensors and handling of the massive data coming from the WSN [74]. Moreover, long-term stability of the polymers should be considered because inadequate long-term stability of many research prototypes of gas sensors prevents their reliable applications in WSNs [74]. Therefore, the stability of the PEI-based sensors developed in this work should be tested further for a long time before they can be used in WSNs for greenhouses. Furthermore, these WSNs with PEI-based sensors can have various potential other applications, such as in-door air quality monitoring in office buildings, food storage/packaging, healthcare.

For the controlled cultivation (photo-synthesis) of plants in greenhouses monitoring of the following parameters are of importance:

- Light
- Temperature
- Humidity
- CO₂ concentration.

With about 50 to 100 nodes distributed over a greenhouse area of about 1,000 to 10,000 m² a good number of nodes is present to monitor appropriate and varying climate conditions. Especially the climate conditions and related growth parameters covering a long period in a specific area of the greenhouse can be obtained. For a specific crop optimal growth conditions can be extracted from the obtained data on light, temperature, humidity and CO₂ stored for the

full growing period of the crop. Furthermore, the total energy input needed to grow a specific crop can be extracted and minimized for the three energy consuming parameters including heat, CO₂ and (electric) light within the greenhouse. In this way energy efficient cultivation of the crop is enabled by the controlled steering of light, temperature, humidity and CO₂ concentration in the greenhouse during the day and during the full growth period.

Reference

- [1] U. Schmidt, Huber, C., Rocks, T., Salazar Moreno, R. and Rojano Aguilar, A., Greenhouse cooling and carbon dioxide fixation by using high pressure fog systems and phytocontrol strategy, *Acta Hort. (ISHS)* 797, (2008) 279-284.
- [2] O. Körner, H. Challa, Process-based humidity control regime for greenhouse crops, *Computers and Electronics in Agriculture*, 39 (2003) 173-192.
- [3] L.M. Mortensen, Effects of air humidity on growth, flowering, keeping quality and water relations of four short-day greenhouse species, *Scientia Horticulturae*, 86 (2000) 299-310.
- [4] M. Hijikagawa, S. Miyoshi, T. Sugihara, A. Jinda, A thin-film resistance humidity sensor, *Sensors and Actuators*, 4 (1983) 307-315.
- [5] L.S. Hwang, J.M. Ko, H.W. Rhee, C.Y. Kim, A polymer humidity sensor, *Synth. Met.*, 57 (1993) 3671-3676.
- [6] T. Taka, Humidity dependency of electrical conductivity of doped polyaniline, *Synth. Met.*, 57 (1993) 5014-5019.
- [7] Y. Sakai, Y. Sadaoka, M. Matsuguchi, Humidity sensors based on polymer thin films, *Sensors and Actuators B: Chemical*, 35 (1996) 85-90.
- [8] K. Ogura, T. Saino, M. Nakayama, H. Shiigi, The humidity dependence of the electrical conductivity of a soluble polyaniline-poly(vinyl alcohol) composite film, *J. Mater. Chem.*, 7 (1997) 2363-2366.
- [9] M. Matsuguchi, A. Okamoto, Y. Sakai, Effect of humidity on NH₃ gas sensitivity of polyaniline blend films, *Sensors and Actuators B: Chemical*, 94 (2003) 46-52.
- [10] H. Bai, G.Q. Shi, Gas sensors based on conducting polymers, *Sensors*, 7 (2007) 267-307.
- [11] D. Nicolas-Debarnot, F. Poncin-Epaillard, Polyaniline as a new sensitive layer for gas sensors, *Anal. Chim. Acta*, 475 (2003) 1-15.
- [12] M. Irimia-Vladu, J.W. Fergus, Suitability of emeraldine base polyaniline-PVA composite film for carbon dioxide sensing, *Synth. Met.*, 156 (2006) 1401-1407.

- [13] S. Neethirajan, M.S. Freund, D.S. Jayas, C. Shafai, D.J. Thomson, N.D.G. White, Development of carbon dioxide (CO₂) sensor for grain quality monitoring, *Biosyst. Eng.*, 106 (2010) 395-404.
- [14] A. Collier, H. Wang, X. Zi Yuan, J. Zhang, D.P. Wilkinson, Degradation of polymer electrolyte membranes, *Int. J. Hydrogen Energy*, 31 (2006) 1838-1854.
- [15] M. Jørgensen, K. Norrman, F.C. Krebs, Stability/degradation of polymer solar cells, *Sol. Energy Mater. Sol. Cells*, 92 (2008) 686-714.
- [16] K. Ogura, A CO₂ sensor with polymer composites operating at ordinary temperature, *J. Electrochem. Soc.*, 147 (2000) 4351-4355.
- [17] T. Oho, T. Tonosaki, K. Isomura, K. Ogura, A CO₂ sensor operating under high humidity, *J. Electroanal. Chem.*, 522 (2002) 173-178.
- [18] E+E Elektronik GmbH, Measure humidity - Basics, Technical Note.
- [19] B. Li, B. Jiang, D.J. Fauth, M.L. Gray, H.W. Pennline, G.A. Richards, Innovative nano-layered solid sorbents for CO₂ capture, *Chem. Commun.*, 47 (2011) 1719-1721.
- [20] Y.G. Ko, S.S. Shin, U.S. Choi, Primary, secondary, and tertiary amines for CO₂ capture: Designing for mesoporous CO₂ adsorbents, *J. Colloid Interface Sci.*, 361 (2011) 594-602.
- [21] A.J. Heeger, S. Kivelson, J.R. Schrieffer, W.P. Su, Solitons in conducting polymers, *Reviews of Modern Physics*, 60 (1988) 781-850.
- [22] T.A.a.M. Mansfield, A.J.S. Pollutants generated in greenhouses during CO₂ enrichment, *Acta Hort. (ISHS)* 162, (1984) 171-178.
- [23] A. Kiel, CO₂ enrichment with natural gas fired hot-air heaters, *Acta Hort. (ISHS)* 268, (1990) 111-120.
- [24] H. Saxe, Relative sensitivity of greenhouse pot plants to long-term exposures of NO- and NO₂-containing air, *Environ. Pollut.*, 85 (1994) 283-290.
- [25] X.B. Yan, Z.J. Han, Y. Yang, B.K. Tay, NO₂ gas sensing with polyaniline nanofibers synthesized by a facile aqueous/organic interfacial polymerization, *Sensors and Actuators B: Chemical*, 123 (2007) 107-113.
- [26] J. Hagin, A. Lowengart, Fertigation for minimizing environmental pollution by fertilizers, *Nutrient Cycling in Agroecosystems*, 43 (1995) 5-7.
- [27] J. Yue, Z.H. Wang, K.R. Cromack, A.J. Epstein, A.G. MacDiarmid, Effect of sulfonic acid group on polyaniline backbone, *J. Am. Chem. Soc.*, 113 (1991) 2665-2671.
- [28] J. Yue, G. Gordon, A.J. Epstein, Comparison of different synthetic routes for sulphonation of polyaniline, *Polymer*, 33 (1992) 4410-4418.

- [29] H.A. Himpler, Conductimetric gas sensor for carbon dioxide, *Anal. Chem.*, 50 (1978) 1623-1627.
- [30] P. Arquint, A. van den Berg, B.H. van der Schoot, N.F. de Rooij, H. Bühler, W.E. Morf, L.F.J. Dürselen, Integrated blood-gas sensor for pO₂, pCO₂ and pH, *Sensors and Actuators B: Chemical*, 13 (1993) 340-344.
- [31] S. Hanstein, D. de Beer, H.H. Felle, Miniaturised carbon dioxide sensor designed for measurements within plant leaves, *Sensors and Actuators B: Chemical*, 81 (2001) 107-114.
- [32] R.M.a.F.J.W.R. R. Brinkman, The Kinetics of the Carbon Dioxide-Carbonic Acid Reaction, *Phil. Trans. R. Soc. Lond. A*, 232 (1934) 65-97.
- [33] B. Serban, A.K.S. Kumar, M. Brezeanu, C. Cobianu, O. Buiu, C. Bostan, N. Varachiu, S. Costea, Amino groups-based polymers for CO₂ detection; A comparison between two sensing mechanism models, in, 2011, pp. 127-130.
- [34] H.A.K.a.F.J.W. Roughton, Carbonic anhydrase as a tool in studying the mechanism of reactions involving H₂CO₃, CO₂ or HCO₃⁻, *Biochem. J.*, 43 (1948) 550-555.
- [35] J. Zosel, W. Oelssner, M. Decker, G. Gerlach, U. Guth, The measurement of dissolved and gaseous carbon dioxide concentration, *Meas. Sci. Technol.*, 22 (2011).
- [36] S. Xing, C. Zhao, S. Jing, Y. Wu, Z. Wang, Morphology and gas-sensing behavior of in situ polymerized nanostructured polyaniline films, *Eur. Polym. J.*, 42 (2006) 2730-2735.
- [37] E. Stussi, R. Stella, D. De Rossi, Chemoresistive conducting polymer-based odour sensors: influence of thickness changes on their sensing properties, *Sensors and Actuators B: Chemical*, 43 (1997) 180-185.
- [38] H. Jiaying, V. Shabnam, H.W. Bruce, B.K. Richard, Nanostructured Polyaniline Sensors, *Chemistry - A European Journal*, 10 (2004) 1314-1319.
- [39] S.-A. Chen, G.-W. Hwang, Structures and properties of the water-soluble self-acid-doped conducting polymer blends: sulfonic acid ring-substituted polyaniline/poly(vinyl alcohol) and poly(aniline-co-N-propanesulfonic acid aniline)/poly(vinyl alcohol), *Polymer*, 38 (1997) 3333-3346.
- [40] R. Gangopadhyay, A. De, G. Ghosh, Polyaniline-poly (vinyl alcohol) conducting composite: material with easy processability and novel application potential, *Synth. Met.*, 123 (2001) 21-31.
- [41] W. Zheng, M. Angelopoulos, A.J. Epstein, A.G. MacDiarmid, Concentration dependence of aggregation of polyaniline in NMP solution and properties of resulting cast films, *Macromolecules*, 30 (1997) 7634-7637.

- [42] J. Janata, M. Josowicz, Organic semiconductors in potentiometric gas sensors, *J. Solid State Electrochem.*, 13 (2009) 41-49.
- [43] J. Huang, S. Virji, B.H. Weiller, R.B. Kaner, Polyaniline Nanofibers: Facile Synthesis and Chemical Sensors, *J. Am. Chem. Soc.*, 125 (2002) 314-315.
- [44] S. Virji, J. Huang, R.B. Kaner, B.H. Weiller, Polyaniline Nanofiber Gas Sensors: Examination of Response Mechanisms, *Nano Lett.*, 4 (2004) 491-496.
- [45] Z.-F. Li, F.D. Blum, M.F. Bertino, C.-S. Kim, S.K. Pillalamarri, One-step fabrication of a polyaniline nanofiber vapor sensor, *Sensors and Actuators B: Chemical*, 134 (2008) 31-35.
- [46] G. Li, M. Carlos, J. Jiri, S.J. Anthony, J. Mira, S. Steve, Effect of morphology on the response of polyaniline-based conductometric gas sensors: Nanofibers vs. thin films, *Electrochem. Solid St.*, 7 (2004) H44-H47.
- [47] X. Yu, Y. Li, K. Kalantar-zadeh, Synthesis and electrochemical properties of template-based polyaniline nanowires and template-free nanofibril arrays: Two potential nanostructures for gas sensors, *Sensors and Actuators B: Chemical*, 136 (2009) 1-7.
- [48] C.H. Sandra , C. Debangshu, C. Wilfred, V.M. Nosang , M. Ashok, Single Polypyrrole Nanowire Ammonia Gas Sensor, *Electroanalysis*, 19 (2007) 2125-2130.
- [49] L. Zhang, F. Meng, Y. Chen, J. Liu, Y. Sun, T. Luo, M. Li, J. Liu, A novel ammonia sensor based on high density, small diameter polypyrrole nanowire arrays, *Sensors and Actuators B: Chemical*, 142 (2009) 204-209.
- [50] L. Jiang, X. Wang, L. Chi, Nanoscaled Surface Patterning of Conducting Polymers, *Small*, 7 (2011) 1309-1321.
- [51] H.-H. Lu, C.-Y. Lin, T.-C. Hsiao, Y.-Y. Fang, K.-C. Ho, D. Yang, C.-K. Lee, S.-M. Hsu, C.-W. Lin, Electrical properties of single and multiple poly(3,4-ethylenedioxythiophene) nanowires for sensing nitric oxide gas, *Anal. Chim. Acta*, 640 (2009) 68-74.
- [52] A.G. MacDiarmid, Synthetic metals: a novel role for organic polymers, *Synth. Met.*, 125 (2001) 11-22.
- [53] N.J. Pinto, I. Ramos, R. Rojas, P.-C. Wang, A.T. Johnson Jr, Electric response of isolated electrospun polyaniline nanofibers to vapors of aliphatic alcohols, *Sensors and Actuators B: Chemical*, 129 (2008) 621-627.
- [54] H. Liu, J. Kameoka, D.A. Czaplewski, H.G. Craighead, Polymeric Nanowire Chemical Sensor, *Nano Lett.*, 4 (2004) 671-675.

- [55] S. Ji, Y. Li, M. Yang, Gas sensing properties of a composite composed of electrospun poly(methyl methacrylate) nanofibers and in situ polymerized polyaniline, *Sensors and Actuators B: Chemical*, 133 (2008) 644-649.
- [56] H. Bai, L. Zhao, C. Lu, C. Li, G. Shi, Composite nanofibers of conducting polymers and hydrophobic insulating polymers: Preparation and sensing applications, *Polymer*, 50 (2009) 3292-3301.
- [57] D. Sun, C. Chang, S. Li, L. Lin, Near-Field Electrospinning, *Nano Lett.*, 6 (2006) 839-842.
- [58] P. Li, Y. Li, B. Ying, M. Yang, Electrospun nanofibers of polymer composite as a promising humidity sensitive material, *Sensors and Actuators B: Chemical*, 141 (2009) 390-395.
- [59] I.D. Norris, M.M. Shaker, F.K. Ko, A.G. MacDiarmid, Electrostatic fabrication of ultrafine conducting fibers: polyaniline/polyethylene oxide blends, *Synth. Met.*, 114 (2000) 109-114.
- [60] A.L. Kukla, Y.M. Shirshov, S.A. Piletsky, Ammonia sensors based on sensitive polyaniline films, *Sens. Actuator B-Chem.*, 37 (1996) 135-140.
- [61] N.E. Agbor, M.C. Petty, A.P. Monkman, Polyaniline Thin-Films for Gas-Sensing, *Sens. Actuator B-Chem.*, 28 (1995) 173-179.
- [62] K. Ogura, H. Shiigi, M. Nakayama, A New Humidity Sensor Using the Composite Film Derived from Poly(o-phenylenediamine) and Poly(vinyl alcohol), *J. Electrochem. Soc.*, 143 (1996) 2925-2930.
- [63] P.D. Harris, W.M. Arnold, M.K. Andrews, A.C. Partridge, Resistance characteristics of conducting polymer films used in gas sensors, *Sensors and Actuators B: Chemical*, 42 (1997) 177-184.
- [64] K. Ogura, H. Shiigi, A CO₂ sensing composite film consisting of base-type polyaniline and poly(vinyl alcohol), *Electrochem. Solid St.*, 2 (1999) 478-480.
- [65] K. Ogura, R.C. Patil, H. Shiigi, T. Tonosaki, M. Nakayama, Response of protonic acid-doped poly(o-anisidine)/poly(vinyl alcohol) composites to relative humidity and role of dopant anions, *J. Polym. Sci., Part A: Polym. Chem.*, 38 (2000) 4343-4352.
- [66] A.C. Partridge, M.L. Jansen, W.M. Arnold, Conducting polymer-based sensors, *Materials Science and Engineering: C*, 12 (2000) 37-42.

- [67] H. Shiigi, T. Oho, T. Tonosaki, K. Ogura, CO₂-sensitive characteristics of base-type polyaniline poly(vinyl alcohol) composites at room temperature and effects of coexisting gases, *Electrochemistry*, 69 (2001) 997-1001.
- [68] M. Irimia-Vladu, J.W. Fergus, Impedance spectroscopy of thin films of emeraldine base polyaniline and its implications for chemical sensing, *Synth. Met.*, 156 (2006) 1396-1400.
- [69] Q. Hao, V. Kulikov, V.M. Mirsky, Investigation of contact and bulk resistance of conducting polymers by simultaneous two- and four-point technique, *Sensors and Actuators B: Chemical*, 94 (2003) 352-357.
- [70] K. Ogura, T. Tonosaki, H. Shiigi, AC Impedance Spectroscopy of Humidity Sensor Using Poly(o-phenylenediamine)/Poly(vinyl alcohol) Composite Film, *J. Electrochem. Soc.*, 148 (2001) H21-H27.
- [71] H. E.C.M, CO, CO₂, CH₄ and H₂O sensing by polymer covered interdigitated electrode structures, *Sensors and Actuators*, 5 (1984) 181-186.
- [72] C.Y. Chang, B.S. Kang, H.T. Wang, F. Ren, Y.L. Wang, S.J. Pearton, D.M. Dennis, J.W. Johnson, P. Rajagopal, J.C. Roberts, E.L. Piner, K.J. Linthicum, CO₂ detection using polyethylenimine/starch functionalized AlGa_N/Ga_N high electron mobility transistors, *Appl. Phys. Lett.*, 92 (2008).
- [73] A. Star, T.R. Han, V. Joshi, J.C.P. Gabriel, G. Grüner, Nanoelectronic Carbon Dioxide Sensors, *Adv. Mater.*, 16 (2004) 2049-2052.
- [74] R.A. Potyrailo, C. Surman, N. Nagraj, A. Burns, Materials and Transducers Toward Selective Wireless Gas Sensing, *Chem. Rev.*, 111 (2011) 7315-7354.

Appendix 1

Supplementary Information for Chapter 2

1. Fourier-Transform Infra-Red Spectroscopy

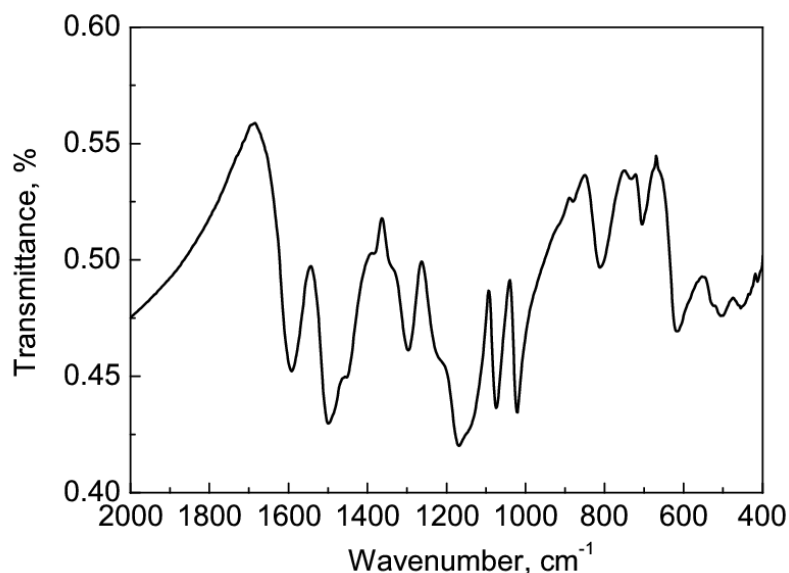


Figure A1. Fourier-transform infra-red (FTIR) spectrum of the sodium salt of sulfonated polyaniline (SPAN-Na).

Table A1. Peak assignments of the FTIR spectrum.

<i>Peak (cm⁻¹)</i>	<i>Vibrational mode</i>
1582	C=C stretching-quinoid rings
1494	C=C stretching-benzenoid rings
1291	C-N stretching-aromatic amine
1129	C-H in-plane bending aromatic
1066, 1015	S=O sulfonate symmetric and antisymmetric stretching
800	C-H out-of-plan bending aromatic
701	C-S aromatic stretching
606	S=O sulfonate stretching

2. UV-Vis Spectroscopy

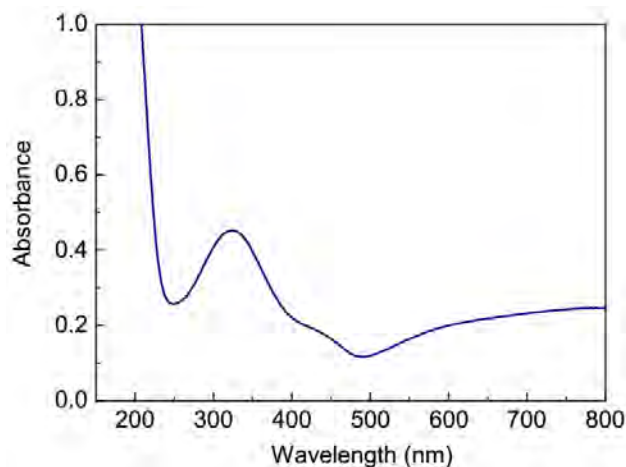


Figure A2. UV-Vis adsorption spectrum of SPAN-Na in water.

3. X-Ray Photoelectron Spectroscopy

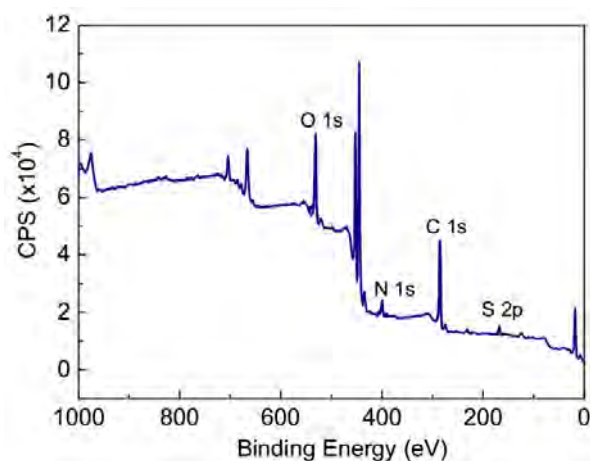


Figure A3. XPS spectrum of SPANI.

Atomic percentages: N 1s (5.82%), S 2p (3.08%), C 1s (65.78%), O 1s (25.33%).

4. Correction Factors for Conductivity Measurements

For calculating the conductivity, $\sigma = (1/R) \times (k) = k \times (I/V)$, correction factors were chosen based on the Zaretsky convention for interdigitated electrodes [1]. For interdigitated devices k is defined as $k = 1/(M \times G^*)$. The meander length M is determined from number of digit fingers (n) and the length (l) of the finger/comb of one electrode, $M = n \times l = 124 \times 300 \mu\text{m} = 3.72 \text{ cm}$. G^* is the dimensionless conductance parameter, defined as $G^* = \lambda/4a$. The spatial periodicity/pitch/lattice constant is given by $\lambda = 2(a+a')$ where a and a' are the electrode spacing and electrode width, respectively. For our samples electrode spacing a is $6 \mu\text{m}$ and

the electrode width a' is $9\text{ }\mu\text{m}$, therefore $\lambda = 2 \times (6+9) = 30\text{ }\mu\text{m}$ and $G^* = \lambda/4a = 30/(4 \times 6) = 1.25$. For our interdigitated devices, $k = 1/(M \times G^*) = 1/(3.72\text{ cm} \times 1.25) = \mathbf{0.215\text{ cm}^{-1}}$. Note: the actual thickness of the polymer is neglected. The distance between the electrodes (electrode spacing) is considered as the thickness of the polymer which is $6\text{ }\mu\text{m}$. **Figure A4** below shows the optical image of the microfabricated interdigitated electrode.

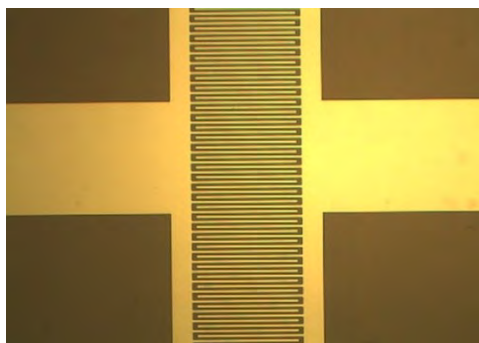


Figure A4. Optical image of the microfabricated interdigitated electrode.

5. Conductivity of Pure PAA Gels

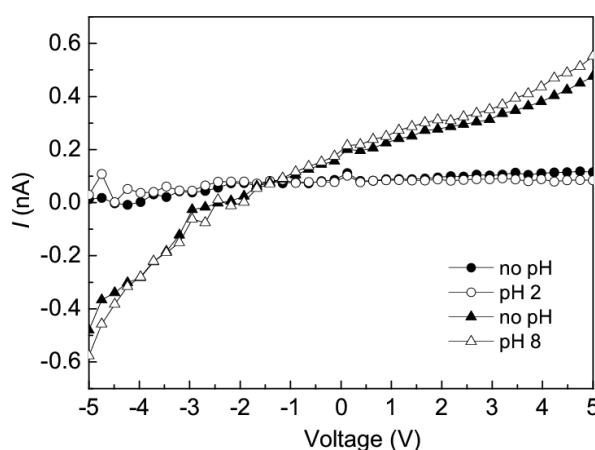


Figure A5. I-V curve measurements of pure PAA gels show that there is no conductivity change of the gels when exposed to pH 2 and pH 8 (measured from two different samples).

6. Electrical Equivalent Circuit Fit for Nyquist Plots for CO₂ detection

For pure SPAN-Na films, when exposed to N₂, CO₂/N₂, the following circuit model gave a reasonable fit.

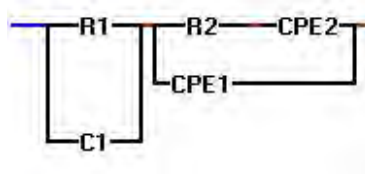


Figure A6. Equivalent circuit diagram for fitting impedance spectrum of SPAN-Na films.

$R1$ and $C1$ are related to the resistance and capacitance of the bulk film, respectively. $R2$, $CPE1$ and $CPE2$ are resistive and capacitive components associated with the film-electrode interface. $CPE1$ and $CPE2$ are the constant phase elements (CPEs), which describe either capacitive ($P1$) or resistive behavior ($P2$) as indicated by the exponential factors. For $CPE1$ $n1 \rightarrow 1$, which means that $CPE1$ acts like a capacitor and for $CPE2$ $n2 \rightarrow 0.5$, which means that $CPE2$ acts as Warburg's impedance related to diffusion of analytes. The values of the extracted parameters for SPAN-Na films when exposed to N_2 and CO_2 are stated below in **Table A2**.

Table A2. Parameter values obtained from fitting of the impedance spectrum for SPAN-Na films when exposed to N_2 and CO_2 .

Parameter	Exposed to N_2		Exposed to CO_2	
	Values	Error (%)	Values	Error (%)
$C1$	7.7E-08	7.1	8.5E-08	7.4
$R1$	1.3E+04	9.3	1.2E+04	6.7
$R2$	8.5E+03	0.09	7.2E+03	0.2
$P1$	1.9E-10	0.1	1.9E-10	0.1
$n1$	0.94	0.007	0.94	0.007
$P2$	1.3E-06	0.04	1.3E-06	0.05
$n2$	0.41	0.01	0.42	0.01

For SPAN-Na:PVA composite films, when exposed to N_2 or CO_2/N_2 , the following circuit model gave a reasonable best fit:

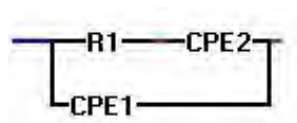


Figure A7. Equivalent circuit diagram used for fitting impedance spectrum of SPAN-Na:PVA films.

Where $R1$ is resistive component of the film and $CPE1$ and $CPE2$ are associated with capacitive ($P1$) ($n1 \rightarrow 1$) or resistive ($P2$) ($n2 \rightarrow 0.5$) behavior (Warburg's impedance related to diffusion of analytes). The parameters obtained from fitting the impedance spectrum of SPAN-Na:PVA films when exposed to N_2 and CO_2 are shown in **Table A3**. As can be seen from **Figure 7b**, the supposedly linear regime of the Nyquist plot for SPAN-Na:PVA films is far from ideal indicating other non-linear processes should be considered.

Table A3. Parameter values obtained from fit of the impedance spectrum for SPAN-Na:PVA films when exposed to N_2 and CO_2 .

<i>Parameter</i>	<i>Exposed to N_2</i>		<i>Exposed to CO_2</i>	
	<i>Values</i>	<i>Error (%)</i>	<i>Values</i>	<i>Error (%)</i>
<i>R1</i>	2.1E+05	0.6	1.3E+05	1.4
<i>P1</i>	1.7E-10	0.5	1.5E-10	1.2
<i>n1</i>	0.95	0.03	0.95	0.06
<i>P2</i>	2.5E-07	1.1	4.5E-07	1.7
<i>n2</i>	0.44	0.3	0.37	0.6

7. Gas Sensor Characterization Setup

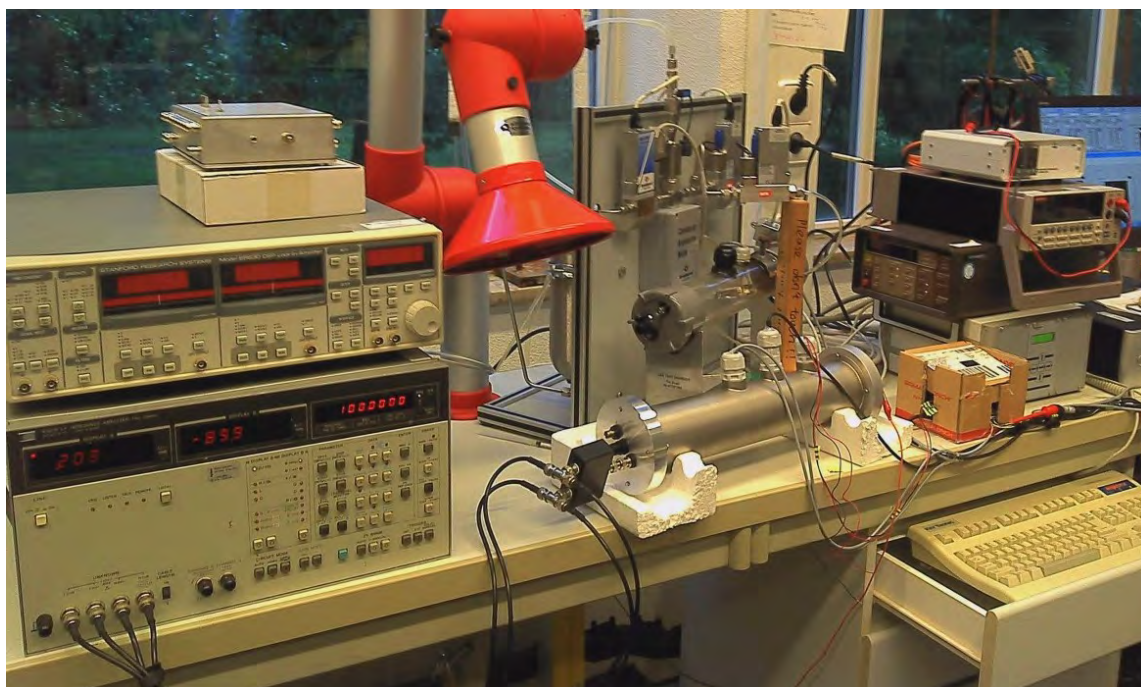


Figure A8. Photo of the automated gas sensor characterization setup.

Reference

- [1] N.F. Sheppard, R.C. Tucker, C. Wu, Electrical conductivity measurements using microfabricated interdigitated electrodes, *Anal. Chem.*, 65 (1993) 1199-1202.

Appendix 2

Supplementary Information for Chapter 3

1. Determination of Re/Rs (Electrode Resistance, Series Resistance)



Figure A1. Electrode configuration.

Resistance $R = \rho * A/l$ where ρ is the resistivity, A is the area cross section of one interdigitated finger, l is length of the finger.

Length and width of each finger/comb is 300 μm and 9 μm respectively. Electrode material deposited by sputtering is Cr/Pt (Cr is used as an adhesion layer). The thickness of Pt layer is 150 nm, the adhesion layer is 20 nm and the total electrode film thickness is 170 nm.

Resistance of Cr/Pt electrodes

From ac impedance measurement, resistance measured from the blank chips is $R_e = 28 \Omega$ at 1 MHz, possibly lower $\sim 20 \Omega$ at 13 MHz (determined from Nyquist plots). Electrode resistance (R_e) measured with polymer on the chips is $R_e = 80 \Omega$ at 1 MHz.

For a 20 nm/150 nm-thick Cr/Pt film, the resistivity of the as-deposited film is $16 \pm 2 \mu\Omega\text{-cm}$ [1]. Resistivity of 20 nm-thick Cr films (deposited by Sputterke, dc sputtering, at MESA+, University of Twente) is 100-1,000 $\mu\Omega\text{-cm}$ and resistivity of 150 nm-thick Pt films is 16 $\mu\Omega\text{-cm}$. So the calculated resistance of the electrodes is in order of $35 \pm 5 \Omega$.

2. Conductivity of the As-casted EB-PANI, SPAN-Na Films under Dry Condition

Table A1. Conductivity of our polymer samples at low humidity.

<i>Polymer</i>	<i>Resistance R (Ω)</i>	<i>1/R</i>	<i>Zaretsky cell constant (K)</i>	<i>$\sigma = (1/R) * k$ (S/cm)</i>	<i>Literature values (S/cm)</i>
<i>EB-PANI</i>	1E+11	1E-11	0.215	2.15E-12	1E-11 [2]
<i>SPANI</i>	2	0.5	0.215	0.108	0.01-0.1 [3, 4]
<i>SPAN-Na</i>	1E+08	1E-08	0.215	2.15E-09	1E-7 [5]
<i>Acid-doped EB-PANI</i>	20	0.05	0.215	1E-02	0.1-5 [6]
<i>Acid-doped SPAN-Na</i>	1E+04	1E-04	0.215	2.15E-05	-

3. Simulations and Data Fitting

3.1. Equivalent Circuit for Decoupling Ionic and Intrinsic Charge Transport

The extended modified Randle's circuit used here is with schematic plot representation.

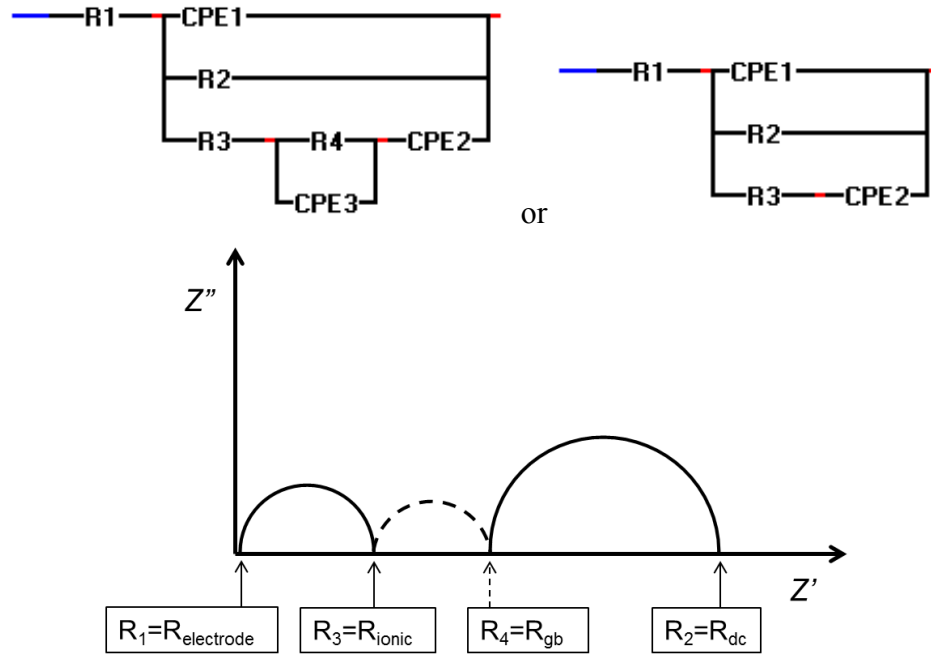


Figure A2. Extended modified Randle's circuit.

3.2. Circuit Elements - Parameter Interpretation

Table A2. Circuit elements and parameter interpretation.

Elements	Parameters	Interpretation
R_1	(R_e)	Electrode resistance (30 Ω)
R_2	(R_q)	Intrinsic charge transport (measured or obtained from dc resistance measurements)
R_3	(R_{ionic})	Ionic charge transport
C_1	CPE_1, P_1, n_1	Film plus blank chip capacitance, pre-factor and exponential factor
CPE_2	$(C_{interface}) - P_2$ $(P_{interface}), n_2$ $(n_{interface})$	Interfacial capacitance pre-factor and exponential factor
R_4 and CPE_3 in parallel (Z_{gb})	R_{gb} (optional) $P_{gb}, n_3 (n_{gb})$	Grain boundary resistance [7] (depends on the samples). Sometimes has no physical functionality in some samples.

3.3. Dc Resistance (I - V Curves) of the Polymers at Different Humidity Levels

a. EB-PANI, acid-doped PANI and acid-doped PANI:PVA blend

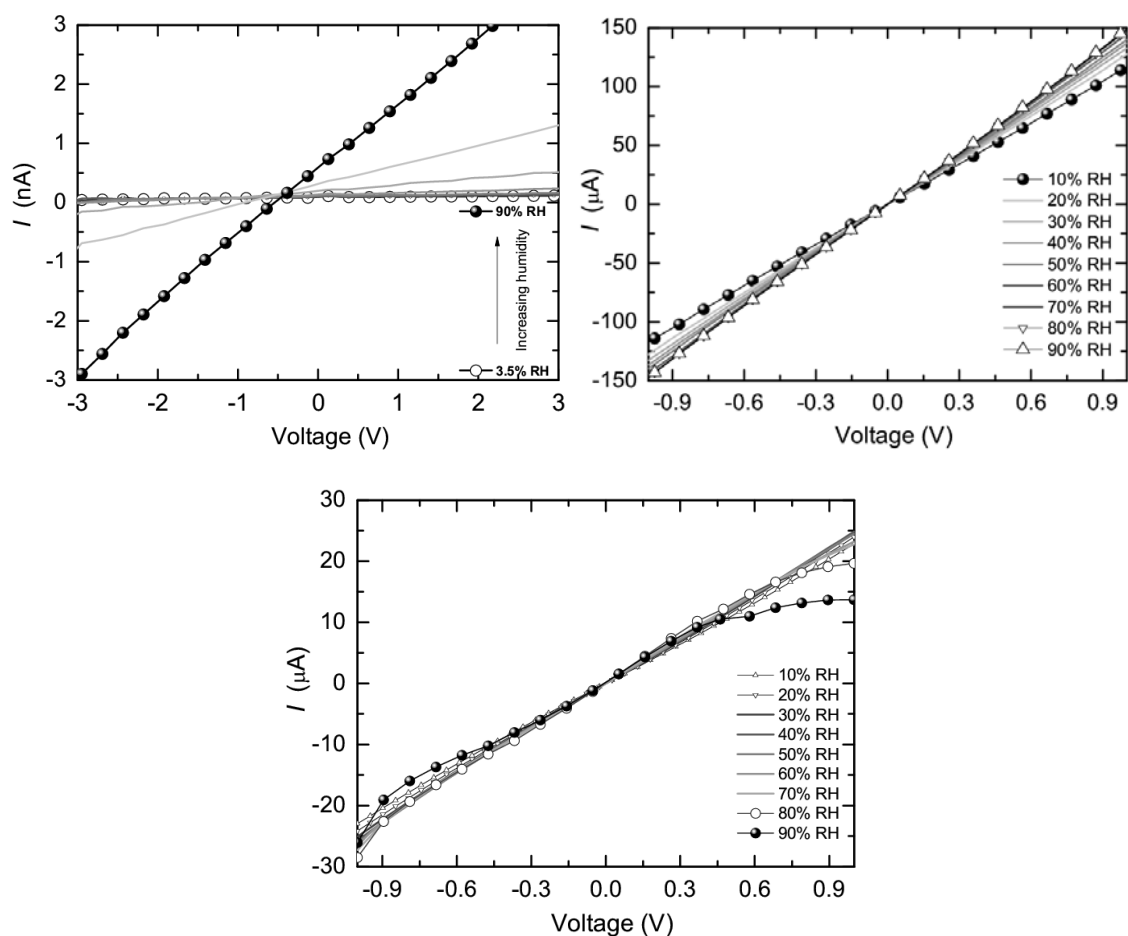
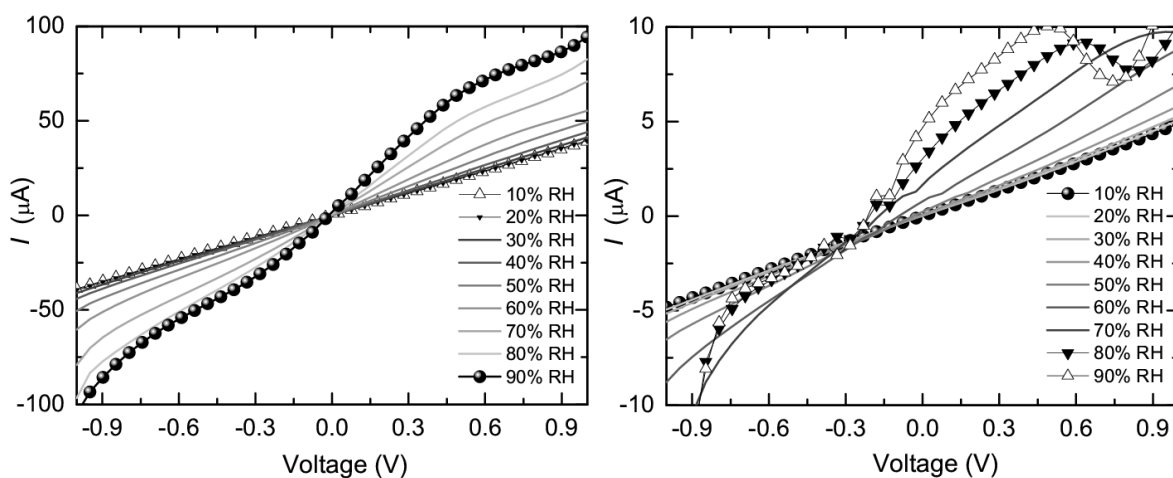


Figure A3. I - V curves of EB-PANI (top left), acid-doped PANI (top right) and acid-doped PANI:PVA (bottom) at different humidity from 10-90% RH.

b. SPANI, SPANI:PVA and acid-doped SPANI



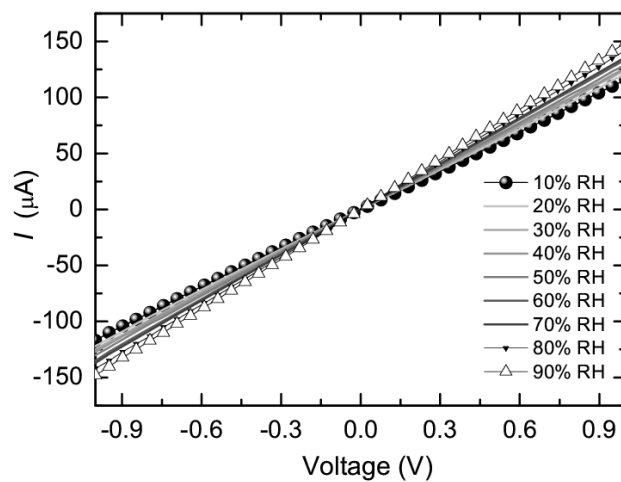


Figure A4. I-V curves of SPANI (top left), SPANI:PVA (top right) and acid-doped SPANI (bottom) at different humidity from 10-90% RH.

c. SPAN-Na, SPAN-Na:PVA and acid-doped SPAN-Na

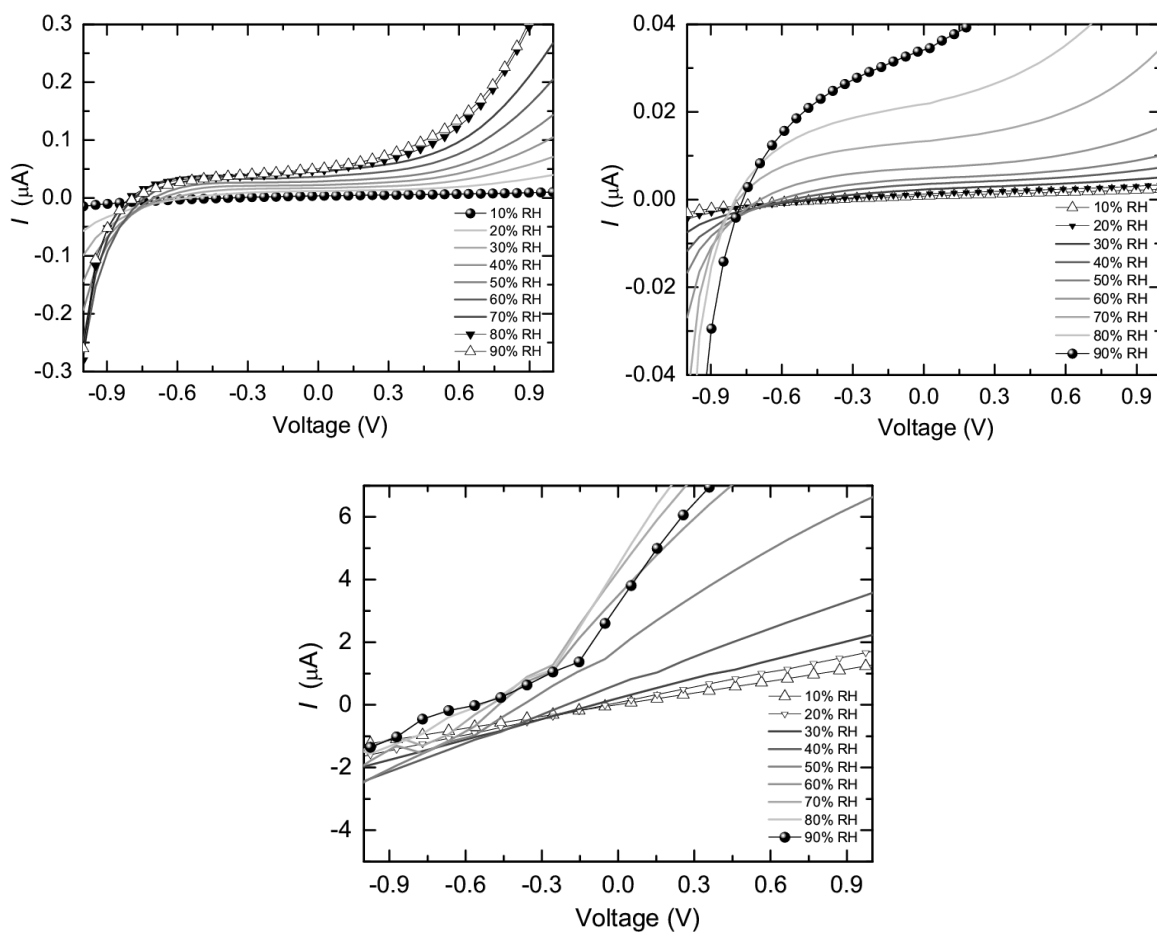


Figure A5. I-V curves of SPAN-Na (top left), SPAN-Na:PVA (top right) and acid-doped SPAN-Na (bottom) at different humidity from 10-90% RH.

d. Pure PVA films at 90% RH and water droplets

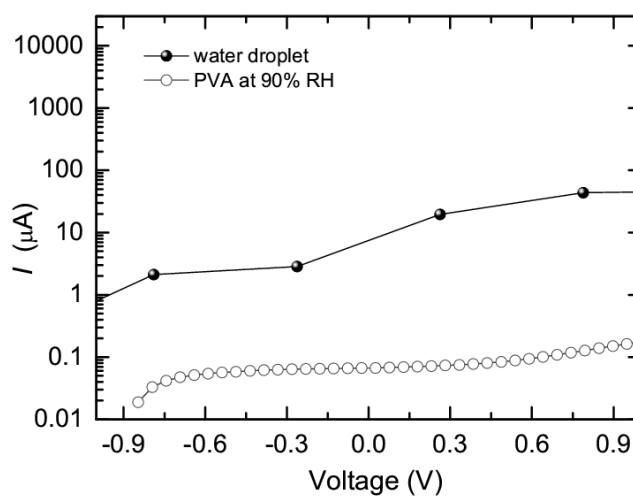


Figure A6. *I-V* curves of pure PVA film and water droplet at 90% RH.

3.4. Fitted Plots of the Polymers at Different Humidity Levels

a. SPAN-Na

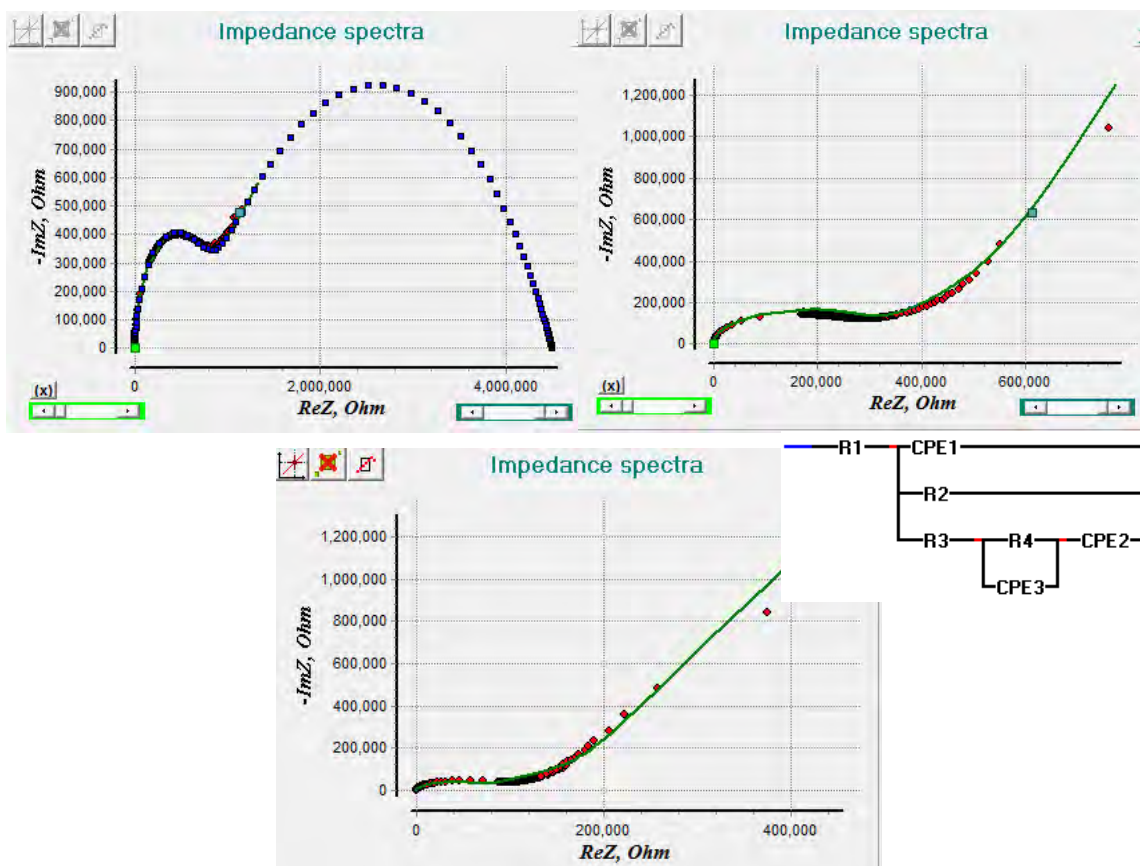


Figure A7. Fitted Nyquist plots of SPAN-Na at 40% RH (top left), 50% RH (top right) and 60% RH (bottom).

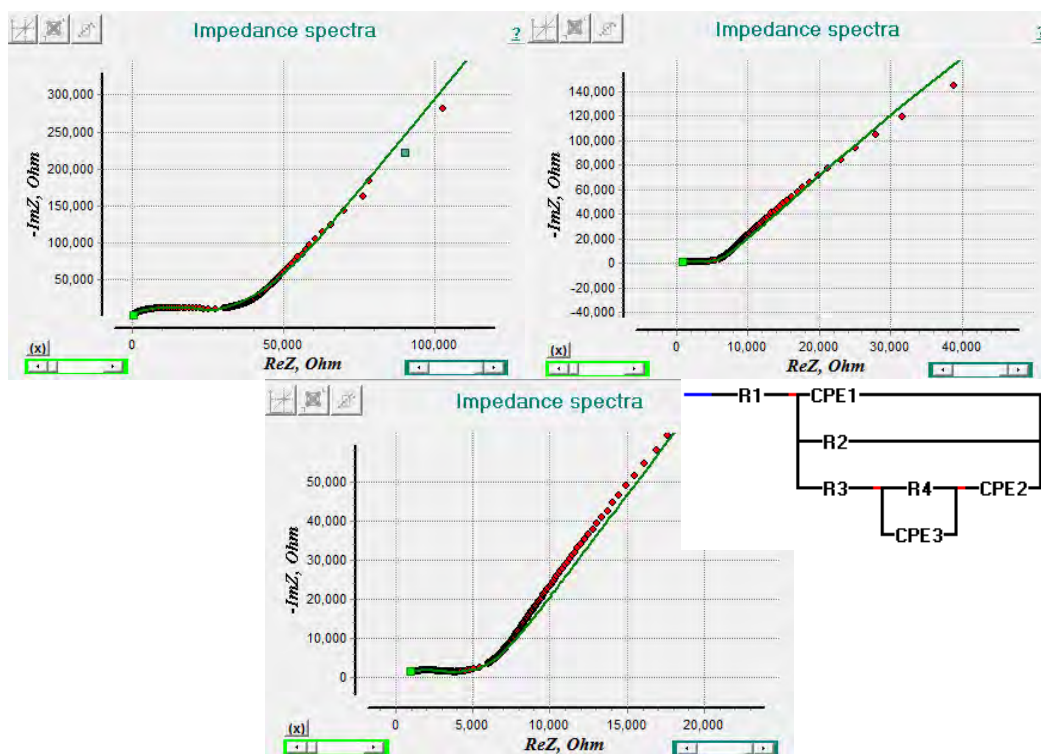


Figure A8. Fitted Nyquist plots of SPAN-Na at 70% RH (top left), 80% RH (top right) and 90% RH (bottom).

b. SPAN-Na:PVA

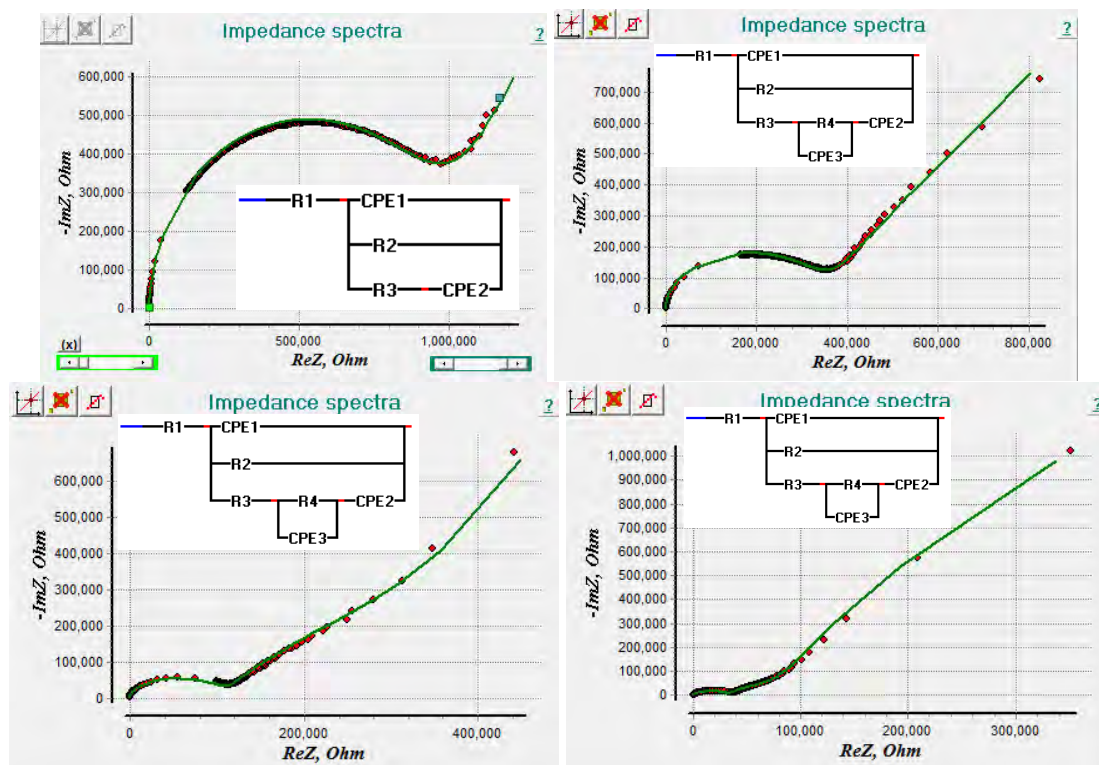


Figure A9. Fitting Nyquist plots of SPAN-Na:PVA at 60% RH (top left), 70% RH (top right), 80% RH (bottom left), 90% RH (bottom right).

c. Acid-doped SPAN-Na:PAA

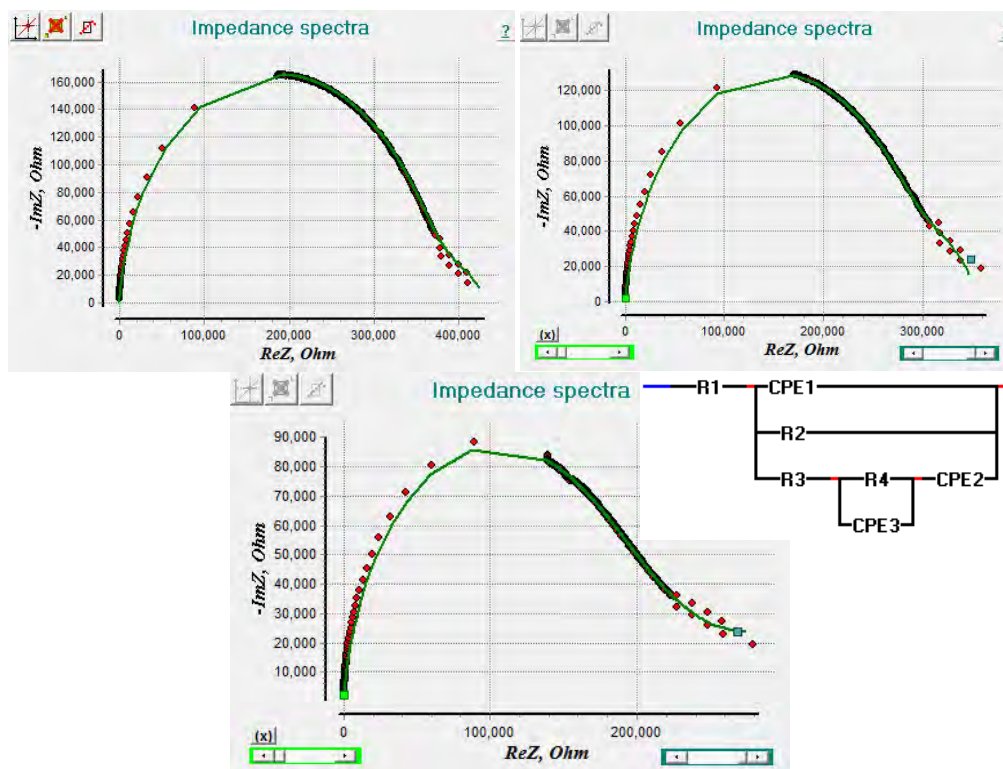


Figure A10. Fitting Nyquist plots of acid-doped SPAN-Na:PAA at 20% RH (top left), 30% RH (top right), 40% RH (bottom).

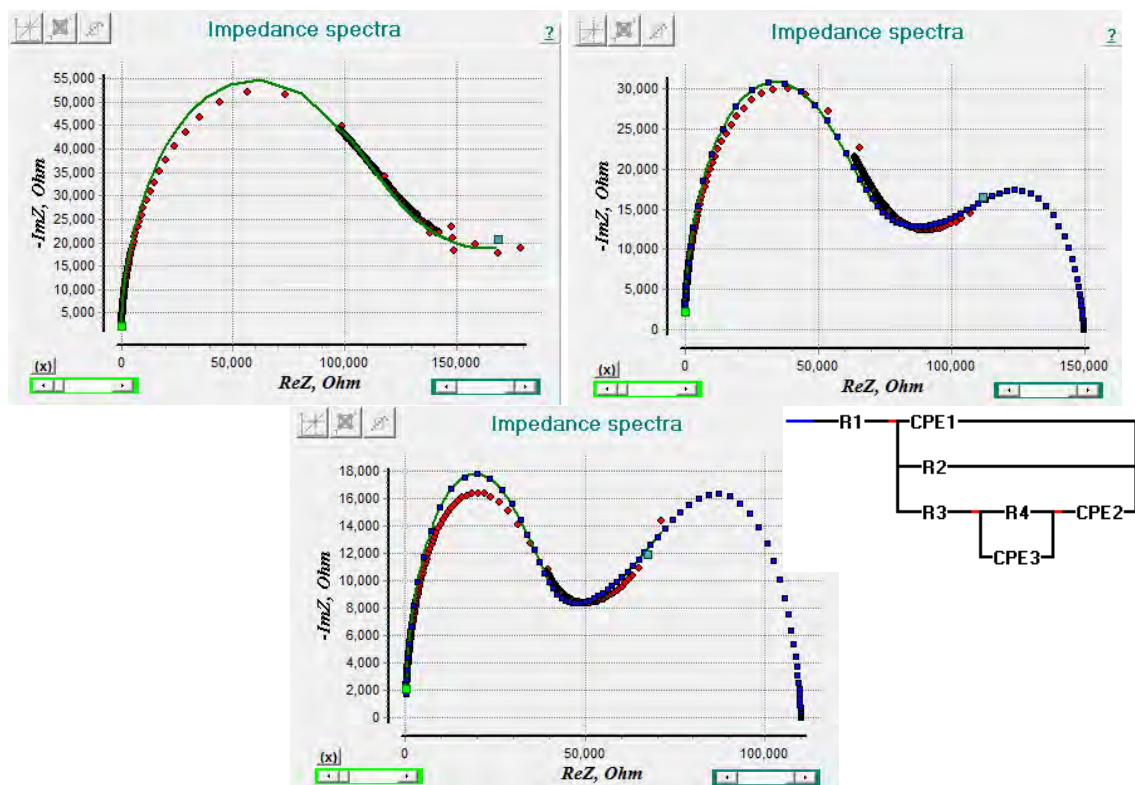


Figure A11. Fitting Nyquist plots of acid-doped SPAN-Na:PAA at 50% RH (top left), 60% RH (top right), 70% RH (bottom).

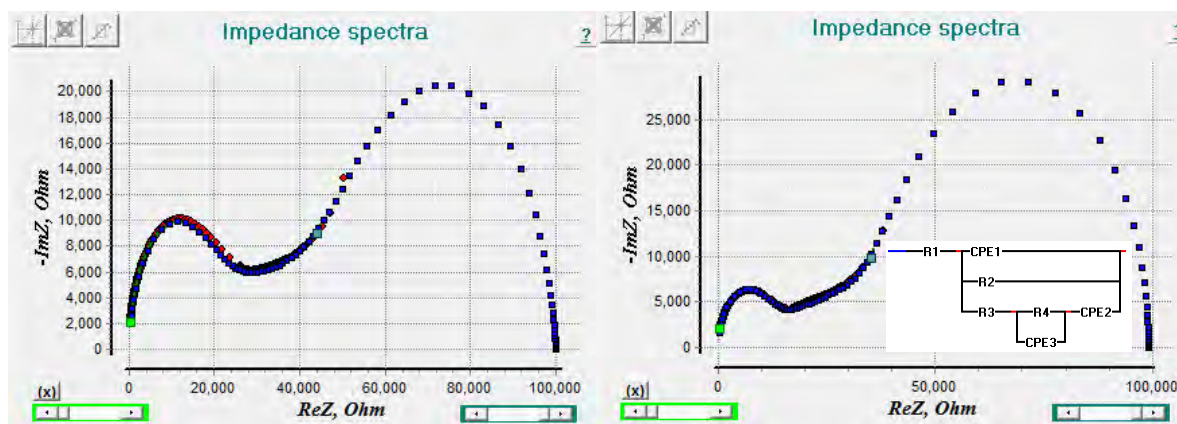


Figure A12. Fitting Nyquist plots of acid-doped SPAN-Na:PAA at 80% RH (left), 90% RH (right).

d. SPANI:PVA

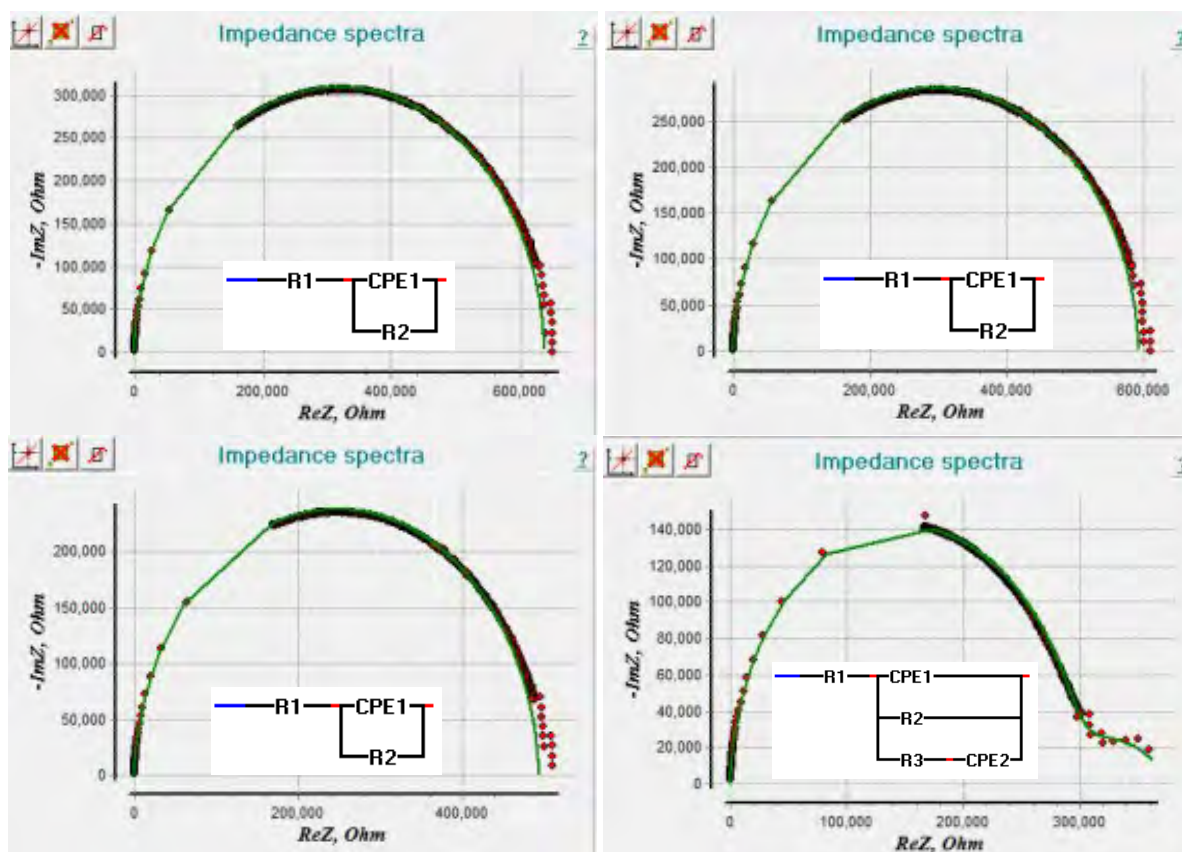


Figure A13. Fitting Nyquist plots of SPANI:PVA at 10% RH (top left), 20% RH (top right), 30% RH (bottom left), 40% RH (bottom right).

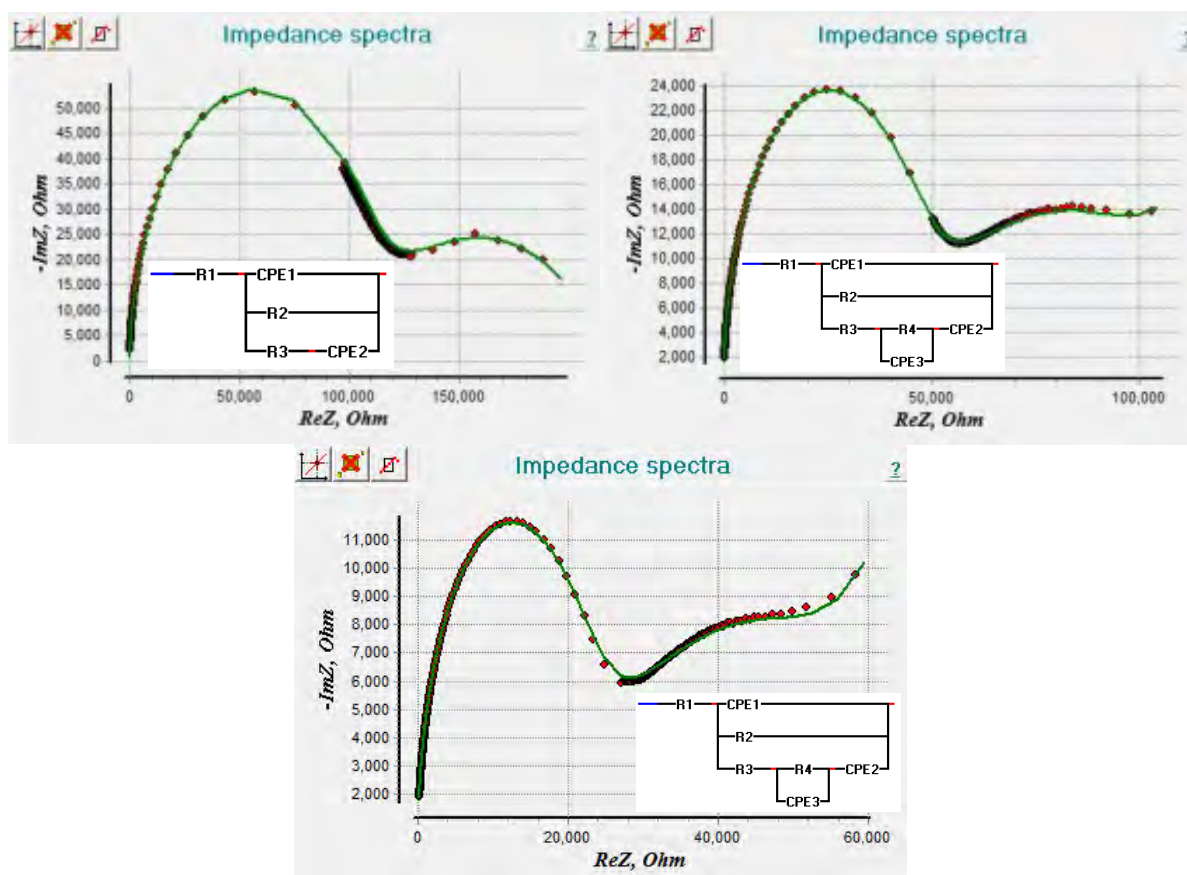


Figure A14. Fitting Nyquist plots of SPANI:PVA at 50% RH (top left), 60% RH (top right), 70% RH (bottom).

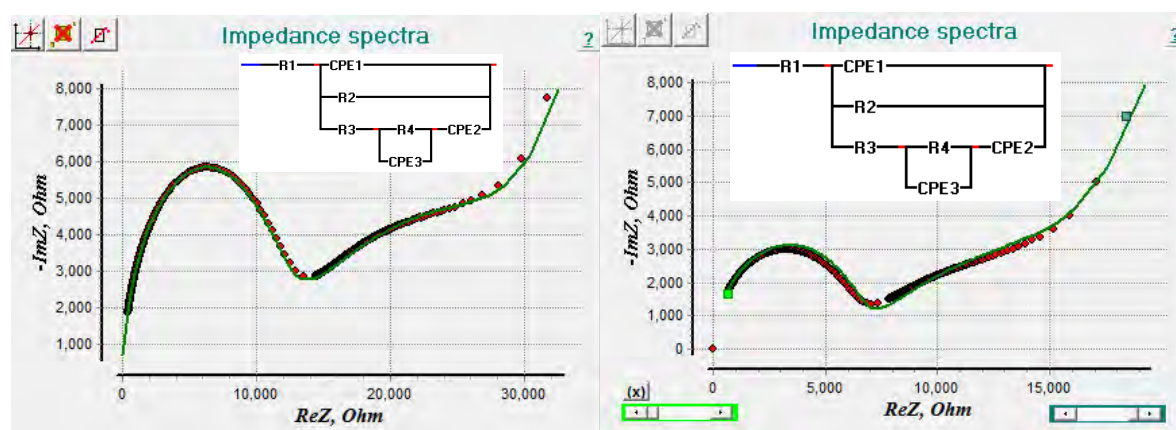


Figure A15. Fitting Nyquist plots of SPANI:PVA at 80% RH (left), 90% RH (right).

e. Acid-doped PANI:PVA

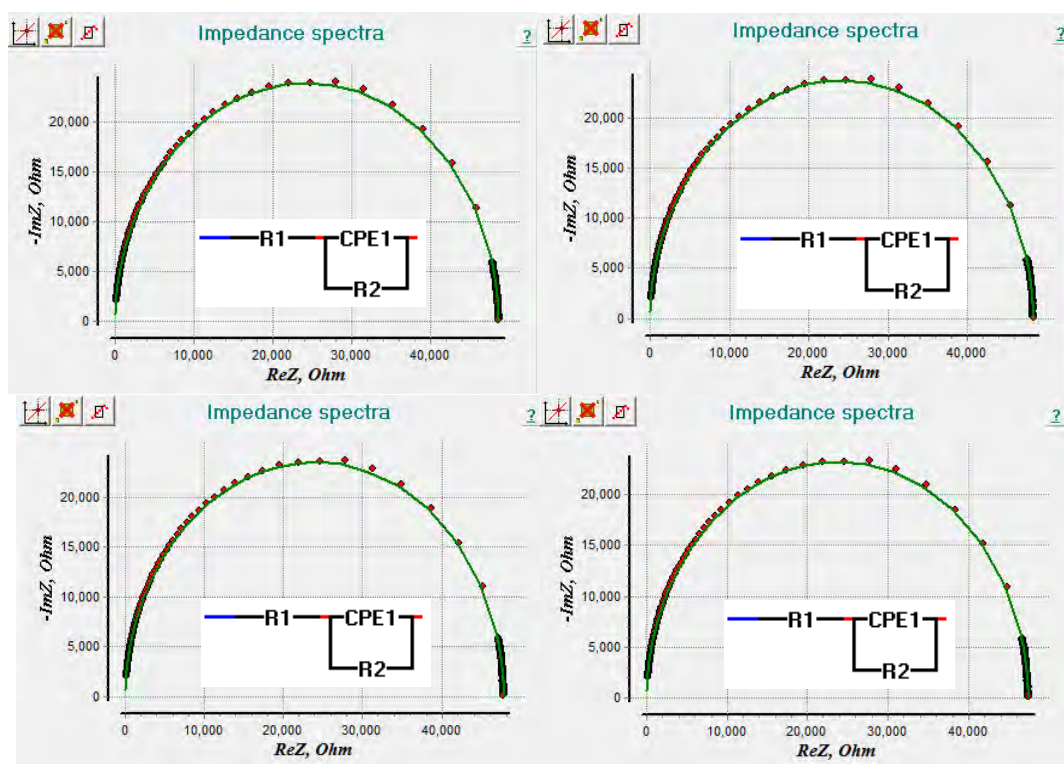


Figure A16. Fitting Nyquist plots of acid-doped PANI:PVA at 10% RH (top left), 20% RH (top right), 30% RH (bottom left), 40% RH (bottom right).

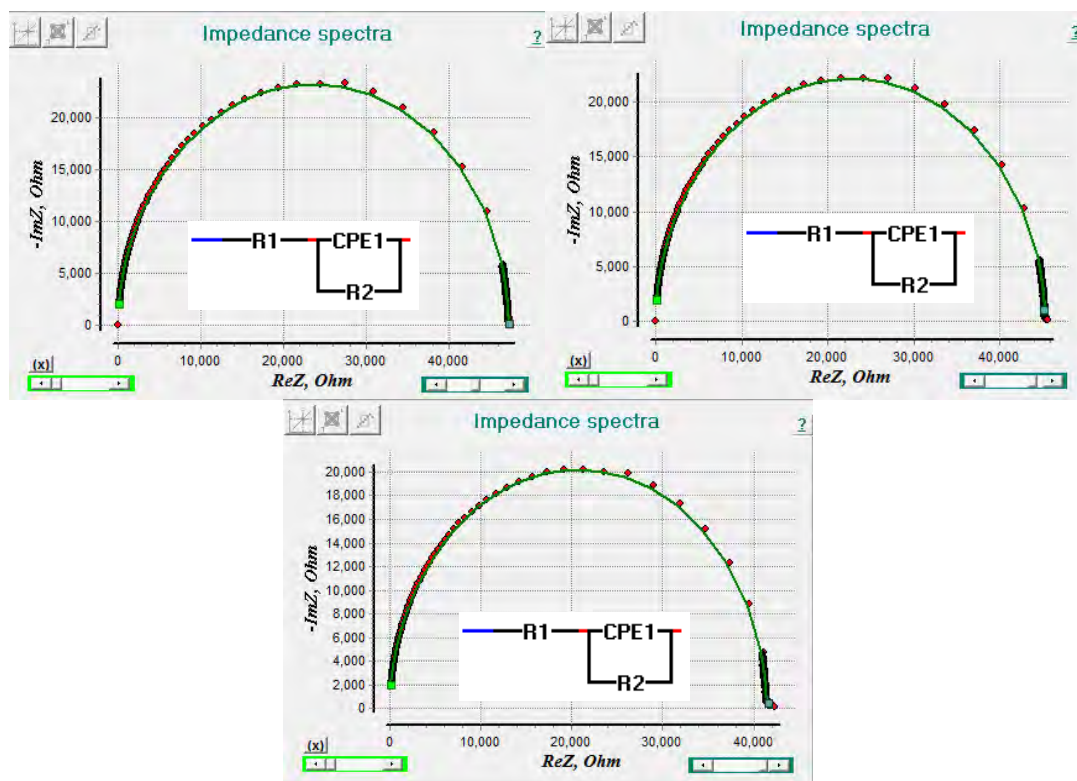


Figure A17. Fitting Nyquist plots of acid-doped PANI:PVA at 50% RH (top left), 60% RH (top right), 70% RH (bottom).

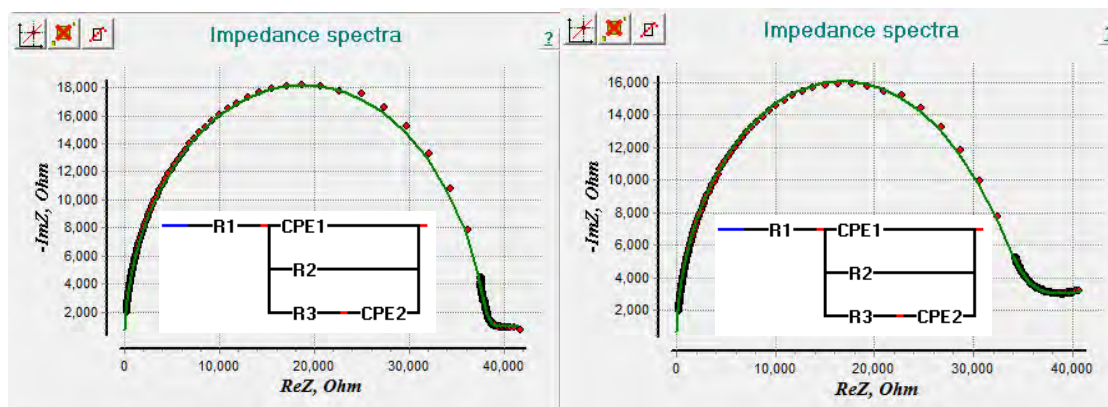


Figure A18. Fitting Nyquist plots of acid-doped PANI:PVA at 80% RH (left), 90% RH (right).

f. Pure PVA sample and DI water droplet

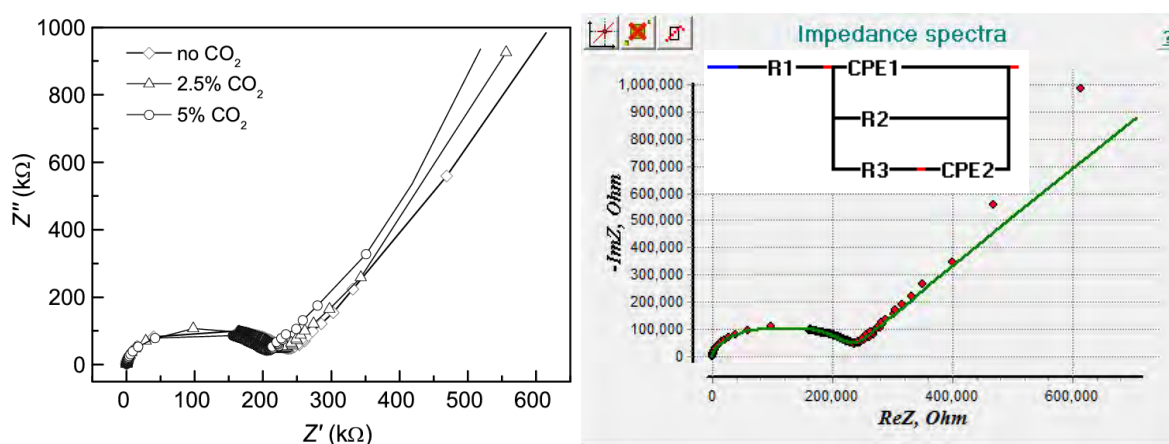


Figure A19. Nyquist plots of pure PVA film at 90% RH with high CO_2 concentrations (left), fitting Nyquist plots of pure PVA at 90% RH (right).

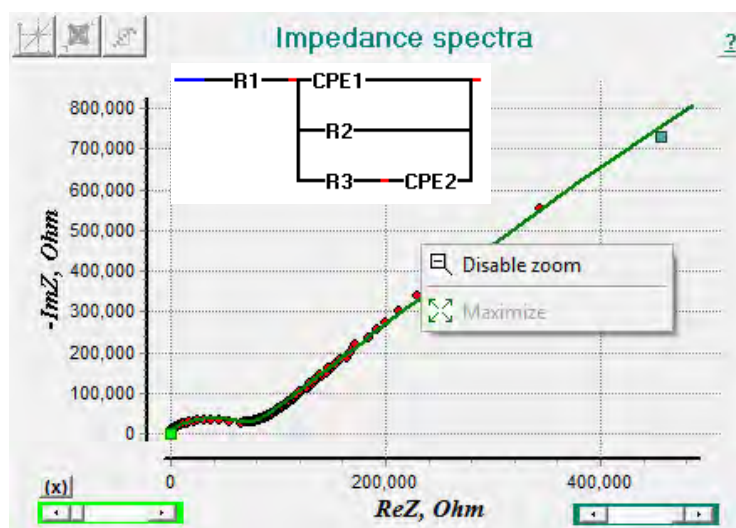


Figure A20. Fitting Nyquist plots of DI water droplet at 90% RH.

3.5. Fitting Parameters

a. SPAN-Na and acid-doped SPAN-Na

Table A3. Fitting parameters of SPAN-Na as a function of humidity.

<i>RH</i> <i>(%)</i>	$R_2 = R_f$ (R_q) (Ω)	$R_3 =$ R_{ionic} (Ω)	R_4 (Ω)	$CPE_3 P_3$ (gb) (F)	n_3 $(undefi$ $ned)$	$CPE_2 P_2$ (F) $(P_{interface})$	n_2 $(n_{inter$ $face)$	CPE_1/C_1 $P_1 = P_f$ (F)	$n_1 = n_f$ $(film)$
20	2.19E+08	-	-	-	-	-	-	9.61E-11	1
30	1.45E+08	-	-	-	-	-	-	9.93E-11	1
40	7.00E+07	520000	350000	-	-	-	-	7.50E-11	0.99
50	5.90E+07	330480	221590	-	-	1.12E-08	-	8.99E-11	0.99
60	4.20E+07	78155	93407	2.40E-08	0.75	1.12E-08	0.88	9.47E-11	0.98
70	2.50E+07	25000	25000	2.44E-08	0.77	1.97E-08	0.88	1.00E-10	0.97
80	1.60E+07	8871.2	8908.3	2.31E-07	0.6	2.00E-08	0.89	7.54E-11	0.96
90	8.72E+06	3404.9	3077.2	2.32E-07	0.61	3.51E-08	0.89	8.08E-11	0.96

Table A4. Fitting parameters of acid-doped SPAN-Na as a function of humidity.

<i>RH</i> <i>(%)</i>	$R_2 = R_f$ (R_q) (Ω)	$R_3 = R_{ionic}$ (Ω)	R_4 (Ω)	$CPE_3 P_3$ (gb) (F)	n_3 $(undefi$ $ned)$	$CPE_2 P_2$ (F) $(P_{interface})$	n_2 $(n_{inter$ $face)$	CPE_1/C_1 $P_1 = P_f$ (F)	$n_1 = n_f$ $(film)$
10	504660	-	-	-	-	-	-	9.53E-11	0.98
20	433860	2.20E+06	-	-	-	6.98E-09	0.6	1.62E-10	0.93
30	355830	1.75E+06	9.97E+06	-	-	1.87E-09	0.76	2.36E-10	0.91
40	307710	473460	1.30E+06	2.85E-08	0.53	1.52E-08	0.85	2.35E-10	0.91
50	211770	165160	886280	9.00E-08	0.43	3.00E-08	0.88	8.24E-11	0.99
60	149540	63215	997490	6.18E-07	0.3	1.11E-07	0.9	7.46E-11	1
70	110090	33127	798250	1.69E-06	0.27	2.59E-07	0.9	9.29E-11	1
80	110000	10497	218860	2.93E-06	0.24	5.23E-07	0.89	7.53E-11	1
90	99000	10926	80065	2.26E-06	0.35	5.45E-07	1	9.33E-11	1

b. SPANI and acid-doped SPANI

Table A5. Fitting parameters of SPANI as a function of humidity.

<i>RH (%)</i>	$R_2 = R_f (R_q) (\Omega)$	$CPE_1/C_1, P_1 = P_f (F)$	$n_1 = n_f (film)$
10	6773.8	9.11E-11	0.99
20	6701.3	8.89E-11	1

30	6565.7	8.93E-11	1
40	6395.3	9.00E-11	0.99
50	6175.5	8.99E-11	1
60	5920.6	9.20E-11	0.99
70	5590.9	9.55E-11	0.99
80	5160.1	1.05E-10	0.99
90	4757.3	1.67E-10	0.96

Table A6. Fitting parameters of acid-doped SPANI as a function of humidity.

<i>RH</i> (%)	R_{dc} (Ω)	$R_2 = R_f (R_q)$	$CPE_l/C_l, P_l = P_f (F)$	$n_l = n_f$
10	8557	4043	9.41E-11	0.99
20	8221	4047.1	9.33E-11	0.99
30	7989	4010.6	9.20E-11	0.99
40	7868	3917.5	9.14E-11	1
50	7700	3798.6	9.18E-11	1
60	7440	3637.8	9.36E-11	0.99
70	7335	3524.8	9.71E-11	0.99
80	7039	3429.9	1.03E-10	0.99
90	6761	3257.2	1.09E-10	0.99

c. Acid-doped PANI and acid-doped PANI:PVA

Table A7. Fitting parameters of acid-doped PANI as a function of humidity.

<i>RH</i> (%)	$R_2 = R_f (R_q)$ (Ω)	$CPE_l/C_l, P_l = P_f (F)$	$n_l = n_f$
10	10984	8.94E-11	0.99
20	10004	8.73E-11	0.99
30	9593.7	8.91E-11	0.99
40	9314.5	8.98E-11	0.99
50	9082.1	9.13E-11	0.99
60	8872.1	9.24E-11	0.99
70	8629.5	9.70E-11	0.98
80	8361.9	1.07E-10	0.98
90	8029.7	1.56E-10	0.95

Table A8. Fitting parameters of acid-doped PANI:PVA as a function of humidity.

RH (%)	$R_2 = R_f$ (R_q) (Ω)	$R_3 = R_{ionic}$ (Ω)	$CPE_2 P_2$ (F) ($P_{interface}$)	n_2 ($n_{interface}$)	CPE_l/C_1 $P_l = P_f$ (F)	$n_l = n_f$ (film)
10	48589	-	-	-	9.42E-11	0.99
20	48328	-	-	-	9.43E-11	0.99
30	47891	-	-	-	9.48E-11	0.99
40	47431	-	-	-	9.59E-11	0.99
50	47229	-	-	-	9.77E-11	0.99
60	45322	-	-	-	1.00E-10	0.99
70	41457	-	-	-	1.04E-10	0.98
80	45490	188030	1.4E-06	0.27	1.04E-10	0.98
90	65200	51059	3.6E-06	0.23	9.62E-11	0.99

*d. SPAN-Na:PVA***Table A9. Fitting parameters of SPAN-Na:PVA as a function of humidity.**

RH (%)	$R_2 = R_f$ (R_q) (Ω)	$R_3 = R_{ionic}$ (Ω)	R_4 (Ω)	$CPE_3 P_3$ (gb) (F)	n_3 (undefined)	$CPE_2 P_2$ (F) ($P_{interface}$)	n_2 ($n_{interface}$) (n_{ace})	CPE_l/C_1 $P_l = P_f$ (F)	$n_l = n_f$ (film)
20	6.98E+08	-	-	-	-	-	-	1E-10	1
30	5.37E+08	-	-	-	-	-	-	1E-10	1
40	4.47E+08	-	-	-	-	-	-	1E-10	1
50	3.88E+08	-	-	-	-	-	-	1E-10	1
60	1.94E+08	980000	-	-	-	2.30E-08	0.68	1E-10	0.98
70	8E+07	348140	70000	5.7E-08	1	4.03E-08	0.69	9.51E-11	0.99
80	4E+07	110000	287420	5.46E-08	0.74	3.53E-08	0.91	1.09E-10	0.98
90	2E+07	33485	41467	3.55E-08	0.86	4.61E-08	0.87	9.49E-11	0.99

*e. SPANI:PVA***Table A10. Fitting parameters of SPANI:PVA as a function of humidity.**

RH (%)	$R_2 = R_f$ (R_q) (Ω)	$R_3 = R_{ionic}$ (Ω)	R_4 (Ω)	$CPE_3 P_3$ (gb) (F)	n_3 (undefined)	$CPE_2 P_2$ (F) ($P_{interface}$)	n_2 ($n_{interface}$)	CPE_l/C_1 $P_l = P_f$ (F)	$n_l = n_f$ (film)
10	638200	-	-	-	-	-	-	1.10E-10	0.98
20	592720	-	-	-	-	-	-	1.13E-10	0.98

30	493770	-	-	-	-	-	-	1.19E-10	0.97
40	375000	1.35E+06	-	-	-	3.00E-08	0.55	1.20E-10	0.97
50	220000	2.11E+05	-	-	-	1.29E-07	0.55	1.31E-10	0.97
60	164500	60411	336210	4.83E-07	0.44	9.00E-07	0.96	1.02E-10	0.99
70	100030	26511	167730	9.49E-07	0.41	1.16E-06	0.96	9.82E-11	0.99
80	88000	12345	49511	2.12E-06	0.41	2.84E-06	0.97	9.77E-11	0.99
90	85000	6800.3	21341	4.01E-06	0.44	3.70E-06	0.96	1.54E-10	0.96

f. Pure PVA and DI water droplet

Table A11. Fitting parameters of pure PVA and water droplet at 90% RH.

Material	R_1 (Ω)	R_2 (Ω)	R_3 (Ω)	P_1 (F)	n_1	P_2 (F)	n_2
PVA	30	4E+07	2.28E+05	1.10E-10	0.97	8.93E-08	0.69
DI water droplet	1E+06	1E+06	1E+06	0.0005	1	0.0005	1

References

- [1] R.M. Tiggelaar, R.G.P. Sanders, A.W. Groenland, J.G.E. Gardeniers, Stability of thin platinum films implemented in high-temperature microdevices, *Sensors and Actuators A*, 152 (2009) 39–47.
- [2] A.G. Macdiarmid, J.C. Chiang, A.F. Richter, A.J. Epstein, Polyaniline: a new concept in conducting polymers, *Synth. Met.*, 18 (1987) 285-290.
- [3] S.-A. Chen, G.-W. Hwang, Structure Characterization of Self-Acid-Doped Sulfonic Acid Ring-Substituted Polyaniline in Its Aqueous Solutions and as Solid Film, *Macromolecules*, 29 (1996) 3950-3955.
- [4] J. Yue, Z.H. Wang, K.R. Cromack, A.J. Epstein, A.G. MacDiarmid, Effect of sulfonic acid group on polyaniline backbone, *J. Am. Chem. Soc.*, 113 (1991) 2665-2671.
- [5] A.J. Epstein, Yue, Jiang Sulfonated polyaniline salt compositions and uses thereof, US patent 5159031, (1992).
- [6] J.C. Chiang, A.G. MacDiarmid, 'Polyaniline': Protonic acid doping of the emeraldine form to the metallic regime, *Synth. Met.*, 13 (1986) 193-205.

[7] S.N. Patel, A.E. Javier, G.M. Stone, S.A. Mullin, N.P. Balsara, Simultaneous Conduction of Electronic Charge and Lithium Ions in Block Copolymers, *ACS Nano*, 6 (2012) 1589-1600.

Appendix 3

Supplementary Information for Chapter 4

1. Equivalent Circuits for Fitting Impedance Data of Pure PEI Film

For pure PEI films upon exposure to different humidity levels, the following circuit models gave reasonable fits.

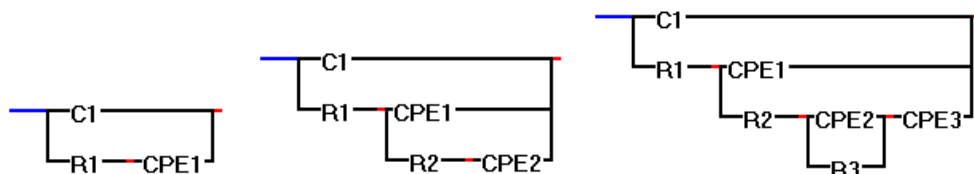
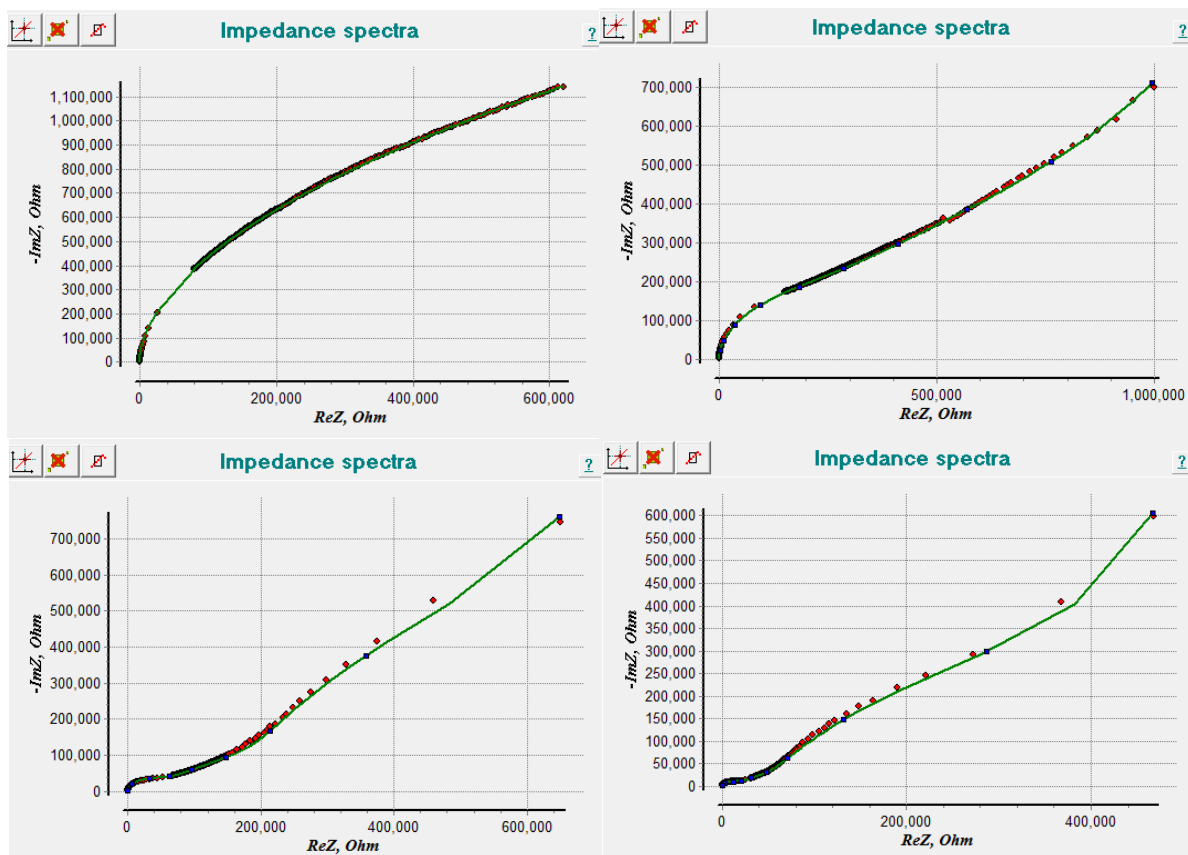


Figure A1. Equivalent circuits for fitting impedance spectra of pure PEI films at 40% RH (left), 50% RH (middle), 60-90% RH (right).

2. Fitted Nyquist Plots of Pure PEI Film at Different Humidity Levels



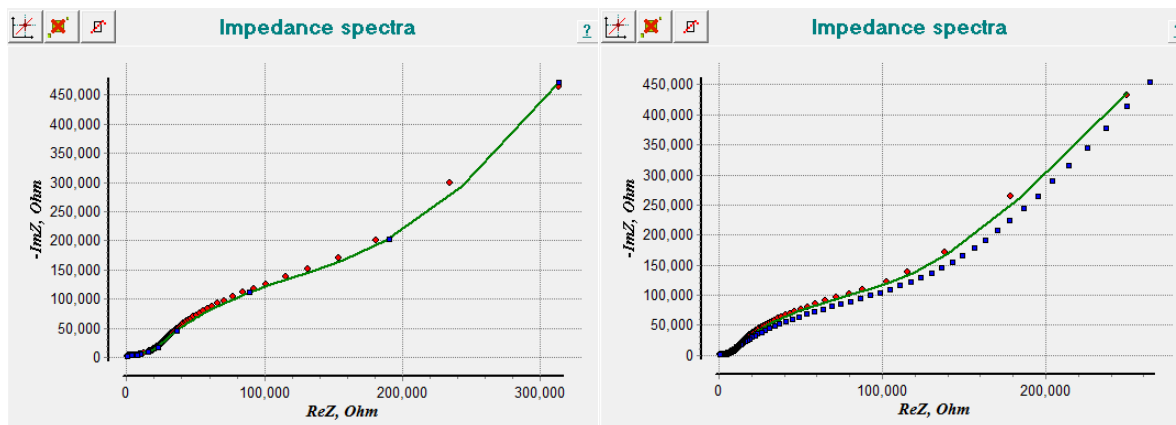


Figure A2. Fitted Nyquist plots of pure PEI film at 40% RH (top left), 50% RH (top right), 60% RH (middle left), 70% RH (middle right), 80% RH (bottom left), 90% RH (bottom right).

Table A1. Parameter values obtained from fitting the Nyquist plots of PEI films.

<i>RH</i> (%)	R_1 (Ω)	R_2 (Ω)	R_3 (Ω)	C_1 (F)	CPE_1 (F)	n_1	CPE_2 (F)	n_2	CPE_3 (F)	n_3
40	1.28 E+06	-	-	7.48E-11	1.27E-08	0.45	-	-	-	-
50	1.62 E+05	5.00 E+06	-	7.10E-11	4.90E-08	0.45	-	-	9.39E-10*	1*
60	5.41 E+04	3.42 E+05	1.38 E+06	8.19E-11	4.29E-08	0.6	1.39E-08	0.84	1.58E-08	1
70	1.82 E+04	7.79 E+04	6.68 E+05	7.56E-11	3.87E-08	0.67	2.37E-08	0.81	4.63E-08	1
80	8.04 E+03	2.44 E+04	1.99 E+05	7.77E-11	1.62E-08	0.79	2.58E-08	0.88	1.15E-07	0.81
90	3.95 E+03	1.31 E+04	1.32 E+05	7.97E-11	2.26E-08	0.8	1.54E-08	0.96	1.23E-07	0.79

* P_3 and n_3 for 50% RH is obtained from CPE_2 in the middle circuit (for 50% RH) of **Figure A1**.

Appendix 4

Supplementary Information for Chapter 5

1. Equivalent Circuits for Fitting Impedance Data of PEI Blend Films

For the PEI:SPAN-Na blend films upon exposure to different humidity levels, the following circuit models gave reasonable fits.

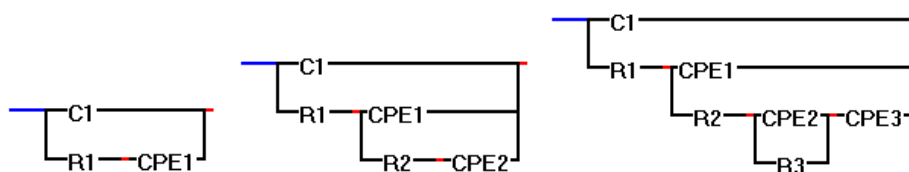


Figure A1. Equivalent circuits for fitting impedance spectra of the PEI:SPAN-Na blend films at 30% RH (left), 40% RH (middle), 50-90% RH (right).

For the PEI:Nafion-Na blend films, the first circuit in **Figure A1** was applied.

2. Fitted Nyquist Plots of PEI:SPAN-Na Film at Different Humidity Levels

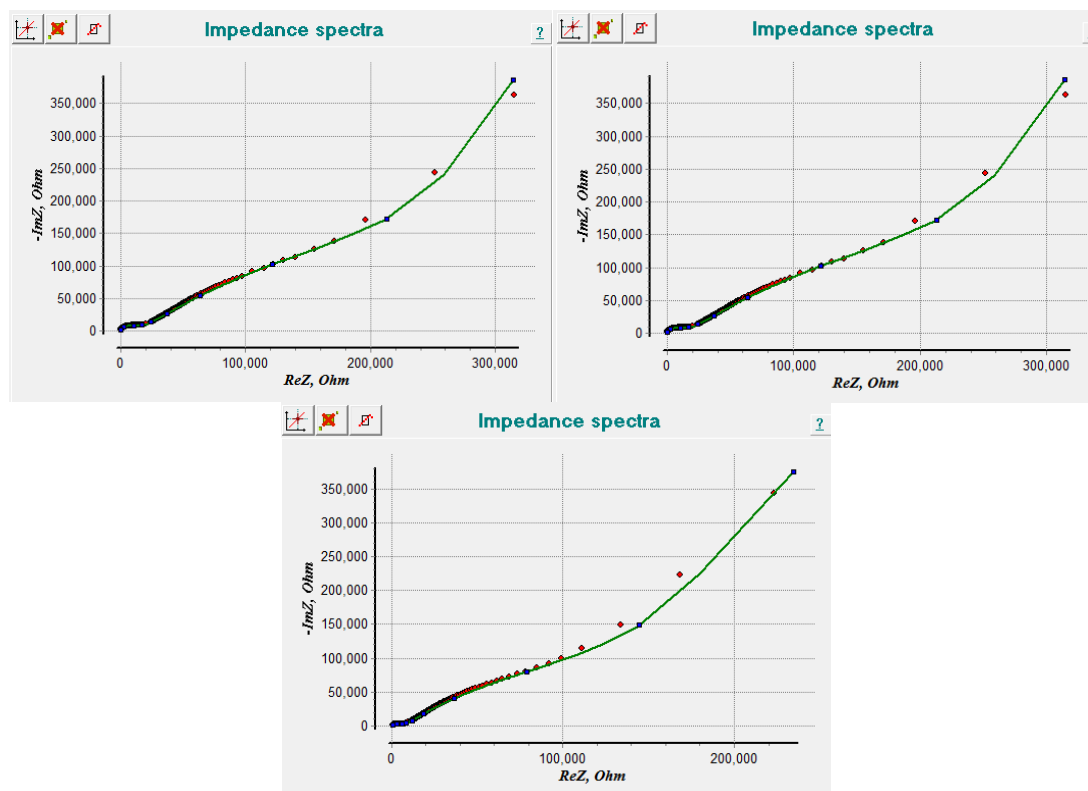


Figure A2. Fitted Nyquist plots of PEI:SPAN-Na film at 50% RH (top left), 60% RH (top right), 70% RH (bottom).

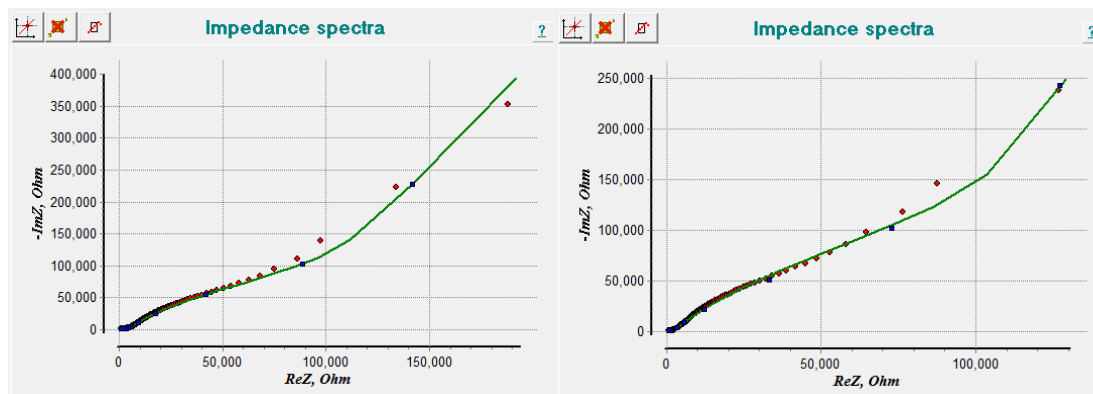
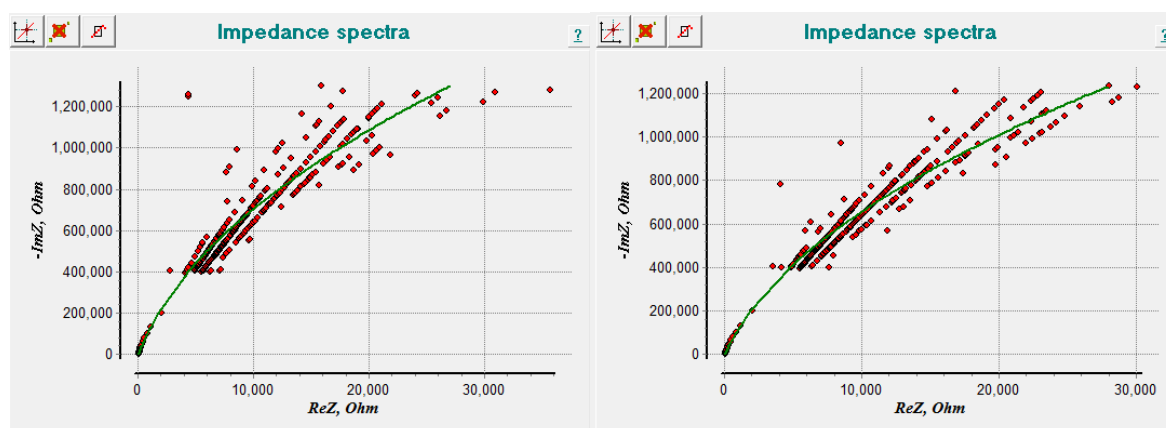


Figure A3. Fitted Nyquist plots of PEI:SPAN-Na film at 80% RH (left), 90% RH (right).

Table A1. Parameter values obtained from fitting the Nyquist plots of PEI:SPAN-Na films.

<i>RH</i> (%)	R_1 (Ω)	R_2 (Ω)	R_3 (Ω)	C_1 (F)	CPE_1 (F)	n_1	CPE_2 (F)	n_2	CPE_3 (F)	n_3
50	4.81E+04	4.56 E+05	1.07 E+06	8.12E-11	1.52E-07	0.47	2.27E-09	0.82	2.62E-08	1
60	1.44E+04	1.81 E+05	4.80 E+05	8.35E-11	1.64E-07	0.57	4.11E-09	0.85	3.60E-08	1
70	6.03E+03	9.68 E+04	3.28 E+05	8.77E-11	1.54E-07	0.63	1.52E-09	1	4.09E-08	0.95
80	2.78E+03	3.69 E+04	2.85 E+05	9.70E-11	1.27E-07	0.68	2.00E-09	1	3.75E-08	0.96
90	1.47E+03	3.28 E+03	2.03 E+05	1.05E-10	2.51E-08	0.81	6.14E-08	1	7.30E-08	0.74

3. Fitted Nyquist Plots of PEI:Nafion-Na Film at Different Humidity Levels



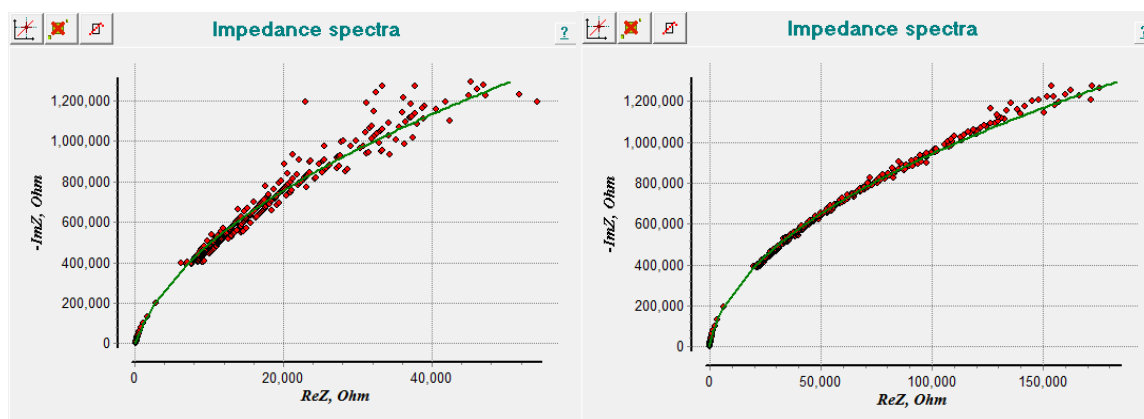


Figure A4. Fitted Nyquist plots of PEI:Nafion-Na film at 10% RH (top left), 20% RH (top right), 30% RH (bottom left), 40% RH (bottom right).

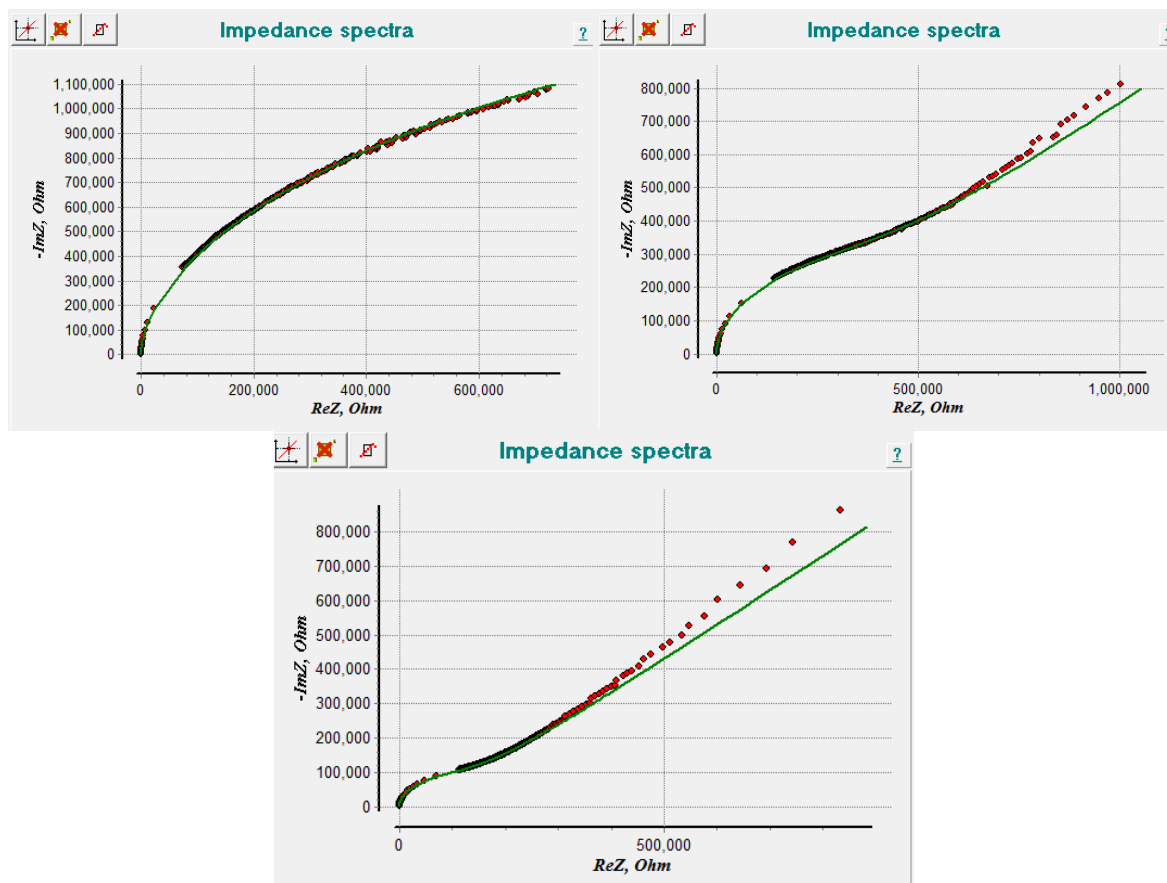


Figure A5. Fitted Nyquist plots of PEI:Nafion-Na film at 50% RH (top left), 60% RH (top right), 70% RH (bottom).

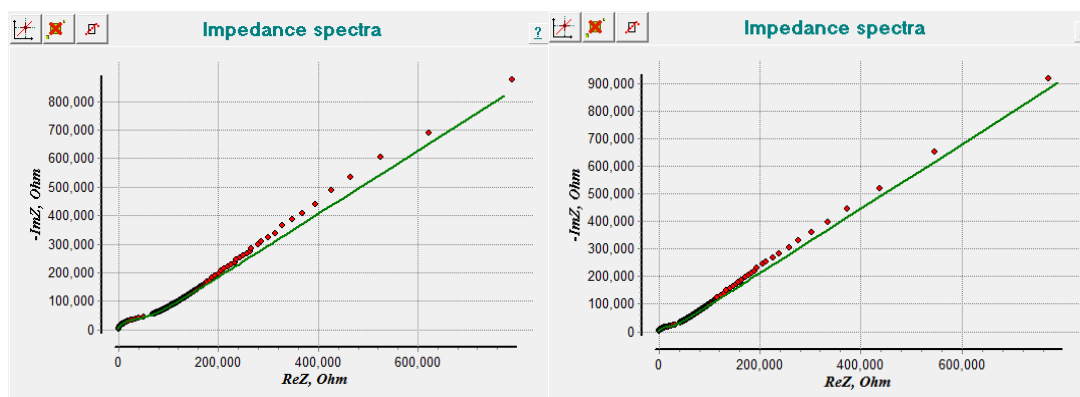
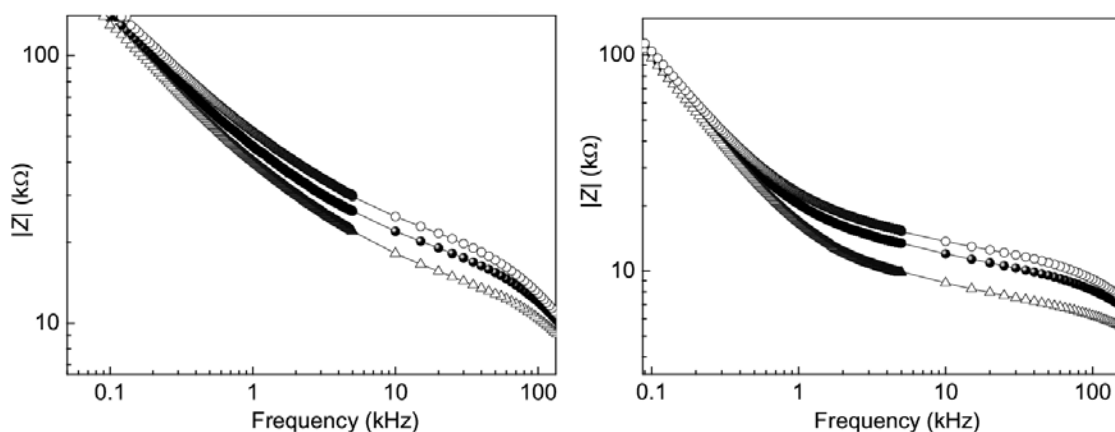


Figure A6. Fitted Nyquist plots of PEI:Nafion-Na film at 80% RH (left), 90% RH (right).

Table A2. Parameter values obtained from fitting the Nyquist plots of PEI:Nafion-Na films.

RH (%)	R_1 (Ω)	$R_2 = R_f(R_g)$ (Ω)	$CPE_1/C_1 P_1 = P_f$ (F)	CPE_2 (Randel) (F)	n_2
10	8.20E+01	8.97E+07	8.36E-11		
20	8.20E+01	7.70E+07	8.39E-11		
30	7.70E+01	4.26E+07	8.55E-11		
40	6.50E+01	1.03E+07	8.99E-11		
50	7.40E+01	1.41E+06	8.90E-11	1.75E-08	0.46
60	1.14E+02	2.98E+05	8.02E-11	4.07E-08	0.46
70	1.19E+02	1.13E+05	8.06E-11	5.37E-08	0.51
80	1.27E+02	4.83E+04	8.13E-11	6.85E-08	0.53
90	1.40E+02	2.37E+04	8.25E-11	8.61E-08	0.55

4. Comparison of Relative Change in Impedance due to Humidity and CO₂



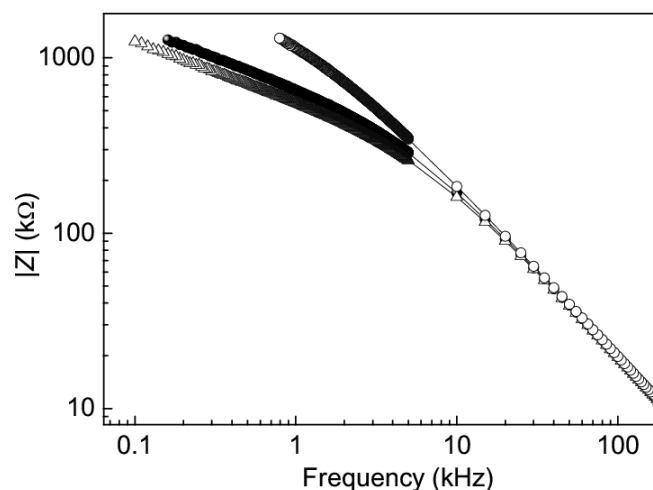


Figure A7. Absolute impedance ($|Z|$) of the blend films as a function of frequency at 60% RH (●), at 60% RH with 1% CO_2 (○) and at 62% RH (△). PEI:SPAN-Na 1:1 (top left), PEI:PSS-Na 1:1 (top right), PEI:Nafion-Na 1:1 (bottom).

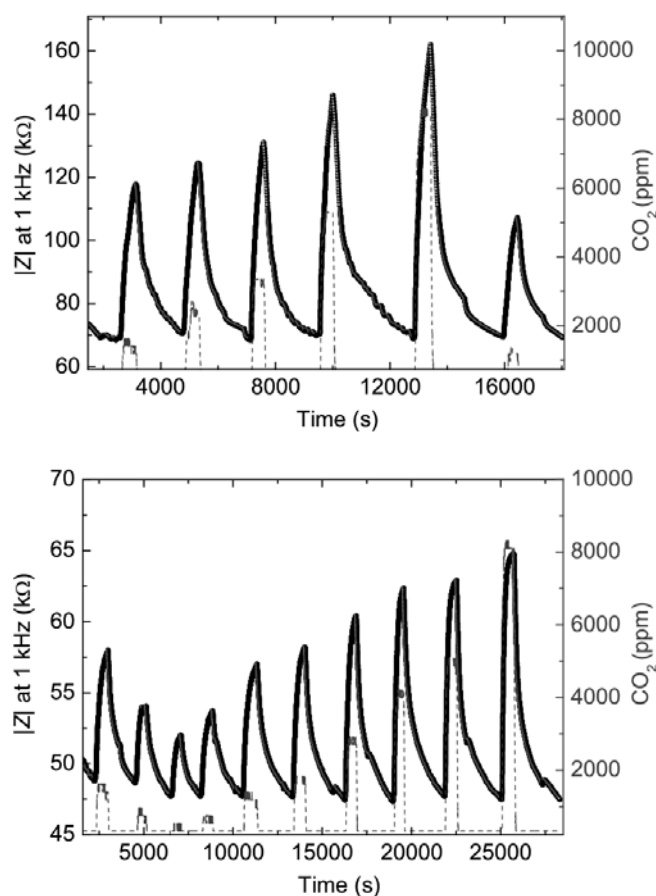


Figure A8. Time dependent impedance measured at 1 kHz of PEI:Nafion-Na 3:1 when the blend was exposed to different CO_2 concentrations (dash line) at 75% RH as prepared - the first measurement (top), after 2 weeks (bottom).

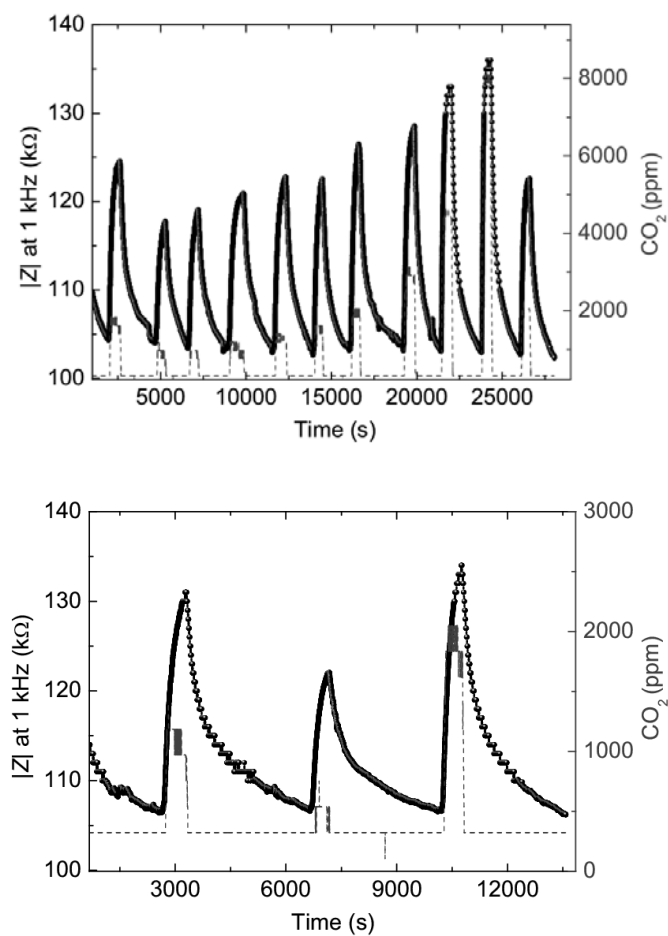


Figure A9. Time dependent impedance response measured at 1 kHz of PEI:Nafion-Na 2:1 when the blend was exposed to different CO_2 concentrations (dash line) at 75% RH in the first measurement after 2 weeks of preparation (top), measured again after drying in vacuum for 1 day (bottom).

Summary

Augmented levels of carbon dioxide (CO₂) in greenhouses can stimulate plant growth through photosynthesis leading to an increase in crop productivity. Monitoring CO₂ concentrations, typically between 1000-2000 ppm, with appropriate sensors is therefore necessary. To monitor and control CO₂ levels over large area of greenhouses, a wireless sensor network seems a good instrument. With preference these networks require low-power sensors to minimize energy consumption; hence room temperature operating polymer-based CO₂ sensors seem favorite. However, climate conditions in greenhouses, such as high humidity (70-90% RH) and presence of various gasses from fertilizers and combustion, like NO₂, SO₂, CH₄ and NH₃, induce cross-sensitivity of different analytes and may reduce long term stability of the active sensor materials. Consequently a polymer-based CO₂ sensor working at room temperature with high selectivity and sensitivity remains a challenge. Therefore, the main objective of this research is to develop CO₂ chemiresistors using conductive polymer/polyelectrolyte blends as sensing layers operating at room temperature. The transduction principle is based on a relative change in conductivity of the polymer/blend film with regard to variation of CO₂ concentrations.

In *Chapter 2* conducting polymers including emeraldine base polyaniline (EB-PANI), sodium salt of sulfonated polyaniline (SPAN-Na) and their blends with poly(vinyl alcohol) (PVA) were investigated for CO₂ sensing. pH-dependent conductivity of EB-PANI and SPAN-Na films was studied with aqueous pH buffers. EB-PANI exhibited a high conductivity only in its protonated form at low pH values. At pH above 4, EB-PANI became unprotonated and its conductivity did not change. Therefore, EB-PANI was verified to be not suitable for CO₂ sensing because conductivity of EB-PANI did not vary in the desired pH range for CO₂ sensing (pH4 - pH7). In contrast, SPAN-Na showed an appropriate conductivity change in this pH range. The extended pH range of conductivity of SPAN-Na is attributed to the sulfonic groups covalently attached to the polymer backbone, acting as inner dopant anions. Frequency-dependent impedance measurements of the polymer films casted on interdigitated electrodes was performed. A significant decrease in impedance of the SPAN-Na:PVA blend films was observed at high CO₂ concentrations (above 20,000 ppm) under high humidity regimes. This work demonstrated the capability of SPAN-Na blends for CO₂ sensing at ambient temperature.

Polymer CO₂ sensors have to operate at a high humidity level inside the greenhouse; hence, water (vapor) is the main cross-sensitive analyte which can interfere with CO₂ sensing. In pH-based indirect CO₂ sensing water vapor is essential to create carbonic acid to protonate the conductive polymers. Water vapor induces a similar sensor response as CO₂ because water is also needed for the dissociation of protons from carbonic acid. The effect of humidity on intrinsic and ionic conductivity of PANI, SPAN-Na, self-doped sulfonated polyaniline (SPANI), and their blends with PVA was investigated in *Chapter 3*. Dc and ac impedance measurements were used to characterize the conductivity responses of the polymers in relation to variations of humidity levels (10-90% RH). Electrochemical impedance spectroscopy (EIS) combined with an “extended Randle’s circuit model” is introduced to decouple ionic and intrinsic conduction paths in the polymer film upon exposure to water vapor. The intrinsic conductivity was found to increase as humidity increased. In acid-doped PANI, SPAN-Na and self-doped SPANI films, the conductivity is mainly due to charge transport of electron-holes induced by doping with acidic pH buffer and by water molecules. Nyquist plots were fitted to single (acid-doped PANI, SPANI) and double (SPAN-Na) semicircles. In case of blending with PVA, the conduction pathway consisted of more complex intrinsic and ionic charge transport through the polymer bulk and ion transport at the polymer/electrode interface, and is described by three semicircles. The increased conductivity at high humidity is partially explained by an increase of intrinsic conductivity due to protonation with protons dissociated from water molecules and by ionic transport of Na⁺ ions (if present). In addition, according to our understanding protons and electron-hole hopping via the Grotthuss mechanism contribute significantly to both ionic and intrinsic conductivity (e.g. SPAN-Na). This research provides a tentative insight on charge transport in conductive polymers under high humidity.

Another achievement of this research is the development of CO₂ chemiresistors based on polyethyleneimine (PEI) and its blends with SPAN-Na, sodium salt poly(styrene sulfonate) (PSS-Na) and Nafion sodium salt (Nafion-Na). These sensors exhibited a good CO₂ sensitivity over a wide range of CO₂ concentrations (from 400 ppm to 10,000 ppm). In *Chapter 4*, chemiresistors using branched PEI as sensing layers were investigated for CO₂ sensing. Both dc resistance and ac impedance of the PEI films increased when the films were exposed to CO₂ at high humidity. The relative change in impedance was about 6-12%. The increase in resistance/impedance is attributed to the formation of carbamates and bicarbonates at amine sites of PEI chain in presence of CO₂. These species reduce the number of free

amine groups, hence hinder proton hopping along the chain leading to a decrease in conductivity of the PEI films. Humidity induced an increase in the conductivity of the PEI films, which is an opposite response in comparison with CO₂. The response time was approximately 4-5 minutes; however, recovery time of the PEI sensor was quite long, in the order of 20 to 60 minutes.

Slow CO₂ desorption or slow reversibility of PEI films might not be a big problem in practical applications because CO₂ concentration in greenhouses is often maintained at a constant level e.g. 1,200 ppm and does not have to change frequently or rapidly. Nevertheless, a novel solution to reduce the recovery time was achieved with a PEI blend. In *Chapter 5*, blends of PEI and other polyelectrolytes including SPAN-Na, PSS-Na and Nafion-Na exhibited better sensing characteristics. The blend of PEI:SPAN-Na exhibited an (unexplained) fast response (about 1.5-4 min) and a short recovery time (1.5-10 min) but at a reduced sensitivity in comparison with the plain PEI. Furthermore, blends of PEI with PSS-Na, Nafion-Na gave a good sensitivity (up to 2-3 order improvement) and relatively short recovery time (10-20 minutes) in comparison with pure PEI. The sulfonate groups and their interactions with amine groups of PEI might be the main reason to explain for a better CO₂ sensitivity of the PEI blends. Therefore, mixing PEI with other polyelectrolytes not only improved CO₂ sensitivity but also shortened desorption time. Better sensing characteristics of the PEI blends bring great possibility of using these blends as CO₂ sensors in greenhouses and offices.

Finally, in *Chapter 6* several factors affecting the performance of the polymer sensors are discussed. Variations in humidity, temperature, solar radiation, temperature and presence of possible contaminants in greenhouse environment can influence the accuracy in CO₂ measurement and life-time of polymer-based sensors. In addition, possible effects of polymer structure, surface morphology and device configuration on CO₂ sensing performance were discussed. Furthermore, some perspectives and further researches are suggested for polymer sensors before these sensors can be applied in wireless sensor network for greenhouses and other potential applications such as in-door air quality monitoring in office buildings, food storage/packaging, healthcare, etc.

Samenvatting

Verhoogde koolstofdioxide (CO_2) niveaus in kassen kunnen de fotosynthese bevorderen, hetgeen leidt tot een toename in gewasproductiviteit. Het is daarvoor noodzakelijk om de gewenste CO_2 concentratie, typisch tussen de 1000 en 2000 ppm, te monitoren en te sturen met behulp van geschikte sensoren. Aangezien dit gewensd is voor grote oppervlakken in kassen zijn draadloze sensor netwerken mogelijk een goede oplossing. Zulke netwerken vereisen energiezuinige sensoren om het stroomverbruik te minimaliseren. Derhalve zijn op polymeren gebaseerde sensoren die bij kamertemperatuur werken veelbelovend. Vanwege de klimaatomstandigheden in kassen, zoals hoge luchtvochtigheid (70-90% RH) en aanwezigheid van diverse restgassen, zoals NO_2 , SO_2 , CH_4 , en NH_3 , kan dit leiden tot kruisgevoeligheid tussen de verschillende analieten en kan het de lange termijn stabiliteit van de actieve sensormaterialen reduceren. Het ontwikkelen van CO_2 sensoren gebaseerd op polymeren die werken bij kamertemperatuur met hoge selectiviteit en gevoeligheid zijn daarom een grote uitdaging.

Het hoofddoel van het onderzoek beschreven in dit proefschrift is het ontwikkelen van CO_2 chemiresistoren werkend bij kamertemperatuur, gebruikmakend van mengsels van geleidende polymeren en polyelectrolyten als sensormateriaal. Het meetprincipe is gebaseerd op veranderingen in de geleidbaarheid van de polymeerlaag veroorzaakt door veranderingen in de CO_2 concentratie.

In *Hoofdstuk 2* zijn de geleidende polymeren emeraldine base polyaniline (EB-PANI) en het natrium zout van gesulfoneerd polyaniline (SPAN-Na) bestudeerd voor CO_2 detectie in pure vorm en ook in mengsels met poly(vinylalcohol) (PVA). Eerst wordt de pH afhankelijkheid van de geleidbaarheid van EB-PANI en SPAN-Na lagen bestudeerd met waterige pH buffers. EB-PANI vertoonde alleen een hoge geleidbaarheid bij lage pH waarden in de geprotoneerde vorm. Bij pH boven de 4 wordt EB-PANI gedeprotoneerd en de geleidbaarheid verdwijnt. Dit is een indicatie dat EB-PANI niet geschikt is voor CO_2 detectie omdat de geleidbaarheid van EB-PANI niet veranderd in het gewenste pH bereik voor CO_2 detectie (pH 4 - 7). In tegenstelling tot EB-PANI vertoont SPAN-Na wel een verandering in de geleidbaarheid in dit pH gebied. Dit wordt toegeschreven aan de sulfonaat groepen die covalent zijn gebonden aan de polyaniline keten en die fungeren hierbij als interne doterende anionen. Frequentieafhankelijke impedantie metingen zijn verricht aan polymeer lagen aangebracht op

zelf-vervaardigde interdigitale electrodes. Een significante afname in de impedantie van SPAN-Na:PVA mengsels is waargenomen bij hoge CO₂ concentraties (boven 20.000 ppm) en hoge luchtvochtigheid. Dit werk demonstreert dat CO₂ detectie bij kamertemperatuur met SPAN-Na mogelijk is, hoewel vooralsnog alleen bij relatief hoge CO₂ concentraties.

Polymere CO₂ sensoren dienen te werken bij hoge luchtvochtigheden (RH>70%) in de kassen. Daarom is waterdamp de belangrijkste kruisgevoelige analiet die kan interfereren met CO₂ detectie. In de op pH-gebaseerde indirecte CO₂ detectie is water essentieel voor het vormen van koolzuur om de geleidende polymeren te protoneren. Waterdamp induceert hierbij een vergelijkbare respons als CO₂ omdat water nodig is voor de vorming van koolzuur en de daaropvolgende dissociatie van protonen van dit koolzuur. Het effect van de luchtvochtigheid op de intrinsieke en ionische geleidbaarheid van PANI, SPAN-Na, zelf-gedoteerd gesulfoneerd polyaniline (SPANI) en mengsels hiervan met PVA is onderzocht in *Hoofdstuk 3*. Dc en ac impedantie metingen zijn gebruikt voor karakterisatie van de respons in de geleidbaarheid van de polymeren als gevolg van variaties in de luchtvochtigheid (10-90% RH). Electrochemische impedantie spectroscopie (EIS) worden gecombineerd met modellering gebaseerd op een zogenaamd “*extended Randle’s circuit*”. Deze is zodanig gekozen opdat de bijdrage aan de respons van de intrinsieke en ionische geleidingspaden in de polymeerfilm als gevolg van blootstelling aan waterdamp worden ontkoppeld. In zuur gedoteerde PANI en zelfgedoteerde SPANI films vindt de (intrinsieke) geleiding voornamelijk plaats door ladingtransport van electrongaten. De Nyquist plots worden hier gekarakteriseerd met een enkele semicirkel. Een dubbele (gesloten) semicirkel wordt gevonden bij SPAN-Na, hetgeen duidt op een combinatie van intrinsieke en ionische geleiding. In het geval van mengsels met PVA is gefit met drie semicirkels, het geleidingspad is hierbij een complexe combinatie van intrinsieke geleiding en ionische ladings-transport door de bulk, en ook het transport proces van ionen naar en van het polymeer/electrode grensvlak. De toename van de geleidbaarheid bij hoge luchtvochtigheid is gedeeltelijke te verklaren door een toename van de intrinsieke geleiding en door ionisch transport van natrium ionen (indien aanwezig). Daarnaast, naar ons inzicht, dragen zowel proton en ook electrongat hopping via het Grotthuss mechanisme significant bij aan zowel de ionische als de intrinsieke geleiding (bijvoorbeeld SPAN-Na). Dit onderzoek geeft een eerste inzicht in ladingtransport in geleidende polymeren bij hoge luchtvochtigheid.

Een ander aspect van het onderzoek beschreven in dit proefschrift is de ontwikkeling van CO₂ chemiresistoren gebaseerd op poly(ethyleenimine) (PEI) en mengsels hiervan met SPAN-Na,

poly(styrene sulfonate) (PSS-Na) en Nafion natrium zout (Nafion-Na). Deze sensoren vertonen een goede CO₂ gevoeligheid over een groot bereik van CO₂ concentraties (van 400 ppm tot 10.000 ppm). In *Hoofdstuk 4* zijn chemiresistoren op basis van vertakt PEI als gevoelige laag onderzocht voor CO₂ detectie. Zowel de dc weerstands als de ac impedantie van PEI lagen neemt toe wanneer het materiaal wordt blootgesteld aan CO₂ bij hoge luchtvochtigheid. De relatieve verandering in impedantie bedraagt 6 tot 12 %. De toename in weerstand/impedantie wordt toegeschreven aan de vorming van carbamaten en bicarbonaten aan de amine groepen van de PEI keten met behulp van CO₂. Deze verbindingen reduceren het aantal vrije amine groepen, hetgeen de proton hopping langs de keten bemoeilijkt, en leidt tot een afname van de geleidbaarheid van de PEI lagen. Een hogere luchtvochtigheid veroorzaakt een toename van de geleidbaarheid, tegenovergesteld aan de respons veroorzaakt door CO₂. De responstijd is 4 tot 5 minuten, hoewel de hersteltijd (desorptie) na blootstelling aan CO₂ vrij lang is, 20 tot 60 minuten.

Langzame CO₂ desorptie of langzame reversibiliteit van PEI lagen hoeft geen groot probleem te zijn in de praktijk omdat de CO₂ concentratie in kassen vaak constant wordt gehouden op bijvoorbeeld 1.200 ppm en niet snel hoeft te worden veranderd. Desondanks, een nieuwe manier om de hersteltijd te verbeteren was door de PEI te mengen met polyelectrolyten. In *Hoofdstuk 5* worden mengsels van PEI met de polyelectrolyten, SPAN-Na, PSS-Na en Nafion-Na, beschreven die betere eigenschappen hebben voor detectie dan puur PEI. Het mengsel van PEI met SPAN-Na vertoont een (onverklaarde) snelle respons (1,5 tot 4 minuten) en korte hersteltijd (1,5 tot 10 minuten) maar een lagere gevoeligheid in vergelijking met puur PEI. Verder bleek dat mengsels met PSS-Na en Nafion-Na een verhoogde gevoeligheid (2 tot 3 keer gevoeliger) met een relatief korte hersteltijd (10 tot 20 minuten) vertonen. De interactie van sulfonaat groepen met amine groepen van PEI kunnen de hoofdoorzaak zijn voor de betere gevoeligheid van de PEI mengsels. Het mengen van PEI met polyelectrolyten verbeterd niet alleen de CO₂ gevoeligheid maar verkort ook de desorptietijd van CO₂. Betere CO₂ detectie eigenschappen van de PEI mengsels opent meer mogelijkheden voor het gebruik hiervan als CO₂ sensor in kassen en kantoren.

In *Hoofdstuk 6* worden verschillende factoren besproken die de prestaties van polymere sensoren beïnvloeden. Variaties in luchtvochtigheid, temperatuur, zonlicht en aanwezigheid van mogelijke vervuilingen in de kasomgeving kunnen invloed hebben op de nauwkeurigheid en levensduur van de polymere sensoren. Daarnaast zijn de mogelijke effecten van polymeer structuur, oppervlakte morphologie en meetconfiguratie beschreven die de prestaties kunnen

beïnvloeden. Tenslotte is er een perspectief geschetst voor verder onderzoek naar polymere sensoren om te komen tot het gebruik van draadloze sensor netwerken in kassen en voor andere toepassingen, zoals bewaking van de luchtkwaliteit in kantoorgebouwen, bij voedsel-opslag, in verpakkingen en in ziekenhuizen.

Tóm Tắt

Nồng độ khí carbon dioxide (CO_2) trong nhà kính (greenhouse) được điều chỉnh cao hơn so với môi trường bên ngoài có thể kích thích cây trồng tăng trưởng thông qua quá trình quang hợp nhằm gia tăng sản lượng thu hoạch. Do đó việc theo dõi kiểm tra nồng độ khí CO_2 , thường dao động trong khoảng 1.000 - 2.000 ppm, bằng các cảm biến (sensor) thích hợp là điều rất cần thiết. Mạng lưới cảm biến không dây là một hệ thống phù hợp giúp đo đạc và điều khiển nồng độ CO_2 trên một diện tích rộng của nhà kính. Các mạng lưới này yêu cầu sử dụng các cảm biến có công suất thấp nhằm giảm thiểu năng lượng tiêu hao; do đó các cảm biến đo nồng độ CO_2 trên cơ sở polymer hoạt động ở nhiệt độ thường có lẽ thích hợp nhất. Tuy nhiên, môi trường bên trong nhà kính với độ ẩm cao (thường từ 70-90% RH) và các khí khác nhau thải ra từ phân bón và quá trình đốt cháy nhiên liệu như khí NO_2 , SO_2 , CH_4 và NH_3 có thể gây ra nhiễu tín hiệu đo (cross-sensitivity) và làm suy giảm độ bền của các vật liệu nhạy khí. Vì vậy cảm biến CO_2 sử dụng polymer làm việc ở nhiệt độ thường với khả năng chọn lọc cao và độ nhạy cao vẫn còn là một thách thức cần vượt qua đối với các nhóm nghiên cứu. Do đó, mục tiêu chủ yếu của nghiên cứu này là phát triển các cảm biến khí CO_2 kiểu điện trở (chemiresistor) sử dụng các hỗn hợp polymer dẫn điện/polymer điện giải (conductive polymers/polyelectrolytes) làm lớp nhạy khí hoạt động ở nhiệt độ thường. Nguyên lý đo dựa trên sự biến thiên độ dẫn điện của lớp phủ polymer khi nồng độ khí CO_2 trong môi trường thay đổi.

Trong *Chương 2* các polymer dẫn điện như emeraldine base polyaniline (EB-PANI), muối Natri của sulfonated polyaniline (SPAN-Na) và các hỗn hợp với poly(vinyl alcohol) (PVA) được nghiên cứu để đo nồng độ CO_2 . Độ dẫn điện tùy thuộc vào pH của các màng mỏng EB-PANI và SPAN-Na được khảo sát bằng các dung dịch đệm pH. EB-PANI chỉ có khả năng dẫn điện cao khi ở dạng được pha tạp bằng các proton (protonated) ở pH thấp. Khi pH cao hơn 4, EB-PANI không bị pha tạp, độ dẫn điện vẫn ở mức thấp và không thay đổi. Do đó, EB-PANI đã được xác định là không phù hợp để đo CO_2 bởi vì độ dẫn điện của EB-PANI không đổi trong khoảng pH cần thiết cho việc đo CO_2 (pH4 – pH7). Trái lại, các kết quả thí nghiệm với SPAN-Na cho thấy độ dẫn điện của SPAN-Na có thay đổi trong khoảng pH này. Độ dẫn điện của SPAN-Na có thể biến thiên trong khoảng pH rộng hơn là do sự có mặt của các nhóm sulfonic có liên kết cộng hóa trị với mạch chính của polymer, đóng vai trò làm các ion âm pha tạp nội tại (inner dopant anion). Các màng mỏng polymer được phủ trên các điện cực Platin xen kẽ nhau và được đo điện trở kháng (impedance) theo tần số. Kết quả đo cho thấy điện trở

kháng của các màng mỏng hỗn hợp SPAN-Na:PVA giảm đáng kể khi nồng độ CO_2 tăng cao (hơn 20.000 ppm) trong môi trường có độ ẩm cao. Kết quả nghiên cứu này chứng minh khả năng nhạy khí CO_2 của hỗn hợp SPAN-Na ở nhiệt độ thường.

Các cảm biến CO_2 trên cơ sở polymer làm việc trong môi trường có độ ẩm cao bên trong nhà kính; do đó hơi nước là tác nhân chính có thể gây nhiễu tín hiệu khi đo nồng độ CO_2 . Trong quá trình đo nồng độ CO_2 theo phương pháp gián tiếp thông qua pH, hơi nước là tác nhân thiết yếu để tạo thành acid carbonic nhằm pha tạp proton cho các polymer dẫn điện. Hơi nước gây ra đáp ứng cảm biến tương tự như khí CO_2 bởi vì hơi nước cũng cần thiết cho quá trình phân ly proton từ acid carbonic. Ảnh hưởng của hơi nước đến độ dẫn điện nội tại và độ dẫn điện ion của PANI, SPAN-Na, sulfonated polyaniline tự pha tạp (SPANI) và các hỗn hợp của chúng với PVA được khảo sát trong *Chương 3*. Các thí nghiệm đo đặc điện trở một chiều (dc) và điện trở kháng xoay chiều (ac) được tiến hành để đánh giá sự biến thiên độ dẫn điện của các polymer khi độ ẩm thay đổi (10-90% RH). Phổ đo điện trở kháng điện hóa (Electrochemical impedance spectroscopy - EIS) kết hợp với “mô hình mạch điện của Randle mở rộng” đã được áp dụng để tách biệt dòng điện nội tại và dòng điện ion trong màng polymer khi tiếp xúc với hơi nước. Kết quả thí nghiệm cho thấy độ dẫn điện nội tại gia tăng khi hơi ẩm tăng cao. Đối với các màng PANI, SPAN-Na pha tạp bằng acid và SPANI tự pha tạp, khả năng dẫn điện cao chủ yếu là do sự chuyển động của hạt tải gồm electron-lỗ trống được tạo ra bằng cách pha tạp với dung dịch đệm pH thấp có tính acid mạnh và bởi các phân tử nước. Các đồ thị Nyquist được tính toán mô phỏng cho khớp (fit) với một nửa vòng tròn (semicircle) (đối với PANI, SPANI pha tạp bằng acid) và hai nửa vòng tròn (SPAN-Na). Đối với các hỗn hợp với PVA, dòng dẫn bao gồm nhiều chuyển động của các hạt tải nội tại và các ion phức tạp hơn bên trong khối polymer và hạt tải ion ở giao diện polymer/điện cực, và được mô tả bằng ba nửa vòng tròn. Độ dẫn điện gia tăng khi hơi ẩm tăng cao được giải thích một phần là do độ dẫn điện nội tại gia tăng khi polymer được pha tạp bằng proton phân ly từ các phân tử nước và do chuyển động ion của các ion Na^+ (nếu hiện diện). Hơn nữa, theo suy luận của chúng tôi quá trình nhảy ngắn qua lại (hopping) của các proton và electron-lỗ trống theo cơ chế Grotthuss đóng góp đáng kể vào cả độ dẫn điện nội tại và độ dẫn điện ion (ví dụ như trường hợp của SPAN-Na). Nghiên cứu này kiến nghị những phân tích suy luận về chuyển động hạt tải trong các polymer dẫn điện khi tiếp xúc với độ ẩm cao.

Một kết quả đáng chú ý khác trong nghiên cứu này là chúng tôi đã chế tạo thành công các cảm biến điện trở CO_2 trên cơ sở polyethyleneimine (PEI) và hỗn hợp của PEI với SPAN-Na, muối Natri poly(styrene sulfonate) (PSS-Na) và muối Natri Nafion (Nafion-Na). Các cảm

biến này cho độ nhạy cao với CO₂ trong khoảng nồng độ khí CO₂ rộng (từ 400 ppm đến 10.000 ppm). Trong *Chương 4*, các cảm biến điện trở sử dụng PEI mạch nhánh (branched) làm lớp nhạy khí được khảo sát đo nồng độ CO₂. Cả điện trở dc và điện trở kháng ac của các màng mỏng PEI đều tăng khi các màng polymer này tiếp xúc với CO₂ trong môi trường có độ ẩm cao. Biến thiên tương đối của điện trở kháng khoảng 6-12%. Sự gia tăng điện trở/điện trở kháng là do hình thành carbamate và bicarbonate ở các amine của mạch PEI khi có mặt khí CO₂. Những hợp chất này làm giảm các nhóm amine tự do trong PEI, do đó ngăn cản sự nhảy ngắn qua lại của proton dọc theo mạch polymer dẫn đến suy giảm khả năng dẫn điện của các màng PEI. Hơi ẩm làm tăng độ dẫn điện của các màng mỏng PEI, trái ngược với tác dụng làm giảm độ dẫn điện của khí CO₂. Thời gian đáp ứng khoảng 4-5 phút, tuy nhiên thời gian phục hồi của cảm biến PEI khá dài từ 20-60 phút.

Sự giải hấp CO₂ chậm hay nói cách khác khả năng phục hồi của các màng PEI chậm không gây khó khăn nhiều trong các ứng dụng thực tiễn vì nồng độ CO₂ trong các nhà kính thường được duy trì ở mức cố định, ví dụ 1.200 ppm và không phải thay đổi thường xuyên hay nhanh chóng. Tuy vậy, giải pháp mới nhằm rút ngắn thời gian hồi phục đã được nghiên cứu với hỗn hợp PEI. Trong *Chương 5*, các hỗn hợp của PEI với những polymer điện giải khác gồm có SPAN-Na, PSS-Na và Nafion-Na cho kết quả nhạy khí tốt hơn. Hỗn hợp PEI:SPAN-Na cho đáp ứng nhanh khoảng 1,5-4 phút (lý do vì sao vẫn chưa được rõ) và thời gian hồi phục ngắn (1,5-10 phút) nhưng độ nhạy lại kém hơn so với PEI. Hơn nữa, các hỗn hợp giữa PEI với PSS-Na, Nafion-Na cho độ nhạy cao (tăng từ 2-3 lần) và thời gian hồi phục tương đối ngắn (10-20 phút) so với PEI. Sự hiện diện của các nhóm sulfonate và tương tác giữa chúng với các nhóm amine của PEI có thể là lý do chính giải thích vì sao các hỗn hợp PEI có độ nhạy CO₂ tốt hơn. Do đó, pha trộn PEI với các polymer điện giải khác không những cải thiện độ nhạy khí CO₂ mà còn làm giảm thời gian hấp phụ và giải hấp CO₂. Các hỗn hợp PEI với những đặc tính nhạy khí CO₂ tốt hơn thích hợp sử dụng trong các cảm biến CO₂ dùng trong nhà kính và văn phòng.

Cuối cùng, một số yếu tố ảnh hưởng đến hiệu suất của các cảm biến polymer được bàn luận trong *Chương 6*. Sự biến thiên độ ẩm, nhiệt độ, bức xạ ánh sáng mặt trời và sự hiện diện của các tạp chất có trong môi trường nhà kính có thể ảnh hưởng đến độ chính xác của phép đo nồng độ CO₂ và tuổi thọ của các cảm biến polymer. Thêm vào đó, các ảnh hưởng của cấu trúc polymer, hình thái bề mặt và cấu hình cảm biến đến khả năng đo CO₂ cũng được thảo luận. Hơn nữa, một số triển vọng và các nghiên cứu sâu hơn được đề nghị thực hiện trên các cảm biến polymer trước khi được đưa vào ứng dụng trong các mạng lưới cảm biến không dây

trong nhà kính và những ứng dụng tiềm năng khác như theo dõi chất lượng không khí trong môi trường các cao ốc văn phòng, trong lưu trữ/đóng gói thực phẩm, chăm sóc y tế, v.v...

Curriculum Vitae



Đoàn Đức Chánh Tín (Tin C. D. Doan) was born on December 12, 1979 in Ho Chi Minh City, Vietnam. He obtained his Mechanical Engineer degree in Materials for Mechanical Engineering in 2003 and Master's Degree in Materials Technology in 2005 from Ho Chi Minh City University of Technology (HCMUT), Vietnam.

From 2003 to 2005 he worked as an assistant lecturer at Faculty of Materials Technology - HCMUT. After that, he moved to the Laboratory for Nanotechnology (LNT), Vietnam National University - Ho Chi Minh City (VNU-HCM) and worked as a researcher fellow; hold concurrently Director Assistant from 2005 until 2007. From 2008 he worked as a Ph.D. student at the Laboratory of Organic Chemistry, Wageningen University, the Netherlands. His research focused on development of polymer-based sensors for CO₂ detection in greenhouses and offices. The main achievements were reported in this thesis.

Email: chanhtindoan@gmail.com

List of Publications

“*Carbon Dioxide Sensing with Sulfonated Polyaniline*”, Tin C. D. Doan, Rajesh Ramaneti, Jacob Baggerman, J. Franc van der Bent, Antonius T. M. Marcelis, Hien D. Tong, and Cees J. M. van Rijn, *Sensors and Actuators B* 168 (2012) 123–130.

“*Intrinsic and Ionic Conduction in Humidity Sensitive Sulfonated Polyaniline*”, Tin C. D. Doan, Rajesh Ramaneti, Jacob Baggerman, Antonius T. M. Marcelis, Hien D. Tong, and Cees J. M. van Rijn, submitted.

“*Carbon Dioxide Detection at Room Temperature with Polyethyleneimine-based Chemiresistor*”, Tin C. D. Doan, Rajesh Ramaneti, Jacob Baggerman, Antonius T. M. Marcelis, Hien D. Tong, and Cees J. M. van Rijn, *Sensors and Actuators B*, submitted.

Overview of Completed Training Activities

<i>Discipline specific activities</i>	<i>Graduate school/ Institute</i>	<i>Time</i>
Course “ <i>Lab on a chip</i> ”	BIOS group, UTwente	04–06/2008
Summer school “ <i>Highlights in Microtechnology</i> ”	Swiss Foundation for Research in Microtechnology, Institute of Micro-technology - University of Neuchâtel, École Polytechnique Fédérale de Lausanne, Switzerland	06–07/2009
3 rd International GASMEMS Summer school & Workshop “ <i>Gas Flows in Micro Electro Mechanical Systems</i> ”	7FP GASMEMS project, Centro Residenziale Universitario di Bertinoro, Italy	6/2011
Netherlands Micro-Nano Conference	MicroNed - NanoNed - MinacNed	11/2008, 2009
2 nd and 3 rd International Workshop on Nanotechnology and Application	Laboratory for Nanotechnology, National University Ho Chi Minh City, Vietnam	11/2009, 2011
STW.ICT Conference - SAFE Workshop on Microsystems, Materials, Technology and RF-devices and Sensors	STW	11/2010
3 rd Conference on Nanosensors for Industrial Applications	Nanosens, Tech Gate Vienna, Austria	12/2010
Workshop Sense of Contact 13	FHI and STW	6/2011
<i>General courses</i>		
Academic Writing II	Centa, WUR	02–07/2008
Techniques for Writing and Presenting a Scientific Paper	WUR	07/2008
Introduction course of MESA+ cleanroom and MTE Workshop “ <i>Fundamentals of Nanotechnology</i> ”	MESA+ Institute for Nanotechnology, UTwente	03/2008
<i>Optional courses and activities</i>		
Analytical Methods in Organic Chemistry	ORC-WUR	09–10/2008
Sensor technology	SCO-WUR	01–02/2009
Colloquia	ORC-WUR	2008–2012
STW progress project meeting, group meetings with other collaborative partners	STW, ORC-WUR, Nanosens, Delft, CHESS	2008–2011
Preparing Ph.D. research proposal	VLAG-WUR	2008
Ph.D. trip in China (Beijing and Shanghai)	ORC-WUR	05/2009
Ph.D. trip in UK (Scotland and North England)	ORC-WUR	05/2011

Acknowledgement

This thesis could not be accomplished without the valuable support of many people whose contributions will never be forgotten. Therefore I would like to express my gratitude to them.

The first sincere thank I would like to give to my promoter and supervisor, *Prof. Cees J.M. van Rijn*, for giving me the position in a very stimulating and challenging project. Dear Sir, I still remember what you told me when we had the first meeting “You were chosen because you are flexible”. Personally I thought that you and I took a risk when you chose me and I chose this topic for my Ph.D. research. I had anticipated the difficulties in dealing with conductive polymer based sensors before I arrived at Wageningen, but I had not expected so many tough problems to be encountered. Luckily we could manage to overcome and to reach the Aula in the end. Thank you so much for giving me a chance to correct my mistakes during the project and learn many new things. I really appreciate your quick action whenever I need your letters/signatures, your direction in writing our articles and also your day and night correction for my thesis. So thank you again, Sir!

I would like to give my special thanks to *Rajesh Ramaneti* who contributed a great deal in this achievement. Dear Rajesh, you did drive me back on the track and push the progress of our project faster when you joined. Many useful instruments arrived after you came and we have an excellent set-up for my measurements. I really appreciated your enthusiasm and working attitude. I have learned a lot from you. Thank you for your questions at any time which stimulated my thinking and hence improved my knowledge gradually.

I am also grateful to *Jacob Baggerman* for all of his contribution to this work and continuous support during my project timeline. Dear Jacob, you not only instructed me with polymer synthesis, characterization but also helped me with many things during my project. I really appreciate your original ideas, critical reviews, useful advices and corrections which helped my thesis to be submitted on time. Thank you so much for your kind help with Dutch translation and preparation of my thesis, especially the PEI part owes a lot to you.

There are some other people *Franco van der Bent*, *Ton Marcelis* and *Hien D. Tong* in our working team to whom I would like to give many thanks for their scientific contributions. Dear Franco, thank you so much for helping me a lot in the beginning of the project, lending me many electrical instruments and many valuable technical suggestions you gave during discussions. Dear Ton, I would like to express gratefulness to you for your kind explanation

on chemicals, polymers, doping mechanism, your helpful scientific discussions and suggestions and also your quick critical comments for our articles. I also would like to appreciate *Hien D. Tong* for his introduction to this project and his support in device processing. Dear anh Hiên, I really appreciate your kind instructions when we did processing in MESA+ clean room, your sharing on Ph.D. life and various social aspects.

I also greatly appreciate *Dutch Technology Foundation STW* for funding our research, participation of *Nanosens*, *CHESS* and *Delft University* as involved partners in our project.

It is time to say how I appreciated to work with all of my colleagues at ORC. I would like to say thank you to *Han*, *Elly* and *Aleida*, who helped me a lot with paper work for my residence permit application/extension, booking air plane ticket, hotel for conferences, optare, etc. Great thanks to *Barend* and *Marcel* for FTIR and XPS measurements, to *Frank* and *Elbert* for helping me with gas cylinders, gas tubes and connectors. I am especially grateful to *Ronald* for helping me with ordering chemicals, tools, instruments. Many thanks to *Remco* and *Teris* when we would like to try polymer dropping with silica capillary tubing. I also would like to thank *Cees*, *Erik*, *Maurice*, *Teris*, *Nishant* for helping me in tasks of exam supervision, *Anne-Marie* for teaching me practical knowledge in organic chemistry course.

I would like to thank my friendly colleagues *Ai*, *Jerome*, *Nagesh*, *Willem*, *Ganesan*, *Rokus*, *Bart*, *Loes*, *Wouter*, *Sidhu*, *Umesh*, *Aline* who are always willing to help me in lab work, and research issues. Thank you *Alexandre*, *Ai*, *Jerome*, *Willem*, *Rokus* for playing badminton sometimes at the sport center and playing a beach volleyball We Day together as a “jet-lag” team right after we were back from our Ph.D. trip in China. I will miss all you guys and the time we had together. I also greatly thank *Nagesh*, *Sourav* and *Alexandre* for sharing their experience and ideas when I was preparing my thesis. Many thanks to *Luc*, *Jurien*, *Feng*, *Kim*, *TuHa*, *Jaime*, *Radostina*, *Anke*, *Jacinthe*, *Yessie*, *Saurabh*, *Satesh*, *Nagendra*, *Florine*, *Yao*, *Bas*, *Peter*, *Jos*, *Tom* for all their help during my stay in the lab and during two interesting Ph.D. trips to China and UK. I wish you all the best for your research and career.

I especially acknowledge *Hans Meijer*, *Frans van Korlaar* and *Reinoud Hummelen* from WUR workshop who helped me a lot with my experimental set-up and ordering some tools. Many thanks to *Remco Fokkink* (Laboratory of Physical Chemistry and Colloid Science) for helping me in use of high temperature furnace. I appreciate *Jos Balendonck* (Greenhouse Horticulture) and *Jeremy Harbison* (Horticultural Supply Chains Group) for lending me the

impedance analyzer in several months. I also thank *Nicole de Vries* and *Jacqueline de Graaf* (HRM department) for helping me with my contract, insurance, residence permit extension.

I greatly appreciate the kindness of my Director, *Prof. Chien Mau Dang* - Director of Laboratory for Nanotechnology (LNT) - for accepting me to do Ph.D. here and his support during the past four years. Many thanks to my colleagues in LNT (*Nhân Ái, Tuấn Anh, Tuyền, Đám, Hằng, Lê, Trang, Vinh,...*) for helping me in measurements when I visited LNT and attended International Workshops on Nanotechnology and Application in 2009 and 2011.

I would like to thank my Vietnamese friends who shared lots of time with me during the time this thesis was done. I express my thankfulness to *Ai T. Nguyen*, my colleague in Ho Chi Minh city and Wageningen and also one of my best friends. Dear Ái, thanks a lot for your kind help when I arrived and during my stay in Wageningen. I really appreciate your delicious meals, chatting, scientific suggestions/discussions, and also thank you for your helpful advices in my thesis writing and preparation. I am also grateful to my close friends namely *chị Hương, Duyên, chị Dung, Thắng - Trang, Peter - Yuni, chị Thu Hà*. I also thank my other friends in Vietnam Student Association in Wageningen. Thank you all for spending time with me in playing badminton, eating, shopping and wandering around. I would like to thank *So V. Pham* for helping me during my courses in University of Twente and when I worked in the clean room. I also thank my friends *Tuấn, Uyên* for sharing time with me in journeys around Europe. I wish you guys all the best and I hope we will keep in touch later on. Many thanks to my teachers *Ms. Lan* and *Ms. Thu* for your guidance and encouragement.

Finally, it is my pleasure to express my gratefulness to my family and my relatives for their everlasting love and support. Thank you so much my parents, my sisters, my niece who are always beside me to support and encourage me. I also would like to thank my grandmother, my aunts and uncles, my cousins who helped my family when I was away from home and always welcome me anytime I am back. Last but not least, I would say thank you to my love “*Little Turtle*”, thank you for your love, your sharing and continuous encouragement which bring happiness in my life and open my soul.

Best regards,



Tin C. D. Doan

The research described in this thesis was financially supported by Dutch Technology Foundation STW (Project no. 10058).

Design & Layout: Tin C. D. Doan

Printed by Wöhrmann Print Service, Zutphen, The Netherlands